AEROSOLFORSCHUNG AM

INSTITUT FÜR EXPERIMENTALPHYSIK DER UNIVERSITÄT WIEN

(VORMALS I. PHYSIKALISCHES INSTITUT)

AEROSOL RESEARCH AT THE

INSTITUTE FOR EXPERIMENTAL PHYSICS OF THE UNIVERSITY OF VIENNA

(FORMERLY FIRST PHYSICS INSTITUTE)

PART III

HETEROGENEOUS NUCLEATION AND DROPLET GROWTH

MEASUREMENTS WITH A PROCESS CONTROLLED FAST EXPANSION CHAMBER, THE SIZE ANALYZING NUCLEI COUNTER SANC

FEBRUARY 1981

Mit herzlichen Grüßen

Paul Hagen

AEROSOLFORSCHUNG AM INSTITUT FÜR EXPERIMENTALPHYSIK DER UNIVERSITÄT WIEN

(VORMALS I. PHYSIKALISCHES INSTITUT)

AEROSOL RESEARCH AT THE INSTITUTE FOR EXPERIMENTAL PHYSICS OF THE UNIVERSITY OF VIENNA

(FORMERLY FIRST PHYSICS INSTITUTE)

O. PREINING

PART I: *Aerosol Measurements in the Submicron Size Range (Studies with an Aerosol Centrifuge, a New Diffusion Battery, a Low Pressure Impactor, and an Advanced Condensation Nuclei Counter).*
By A. Berner, O. Preining

PART II: *Measurements of Visibilities in Simulated Atmospheres (Hydrosols) and Applications to Real Atmospheres.*
By H. Horvath, G. Presle

PART III: *Heterogeneous Nucleation and Droplet Growth (Measurements with a Process Controlled Fast Expansion Chamber, the Size Analyzing Nuclei Counter SANC)*
By O. Preining, P.E. Wagner, F.G. Pohl, W. Szymanski

INSTITUTE FOR EXPERIMENTAL PHYSICS OF THE UNIVERSITY OF VIENNA
BOLTZMANNGASSE 5, 1090 WIEN, AUSTRIA.

FOREWORD

Aerosol Research at the Institute for Experimental Physics of the University of Vienna has a long tradition starting in the first decade of this century with Ehrenhaft's work on the elementary charge and continuing with related programs on material dependence of slip correction factors and on photophoresis. During the past decade the main interest was directed to characterization of physical aerosol properties as documented by this report.

The first volume of the report covers the work on instrumentation for acquiring size and size distribution data, the second one represents independently conducted visibility research, and the third volume summarizes studies of heterogeneous nucleation and droplet growth, performed with the Size Analyzing Nuclei Counter SANC. Almost all the scientific work reported here was finished by the end of January 1980. For personal reasons the preparation of this report was delayed.

February, 1981. O. Preining

Aerosol Measurement in the Submicron Size Range (Studies with an Aerosol Centrifuge, a New Diffusion Battery, a Low Pressure Impactor, and an Advanced Condensation Nuclei Counter)

By.A. Berner, O. Preining

ABSTRACT

The report summarizes the investigations of four aerosol classifiers which cover finite, but overlapping ranges of the aerosol particle size spectrum.

The first part is concerned with a cylindrical aerosol centrifuge, which measures aerodynamic equivalent diameters precisely. This instrument has been used as a reference instrument in diffusion battery experiments reported in the second part. The diffusion battery has been investigated for fairly large particle sizes (o,3 µm to o,5 µm) to investigate the influence of sedimentation, interception and impaction on the transmission of the diffusion battery. These experiments have been performed with highly monodispersed NaCl aerosols.

In the third part a five stage low pressure impactor is described, which covers the size range from o,1 µm to 25 µm diameter. It has been developed specifically for the determination of the deposited particulate mass. First data on mass size distributions of atmospheric aerosols are reported. The final chapter summarizes the development of a special condensation nuclei counter which measures number size distributions in the size range from o,oo2 µm to o,1 µm of KELVIN-equivalent diameter. The applicability to urban atmospheric aerosols is demonstrated.

Measurement of Visibility in Simulated Atmospheres (Hydrosols) and Applications to Real Atmospheres

By H. Horvath , G. Presle

ABSTRACT

For laboratory measurements reduced visibilities have been simulated in a hydrosol of high particle concentration, using different types of hydrosols, which were representative for different levels of pollution in the atmosphere. The hydrosol was normally illuminated homogeneously, within ± 3 %, but innomogeneous illumination could be simulated by shading part of the hydrosol. Seven visibility targets were suspended in the hydrosols such, that they were increasingly distant from the observer, and only some were visible. The visibility was determined by counting the number of visible targets. The extinction coefficient of the hydrosol was determined by means of a specially designed long path photometer. The visibilities were calculated from the extinction coefficients by means of the Koschmieder Visibility formula. An agreement between the calculated and measured visibilities was only found if the extinction coefficient was used at a wavelength longer than 550 nm, since the contrast of the target seen through the turbid medium increases with wavelength.

The visibilities measured in inhomogeneous media were found to be in agreement with an expanded visibility formula.

The visibility of colored and grey targets normally is lower than that of black targets, since the inherent contrast is usually larger than -1 and less than 1. A color is better visible the smaller its reflection in the spectral range of maximum perception.

Since visibility in the atmosphere is due to contrast reduction, a measurement of the contrast reduction permits the determination of visibility or extinction coefficient. A small astronomic telescope has been adapted for this purpose (telephotometer). By means of spectral extinction measurements it is possible to estimate the size distribution of the aerosol and the mass of the suspended particles.

PART III

HETEROGENEOUS NUCLEATION AND DROPLET GROWTH

MEASUREMENTS WITH A PROCESS CONTROLLED FAST EXPANSION CHAMBER, THE SIZE ANALYZING NUCLEI COUNTER SANC

O. PREINING, P.E. WAGNER, F.G. POHL, W. SZYMANSKI

FEBRUARY 1981

ACKNOWLEDGMENTS

The support by the Österreichisches Bundesministerium für Wissenschaft und Forschung, the University of Vienna and the EDV-Zentrum der Universität Wien, Abteilung Prozeßrechenanlage Physik is acknowledged as well as the very important support by the Fonds zur Förderung der wissenschaftlichen Forschung in Österreich, Proj. Nr. 2429 and 3481. We also acknowledge the support by the Hochschuljubiläumsstiftung der Stadt Wien.

We appreciate the help of the machine shop for building much complicated equipment and the help of the secretary, Mrs. H. Kranner, in preparing manuscripts and the report.

Part of the subject, covered by this report, has been published:

Wagner, P., "Optical Determination of the Size of Fast-Growing Water Droplets in an Expansion Cloud Chamber", J. Colloid Interface Sci. 44, 181 (1973).

Wagner, P.E., and Pohl, F.G., "The Interdependence of Droplet Growth and Concentration. I. Theory of Droplet Growth and Applications on Condensation Nuclei Counters", J. Colloid Interface Sci. 53, 429 (1975).

Wagner, P.E., "The Interdependence of Droplet Growth and Concentration. II. Experimental Test of Droplet Growth Theory", J. Colloid Interface Sci. 53, 439 (1975).

Wagner, P.E., and Pohl, F.G., "Eine prozeßgesteuerte Anlage zur Untersuchung der Kinetik von Kondensationsvorgängen", Staub-Reinhalt. Luft 38, 72 (1978).

Wagner, P.E., "Droplet Growth Kinetics and Design Principles for Condensation Nuclei Counters", in "Aerosol Measurement" (D.A. Lundgren, et al., eds.), p. 574. University Presses of Florida, Gainesville, Florida, 1979.

Pohl, F., "Zur Untersuchung der Wasserdampfkondensation in einer prozeßgesteuerten Expansionsnebelkammer und deren Anwendung zur Analyse des urbanen Aerosols", Ph.D. Thesis, University of Vienna, 1979.

Pohl, F.G., and Wagner, P.E., "Measurement of Size Distributions of Urban Aerosols in the Size Range Below 0,1 um", J. Aerosol Sci. 1o, 2o9 (1979).

Pohl, F.G., and Wagner, P.E., "Measurement of Kelvin-equivalent Size Distributions of Urban Aerosols", J. Phys. Chem. 84, 1642 (198o).

Wagner, P.E., and Pohl, F.G., "Experimental Test of Recent Droplet Growth Theories by Means of a Process Controlled Expansion Cloud Chamber", J. Aerosol Sci. 1o, 2o4 (1979).

Berner, A., Lürzer, Ch., Pohl, F., Preining, O., and Wagner, P., "The Size Distribution of the Urban Aerosol in Vienna", Sci. Total Env. 13, 245 (1979).

Szymanski, W., Pohl, F.G., and Wagner, P.E., "The Optical Determination of Droplet Size Distribution During a Growth Process in Supersaturated Vapor", J. Aerosol Sci. 11,268 (198o).

CONTENTS

Kurzfassung

Kondensationsvorgänge können in einer Anzahl von Systemen beobachtet werden, die in der Praxis von Bedeutung sind. In vielen Fällen wird der Kondensationsvorgang ausgelöst durch heterogene Keimbildung an der Oberfläche von Fremdpartikeln (Kondensationskerne). Nachdem Keimbildung stattgefunden hat, schreitet der Kondensationsvorgang fort in Form von Wachstumsvorgängen und Koagulation. Beispielsweise in der Atmosphäre wirken verschiedene Arten von Aerosolteilchen als Kondensationskerne und lösen Wolkenbildung und Niederschlag aus.

Eine wichtige technische Anwendung der heterogenen Keimbildung ist der Kondensationskernzähler (CNC). Die Wirkungsweise eines CNC basiert auf heterogener Keimbildung übersättigten Dampfes an Aerosolteilchen und anschließendem Tröpfchenwachstum. Teilchen, die zu klein sind, um mit den meisten anderen Meßmethoden registriert zu werden, wachsen dadurch zu sichtbaren Größen und können mit Hilfe optischer Verfahren gezählt werden. Unter der Voraussetzung, daß jedem wachsenden Tröpfchen genau ein Aerosolteilchen entspricht, ist die gemessene Tröpfchenkonzentration gleich der Aerosol-Teilchenzahlkonzentration. In den meisten CNC's wird die erforderliche Übersättigung durch schnelle Expansion einer nahezu gesättigten Dampf-Gas-Mischung erzielt. Die Anzahlkonzentration der entstehenden Tröpfchen wird entweder durch direkte visuelle Zählung oder durch Messung der Lichtextinktion oder Lichtstreuung bestimmt. Während visuelle Zählung "absolute" Anzahlkonzentrationen liefert, sind die meisten Lichtextinktions- und Lichtstreuverfahren abhängig von empirischer Eichung mittels Eichstandards.

Zur Untersuchung der heterogenen Keimbildung und des Tröpfchenwachstums in übersättigtem Dampf wurde eine prozeßgesteuerte, schnelle Expansionskammer, der Size Analyzing Nuclei Counter SANC, entwickelt. Die experimentelle Anordnung besteht im wesentlichen aus einem Befeuchter,

einer Expansionskammer, Unterdruckrezipienten und Pumpen. Befeuchter und Expansionskammer sind getrennt thermostatisiert, die Verbindungsrohre sind geheizt, um Dampfverluste durch Kondensation zu vermeiden. Der Meßvorgang wird mittels einer elektronischen Steuereinheit in Verbindung mit fünf Magnetventilen gesteuert. Das Kernaerosol strömt zunächst durch den Befeuchter, um eine nahezu gesättigte Dampf-Gas-Mischung zu erzielen, und dann tritt das befeuchtete Aerosol in die Expansionskammer ein. Anschließend wird durch Öffnen eines Magnetventils die Expansionskammer mit einem Unterdruckrezipienten verbunden und damit eine Expansion mit einer Dauer von etwa 5 - 7 ms hervorgerufen. Dadurch wird Dampfübersättigung in der Expansionskammer erzielt und heterogene Keimbildung wird verursacht durch Aerosolteilchen, die als Kondensationskerne wirken. Zur Beobachtung werden die in der Expansionskammer wachsenden Tröpfchen mittels eines He-Ne-Laserstrahls beleuchtet. Der von den wachsenden Tröpfchen gestreute Lichtfluß wird unter einstellbaren Streuwinkeln registriert. Ferner werden der durch die Expansionskammer hindurchtretende Laser-Lichtfluß und der gesamte Gasdruck während der Expansion und des Tröpfchenwachstums registriert. Diese drei Signale werden mittels eines digitalen Transientenrecorders aufgezeichnet. Abhängig vom eingestellten Streuwinkel zeigt der experimentelle Streulichtlichtfluß als Funktion der Zeit Maxima und Minima in ausgezeichneter Übereinstimmung mit dem theoretischen Streulichtfluß als Funktion der Teilchengröße, berechnet gemäß Mie-Theorie. Nach Herstellung einer eindeutigen Zuordnung von experimentellen und theoretischen Streulichtextrema werden deren Lagen und Höhen verglichen. Damit ist eine gleichzeitige und unabhängige quantitative Bestimmung von Tröpfchenradius und Tröpfchenkonzentration zu bestimmten Zeiten während des Wachstumsvorganges möglich. Die bei hohen Tröpfchenkonzentrationen in der Expansionskammer auftretende Lichtextinktion wird berücksichtigt durch Normierung des experimentellen Streulichtflusses relativ zu dem durch die Expansionskammer hindurchtretenden Laser-Lichtfluß. Die Expansionszeit erwies sich als hinreichend kurz im Vergleich zu

den Tröpfchenwachstumszeiten, sodaß der Expansionsvorgang als weitgehend trockenadiabatisch angesehen werden kann. Dementsprechend kann die Übersättigung am Ende der Expansion aus dem Gesamtdruckabfall berechnet werden, der auf Grund des gemessenen zeitlichen Druckverlaufes bestimmt wird.

Die Meßserien werden im allgemeinen mit Computersteuerung durchgeführt. Entsprechend einer vorher festgelegten Reihenfolge werden Streuwinkel und Expansionsverhältnis eingestellt. Die Meßdaten werden zum Computer übertragen und für die anschließende Datenauswertung auf Magnetband gespeichert. Das Datenauswerteprogramm ist für interaktive Bedienung ausgelegt, um eine sichere Identifizierung der experimentellen Streulichtextrema durch den Experimentator zu ermöglichen. In verschiedenen Programmsektionen können Mittelwerte der experimentellen Daten berechnet und eine statistische Auswertung durchgeführt werden. Experimentell ermittelte Tröpfchenwachstumskurven können mit verschiedenen theoretischen Modellen verglichen werden. Ferner können Tröpfchenkonzentrationen ermittelt werden in Abhängigkeit von der eingestellten Übersättigung und dem entsprechenden Kelvin-Äquivalentdurchmesser.

Für eine genaue Berechnung des Streulichtflusses als Funktion der Teilchengröße ist die Kenntnis der Tröpfchengrößenverteilung in der Expansionskammer erforderlich. Mit Hilfe eines Best-Fit-Verfahrens wurde die zeitliche Entwicklung der Tröpfchengrößenverteilung während des Tröpfchenwachstumsvorganges bestimmt. Ein Vergleich experimenteller und theoretischer Streulichtkurven zeigt, daß theoretisch vorhergesagte Partialwellenresonanzen experimentell bestätigt werden können.

Messungen des Tröpfchenwachstums wurden für drei verschiedene Anfangsübersättigungen durchgeführt. Berechnungen auf Grund der Standard-Tröpfchenwachstumstheorie lieferten Wachstumsraten, die bedeutend größer sind als die experimentell gefundenen Werte. Es zeigte sich, daß der gegenseitige Einfluß erster Ordnung von Masse- und Wärme-

fluß in der Umgebung der wachsenden Tröpfchen eine signifikante Verringerung der Tröpfchenwachstumsrate bewirkt. Während Thermodiffusion und der Diffusionsthermoeffekt vernachlässigbar sind, ist insbesondere der Energietransport durch die diffundierenden Dampfmoleküle von Bedeutung. Der gegenseitige Einfluß von Masse- und Wärmefluß wird in der Standard-Tröpfchenwachstumstheorie vernachlässigt. Durch Berücksichtigung dieser Effekte erster Ordnung kann eine signifikante Verbesserung der Übereinstimmung von Theorie und Experiment für niedrige Übersättigungen erreicht werden. Bei hohen Übersättigungen treten jedoch weiterhin starke Abweichungen auf. Diese Tatsache kann auf Grund der Nichtlinearität des Dampfdruckes als Funktion der Temperatur erklärt werden. In der Standard-Tröpfchenwachstumstheorie wird eine linearisierte Beziehung verwendet. Berücksichtigung der korrekten Temperaturabhängigkeit des Dampfdruckes durch numerische Lösung der Energiebilanzgleichung ergibt gute Übereinstimmung zwischen experimentellen und theoretischen Tröpfchenwachstumskurven für Sättigungsverhältnisse zwischen 12o und 354 %, wobei keine willkürliche Anpassung unbestimmter Parameter erforderlich ist. Insbesondere der Masseakkomodationskoeffizient wurde gleich 1 gesetzt. Wesentlich kleinere Werte, wie sie von vielen Autoren vorgeschlagen wurden, konnten für die betrachteten experimentellen Bedingungen ausgeschlossen werden.

Der SANC kann zur Bestimmung von Kelvin-Äquivalentgrößenverteilungen des Kernaerosols verwendet werden. Zu diesem Zweck werden Meßserien durchgeführt mit schrittweise ansteigender Übersättigung und ansonsten unveränderten experimentellen Bedingungen. Dadurch werden zunehmend kleinere Teilchen als Kondensationskerne aktiviert und man erhält kumulative Kelvin-Äquivalentgrößenverteilungen des Kernaerosols. Messungen von Kelvin-Äquivalentgrößenverteilungen wurden für das urbane Aerosol in Wien durchgeführt bei verschiedenen meteorologischen Bedingungen. Ein Mode der differentiellen Anzahl-

größenverteilung wurde für Teilchendurchmesser zwischen o,o1 und o,o2 µm festgestellt. Dieser Mode wird üblicherweise als "Nucleation Mode" bezeichnet. Im Rahmen experimenteller Workshops, durchgeführt in Wien in den Jahren 1979 und 198o, wurden mittels des SANC Kelvin-Äquivalentgrößenverteilungen für wohldefinierte, monodisperse Aerosole mit Teilchendurchmessern zwischen o,o56 und o,oo6 µm gemessen. Die erhaltenen Ergebnisse werden an anderer Stelle publiziert werden.

Abstract

Condensation processes can be observed in a number of practically important systems. In many cases the condensation process is initiated by heterogeneous nucleation on the surface of foreign particles (condensation nuclei). After nucleation has occured, condensation proceeds by growth processes and coagulation. For example in the atmosphere different kinds of aerosol particles act as condensation nuclei initiating cloud formation and precipitation.

An important technological application of heterogeneous nucleation is the Condensation Nuclei Counter (CNC). The operation of a CNC is based on heterogeneous nucleation of supersaturated vapor on aerosol particles and subsequent droplet growth. Thereby particles, which are too small to be detected by most other methods, grow to visible sizes and can be counted by optical techniques. Provided that each growing droplet corresponds to just one aerosol particle, the measured droplet concentration is equal to the aerosol number concentration. In most CNC's the required supersaturation is obtained by a fast expansion of a nearly saturated vapor-gas mixture. The number concentration of the formed droplets is determined either by direct visual counting or by light extinction or light scattering techniques. While visual counting provides "absolute" number concentrations, most light extinction and light scattering techniques depend on empirical calibration by external reference standards.

For investigation of heterogeneous nucleation and droplet growth in supersaturated vapor a process controlled fast expansion chamber, the Size Analyzing Nuclei Counter SANC, was developed. Essentially the experimental apparatus consists of a humidifier, an expansion chamber, subpressure vessels and pumps. Humidifier and expansion chamber are separately thermostated, the connecting tubes are heated in order to avoid losses due to vapor condensation. The measuring process is controlled by an electronic control unit in connection with five

solenoid valves. The nuclei aerosol first passes the humidifier in order to obtain a nearly saturated vapor-gas mixture and then the humidified aerosol enters the expansion chamber. Subsequently an expansion with a duration of approximately 5 - 7 ms is facilitated by opening of a solenoid valve and thus connecting the expansion chamber to a subpressure vessel. Thereby vapor supersaturation is obtained in the expansion chamber and heterogeneous nucleation is caused by aerosol particles, acting as condensation nuclei. For observation, the droplets, growing in the expansion chamber, are illuminated by a He-Ne laser beam. The light flux, scattered by the growing droplets, is monitored under selectable scattering angles. Furthermore the laser light flux, transmitted through the expansion chamber and the total gas pressure are monitored during expansion and droplet growth. These three signals are recorded by a digital transient recorder. Depending on the selected scattering angle, the experimental scattered light flux vs. time curves show series of maxima and minima in excellent agreement with theoretical scattered light flux vs. size curves, calculated by means of Mie theory. After establishing a one-to-one correspondence between experimental and theoretical light scattering extrema, their positions and heights are compared. This allows a simultaneous and independent quantitative determination of droplet radius and droplet concentration at specific times during the growth process. The light extinction, occuring at high droplet concentrations in the expansion chamber, is taken into account by normalizing the experimental scattered light flux relative to the laser light flux, transmitted through the expansion chamber. The expansion time was found to be sufficiently small compared to the droplet growth times, so that the expansion process can be regarded as approximately dry-adiabatic. Accordingly, the supersaturation at the end of the expansion can be calculated from the total pressure drop, as obtained from the experimental pressure vs. time curve.

Measuring series are usually performed under computer control. Scattering angle and expansion ratio are set according to a preselected measuring sequence. The experimental data are transferred to the

computer and stored on magnetic tape for subsequent data evaluation. The data evaluation software is designed for interactive operation in order to allow a safe identification of the experimental light scattering extrema by the experimentalist. In different program sections averages of the experimental data can be calculated and a statistical evaluation performed. Experimentally obtained droplet growth curves can be compared with various theoretical predictions. Furthermore droplet concentrations can be determined as functions of the applied supersaturation and the corresponding Kelvin-equivalent diameter.

For accurate calculation of the theoretical scattered light flux vs. size curves, knowledge of the actual droplet size distribution in the expansion chamber is required. Using a best fit procedure, the time development of the droplet size distribution was determined during the droplet growth process. Comparison of experimental and theoretical light scattering curves shows that theoretically predicted partial wave resonances can be verified experimentally.

Measurements of droplet growth were performed for three different initial supersaturations. Calculations based on standard droplet growth theory resulted in growth rates substantially higher than experimentally observed. It turned out that the first order mutual influence of mass and heat flux in the vicinity of the growing droplets causes a significant reduction of the droplet growth rate. While thermal diffusion and the diffusion-thermo effect are negligible, particularly the energy transport by the diffusing vapor molecules is important. The mutual influence of mass and heat flux is neglected in standard droplet growth theory. By taking these first order effects into account, a significant improvement of the theoretical fit can be achieved for low supersaturations. However, strong deviations still occur at high supersaturations. This fact is explained by the nonlinearity of the vapor pressure vs. temperature curve. In standard

droplet growth theory a linearized relationship is used. Taking into account the correct temperature dependence of the vapor pressure by numerical solution of the energy balance equation, good agreement between experimental and theoretical droplet growth curves is obtained for saturation ratios ranging from 12o to 354 % without arbitrary adjustment of undetermined parameters. Particularly the mass accomodation coefficient was chosen to be unity. Much smaller values, as proposed by many authors, were ruled out for the considered experimental conditions.

The SANC can be used for determination of Kelvin-equivalent size distributionsof the nuclei aerosol. To this end measuring series are performed with stepwise increasing supersaturation and otherwise unchanged experimental conditions. Thereby gradually smaller particles are activated as condensation nuclei and cumulative Kelvin-equivalent size distributions of the nuclei aerosols are obtained. Measurements of Kelvin-equivalent size distributions were performed for the urban aerosol in Vienna at different meteorological conditions. A mode of the differential number size distribution was observed between o,o1 and o,o2 μm diameter. This mode is usually called "Nucleation Mode". During experimental workshops, performed in Vienna 1979 and 198o, Kelvin-equivalent size distributions were measured by means of the SANC for well-defined monodispersed aerosols with particle diameters ranging from o,o56 to o,oo6 μm. The obtained results will be presented elsewhere.

LIST OF FIGURES

page

page

page

page

page

page

page

page

page

Table of Symbols

A_{gv}, A_{vg}	empirical coefficients in the Wassiljewa equation
a	droplet radius
a_M	modal radius of the droplet size distribution
a_v, a_g	specific chemical reaction rates
B	Humidification
b	diameter of the laser beam
C	droplet concentration (number per unit volume)
$\bar{c}$	average absolute velocity of the gas molecules
C_p	molar heat capacity at constant pressure
C_v	molar heat capacity at constant volume
c_L	specific heat capacity of the liquid
c_p	specific heat capacity at constant pressure
c_v	specific heat capacity at constant volume
D	binary diffusion coefficient
D_{ch}	diameter of the expansion chamber
d	diameter of circular stop S_c
$\vec{E}$	complex amplitude of the electric field vector
F_c	cross sectional area of circular stop S_c
F_T, F_M	first order thermal and diffusional correction factors
$\vec{H}$	complex amplitude of the magnetic field vector
h	specific enthalpy
I	total mass flux towards the droplet
I_c	total mass flux in the continuum regime
I_T	total mass flux in the transition regime
i	Van't Hoff-factor of a soluble condensation nucleus
I_o	intensity of the incident light
$i_\perp$, $i_\parallel$	intensity functions
$I_\perp$, $I_\parallel$	intensities of the scattered wave polarized perpendicular or parallel to the plane of observation
I_u	intensity of unpolarized scattered radiation

$\vec{J}$	mass flux density
K_{ext}	extinction cross section
K_{sca}	scattering cross section
K_{abs}	absorption cross section
$Kn = \frac{\lambda}{a}$	Knudsennumber
Kn_T, Kn_M	Knudsennumber with respect to gas or vapor molecules
K	thermal conductivity
k_T	thermal diffusion ratio
L	specific heat of condensation of the liquid, length of the scattering volume
M	molecular weight
m	molecular mass
M_N	molecular weight of a soluble condensation nucleus
m_N	mass of a soluble condensation nucleus
m_D	mass of a droplet
N	molar concentration
n	number of molecules per unit volume
N_d	number of droplets in the volume V
p	pressure
p_s	saturation (equilibrium) vapor pressure
Q	total heat flux towards the droplet
Q_c	total heat flux in the continuum regime
Q_T	total heat flux in the transition regime
Q_{rad}	radiative heat flux
$\vec{q}$	heat flux density
R	universal gas constant
r	distance from the center of the droplet
S	saturation ratio
S_c	circular stop
S_r	rectangular stop

T	absolute temperature
T_B	temperature of the humidifier
T_i	initial temperature before the expansion (chamber temperature)
t	time, distance between S_r and S_c
u_v, u_g	internal energy per unit mass
V	considered volume of the system, occupied by a particular amount of gas and condensate
V_S	scattering volume
$\vec{v}$	average diffusion velocity
w	width of rectangular stop S_r
X	mole fraction

α	Thermal diffusion factor
$\alpha = \frac{2 \pi a}{\lambda}$	Size parameter
α_T, α_M	thermal or mass accomodation coefficient
β	pressure expansion ratio
β_T, β_M	transitional correction factors
Δ_p	total pressure drop during the expansion in the expansion chamber
ε	aperture of the light measuring system
θ	scattering angle
θ_o	scattering angle, at which the light measuring system is centered
κ	adiabatic index
κ_{pol}	polytropic index
λ	mean free path, light wavelength
μ	exponent describing the temperature dependence of D
μ_g, μ_v	mass of gas or vapor in the volume V
Π	polytropic factor
Π_e, Π_m	Debye potentials
ρ	mass concentration
σ	breadth parameter of the droplet size distribution
σ_{LV}	surface tension at the liquid-vapor interface
Φ_o	primary light flux (power) of the laser beam
Φ_{sca}	scattered light flux
Φ_{trans}	transmitted light flux
ω	angular frequency of the incident light

Subscripts

g	gas
L	liquid
v	vapor
a	at the droplet surface
∞	at a large distance from the droplet
i	initial value before the expansion
o	value at the end of the expansion

1) INTRODUCTION

Phase transitions are frequently observed in various physical systems. The formation process of a new phase can usually be divided into three steps. First, a small amount of the new phase is formed spontaneously (nucleation). Secondly, an increasing amount of the new phase accumulates around the initially formed nuclei (growth). Finally, the growing aggregates (droplets, crystallites, etc.) coagulate to form a bulk amount of the new phase (coagulation). Depending on the actual physical situation, two or even all three of these processes can occur simultaneously.

Nucleation can take place in a homogeneous bulk phase by statistical formation of clusters of the new phase (homogeneous nucleation). However, the energy of cluster formation is comparatively high in most cases. Accordingly, an appreciable homogeneous nucleation rate can only be expected at high supersaturations. In the presence of discontinuities in the bulk phase (walls enclosing the considered system, condensation nuclei, etc.), the energy of cluster formation is significantly reduced in most cases. Accordingly, the new phase preferably forms at the surface of these discontinuities at comparatively low supersaturations (heterogeneous nucleation). Many practically important systems contain discontinuities and in these systems phase transitions are generally initiated by heterogeneous nucleation. An important example is the atmosphere, where different kinds of natural and anthropogenic aerosol particles act as condensation and ice nuclei thereby initiating cloud formation and precipitation (Coulier, 1875).

Among a number of technological applications of heterogeneous nucleation, the Condensation Nuclei Counter (CNC), invented by Aitken (189o/91), is of considerable practical importance. The operation of a CNC is based on heterogeneous nucleation of supersaturated vapor on aerosol particles and subsequent droplet growth. Assuming that each growing

droplet corresponds to just one aerosol particle, the measured droplet concentration is equal to the aerosol number concentration. It is an important feature of CNC's that particles, which are too small to be detected by most other experimental techniques, can still be activated as condensation nuclei and thus counted.

In most CNC's the supersaturated vapor is obtained by fast expansion of a nearly saturated vapor-gas mixture in an expansion chamber. The number concentration of the growing droplets can be measured using various experimental techniques. Some CNC's require direct visual counting of the droplets, in other instruments light extinction or light scattering by the growing droplets is used as a measure for the droplet number concentration. Most instruments require an empirical calibration, only a few "absolute" CNC's are available.

Obviously the operation of CNC's is determined by heterogeneous nucleation and droplet growth in supersaturated vapors. Furthermore the light scattering properties of growing droplets are important. In section 2 of this report the theory of droplet growth is reviewed and some extensions of the usually applied theory are described. In section 3 the calculation of thermodynamic parameters in an expansion chamber is described. Section 4 contains a review of the theory of light scattering by spherical particles, as far as it is important for the present investigations.

In order to perform experimental investigations of heterogeneous nucleation and droplet growth, a process controlled expansion chamber, the Size Analyzing Nuclei Counter SANC, was developed in this laboratory. A view of the experimental apparatus is shown below. By means of the SANC time resolved light scattering measurements were performed during the droplet growth process in the expansion chamber. The obtained light scattering curves allow quantitative and independent determinations of droplet radius and number concentration at specific times during

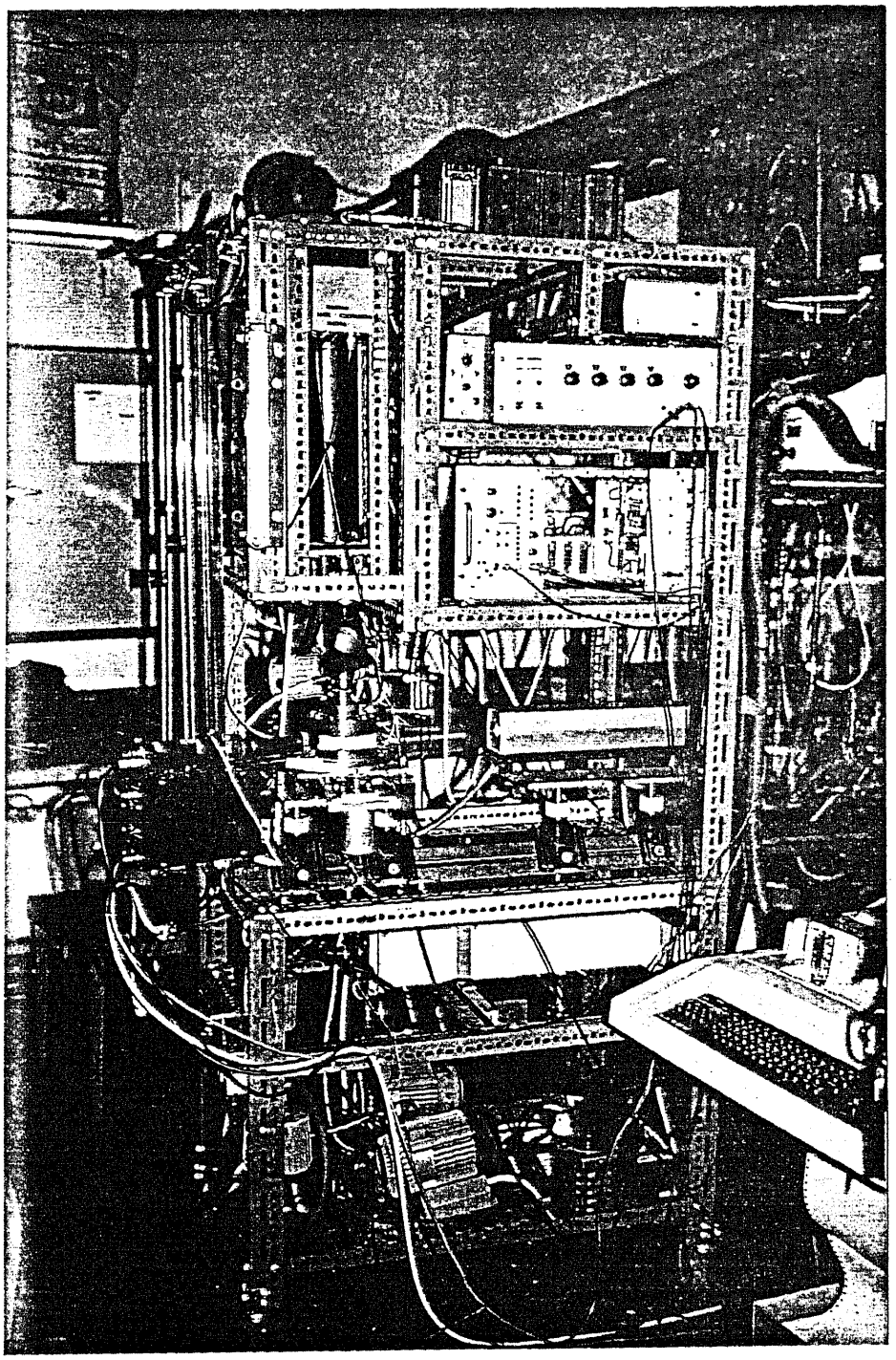

View of the experimental apparatus

2) THEORY OF DROPLET GROWTH AND EVAPORATION

The theory of droplet growth and evaporation has been investigated by many authors and reviewed e.g. by Fuchs (1959) and Sedunov (1974). Here a review of the theory is given as far as it is important for the present investigations. Extensions of the usually applied theory are described.

Droplet growth calculations were performed, which are based on the full, first order phenomenological equations for mass and heat transport. The influence of the interactions of heat and mass flux on the droplet growth process was determined quantitatively. Different expressions were used to take transitional effects into account. Furthermore the mutual influence of the growing droplets was taken into account. Theoretical growth curves were obtained by means of numerical methods. A comparison of the numerical results with experimentally determined droplet growth curves was performed.

2.1 Statement of the problem

A system, consisting of essentially two different chemical components is considered, in which no chemical reactions take place. One component is the carrier gas, which is assumed to be an ideal gas. The other component, the condensate, occurs in both the gaseous (vapor) and the liquid state (droplets). The droplets may be dilute solutions of additional chemical components. The vapor concentration is sufficiently small compared to the concentration of the carrier gas so that the vapor can be considered approximately as an ideal gas. The total pressure in the system is constant and uniform. The droplets are spherical and randomly located. The droplet aerosol is monodispersed.A typical system dimension is assumed to be large compared to the droplet radius. The droplet concentration is sufficiently small, so that the average distance of

two neighboring droplets is large compared to the droplet radius. The influence of external forces on vapor diffusion and heat conduction is assumed to be negligible. The fluxes of vapor and heat across the system borders are assumed to be very small. The validity of the above assumptions depends on the experimental conditions and will be discussed later.

Furthermore the movement of the droplets relative to the carrier gas is assumed to be sufficiently slow, so that the influence of the convective mass and heat transfer to the droplets can be disregarded. Fuchs (1934) considered small droplet velocities, where the mass transport due to convection is small compared to the diffusive transport. In this case it is found that an increase of the vapor flux on one side of the droplet is compensated by a decrease of the vapor flux on the other side. Accordingly at low Reynolds numbers no influence of the droplet movement on the growth rate is expected. From theoretical considerations Frössling (1938) obtained the general form of a correction factor for the mass flux to a ventilated drop. Frössling performed experiments with suspended drops in a wind channel and showed the validity of this correction factor in a range of Reynoldsnumbers between 2 and 8oo. These results were applied by Squires (1952) to calculate the influence of ventilation on the growth rate of cloud droplets, falling with terminal velocity. The numerical results of Squires show that for freely falling cloud droplets with a radius less than 1o µm, the deviations from the theory for droplets at rest are smaller than 1 % of the droplet radius. The above mentioned calculations are restricted to droplets in the continuum regime. Brock (1967 b) considered the evaporation of a moving droplet in the transition and free molecule regimes. From the above mentioned results it can be concluded that the effect of ventilation due to gravitational settling of the droplets is negligible, if the droplet radius is assumed to be less than 1o µm.

Finally the droplet growth or evaporation process is assumed to be quasistationary. Accordingly it is assumed that the vapor concentration and temperature profiles always correspond to steady state solutions and changes during the growth process are determined only by the changing boundary conditions. The range of applicability of the quasi steady state assumption has been investigated by a number of authors. Most studies of non-stationary growth and evaporation are restricted to the continuum regime. Luchak and Langstroth (1950) considered the evaporation of a droplet, situated in the center of a spherical enclosure, whose surface maintains zero vapor concentration. The non-stationary diffusion equation was solved by a method of successive approximation. It was found that the nonstationary correction for the mass flux is less than 1 % for water at 20°C. However, the radius of the enclosure must not exceed the droplet radius by more than a factor of about 1700. The heat flux to the droplet was neglected. Frisch and Collins (1953) solved the nonstationary diffusion equation for a single droplet located in an infinite region with initially constant vapor concentration. After an initial growth period the well known quadratic growth law is obtained. A size dependent accomodation coefficient is considered. The effect of the moving boundary on the droplet growth process was taken into account by Kirkaldy (1958) by introducing a convection term in the phenomenological equation for the mass flux, whose time dependence was chosen as a trial. The resulting vapor concentration field agrees with the quasi steady state solution. However, Kirkaldy concludes that this agreement is caused by a "lucky combination of compounded errors". Carstens and Zung (1970 a) solved the nonstationary equations for simultaneous mass and heat transport in the continuum regime. The growing droplet is surrounded by an impermeable sphere. The nonstationary solutions show slightly higher gradients of vapor concentration and temperature than in the case of quasi steady state. However, after an initial growth period of about 10^{-4} sec the quasi steady state solution is reached. Chang and Davis (1974) solved

the nonstationary continuum equations taking into account the nonuniform temperature field inside the droplet. It is found that droplet evaporation can be approximated by quasi steady state equations except for a short initial period. Nix and Fukuta (1973) used time dependent source functions in the nonsteady state continuum equations for mass and heat transfer. Accordingly, changes of the environmental conditions during the growth process, as occuring for example during the expansion period in an expansion cloud chamber, can be taken into account. It is found that the nonsteady state droplet growth "overshoots" the quasi steady state conditions during the initial stages of condensation. The relative error R_m for the growth rate caused by the use of quasisteady state equations, is proportional to the droplet radius. Furthermore R_m decreases with an increasing time constant for the environmental changes (e.g. expansion time) and with increasing growth time. For the experimental conditions of the present investigations, as described later, a maximum error of about 1 % is predicted. A condition for the applicability of quasi steady state solutions has been given by Twomey (1977), p. 71. Twomey assumes that a steady state vapor concentration field has developed around a droplet. At a particular time the droplet radius is abruptly increased by a certain amount ξ . Calculation of the corresponding nonsteady state flux shows that quasi steady state is a good approximation, if ξ is sufficiently small. This translates into the condition that the vapor density must be much smaller than the liquid density, which is fulfilled in most practical cases. The above mentioned nonsteady state calculations were based on continuum equations. Brock (1967 a) investigated the case of non continuum nonsteady state transfer. His results indicate that "a quasistationary assumption is valid in general for aerosol collisions and molecular transfer". Although most theoretical treatments show that the quasistationary theory of droplet growth provides a good approximation, the actual validity of the quasisteady state equations can only be checked by comparison with experimental data.

As a consequence of the assumed quasistationarity, the temperature profiles inside the droplets are flat and no heat fluxes into the droplets occur. Accordingly, the influence of the heat capacity of the droplets on the growth or evaporation process is not taken into account.

Without introducing further restrictions, the mass flux to the droplets can only be calculated by means of numerical computation. Then a numerical integration of the calculated mass flux is necessary in order to obtain the droplet radius as a function of time. A considerable simplification of the calculations can be achieved by assuming that the temperature in the system is nearly uniform, i.e. the temperature profiles are very flat. In this case the temperature of the droplets is nearly equal to the gas temperature at a large distance from the droplets. This condition will be fulfilled approximately for very slow processes and for condensates with small specific latent heat of condensation. With the above restriction it is possible to use a linear expression as an approximation for the vapor pressure vs temperature function. Furthermore a number of parameters, e.g. diffusion coefficient, coefficient of thermal conductivity, specific latent heat of condensation, etc., can be taken as constant and uniform. In this case the mass flux to the droplets can be expressed in analytical form. However, a numerical integration of the mass flux is still necessary to obtain the droplet radius as a function of time.

A further simplification can be obtained by the additional assumption that the droplets are in the continuum regime and that the droplet concentration is sufficiently small, so that the mutual interactions of the droplets can be neglected. In this case the analytical expression for the mass flux can be integrated and the well known quadratic growth law is obtained.

2.2 Quasistationary fluxes to a single droplet in the Continuum Regime

Growth and evaporation of liquid droplets are determined by the nonstationary fluxes of vapor and heat to the droplets. These fluxes can only be calculated under certain simplifying assumptions. In connection with the theory of the wet bulb thermometer Maxwell (1877) was the first to calculate the fluxes of vapor and heat to a single sphere. These fluxes were obtained by solving the stationary equations for diffusion and heat conduction, thereby assuming stationary transport of mass and energy under diffusion control. Accordingly, the obtained expressions are restricted to spheres, whose radii are large compared to the mean free path of the surrounding gas (continuum regime). Based on Maxwell's results Fuchs (1934) derived an approximate stationary droplet growth equation taking into account the effect of the latent heat of condensation. Mason (1971) obtained a somewhat better approximation and took into account the effect of curvature and solution concentration on the vapor pressure at the droplet surface.

For the following calculations it will be assumed that the droplet radius is large compared to the mean free path in the surrounding gas (continuum regime). Later this assumption will be eliminated and appropriate corrections to the continuum expressions will be applied.

2.2.1 Conservation laws

From the conservation of mass in the binary mixture of carrier gas and vapor, the continuity equation

$$\frac{\partial \rho}{\partial t} + \operatorname{div} \vec{j} = 0 \qquad (2.1)$$

can be obtained, where $\rho = \rho_v + \rho_g$ designates the total mass concentration of the binary mixture, $\vec{j}$ is the total mass flux

density and t the time. ρ_v and ρ_g are the partial densities of the vapor and the carrier gas, respectively. Because of the assumed quasi steady state, ρ will not be explicitly time dependent and equ. (2.1) reduces to

$$\operatorname{div} \vec{j} = 0 \ . \tag{2.2}$$

The conservation of energy in the binary mixture yields the continuity equation

$$\frac{\partial}{\partial t} (\rho_v u_v + \rho_g u_g) + \operatorname{div} \vec{q} = 0, \tag{2.3}$$

where u_v, u_g designate the internal energies of vapor and gas per unit mass, respectively, and $\vec{q}$ is the heat (energy) flux density. The internal energies can be expressed as

$$\begin{aligned} u_v &= a_v \ . \ t + c_{v,v} \ . \ T \ , \\ u_g &= a_g \ . \ t + c_{v,g} \ . \ T \ , \end{aligned} \tag{2.4}$$

where a_v, a_g are specific chemical reaction rates, $c_{v,v}$, $c_{v,g}$ are specific heat capacities at constant volume, and T is the absolute temperature. Inserting equ. (2.4) into equ. (2.3) and assuming that ρ_v, ρ_g, a_v, a_g are constant, the equation

$$(\rho_v . c_{v,v} + \rho_g . c_{v,g}) \frac{\partial T}{\partial t} + \operatorname{div} \vec{q} = - \rho_v a_v - \rho_g a_g \tag{2.5}$$

is obtained. It can be seen that the chemical reactions cause a source (sink) term in the continuity equation. In the present investigation no chemical reactions are considered. Accordingly equ. (2.5) reduces to

$$(\rho_v . c_{v,v} + \rho_g . c_{v,g}) \frac{\partial T}{\partial t} + \operatorname{div} \vec{q} = 0. \tag{2.6}$$

For the assumed quasi steady state, equ. (2.6) further reduces to

$$\text{div } \vec{q} = 0. \qquad (2.7)$$

2.2.2 Phenomenological equations

The conservation laws are not sufficient for a determination of the density and temperature profiles. In addition, relations between mass concentration and mass flux density on the one hand and between temperature and heat flux density on the other hand are required. It has been found that these relations are linear to a high degree of approximation. Accordingly, linear phenomenological expressions are chosen with empirical coefficients. Fortunately, in the case of dilute gases these phenomenological equations can be rigorously derived by solution of the Boltzmann transport equation. For the present calculations, the first order phenomenological equations, obtained by means of Enskog's perturbation technique (Hirschfelder, et al., 1954, Chapman and Cowling, 197o) are used.

It should be mentioned that the first order phenomenological equation for mass transport has been derived by Fürth (1942) using an elementary theory. By means of the first order phenomenological equations the mutual interactions of mass and heat flux (e.g. thermal diffusion) can be taken into account, whereas usually mass and heat flux to the droplets are calculated independently in the theory of droplet growth. Furthermore the usual restriction to very low vapor concentrations can be eliminated.

Stefan (1874, 1881) was the first to present a phenomenological equation for mass transport which is somewhat more rigorous than Fick's law. For the validity of Stefan's equation a restriction to small vapor concentrations is not required. However, Stefan's

equation only applies in the absence of thermal gradients. The solutions, obtained by means of Stefan's equation, include a description of the additional mass flux from an evaporating surface, caused by the center-of-mass motion of the air-vapor mixture relative to the surface. The effect of this Stefan flow on droplet growth and evaporation is small if the vapor concentration is small compared to the gas concentration. Volkov and Golovin (197o) give a description of nonsteady state effects for droplet evaporation, based on the full, first order phenomenological equations.

The first order phenomenological equation for the mass transport in a binary mixture in the absence of external forces and pressure gradients is usually given in the form

$$\vec{v}_V - \vec{v}_g = - \frac{D}{X_V X_g} \left(\text{grad } X_V + \frac{k_T}{T} \text{ grad } T \right), \qquad (2.8)$$

where $\vec{v}_V$, $\vec{v}_g$ are the average diffusion velocities of vapor and gas, respectively. $X_V = N_V/N$ and $X_g = N_g/N$ are the mole fractions of vapor and gas, respectively. $N = N_V + N_g = \rho/M$ is the total molar concentration of the binary mixture. $N_V = \rho_V/M_V$ and $N_g = \rho_g/M_g$ are the molar concentrations of vapor and gas, respectively. M_V, M_g, and M are the molecular weights of vapor, gas, and the binary mixture, respectively. Because vapor and gas are assumed to be ideal gases, the mole fractions can be expressed as $X_V = p_V/p_o$, and $X_g = p_g/p_o$, where $p_o = p_V + p_g$ is the total pressure of the binary mixture and p_V, p_g are the partial pressures of vapor and gas, respectively.

From equ. (2.8) it can be seen that an exchange of vapor and gas does not affect the binary diffusion coefficient D, while the thermal diffusion ratio k_T will change sign. If in equ. (2.8) $k_T > 0$, the diffusion of vapor towards the cooler region and the diffusion of gas towards the warmer region will be enhanced.

The theoretical expression for the binary diffusion coefficient D, as obtained from the rigorous kinetic theory of gases, shows that D is independent from the composition of the binary mixture to a high degree of approximation (Hirschfelder et al., 1954). Only higher order corrections are dependent on the composition. Accordingly, because of the assumed small vapor concentration, D can be considered as independent from the mole fractions of vapor and gas. The dependence of D on temperature T and total pressure p_o can be expressed approximately as

$$D(T,p_o) = D_N \left(\frac{T}{T_N} \right)^{\mu} \frac{p_N}{p_o} , \qquad (2.9)$$

where D_N is the binary diffusion coefficient at temperature T_N and pressure p_N, and $1{,}6 < \mu < 2$ in most cases.

The dependence of k_T on the mole fractions is approximately given by

$$k_T = \alpha . X_v X_g , \qquad (2.10)$$

where the absolute value of the thermal diffusion factor α is usually less than o,6 .

Because of the assumptions that vapor and gas are ideal and that the gradient of the total pressure can be neglected, equ. (2,8) can be transformed into

$$\vec{v}_v - \vec{v}_g = - \frac{\rho}{\rho_v \rho_g} D^{(v)} \left(\text{grad } \rho_v + \frac{\rho_v + \rho . k_T^{(v)}}{T} \text{ grad } T \right), \qquad (2.11)$$

where a modified binary diffusion coefficient $D^{(v)}$ and a modified thermal diffusion ratio $k_T^{(v)}$ are defined as

$$D^{(v)} \equiv \frac{1}{\rho}\left(\rho_g + \frac{M_g}{M_v}\rho_v\right).D = \frac{M_g}{M} \cdot D \quad , \qquad (2.12 - 1)$$

$$k_T^{(v)} \equiv \frac{1}{\rho}\left(\rho_v + \frac{M_v}{M_g}\rho_g\right) \cdot k_T = \frac{M_v}{M} \cdot k_T \quad . \qquad (2.12 - 2)$$

Because of the assumed low vapor concentration, the modified coefficients $D^{(v)}$, $k_T^{(v)}$ can be approximately expressed as

$$D^{(v)} \cong D \quad , \qquad (2.13 -1)$$

$$k_T^{(v)} \cong \frac{M_v}{M_g} \cdot k_T \quad . \qquad (2.13 -2)$$

A further transformation of the phenomenological equation can be achieved by introduction of the mass average velocity $\vec{v} = (\rho_v \vec{v}_v + \rho_g \vec{v}_g)/\rho$. It can be verified easily that the mass flux density $\vec{j}_v = \rho_v \vec{v}_v$ of the vapor can be expressed as

$$\vec{j}_v = \frac{\rho_v \rho_g}{\rho}(\vec{v}_v - \vec{v}_g) + \rho_v \vec{v} \quad . \qquad (2.14)$$

By inserting equ. (2.11) into equ. (2.14), the first order phenomenological equation

$$\vec{j}_v = - D^{(v)}\left(\text{grad } \rho_v + \frac{\rho_v + \rho k_T^{(v)}}{T} \text{ grad } T\right) + \rho_v.\vec{v} \qquad (2.15)$$

for the mass flux density of the vapor can be obtained.

The first term of equ. (2.15),

$$- D^{(v)} \text{ grad } \rho_v \quad ,$$

describes the mass flux of the vapor due to the vapor density gradient.

The second term of equ. (2.15),

$$-D^{(v)} \cdot \frac{\rho_v}{T} \text{ grad } T,$$

is caused by the fact that, according to equ. (2.8), the driving force for the mass flux is the gradient of the mole fraction X_v, not the gradient of the partial density ρ_v. For the case of a binary mixture of ideal gases at uniform total pressure p_o, it can be seen easily that grad X_v is proportional to grad p_v, but not proportional to grad ρ_v.grad X_v will be proportional to grad ρ_v only in the case of uniform temperature. In this case the above mentioned term vanishes.

The third term of equ. (2.15),

$$-D^{(v)} \cdot \frac{\rho . k_T^{(v)}}{T} \text{ grad } T \quad ,$$

describes the effect of thermal diffusion (Soret-effect).

The fourth term of equ. (2.15),

$$\rho_v . \vec{v} \quad ,$$

describes the mass flux of the vapor, caused by the mass average (convective) velocity $\vec{v}$ relative to the observer. This flux is often called Stefan flow.

For the case, where temperature gradients and the mass average velocity are negligible, equ. (2.15) reduces to the well-known zeroth order phenomenological equation

$$\vec{j}_v = - D^{(v)} \text{ grad } \rho_v, \qquad (2.16)$$

which is known as Fick's law of diffusion. In this case the above mentioned first order effects can be disregarded.

The first order phenomenological equation for the heat (energy) transport in a binary mixture is given in the form

$$\vec{q} = - K \text{ grad } T + \frac{\rho RT}{M} k_T(\vec{v}_v - \vec{v}_g) + \rho_v h_v \vec{v}_v + \rho_g h_g \vec{v}_g, \quad (2.17)$$

where h_v and h_g are the specific enthalpies of vapor and gas, respectively, and R is the universal gas constant.

The coefficient of thermal conductivity K of the binary mixture of vapor and gas depends on the temperature and the mole fractions (Reid and Sherwood, 1966). Based on kinetic theory, Wassiljewa (19o4) proposed an approximate expression of the form

$$K(T, X_v/X_g) = \frac{K_v(T)}{1 + A_{vg} X_g/X_v} + \frac{K_g(T)}{1 + A_{gv} X_v/X_g} . \quad (2.18)$$

The temperature dependence of the thermal conductivities K_v, K_g of vapor and gas can be approximated for a limited temperature range by the linear expressions

$$K_v(T) = K_v^{(o)} + K_v^{(1)}.T \quad , \quad (2.19 - 1)$$

$$K_g(T) = K_g^{(o)} + K_g^{(1)}.T \quad , \quad (2.19 - 2)$$

where $K_v^{(o)}$, $K_v^{(1)}$, $K_g^{(o)}$, $K_g^{(1)}$ are empirical coefficients. The parameters A_{vg} and A_{gv} are nearly independent from temperature and can be obtained from the semiempirical theory of Lindsay and Bromley (195o)

$$A_{vg} = \frac{1}{4}\{1 + [\frac{\eta_v}{\eta_g}\ (\frac{M_g}{M_v})^{3/4} \cdot \frac{1 + S_v/T}{1 + S_g/T}]^{1/2}\}^2$$

$$\cdot \frac{1 + S_{vg}/T}{1 + S_v/T}\ , \qquad (2.2o - 1)$$

A_{gv} analogous,

where

$$\frac{\eta_v}{\eta_g} = \frac{K_v M_v}{K_g M_g} \cdot \frac{C_{p,g} + (5/4)R}{C_{p,v} + (5/4)R}\ , \qquad (2.2o - 2)$$

$$S_v = \frac{3}{2} \cdot T_{b,v}\ , \qquad (2.2o - 3)$$

$$S_g = \frac{3}{2} \cdot T_{b,g}\ , \qquad (2.2o - 4)$$

$$S_{vg} = S_{gv} = \begin{cases} \sqrt{S_v S_g}, & \text{if both gases nonpolar,} \\ 0{,}733 \cdot \sqrt{S_v S_g}, & \text{if one gas strongly polar.} \end{cases} \qquad (2.2o - 5)$$

$C_{p,v}$, $C_{p,g}$ are the molar heat capacities at constant pressure and $T_{b,v}$, $T_{b,g}$ are the normal boiling temperatures of vapor and gas, respectively.

The specific enthalpies h_v and h_g can be calculated by means of the expressions

$$h_v(T) = \int_0^T c_{p,v}\, dT'\ , \qquad (2.21 - 1)$$

$$h_g(T) = \int_0^T c_{p,g}\, dT'\ , \qquad (2.21 - 2)$$

where $c_{p,v}$ and $c_{p,g}$ are the specific heat capacities at constant pressure of vapor and gas, respectively. Sometimes h_v and h_g are given in the form

$$h_v(T) = \gamma_v(T).T, \qquad (2.22 - 1)$$

$$h_g(T) = \gamma_g(T).T, \qquad (2.22 - 2)$$

where γ_v and γ_g are slightly smaller than $c_{p,v}$ and $c_{p,g}$. γ_v and γ_g are slowly varying with temperature, actual values for different gases are tabulated as functions of temperature.

The first term of equ. (2.17),

$$-K.\text{grad } T,$$

describes the heat flux due to the temperature gradient.

The second term of equ. (2.17),

$$\frac{\rho RT}{M} k_T (\vec{v}_v - \vec{v}_g),$$

describes the diffusion thermal effect (Dufour - effect). This effect is reciprocal to the effect of thermal diffusion (Soret - effect). As a consequence of Onsager's symmetry theorem, the Dufour-effect and the reciprocal Soret-effect are determined by the same coefficient k_T.

The third term of equ. (2.17),

$$\rho_v h_v \vec{v}_v + \rho_g h_g \vec{v}_g \quad ,$$

describes the heat flux, caused by the energy, which is carried with the diffusing vapor and gas molecules.

For the case, where the average diffusion velocities are negligible, equ. (2.17) reduces to the well-known zeroth order phenomenological equation

$$\vec{q} = - K.\text{grad } T, \tag{2.23}$$

which is known as Fourier's law of heat conduction. In this case the above mentioned first order effects can be disregarded.

Fick's law (2.16) and Fourier's law (2.23) are usually applied in the theory of droplet growth. However, Fourier's law of heat conduction only applies in the absence of diffusive mass transport. Furthermore, Fick's law of diffusion is valid only in isothermal gas mixtures, whereas considerable temperature gradients will occur in the neighborhood of growing droplets. Accordingly it can be expected that Fick's and Fourier's law will not yield an accurate theoretical description of droplet growth, particularly for liquids with high specific latent heat, e.g. water. Based on the first order phenomenological equation for mass transport, Sedunov (1974) concludes that the error caused by the use of Fick's law is negligible for growth processes under atmospheric conditions. This point will be discussed later.

2.2.3 Integration of the fundamental equations

The continuity equations combined with the phenomenological equations, can be solved and vapor concentration and temperature profiles can be obtained, which satisfy the boundary conditions at the droplet surface and at infinity.

Because of the assumed quasi steady state, the continuity equations corresponding to the conservation of mass, equ. (2.2), and energy, equ. (2.7), are of the general form

$$\operatorname{div} \vec{f} = 0, \tag{2.24}$$

where $\vec{f}$ stands for the mass or the heat flux density.

As will be shown below, the first order phenomenological equations for the mass and heat transport can be brought into the general form

$$\vec{f} = - \delta . \operatorname{grad} \psi \ , \tag{2.25}$$

where ψ stands for the mass concentration or the temperature. It will be shown that the coefficient δ is weakly dependent on ψ . This dependence can be expressed approximately as

$$\delta = \delta_0 \ (1 + \varepsilon . \psi), \tag{2.26}$$

where δ_0 and ε are constants and $(\varepsilon . \psi)^2 << 1$.

The boundary conditions at the droplet surface and at infinity are

$$\psi \ (r = a) = \psi_a, \tag{2.27 - 1}$$

$$\psi \ (r = \infty) = \psi_\infty, \tag{2.27 - 2}$$

where r is the distance from the droplet center and a is the droplet radius.

The solution of equ. (2.24), (2.25), (2.26) and (2.27) is approximately given by

$$\psi(r) = \frac{1}{\varepsilon} \left[1 - (1 - \varepsilon . \psi_a)^{a/r} . (1 - \varepsilon \ \psi_\infty)^{1-a/r} \right]. \tag{2.28}$$

By means of a series expansion of equ. (2.28), the zeroth order approximation

$$\psi(r) = \psi_\infty + (\psi_a - \psi_\infty)\cdot\frac{a}{r} \qquad (2.29)$$

can be obtained. Equ. (2.29) corresponds to the well known hyperbolic profiles, which are usually considered in droplet growth theory.

From the first order profile, equ. (2.28), the corresponding flux through the droplet surface can be obtained by means of the phenomenological equation (2.25). By inserting equ. (2.26) and (2.28) into equ. (2.25), the flux density at the droplet surface can be calculated. Integration over the droplet surface yields the total flux towards the droplet surface

$$F = \frac{4\pi a \delta_o}{\varepsilon}\left[\ln(1-\varepsilon\psi_a) - \ln(1-\varepsilon\psi_\infty)\right] . \qquad (2.3o)$$

Expanding as a logarithmic series and retaining the first two terms results in

$$F = 4\pi\, a\, \delta_o \left(1+\varepsilon\frac{\psi_\infty + \psi_a}{2}\right)(\psi_\infty - \psi_a) \quad . \qquad (2.31)$$

Finally, using equ. (2.26), the first order total flux towards the droplet surface can be written as

$$F = 4\pi a \frac{\delta(\psi=\psi_\infty) + \delta(\psi=\psi_a)}{2}(\psi_\infty - \psi_a) \; . \qquad (2.32)$$

For the case, where the dependence of δ on ψ can be neglected, the arithmetic mean in equ. (2.32) can be replaced by δ and the zeroth order approximation

$$F = 4\pi a\, \delta\, (\psi_\infty - \psi_a) \qquad (2.33)$$

can be obtained, which is usually applied in the theory of droplet growth.

2.2.4 Heat flux Q_c in the continuum regime

In the phenomenological equation (2.17) for heat transfer, the average diffusion velocities can be calculated by means of the phenomenological equations (2.11), (2.15) for mass transfer. Taking into account that in the present case $\vec{v}_g = o$, inserting $D^{(v)}$, $k_T^{(v)}$, and k_T according to equ. (2.13-1), (2.13-2) and (2.1o), respectively, and neglecting higher order terms, the expression

$$\vec{q} = - K \operatorname{grad} T - D \left(\operatorname{grad} \rho_v + \frac{\rho_v}{T} (1 + \alpha) \operatorname{grad} T\right) \cdot \left(\frac{RT}{M_v} \alpha + h_v\right) \qquad (2.34)$$

can be obtained, where α is the thermal diffusion factor.

It can be seen that the heat flux density $\vec{q}$ depends on the temperature gradient as well as on the vapor concentration gradient. In order to separate the problem, a relation between the gradients of temperature and vapor concentration is required. This relation can be obtained from the heat balance at the droplet surface

$$\frac{4\pi}{3} \rho_L a^3 c_L \frac{d T_a}{dt} = Q + L I , \qquad (2.35)$$

where Q and I are the total fluxes of heat and mass, directed towards the droplet, respectively. ρ_L, c_L and L are the density, specific heat capacity and specific heat of condensation of the liquid, respectively. The temperature dependence of L can be approximated for a limited temperature range by the linear expression

$$L(T) = L^{(o)} + L^{(1)} \cdot T,$$

where $L^{(o)}$, $L^{(1)}$ are empirical coefficients. T_a is the temperature at the droplet surface. Because of the assumed quasi steady state, T_a is not explicitly time dependent, i.e., $dT_a/dt = 0$. Accordingly, no heat fluxes into the droplet are considered and the influence of the heat capacity of the droplet is not taken into account. In this case equ. (2.35) yields the balance equation

$$Q + L\, I = 0 \,. \tag{2.36}$$

From this equation a corresponding relation

$$\vec{q} + L\, \vec{J}_V = 0 \tag{2.37}$$

between the flux densities can be derived. By inserting the zeroth order phenomenological equations (2.16) and (2.23), the relation

$$K \operatorname{grad} T + L \,.\, D \operatorname{grad} \rho_V = 0 \tag{2.38}$$

between the gradients of T and ρ_V is obtained.

By means of equ. (2.38), equ. (2.34) can be transformed into

$$\vec{q} = - K F_T \,.\, \operatorname{grad} T \,, \tag{2.39}$$

where the thermal correction factor F_T is given by

$$F_T \equiv 1 - \left(\frac{1}{L} - \frac{D\rho_V}{KT} (1 + \alpha) \right) \left(\frac{RT}{M_V} \alpha + h_V \right). \tag{2.4o}$$

The first correction term in F_T,

$$\left(\frac{1}{L} - \frac{D\rho_V}{KT} (1 + \alpha) \right) \frac{RT}{M_V} \alpha \,,$$

describes the influence of the diffusion thermo effect on the heat transfer. This correction term includes one expression proportional α^2, which can usually be neglected.

The second correction term in F_F,

$$\left(\frac{1}{L} - \frac{D\rho_v}{KT} (1 + \alpha) \right) h_v,$$

corresponds to the heat flux, caused by the energy, which is carried with the diffusing vapor molecules. It can be seen that this correction term depends on the thermal diffusion factor α . This is explained by the fact that the heat flux, carried by the diffusing vapor molecules, depends on the diffusive flux of the vapor, and that this mass flux is, in turn, influenced by the thermal diffusion effect.

For atmospheric conditions (air-watervapor-mixture, $T = 20^{o}C$, $p_o = 760$ Torr, $p_v = 15$ Torr), the first correction term in F_T amounts to $0{,}049\ \alpha$, the second correction term has the numerical value $0{,}194 - 0{,}027\ \alpha$.

Unfortunately, reliable experimental values for α are not available. As mentioned above, usually $|\alpha| < 0{,}6$ is assumed. Based on experimental data from Whalley (1951) and theoretical investigations by Mason and Monchick (1965), Katz and Mirabel (1975) conclude that α is "probably equal to 0,01" for the mixture of water vapor and air.

From the above mentioned numerical values it can be seen that the diffusion thermal effect influences the heat flux by only a few percents or even less, depending on the choice of α . Furthermore it is partly compensated by the second correction term. However, the heat, carried by the diffusing vapor molecules, causes a reduction of the heat flux by nearly 20 %.

In the equations, which are usually applied in droplet growth theory, the above mentioned corrections are not included.

The phenomenological equation (2.39) is of the general form (2.25). Accordingly, the solutions of section 2.2.3) can be used. The zeroth order temperature profile is given by (equ.(2.29))

$$T(r) = T_\infty + (T_a - T_\infty) \cdot \frac{a}{r} \quad , \tag{2.41}$$

where T_a and T_∞ are the temperatures at the droplet surface and at infinity, respectively. The first order total continuum heat flux towards the droplet surface can be expressed as (equ.(2.32))

$$Q_c = 2\pi\, a\, (K_\infty F_{T,\infty} + K_a F_{T,a})\, (T_\infty - T_a) \quad , \tag{2.42}$$

where K_a, K_∞ are the thermal conductivities and $F_{T,a}$, $F_{T,\infty}$ the thermal correction factors at the droplet surface and at infinity, respectively.

For the determination of the thermal conductivity K_a of the binary mixture, and the thermal correction factor $F_{T,a}$, at the droplet surface, the vapor pressure $p_{v,a}$ at the droplet surface must be calculated. For the present calculations it is assumed that the droplet is in the continuum regime. Therefore the droplet surface is in equilibrium with the vapor phase to a high degree of approximation. In this case, the vapor pressure $p_{v,a}$ at the droplet surface can be calculated from the equilibrium vapor pressure $p_s(T_a)$, taking into account the curvature effect (Kelvin's law), and the solution effect (Raoult's law):

$$p_{v,a} = p_s(T_a) \exp\left(\frac{2\, M_v \sigma_{LV}}{R \rho_L T_a} \cdot \frac{1}{a}\right) \cdot \left(1 - \frac{3 m_N\, M_v\, i}{4\pi \rho_L\, M_N} \cdot \frac{1}{a^3}\right) . \tag{2.43}$$

Series expansion of the exponential function yields the approximate expression

$$p_{v,a} = p_s(T_a) \cdot \left(1 + \frac{2M_v \sigma_{LV}}{R \rho_L T_a} \cdot \frac{1}{a} - \frac{3\, m_N\, M_V\, i}{4\pi \rho_L\, M_N} \cdot \frac{1}{a^3}\right). \qquad (2.44)$$

Here ρ_{LV} denotes the surface tension and ρ_L the density of the liquid. m_N and M_N are the mass and the molecular weight of a soluble condensation nucleus, i is the Van't Hoff-factor. The saturation vapor pressure p_s is usually given as a function of temperature by empirical equations. In many cases expressions of the form

$$\ln p_s(T) = A_1 - \frac{A_2}{T - A_3} - A_4 \ln T + A_5 T \qquad (2.45)$$

are applied, where $A_1, \ldots, A_5$ are empirical coefficients. If $A_4 = A_5 = 0$, equ. (2.45) reduces to the so called Antoine-form. The temperature dependence of σ_{LV} and ρ_L can be approximated for a limited temperature range by the linear expressions

$$\sigma_{LV}(T) = \sigma_{LV}^{(o)} + \sigma_{LV}^{(1)} \cdot T, \qquad (2.46)$$

$$\rho_L(T) = \rho_L^{(o)} + \rho_L^{(1)} \cdot T, \qquad (2.47)$$

where $\sigma_{LV}^{(o)}$, $\sigma_{LV}^{(1)}$, $\rho_L^{(o)}$, $\rho_L^{(1)}$ are empirical coefficients.

In addition to the above mentioned heat flux Q_c, the heat flux Q_{rad} due to radiation has to be taken into account. According to Stefan-Boltzmann's law, the total radiative heat flux, directed towards the droplet, is given by

$$Q_{rad} = 4\pi a^2 \sigma \left(\varepsilon_\infty T_\infty^4 - \varepsilon_a T_a^4\right), \qquad (2.48)$$

where σ is a constant, and $\varepsilon_a, \varepsilon_\infty$ are the emissivities of the droplet surface and the environment, respectively. Assuming $\varepsilon_a = \varepsilon_\infty = 1$, and neglecting higher order terms, equ. (2.48) can be transformed into

$$Q_{rad} = 16\pi\, a^2 \sigma T_\infty^3\, (T_\infty - T_a). \tag{2.49}$$

By comparison with equ. (2.42) it can be estimated that

$$\frac{Q_{rad}}{Q_c} \cong \frac{4\sigma T_\infty^3}{K}\, a. \tag{2.5o}$$

In most practically important cases, $4\sigma\, T_\infty^3/K$ does not exceed $2oo\ m^{-1}$. According to the general assumptions in section 2.1), the droplet radius a is restricted to $a < 1o\ \mu m$, so that the influence of gravitational settling on the growth process can be neglected. Therefore it can be seen from equ. (2.5o) that the heat transport by radiation is negligible for the assumed experimental conditions.

2.2.5 Mass flux I_C in the continuum regime

In the phenomenological equation (2.11) for mass transfer, $D^{(v)}$ can be inserted from equ. (2.12-1), and $k_T^{(v)}$ can be substituted according to equ. (2.13-2) and (2.1o). Taking into account that in the present case $\vec{v}_g = 0$, the mass flux density $\vec{j}_V = \rho_V \vec{v}_V$ of the vapor can be expressed to a high degree of approximation as

$$\vec{j}_V = \frac{1}{1 - \frac{p_V}{p_o}}\, D\, (\operatorname{grad} \rho_V + \frac{\rho_V(1+\alpha)}{T} \operatorname{grad} T). \tag{2.51}$$

Replacing grad T according to equ. (2.38) yields

$$\vec{j}_v = - D \quad F_M \text{ grad } \rho_v, \tag{2.52}$$

where the diffusional correction factor F_M is given by

$$F_M \equiv \frac{1 - \frac{\rho_v L D}{KT}(1 + \alpha)}{1 - \frac{p_v}{p_o}} . \tag{2.53}$$

Because of the assumed low vapor pressure, F_M can be approximated by

$$F_M = 1 + \frac{p_v}{p_o} - \frac{\rho_v L D}{K T} (1 + \alpha). \tag{2.54}$$

The first correction term in F_M,

$$\frac{p_v}{p_o} ,$$

describes the influence of the Stefan flow on the mass transfer. The second correction term in F_M,

$$\frac{\rho_v L D}{K T} ,$$

is caused by the fact that the driving force for the mass flux is grad X_v, not grad ρ_v. grad X_v is proportional to grad ρ_v only for uniform temperature. This condition will be approximately fulfilled for low specific latent heat L and high thermal conductivity K. In this case the above mentioned term is negligible.

The third correction term in F_M ,

$$\frac{\rho_v L\ D}{K\ T} \cdot \alpha \ ,$$

describes the effect of thermal diffusion on the mass flux.

For atmospheric conditions (air-watervapor-mixture, T = 20°C, p_o = 760 Torr, p_v = 15 Torr), the numerical values of the above correction terms are 0,020 for the first term, 0,121 for the second term and 0,121 α for the third terms. As mentioned earlier, α is probably equal to 0,01.

It can be seen that the Stefan flow is negligible for atmospheric conditions. Furtheremore, the thermal diffusion effect influences the mass flux by only a few percents or even less, depending on the choice of α . However, the correction due to the difference between grad X_v and grad ρ_v, amounts to about 12 %. Although the latter effect is more important than Stefan flow and thermal diffusion, only the influence of the Stefan flow has been usually estimated in droplet growth theory.

The phenomenological equation (2.52) is of the general form (2.25). Accordingly, the solutions of section 2.2.3) can be used. The zeroth order vapor concentration profile is given by (equ. 2.29)

$$\rho_v(r) = \rho_{v,\infty} + (\rho_{v,a} - \rho_{v,\infty}) \cdot \frac{a}{r} \ , \qquad (2.55)$$

where $\rho_{v,a}$ and $\rho_{v,\infty}$ are the vapor concentrations at the droplet surface and at infinity, respectively. The first order total continuum mass flux towards the droplet surface can be expressed as (equ. (2.32))

$$I_c = 2\pi\ a\ D\ (F_{M,\infty} + F_{M,a})\ (\rho_{v,\infty} - \rho_{v,a})\ , \qquad (2.56)$$

where $F_{M,a}$ and $F_{M,\infty}$ are the diffusional correction factors at the droplet surface and at infinity, respectively.

The temperature dependence of the diffusion coefficient D can be taken into account, similar to equ. (2.42), by inserting $D_\infty F_{M,\infty} + D_a F_{M,a}$, where D_a and D_∞ are the diffusion coefficients at the droplet surface and at infinity, respectively. However, a somewhat better approximation, based on the exponential temperature dependence (equ. (2.9)), can be achieved as follows (Fuchs, 1959). Inserting the zeroth order phenomenological equation (2.16) into the steady state continuity equation (2.2), the equation

$$\text{grad}\ \rho_v\ .\ \text{grad}\ D + D.\Delta\rho_v = 0 \qquad (2.57)$$

can be obtained. Two integrations yield the solution of equ. (2.57) in the form

$$\rho_v = C_1 \int \frac{dr}{r^2.D} + C_2, \qquad (2.58)$$

where C_1 and C_2 are constants of integration. By differentiation of the zeroth order temperature profile, equ. (2.41), it can be seen that the integral in equ. (2.58) can be expressed as

$$\int \frac{dr}{r^2.D} = -\int \frac{dT}{D.a.(T_a - T_\infty)} \ . \qquad (2.59)$$

This integral can be evaluated in a closed analytical form taking into account the temperature dependence of D (equ.(2.9)). Now the solution of equ. (2.57), which satisfies the boundary conditions (2.27), can be obtained from equ. (2.58) after inserting the zeroth

order temperature profile (2.41):

$$\rho_v = \rho_{v,\infty} + \frac{\rho_{v,a} - \rho_{v,\infty}}{T_a^{1-\mu} - T_\infty^{1-\mu}} \left\{ \left[T_\infty + (T_a - T_\infty) \frac{a}{r} \right]^{1-\mu} - T_\infty^{1-\mu} \right\} . \quad (2.6o)$$

The corresponding flux through the droplet surface can be calculated by means of the zeroth order phenomenological equation (2.16). By inserting equ. (2.9) and (2.6o) into equ. (2.16), the flux density at the droplet surface can be obtained. Integration over the droplet surface yields the total mass flux towards the droplet surface

$$I_c = 4\pi a \, D_\infty \left[\frac{T_a^{\mu-1}}{T_\infty} \cdot \frac{T_\infty - T_a}{T_\infty^{\mu-1} - T_a^{\mu-1}} \cdot (\mu - 1) \right] . (\rho_{v,\infty} - \rho_{v,a}) . \quad (2.61)$$

If $\mu = 2$, equ. (2.61) reduces to

$$I_c = 4\pi \, a \, \sqrt{D_\infty \cdot D_a} \cdot (\rho_{v,\infty} - \rho_{v,a}) . \quad (2.62)$$

From equ. (2.61) it can be concluded that the temperature dependence of D can be taken into account by multiplication of D_∞ with the expression in square brackets. Accordingly, the first order total continuum mass flux towards the droplet surface, can be obtained from equ. (2.56):

$$I_c = 2\pi a \, D_\infty \left[\frac{T_a^{\mu-1}}{T_\infty} \cdot \frac{T_\infty - T_a}{T_\infty^{\mu-1} - T_a^{\mu-1}} \cdot (\mu - 1) \right] . (F_{M,\infty} + F_{M,a}) . (\rho_{v,\infty} - \rho_{v,a}) .$$

(2.63)

2.3 Quasistationary fluxes to a single droplet in the Transition Regime

Up to this point, the calculations were based on the assumption that the droplet is in the continuum regime. In several practically important systems, however, the mean free path λ of the surrounding gas cannot be neglected compared to the droplet radius a. In this case corrections to the continuum fluxes can be applied, which are based on the rigorous theory or on semiempirical interpolation techniques.

In the case of a droplet, whose radius is much smaller than the mean free path of the surroundig gas (free molecule regime), the diffusion theory predicts mass fluxes at the droplet surface, with are much higher than the rate of evaporation. In this case the rate of evaporation is too small to keep the droplet surface saturated and the equilibrium is disturbed. Accordingly the transport is under kinetic control and the stationary fluxes of mass and energy can be calculated according to kinetic theory.

A difficult situation arises if the droplet radius is of the order of the mean free path of the surroundig gas (transition regime). In this case the transport of mass and energy is partly under diffusion control and partly under kinetic control. At the surface a jump of temperatur and vapor concentration occurs, which was already pointed out by Langmuir (1915), p. 426. Schäfer (1932) attempted to calculate the transitional mass flux by equating the stationary continuum and free molecule fluxes at the droplet surface. By matching the fluxes at a jump distance Δ outside the droplet (model of the boundary sphere) Fuchs (1934) obtained an expression for the stationary mass flux in the transition regime. Fuchs (1958) argued that Δ should be chosen somewhat larger than the mean free path in the surrounding gas. The actual value of Δ has been estimated by Bradley, et al. (1946) and Wright (1960).

Carstens and Kassner (1968) and Fukuta and Walter (197o) obtained approximate expressions for the mass and heat flux in the transition regime by equating the continuum and kinetic fluxes at the droplet surface thereby neglecting Fuchs' jump distance Δ . Based on these results Fukuta and Walter (197o) and Carstens et al. (1974 a) derived approximate stationary droplet growth equations taking into account the jump of vapor concentration as well as the temperature jump at the droplet surface. Because the jump distance Δ was neglected, the growth equation will be valid only for droplets with radius > 1 µm. Recently Dahneke (1977) proposed a simple kinetic theory of the mass and heat transport in the transition regime. Using the continuum theory with certain boundary conditions at the droplet surface (kinetic boundary conditions), Dahneke obtains expressions, which are in agreement with Fuchs' semiempirical interpolation, if the Δ of Wright (196o) is chosen.

The above mentioned semiempirical interpolations are limited by the insufficient knowledge of the jump distance and are therefore restricted to sufficiently large droplets. In order to obtain growth equations which are valid for arbitrary droplet sizes, a solution of the rigorous Boltzmann transport equation must be attempted. Because of the complexity of this equation, most authors use a linearization of the collision term, which was suggested by Bhatnagar et al. (1954) (BGK-model). This approximation was first used by Brock (1966) to obtain a first order correction to the free molecule flux, which is valid in the near free molecule regime. Sahni (1966) achieved a solution of the Boltzmann equation in order to calculate the neutron flux intensity onto a spherical absorber (black sphere). These results were generalized by Smirnov (1971) for the case of a partially absorbing sphere (grey sphere) and were used in the theory of droplet growth. Smirnov obtained expressions for the mass and heat flux to a droplet of arbitrary size and with arbitrary values of the mass and thermal accomodation

coefficient. These expressions were used to derive an approximate stationary droplet growth equation for droplets of arbitrary size. Sahni (1966) and Smirnov (1971) assumed that the magnitude of the velocity of the molecules is constant. This assumption was eliminated by Loyalka (1973). Another important generalization is due to Williams (1975), who took into account anisotropic scattering of the vapor molecules thereby allowing for persistence of velocity. Accordingly in Williams' treatment it is not necessary to assume the mass of a vapor molecule to be small compared to the mass of a gas molecule.

A somewhat different approach was chosen by Shankar (197o), who solved the Boltzmann equation by means of the Maxwell moment method. The advantage of this method lies in the fact that the Boltzmann equation need not be solved directly but is solved only for the lower moments of the distribution function. These moments correspond to macroscopic quantities. Numerical calculations show excellent agreement with Fuchs' Δ-method, if Δ is set equal to zero. The calculations of Loyalka (1973), Williams (1975) and Shankar (197o) result in expressions for the mass flux to the droplet, but the heat flux has not been calculated. Loyalka and Williams assume an isothermal carrier gas. However, in general the heat, released during the phase transition, will cause temperature gradients in the vicinity of the droplet and explicit expressions for the heat flux to the droplet are required for droplet growth calculations.

2.3.1 Knudsennumbers

The transitional correction depends on the Knudsennumber

$$Kn \equiv \frac{\lambda}{a} \quad , \tag{2.64}$$

where λ is the mean free path in the surrounding gas and a is the droplet radius.

The mean free path in a gas is well defined only in the case, where the molecules can be approximated as rigid particles. For a pure gas in the rigid elastic sphere model the mean free path is given by (Chapman and Cowling, 197o)

$$\lambda = \frac{1}{\sqrt{2}\, n\, \pi\, \sigma^2} \quad , \tag{2.65}$$

where n is the number of molecules per unit volume and σ is the diameter of a molecule. $\pi\sigma^2$ is the collision cross section. In the binary mixture of vapor and gas, the mean free path λ_v of the vapor molecules will be different, in general, from the mean free path λ_g of the gas molecules. It can be shown (Jeans, 1954) that

$$\lambda_v = \frac{1}{\sqrt{2}\, n_v\, \pi\sigma_v^2 + \sqrt{1 + m_v/m_g}\, n_g\, \pi\sigma_{vg}^2} \quad , \tag{2.66}$$

λ_g analogous,

where n_v, n_g are the numbers of molecules per unit volume, m_v, m_g are the molecular masses and σ_v, σ_g the molecular diameters

of vapor and gas, respectively. $\pi\sigma_{vg}^2 = (\pi/4)(\sigma_v + \sigma_g)^2$ is the collision cross section for unlike-molecule interactions. $\pi\sigma_v^2$ and $\pi\sigma_g^2$ are the collision cross sections for like-molecule interactions for vapor and gas molecules, respectively. Because of the assumed low vapor concentration, the equations (2.66) reduce to

$$\lambda_v = \frac{1}{\sqrt{1 + m_v/m_g}\, n_g\, \pi\sigma_{vg}^2} \quad , \tag{2.67 - 1}$$

$$\lambda_g = \frac{1}{\sqrt{2}\, n_g\, \pi\sigma_g^2} \quad . \tag{2.67 - 2}$$

For the determination of the mean free path λ, relations between λ and the transport coefficients D, K and η for diffusion, thermal conductivity and viscosity, respectively, can be applied. From simple kinetic theory the zeroth order approximations (Hirschfelder, et al., 1954)

$$D = \frac{1}{3}\,\bar{c}\,\lambda = \frac{2}{3\pi}\,\frac{\sqrt{\pi\, m\, k\, T}}{\pi\sigma^2}\,\frac{1}{\rho} \quad , \tag{2.68 - 1}$$

$$K = \frac{1}{3}\, n\, m\, c_v\, \bar{c}\lambda = \frac{2}{3\pi}\,\frac{\sqrt{\pi\, m\, k\, T}}{\pi\sigma^2}\, c_v \quad , \tag{2.68 - 2}$$

$$\eta = \frac{1}{3}\, n\, m\, \bar{c}\, \lambda = \frac{2}{3\pi}\,\frac{\sqrt{\pi\, m\, k\, T}}{\pi\sigma^2} \quad , \tag{2.68 - 3}$$

can be obtained for pure gases, where

$$\bar{c} = \sqrt{\frac{8\, k\, T}{\pi\, m}} = \sqrt{\frac{8\, R\, T}{\pi\, M}} \tag{2.69}$$

is the average absolute velocity of the gas molecules. c_v is the specific heat capacity at constant volume, m is the molecular mass and k is Boltzmann's constant. $\rho = nm$ is the mass concentration of the gas. From equ. (2.68) it can be seen that D, K and η are expressed in terms of λ . Therefore diffusion, heat conduction and viscosity are sometimes called mean free path phenomena. According to equ. (2.68), the zeroth order relations

$$D = \eta/\rho \quad , \qquad (2.7o\text{ -}1)$$

$$K = \eta . c_v \quad , \qquad (2.7o\text{ -}2)$$

between D, K and η can be derived. From equ. (2.68-1) and (2.68-2) the expressions

$$\lambda = \frac{3\ D}{\bar{c}} \quad , \qquad (2.71 - 1)$$

$$\lambda = \frac{3\ K}{\rho c_v \bar{c}} \quad , \qquad (2.71 - 2)$$

These approximate equations can be used to determine λ from D or K. Strictly speaking, in the above equations D is the coefficient of self-diffusion.

In the rigorous theory of transport phenomena, the persistence of velocities has to be taken into account. The first order kinetic theory formulae for the transport properties of a pure gas are (Hirschfelder, et al.,1954)

$$D = \frac{3}{8.\Omega^{(1,1)*}} \cdot \frac{\sqrt{\pi\ m\ k\ T}}{\pi\sigma^2} \cdot \frac{1}{\rho} \quad , \qquad (2.72\text{ -}1)$$

$$K = \frac{25}{32.\Omega^{(2,2)*}} \cdot \frac{\sqrt{\pi\, m\, k\, T}}{\pi\sigma^2} \cdot c_v \frac{9\kappa - 5}{10} \quad , \qquad (2.72 - 2)$$

$$\eta = \frac{5}{16.\Omega^{(2,2)*}} \cdot \frac{\sqrt{\pi\, m\, k\, T}}{\pi\sigma^2} \quad , \qquad (2.72 - 3)$$

where $\Omega^{(1,1)*}$ and $\Omega^{(2,2)*}$ are reduced collision integrals, which are equal to unity for the rigid sphere model. Numerical values for other intermolecular potentials are tabulated, e.g. in Hirschfelder, et al.(1954).
$\kappa = c_p/c_v$ is the ratio of specific heat capacities, $(9\kappa-5)/10$ is the semiempirical Eucken-correction for polyatomic gases, which is equal to unity for monoatomic gases. The expressions for K and η cannot be simply generalized to binary gas mixtures. However, direct generalization of the formula for D yields the correct first order expression for the binary diffusion coefficient

$$D_{vg} = \frac{3}{8.\Omega_{vg}^{(1,1)*}} \frac{\sqrt{\pi k^3 T^3 (m_v+m_g)/2m_v\, m_g}}{\pi\sigma_{vg}^2} \frac{1}{p_o} \quad , \qquad (2.73)$$

which reduces to equ. (2.72-1), if $m_v = m_g = m$ and $\sigma_{vg} = \sigma_v = \sigma_g = \sigma$.

According to equ. (2.73) the binary diffusion coefficient is independentfrom the composition of the binary mixture to the first order of approximation, as already mentioned earlier. It can be seen that the mean free path λ does not appear naturally in the first order equations (2.72) and (2.73). Furthermore the relations between D, K and η are different from the zeroth order approximations (2.7o).

By means of equ. (2.67-1) and (2.73), the expression

$$\lambda_v = \frac{32.\Omega_{vg}^{(1,1)*}}{3\pi(1 + m_v/m_g)} \cdot \frac{D_{vg}}{\bar{c}_v} \qquad (2.74\text{-}1)$$

can be derived (Davis and Ray, 1978), where $\bar{c}_v$ is the average absolute velocity of the vapor molecules. Similarly equ. (2.67-2) and (2.72-2) yield the expression

$$\lambda_g = \frac{64\Omega_g^{(2,2)*}}{25\,\pi} \cdot \frac{10}{9\,\kappa - 5} \cdot \frac{K_g}{\rho_g c_{v,g} \bar{c}_g}\,, \qquad (2.74\text{-}2)$$

where $\bar{c}_g$ is the average absolute velocity of the gas molecules. The first order equations (2.74) can be used to determine more accurate values of λ_v and λ_g from the measured quantities D_{vg} and K_g. Comparison of equ. (2.71) and (2.74) shows that equ. (2.71-1) is a fairly good approximation for the mean free path of the vapor molecules, if $m_v << m_g$ and $\Omega_{vg}^{(1,1)*} \cong 1$. However, equ. (2.71-2) is quite different from equ. (2.74-2). In this connection it is important to note that the equations (2.71) were derived only from simple kinetic theory for the case of self-diffusion and heat conduction in a pure gas.

The higher order approximations for D are very complicated and depend on the composition of the binary mixture and other parameters. However, for most binary mixtures these corrections do not exceed 3 % (Hirschfelder, et al.,1954). Expressions for K and η of a pure gas have been calculated up to the fourth order of approximation assuming the rigid elastic sphere model. It turns out that the first order expressions for K and η according to equ. (2.72-2), (2.72-3) should be multiplied by the factors 1,o2513 and 1,o16oo, respectively

(Chapman and Cowling, 197o). The fourth order approximations may be taken as accurate to within o,1 %. It can be concluded that the error of the first order approximations (2.72) (2.73) will not exceed 3 %.

In the theory of droplet growth in the transition regime the transitional corrections for the mass and heat flux to a droplet will be dependent on different Knudsennumbers. The transitional correction for the mass flux will be dependent on the Knudsennumber

$$Kn_M \equiv \lambda_v / a \qquad (2.75\text{-}1)$$

with respect to the vapor molecules. Because of the low vapor concentration it is usually assumed that the transitional correction for the heat flux is dependent on the Knudsennumber

$$Kn_T \equiv \lambda_g / a \qquad (2.75\text{-}2)$$

with respect to the gas molecules. These Knudsennumbers can be calculated by means of the first order expressions (2.74) for λ_v and λ_g. However, most authors use expressions for Kn_M and Kn_T, which are based on the zeroth order equations (2.71), where slight modifications are sometimes applied. For comparison of different droplet growth theories, the particular definitions of Kn_M and Kn_T, as chosen by the authors, have to be taken into consideration. The Knudsennumbers, based on the first order expressions (2.74) should be used as a common reference (Davis and Ray, 1978).

For the calculations, described here, the theories due to Fukuta and Walter (197o) and Smirnov (1971) were chosen. In both investigations

the same expressions for the Knudsennumbers were used:

$$Kn_M = \frac{3.D_{vg}.\sqrt{\pi}.M_v}{2\sqrt{2\,RT_\infty}.a}\,, \qquad (2.76\text{ -1})$$

$$Kn_T = \frac{3\,K_g\sqrt{\pi M_g}.R.T_\infty}{2\sqrt{2}\,p_o\,(C_{v,g} + R/2).a}\,, \qquad (2.76\text{ -2})$$

where $C_{v,g}$ is the molar heat capacity of the gas at constant volume. The temperature dependence of $C_{v,g}$ can be approximated for a limited temperature range by the linear expression

$$C_{v,g}(T) = C_{v,g}^{(o)} + C_{v,g}^{(1)}.T \quad , \qquad (2.77)$$

where $C_{v,g}^{(o)}$, $C_{v,g}^{(1)}$ are empirical coefficients. The equations (2.76) are direct consequences of the zeroth order approximations (2.71) except for the introduction of the "apparent molar heat capacity" $C_{v,g} + R/2$ of the gas.

2.3.2 Expressions for mass and heat flux

The mass and heat flux in the transition regime can be expressed as

$$I_T = \beta_M.I_C \quad , \qquad (2.78\text{-1})$$

$$Q_T = \beta_T.Q_C \quad , \qquad (2.78\text{-2})$$

where I_C, Q_C are the continuum fluxes and β_M, β_T are transitional correction factors for the continuum fluxes of mass and heat, respectively.

In general, β_M and β_T are dependent on the Knudsennumbers Kn_M and Kn_T and on the accomodation coefficients α_M and α_T for mass and energy, respectively. The mass accomodation coefficient α_M is the probability for a vapor molecule hitting the liquid-gas-interface to stay within the liquid. The energy (thermal) accomodation coefficient α_T is the probability for a gas molecule hitting the liquid-gas-interface to come into thermal equilibrium with the liquid before being diffusely reflected.

According to equ. (2.63) and (2.42) the continuum fluxes I_c and Q_c are proportional to D and K, respectively. In order to express the transitional fluxes I_T and Q_T in the same general form, "compensated" transport coefficients $D^* \equiv \beta_M.D$ and $K^* \equiv \beta_T.K$ are sometimes introduced. Here this notation will not be adopted.

Various expressions for the transitional correction factors have been proposed. Fukuta and Walter (197o) obtained expression for β_M and β_T, which can be written in the form

$$\beta_M^{(F)} = \frac{1}{1 + 4\ Kn_M/3\alpha_M} \quad , \qquad (2.79)$$

$$\beta_T^{(F)} = \frac{1}{1 + 4\ Kn_T/3\alpha_T} \quad ,$$

where Kn_M and Kn_T are defined by equ. (2.76).
It can be expected that the equations (2.79) are approximately valid at low Knudsennumbers.

Smirnov (1971) obtained the expressions

$$\beta_M^{(s)} = \frac{1}{1 + (\Lambda(Kn_M) - 4/3 + 4/3\alpha_M)\, Kn_M}\,,$$

$$\beta_T^{(s)} = \frac{1}{1 + (\Lambda(Kn_T) - 4/3 + 4/3\alpha_T)\, Kn_T}\,, \qquad (2.8o)$$

where Kn_M and Kn_T are defined by equ. (2.76), and Λ is a monotonous function of Kn. Numerical values of Λ have been calculated by Sahni (1966) and are tabulated for different values of Kn. The limiting values of Λ are given by

$$\Lambda = o,71o \quad \text{for Kn} << 1,$$

$$\Lambda = 4/3 \quad \text{for Kn} >> 1. \qquad (2.81)$$

Fuchs (1969) proposed the interpolation formula

$$\Lambda(Kn) = \frac{(4/3)Kn + o,71o}{Kn + 1} = \frac{4/3 + o,71o/Kn}{1 + 1/Kn}\,, \qquad (2.82)$$

which results in Λ-values deviating from Sahni's values by less than 3 %. From equ. (2.8o) and (2.82) the expressions

$$\beta_M^{(s)} = \frac{1}{(o,377.Kn_M + 1)/(Kn_M + 1) + 4\, Kn_M/3\alpha_M}\,,$$

$$\beta_T^{(s)} = \frac{1}{(o,377.Kn_T + 1)/(Kn_T + 1) + 4\, Kn_T/3\alpha_T}\,, \qquad (2.83)$$

can be derived. Equ. (2.83) can be applied for arbitrary values of Kn. However, strictly speaking, the validity is restricted to isotropic scattering, i.e. $m_v << m_g$.

Comparison between equ. (2.79) and (2.8o) shows that the expressions of Fukuta and Walter (197o) and Smirnov (1971) differ by the term

$$(\Lambda - 4/3).Kn$$

in the denominator. As can be seen from above, $\Lambda \lesssim 4/3$. Therefore the values of the transitional fluxes according to Fukuta and Walter (197o) will be somewhat smaller than Smirnov's (1971) values. For large Knudsennumbers, Λ approaches 4/3, but the term $(\Lambda - 4/3).Kn$ does not approach zero. From equ. (2.83) it can be seen that for Kn >> 1

$$\beta_M^{(s)} \cong \frac{1}{o,377 + 4\ Kn_M/3\alpha_M}\ ,$$

$$\beta_T^{(s)} \cong \frac{1}{o,377 + 4\ Kn_T/3\alpha_T}\ . \qquad (2.84)$$

For Kn << 1 equ. (2.8o) yields

$$\beta_M^{(s)} \cong \frac{1}{1 + (4/3\alpha_M - o,623)Kn_M}\ ,$$

$$\beta_T^{(s)} = \frac{1}{1 + (4/3\alpha_T - o,623)Kn_T}\ . \qquad (2.85)$$

From the above equations it can be seen that for very small Knudsennumbers β_M and β_T approach unity and the fluxes become independent from the accomodation coefficients. This is explained by the fact that for the case of negligible mean free path the droplet growth process is under diffusion control and surface kinetic effects have negligible influence. Accordingly, measurements of the accomodation coefficients cannot be performed in the continuum regime.

Because of a modification of the distribution function, caused by the density gradient near the droplet surface, the quantities α_M, α_T occuring in the above equations, are not identical with the true accomodation coefficients α_M', α_T'. It can be shown that $\alpha_M = \alpha_M'/(1 - \alpha_M'/2)$ with a similar expression for α_T. However, mass and heat flux will be significantly affected by the accomodation coefficients only if α_M, α_T are sufficiently smaller than unity and in this case the above distinction is unimportant. Therefore α_M and α_T are treated here as if they were the actual microscopically significant quantities.

For a droplet with o,5 µm radius under atmospheric conditions, the Knudsennumbers according to equ. (2.76) are

$$Kn_M = o,25 \quad ,$$
$$Kn_T = o,32 \quad .$$

Under the assumption that the accomodation coefficients α_M and α_T are equal to unity, the numerical values of the transitional correction factors are

$$\beta_M^{(F)} = o,75 \quad , \quad \beta_T^{(F)} = o,7o \qquad \text{(Fukuta, Walter)},$$
$$\beta_M^{(s)} = o,83 \quad , \quad \beta_T^{(s)} = o,78 \qquad \text{(Smirnov)}.$$

It can be seen that the transitional corrections for a o,5 µm droplet are of the same order as the diffusional and thermal corrections, which have been calculated in section 2.2). With increasing droplet radius the transitional correction factors approach unity and thus become less important, whereas the diffusional and thermal corrections are size-independent. However, the diffusional and thermal corrections have not yet been included in the usually applied droplet growth theory.

The accomodation coefficients play the role of adjustable parameters in droplet growth theory. For most liquids it has been found that α_M and α_T are close to unity (Paul, 1962, Pound 1972). However, for a number of liquids, particularly including water, values much less than unity have been measured and severe disagreements between different investigations can be observed. In a series of papers, starting 1931, Alty and coworkers report investigations of the accomodation coefficients of water. Finally Alty and Mackay (1935) conclude from their measurements that α_M = o,o36 and α_T = 1,o. Hickman (1954) found α_M to be "not less than" o,25. In a re-analysis of Hickman's data Mills and Seban (1967) found that α_M = 1 "is indeed the best conclusion from the experimental data". Values of α_M between o,o265 and o,o415 were found by Delany, et al.(1964). The experiments of Mills and Seban (1967) indicate that α_M > o,45. Akoy (1971) finds α_M between o,55 and 1,17 with a mean value at o,82. Akoy discussed the possible errors caused by surface contamination, by the presence of a diffusion barrier, and by difficulties involved in measuring the temperature of the surface layer.
Measurements by Sinnarwalla, et al.(1975) result in α_M = o,o22 to o,o32 and α_T = 1. Sinnarwalla et al.(1975) and Narusawa and Springer (1975) discuss surface contamination as a possible source of error. Narusawa and Springer (1975) obtain α_M = o,o38 for a stagnant surface and α_M = o,17 to o,19 for a replenished (moving) surface.

Based on a comparison of theoretical and experimental droplet growth curves, an estimate for the accomodation coefficients of water will be given below.

2.3.3 Jumps of Density and Temperature

Inserting the zeroth order profiles (2.55) and (2.41) into the first order phenomenological equations (2.52) and (2.39), respectively, and integrating over the droplet surface yields the expressions

$$I_c = 4\pi a\, D\, F_M\, (\rho_{v,\infty} - \rho_{v,a}) \quad , \tag{2.86-1}$$

$$Q_c = 4\pi a\, K\, F_T\, (T_\infty - T_a) \quad , \tag{2.86-2}$$

for the total fluxes of mass and heat towards the droplet surface. Equ. (2.86) agree with the first order continuum expressions (2.56) and (2.42), if D, F_M, K and F_T are assumed to be uniform.

According to equ. (2.78) the transitional fluxes I_T and Q_T differ from the continuum fluxes I_c and Q_c by factors β_M and β_T, respectively. However, at distances, large compared to the mean free path in the surrounding gas, the zeroth order profiles of vapor concentration and temperature will be similar to the continuum profiles and can be expressed as

$$\rho_v(r) = \rho_{v,\infty} + \beta_M\, (\rho_{v,a} - \rho_{v,\infty})\, \frac{a}{r} \quad , \tag{2.87-1}$$

$$T(r) = T_\infty + \beta_T\, (T_a - T_\infty)\, \frac{a}{r} \quad . \tag{2.87-2}$$

Inserting the profiles (2.87) into the first order phenomenological equations (2.52) and (2.39) and integrating over the droplet surface yields the expressions

$$I_T = 4\pi a\, D\beta_M F_M\, (\rho_{v,\infty} - \rho_{v,a}) \quad , \tag{2.88-1}$$

$$Q_T = 4\pi a\, K\beta_T F_T\, (T_\infty - T_a) \quad , \tag{2.88-2}$$

for the total fluxes of mass and heat towards the droplet surface. Equ. (2.88) agree with the first order transitional expression (2.78) in connection with equ. (2.56) and (2.42), if D, F_M, K and F_T are assumed to be uniform.

The profiles (2.87) will only be valid at sufficiently large distances from the droplet surface. At distances of the order of the mean free path in the surrounding gas, deviations from the hyperbolic profiles (2.87) will occur. These deviations can be estimated by extrapolating the profiles (2.87) towards the droplet surface and comparing the extrapolated values $\rho_v(a)$, $T(a)$, with the actual values of vapor concentration $\rho_{v,a}$ and temperature T_a at the droplet surface. It can be seen that jumps of the vapor concentration,

$$\Delta_M \equiv \rho_v(a) - \rho_{v,a} = (\rho_{v,\infty} - \rho_{v,a})\ (1 - \beta_M), \qquad (2.89\text{-}1)$$

and the temperature,

$$\Delta_T \equiv T(a) - T_a = (T_\infty - T_a)\ (1 - \beta_T), \qquad (2.89\text{-}2)$$

will occur close to the droplet surface. Equ. (2.79), (2.8o) show that β_M, β_T decrease with increasing Knudsennumbers. Accordingly, the jumps of vapor concentration, Δ_M, and temperature, Δ_T, become more pronounced at higher Knudsennumbers. On the other hand, as mentioned earlier, β_M and β_T approach unity for very small Knudsennumbers. In this case the jumps Δ_M and Δ_T become insignificant and the hyperbolic continuum profiles extend all the way to the droplet surface.

2.4 Quasistationary droplet growth and evaporation

2.4.1 Mass flux to a single droplet

The growth rate of a droplet can be determined from the total mass flux to the droplet. For calculation of the total transitional mass flux I_T from equ. (2.78-1) and (2.63), the temperature T_a at the droplet surface must be inserted. T_a can be obtained from the heat balance at the droplet surface. According to equ. (2.36), for quasi steady state conditions the heat flux Q_T and the mass flux I_T are related by the equation

$$Q_T(a,T_a) + L(T_a).I_T(a,T_a) = 0 \quad , \tag{2.9o}$$

Where $L(T_a)$ is the specific latent heat of condensation at the droplet temperature. After inserting Q_T according to equ. (2.78-2) and (2.42) and I_T from equ. (2.78-1) and (2.63), the equ. (2.9o) can be solved numerically to obtain T_a for different values of the droplet radius a. Then T_a can be inserted into the equation (2.63) and the mass flux $I_T(a)$ can be calculated. This will later be refered to as the numerical solution.

The above described numerical solution requires a considerable computational effort. Accordingly, approximate solutions of equ. (2.9o) are frequently used in droplet growth theory. Similar to the result of Mason (1971) the approximate expression

$$I_T(a) \cong \frac{4\pi a\,(S_\infty - S_a)}{N_M + N_T} \quad , \tag{2.91-1}$$

where

$$N_M = \frac{1}{\beta_M . F_{M,\infty}} \quad \frac{R\,T_\infty}{D_\infty\, M_V\, p_S\,(T_\infty)} \quad , \tag{2.91-2}$$

$$N_T = \frac{1}{\beta_T \cdot F_{T,\infty}} \frac{L(T_\infty)}{K_\infty T_\infty} \left(\frac{L(T_\infty)\, M_V}{R\, T_\infty} - 1 \right), \qquad (2.91\text{-}3)$$

$$S_a = p_{v,a}/p_s(T_a) \cong \exp \left(\frac{2\, M_V \sigma_{LV}(T_\infty)}{R \rho_L(T_\infty) . T_\infty} \cdot \frac{1}{a} \right) \left(1 - \frac{3\, m_N\, M_V . i}{4\pi \rho_L(T_\infty) . M_N} \cdot \frac{1}{a^3} \right), \qquad (2.91\text{-}4)$$

$$S_\infty = p_{V,\infty}/p_S(T_\infty) \qquad (2.91\text{-}5)$$

can be derived using an approximate expression for the equilibrium vapor pressure $p_S(T)$, as obtained from the equation of Clausius and Clapeyron. Using equ. (2.9o), (2.78-2) and (2.42), the approximate expression

$$T_a(a) \cong T_\infty + \frac{1}{\beta_T \cdot F_{T,\infty}} \cdot \frac{L(T_\infty) \cdot I_T(a)}{4\pi a K_\infty} \qquad (2.92)$$

can be derived. Equ. (2.91), (2.92) will later be referred to as the analytical solution. This solution is restricted to systems, where the temperature is nearly uniform. As mentioned earlier, this condition will be fulfilled approximately for very slow processes and for condensates with small specific latent heat of condensation. Considerable deviations from the numerical solution can be expected at high supersaturations and accordingly high temperature gradients.

2.4.2 Mass and heat balance in a monodispersed droplet aerosol

For calculation of the simultaneous growth of randomly located droplets in a supersaturated environment the mutual interaction of the droplets has to be taken into account. A theoretical description of this complicated process can only be performed by the use of simplifying models. Fuchs (1934) proposed a model, which was later called "cellular model". According to this model, each droplet is surrounded by a sphere with impermeable surface. The volume of this sphere is equal to the system volume divided by the number of droplets. Fuchs pointed out that this model has a nonstationary solution and that a rigorous treatment poses great difficulties. A rough estimate was given. Reiss and La Mer (195o) present approximate solutions for the case, where the production of latent heat is neglected. The solutions are applied to a monodispersed aerosol, which is cooled at a constant rate. The nonsteady state calculations of Carstens and Zung (197o a) deal with the simultaneous heat and mass transfer in the cellular model thus taking into account the effect of latent heat.

In another model for the calculation of growth processes in droplet populations it is assumed that steep concentration and temperature gradients only occur in the immediate vicinity of the droplets and that the vapor concentration and temperature profiles between the growing droplets are fairly flat. Accordingly, average bulk parameters of vapor concentration and temperature can be defined. The simultaneous droplet growth can be described by single droplet growth theory with bulk values of supersaturation and temperature, which are time dependent due to vapor depletion and production of latent heat. This model of time dependent bulk parameters was first proposed by Reiss (1951), who calculated the growth process in monodispersed and polydispersed aerosols, neglecting temperature changes due to latent heat production.

The results of Reiss (1951) are in agreement with the calculations of Reiss and La Mer (195o), which are based on the cellular model. Based on the model of time dependent bulk parameters, cloud droplet spectra were calculated by Mordy (1959), Neiburger and Chien (196o), Brown and Arnason (1973) and others. Wagner and Pohl (1975 a) used this model to calculate the growth processes at different droplet concentrations in a condensation nucleus counter, taking into account the effect of the production of latent heat.

Both models can only be applied at sufficiently low droplet concentrations, when the mean distance between neighboring droplets is large compared to the droplet radius. If the distance between two droplets is of the order of the droplet radius, an interaction of the density and temperature profiles around the droplets occurs. as described by Carstens et al. (197o b). In this case the droplets do not grow independently and the process cannot be reduced to single droplet growth. However, for sufficiently low droplet concentrations, an interaction between two droplets is unlikely and furthermore the interaction time is short, as pointed out by Williams and Carstens (1971). Accordingly, a monodispersed droplet aerosol remains monodispersed during the growth process. Reiss (1951) estimated an upper concentration limit of 10^6 cm^{-3} for droplet radii smaller than 5 µm. However the assumption of large droplet distances causes no serious limitation of droplet concentration, because at high concentrations, droplet growth terminates at small droplet sizes, so that the ratio of droplet radius and mean droplet distance remains small.

The model of time dependent bulk parameters has the advantage that a random space distribution of the droplets may be considered whereas, strictly speaking, in the cellular model equidistant droplets are supposed. Furthermore the calculations are much simpler than in the cellular model, because the usual quasi steady state

equations can be used. However, it is a disadvantage of the model of time dependent bulk parameters that it may not be applicable at too small droplet concentrations. As Mason (1951) pointed out, transient inhomogeneities in the density and temperature field may occur due to the fast changes of vapor density and temperature at the droplet surfaces. This effect will be more pronounced at large distances between neighboring drops. The actual limits of applicability of the above described models have not been established. The validity of the approximations must be checked experimentally.

According to the assumed experimental conditions, the droplet aerosol is monodispersed and size and concentration of the growing droplets are sufficiently small, so that the total volume of the droplets can be neglected compared to the system volume. Furthermore, the vapor concentration and temperature profiles between the growing droplets will be fairly flat and steep concentration and temperature gradients will only occur in the immediate vicinity of the droplets. Therefore the model of time dependent bulk parameters can be applied. The simultaneous droplet growth can be described by single droplet growth theory, where time dependent bulk values of vapor concentration $\rho_{V,\infty}$, vapor pressure $p_{V,\infty}$, temperature T_∞ , etc. are inserted.

The calculation of the above mentioned bulk parameters is based on the balance of mass and heat in a volume V of the system, which is occupied by a particular amount of gas and condensate. μ_g and μ_V are the masses of gas and vapor in the volume V. N_d is the number of droplets in the volume V, $C = N_d/V$ is the droplet concentration. μ_g, N_d and the total pressure p_0 are constant during the droplet growth process. However, V and accordingly $C = N_d/V$ will change due to temperature changes and μ_V will change

due to vapor depletion. The equation of state for mixtures of ideal gases yields

$$V = \frac{R\,T_\infty}{p_0}\left(\frac{\mu_g}{M_g} + \frac{\mu_V}{M_V}\right). \qquad (2.93)$$

Accordingly the approximations

$$V = V_0 \cdot T_\infty / (T_\infty)_0 \quad , \qquad (2.94\text{-}1)$$

$$C = C_0 \cdot (T_\infty)_0 / T_\infty \quad , \qquad (2.94\text{-}2)$$

can be derived, where V_0, C_0 and $(T_\infty)_0$ are the initial values of V, C and T_∞, respectively. In equ. (2.94) a term of the order of $M_g(\mu_V-(\mu_V)_0)/M_V\mu_g$ has been neglected, where $(\mu_V)_0$ is the initial value of μ_V.

The conservation of the total mass of the condensate in the volume V during the growth process yields the equation

$$(\mu_V)_0 - \mu_V = \frac{4\pi}{3} \cdot \rho_L . N_d \,(a^3 - a_0^3), \qquad (2.95)$$

where a_0 is the initial droplet radius. Using equ. (2.94-1) and (2.95), the following expression for the bulk vapor concentration $\rho_{V,\infty} = \mu_V/V$ can be derived:

$$\rho_{V,\infty} = \frac{(T_\infty)_0}{T_\infty}\left[(\rho_{V,\infty})_0 - \rho_L \frac{4\pi}{3} C_0 \,(a^3 - a_0^3)\right] , \qquad (2.96)$$

where $(\rho_{V,\infty})_0$ is the initial bulk vapor concentration. By means of the equation of state for ideal gases, equ. (2.96) can be transformed into the expression

$$p_{v,\infty} = (p_{v,\infty})_o - \frac{R.(T_\infty)_o}{M_v} \rho_L \frac{4\pi}{3} C_o (a^3 - a_o^3) \qquad (2.97)$$

for the bulk vapor pressure, where $(p_{v,\infty})_o$ is the initial bulk vapor pressure.

The conservation of thermal energy in the volume V during the growth process yields the equation

$$(\mu_g c_{p,g} + (\mu_v)_o c_{p,v}) (T_\infty - (T_\infty)_o) = \frac{4\pi}{3} \cdot \rho_L . L(T_a) . N_d (a^3 - a_o^3) , \qquad (2.98)$$

where $c_{p,g}$ and $c_{p,v}$ are the specific heat capacities at constant pressure for gas and vapor, respectively. The term $(\mu_v)_o . c_{p,v}$ in equ. (2.98) is only approximately correct, because μ_v as well as the bulk vapor pressure $p_{v,\infty}$ will change during the growth process. Furthermore the term $\mu_g . c_{p,g}$ in equ. (2.98) is not strictly correct, because the total pressure $p_o = p_{g,\infty} + p_{v,\infty}$ is constant, whereas the bulk gas pressure $p_{g,\infty}$ will change slightly due to changes of the bulk vapor pressure $p_{v,\infty}$. However, the errors, caused by these approximations, are negligible. From equ. (2.98) the expression

$$T_\infty = (T_\infty)_o + \frac{\rho_L . L (T_a)}{(\rho_{g,\infty})_o . c_{p,g} + (\rho_{v,\infty})_o . c_{p,v}} \frac{4\pi}{3} C_o (a^3 - a_o^3) \qquad (2.99)$$

can be derived. Equ. (2.96), (2.97) and (2.99) describe the dependence of the bulk parameters $\rho_{v,\infty}$, $p_{v,\infty}$ and T_∞ on the droplet radius a. By inserting these equations into the expression for the mass and heat flux, the fluxes to a single droplet of the considered droplet aerosol can be obtained, and the mutual interaction of the droplets is taken into account.

It should be mentioned that the equations (2.97) and (2.99) are somewhat different from the equ. (8) and (6) of Wagner and Pohl (1975 a). These differences occur, because in the equations of Wagner and Pohl (1975 a) the change of V during the growth process and the heat capacity of the vapor has not been taken into account. Numerical calculations have shown, however, that these differences are very small.

2.4.3 Calculation of droplet growth

The quasisteady state growth rate of the droplets can be calculated according to the equation

$$\frac{d\, m_D}{dt} = I_T \quad , \tag{2.100}$$

where $m_D = 4\pi\, a^3 \rho_L / 3$ is the mass of the droplet. Integration of equ. (2.100) yields the growth time t as a function of the droplet radius a:

$$t(a) = \int_{a_o}^{a} \frac{4\pi\rho_L\, r^2}{I_T(r)}\, dr, \tag{2.101}$$

where a_o is the initial droplet radius. After inserting the bulk parameters according to equations (2.96), (2.97) and (2.99) and calculating the droplet temperature T_a and the mass flux I_T by means of the numerical or the analytical solution, the integral in equ. (2.101) can be evaluated numerically and the growth time t(a) can be obtained for various droplet radii a. Numerical inversion of the function t(a) finally yields the droplet radius a(t) as a function of time and the droplet growth calculation is completed. The bulk parameters $p_{V,\infty}$, T_∞ and $S_\infty = p_{V,\infty}/p_S(T_\infty)$ can be obtained

as functions of time by inserting the droplet radius a(t) into the equations (2.97) and (2.99). Furthermore the droplet temperature T_a can be calculated as a function of time.

A considerable simplification of the numerical calculations can be achieved by the assumptions that the temperature in the system is nearly uniform, that the droplets are in the continuum regime and that the droplet concentration is sufficiently small, so that the mutual interactions of the droplets can be neglected. In this case the analytic solution for the mass flux in the continuum regime can be inserted into equ. (2.1o1) with constant bulk parameters. The integration in equ. (2.1o1) can be performed in closed analytic form and the well known quadratic growth law is obtained.

Fig. 1, 2 show curves, resulting from numerical calculation. It can be seen that the droplet temperature T_a remains approximately constant during the growth process. The bulk temperature T_∞ approaches a limiting value, the bulk vapor saturation ratio S_∞ approaches the value 1. During the first stages of droplet growth, a considerable difference between droplet and ambient temperature can be observed. As mentioned earlier, substantial temperature gradients only exist inthe vicinity of the droplets. Accordingly the temperature gradient over some 1o µm in the neighborhood of the droplets will be extremely high. This explains the importance of the above mentioned mutual interactions of mass and heat flux.

The theory can be tested by means of comparison between experimental and theoretical droplet growth curves. Theoretical growth curves and a comparison with experimental data will be presented in section 8.2). Direct measurements of droplet and ambient temperature, ambient vapor pressure and vapor saturation ratio during the growth process are difficult and have not yet been performed.

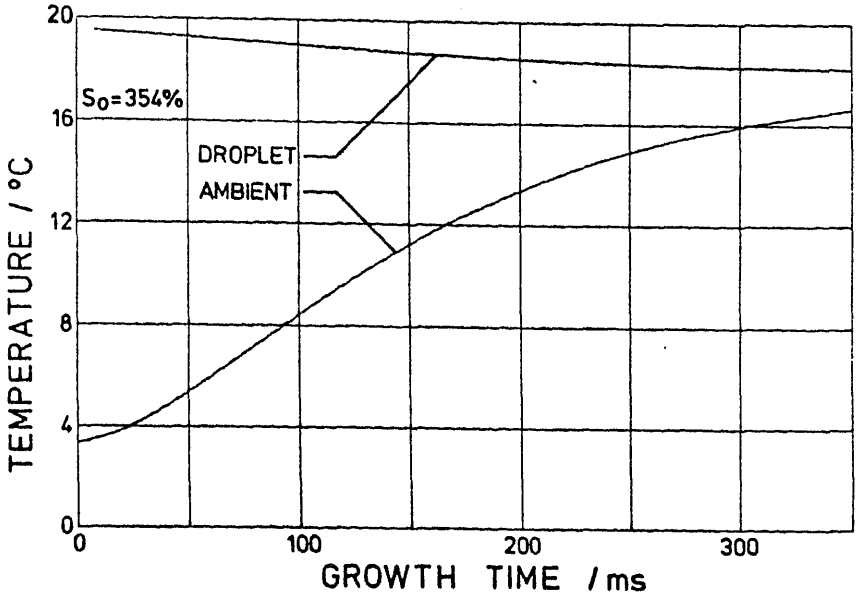

Fig. 1

Theoretical droplet temperature (Upper curve) and ambient temperature (lower curve) as functions of growth time for an initial saturation ratio of 354 % and a droplet number concentration of 4.6 .10^{3} cm^{-3}. The calculation was based on the numerical solution, using the Knudsen correction of Smirnov (1971).

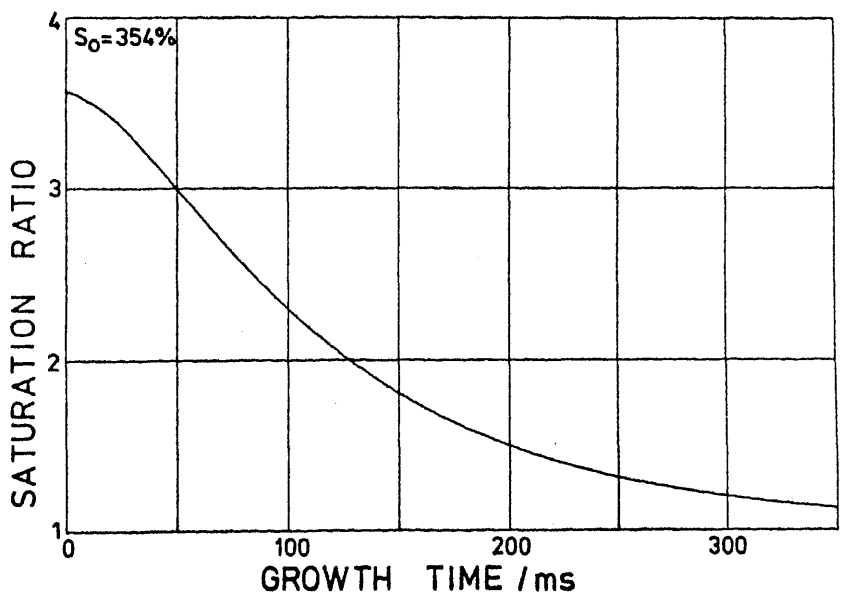

Fig. 2

Theoretical saturation ratio as a function of growth time. Conditions as in fig. 1.

3) THERMODYNAMIC PARAMETERS IN THE MEASURING CHAMBER

3.1 Principles of operation

Before a measurement is performed, the condensation nuclei aerosol with initial number concentration C_i is humidified in a humidifier with temperature T_B. The relative humidity (saturation ratio) B at the exit of the humidifier will be close to 1oo % in most cases. Then the humidified nuclei aerosol enters the expansion chamber with temperature T_i. The initial total gas pressure p_i before the expansion in the expansion chamber is usually equal to the atmospheric pressure. The initial partial pressure of the vapor before the expansion is

$$(p_v)_i = B.p_s(T_B) \ , \qquad (3.1.)$$

where $p_s(T_B)$ is the saturation vapor pressure at the temperature of the humidifier. Supersaturation in the expansion chamber is then achieved by a fast expansion of the humidified nuclei aerosol. The expansion is initiated by the opening of a solenoid valve, which connects the expansion chamber to a low pressure vessel, whose volume is large compared to the chamber volume. The total gas pressure in the expansion chamber drops by an amount of Δ_p and a final total gas pressure

$$p_o = p_i - \Delta_p \qquad (3.2)$$

is established in the expansion chamber. Because the low pressure vessel is large compared to the expansion chamber, changes of the total gas pressure during the droplet growth process will be negligible (pressure defined expansion chamber).

3.2 Assumptions about the expansion process

The final total gas pressure p_0 at the end of the expansion can be determined by means of a fast pressure transducer. Direct measurements of other thermodynamic parameters at the end of the expansion appear to be extremely difficult and have not yet been performed. Therefore these parameters must be calculated.

In order to calculate the thermodynamic parameters at the end of the expansion, certain assumptions have to be made. Here it is assumed that the expansion is dry-adiabatic, which means that negligible vapor and heat exchange with the chamber walls takes place and vapor depletion and production of latent heat due to droplet growth can be disregarded during the expansion period. The expansion is considered as quasistatic, so that the well-known thermodynamic relations for adiabatic processes can be applied. Measurements of Israel and Nix (1966 a,b) and Semonin and Hayes (1968) seem to indicate that a fast expansion is not a reversible process. Furthermore it is assumed that no decomposition of the gas mixture takes place during the expansion period. Accordingly the ratio of the partial densities of vapor and carrier gas remains unchanged and the molecular weight of the gas mixture is constant during the expansion period. In addition the ratio of the particle number concentration and the total gas density is assumed to be constant during the expansion period. Accordingly movements of the particles relative to the gas mixture due to inertial effects during the expansion period are disregarded. The validity of the above assumptions depends on the experimental conditions and will be discussed later.

3.3 Calculation of the initial thermodynamic parameters at the end of the expansion

The expansion process in the expansion chamber can be characterized by the (pressure) expansion ratio

$$\beta \equiv \frac{p_i}{p_o} = \frac{p_i}{p_i - \Delta_p} , \tag{3.3}$$

where p_i is the initial total gas pressure before the expansion, p_o is the (constant) final total gas pressure after the expansion, and Δ_p is the total pressure drop during the expansion. The assumption that no decomposition of the gas mixture occurs during the expansion period, yields

$$\frac{(p_v)_i}{p_i} = \frac{(p_{v,\infty})_o}{p_o} , \tag{3.4}$$

because carrier gas and vapor are assumed to be ideal gases and have always equal temperatures. Accordingly, the partial pressure of the vapor at the end of the expansion is

$$(p_{v,\infty})_o = \frac{B.p_s(T_B)}{\beta} . \tag{3.5}$$

For calculation of the temperature $(T_\infty)_o$ at the end of the expansion, the adiabatic index κ of the gas mixture must be determined. The specific heat capacities c_p, c_v of ideal gases are related by the equation

$$c_p - c_v = \frac{R}{M} , \tag{3.6}$$

which can be rewritten as

$$c_v = \frac{R}{M(\kappa-1)} , \tag{3.7}$$

where $\kappa = c_p/c_v$ is the adiabatic index. Assuming that the heat capacity at constant volume of the gas mixture is the sum of the heat capacities at constant volume of the components, the relation

$$\rho c_v = \rho_v \, c_{v,v} + \rho_g \, c_{v,g} \qquad (3.8)$$

can be obtained, where $c_{v,v}$, $c_{v,g}$ and c_v are the specific heat capacities at constant volume of vapor, carrier gas and the gas mixture, respectively. Inserting equ. (3.7) into equ. (3.8) and using the equation of state for ideal gases yields

$$\frac{p}{\kappa-1} = \frac{p_v}{\kappa_v-1} + \frac{p_g}{\kappa_g-1} \quad , \qquad (3.9)$$

where κ_v, κ_g and κ are the adiabatic indices of vapor, carrier gas and the gas mixture, respectively. A similar expression has been obtained by Richarz (1906). Remembering that $p = p_v + p_g$, equ. (3.9) can be rewritten as

$$\kappa = 1 + \left[\frac{1}{\kappa_g-1} + \frac{p_v}{p}\left(\frac{1}{\kappa_v-1} - \frac{1}{\kappa_g-1}\right)\right]^{-1} \quad . \qquad (3.10)$$

From equ. (3.4) it can be seen that p_v/p and accordingly κ remains unchanged during the expansion period. Therefore κ can be calculated from equ. (3.10), inserting the <u>initial</u> pressure ratio $(p_v)_i/p_i$. Using the just obtained adiabatic index κ, the temperature $(T_\infty)_0$ at the end of the adiabatic expansion can be calculated from well-known thermodynamic relations as

$$(T_\infty)_0 = T_i/\beta^{\frac{\kappa-1}{\kappa}} \quad . \qquad (3.11)$$

Possible deviations from a quasistatic, adiabatic expansion can be taken into account by introducing a polytropic index

$$\kappa_{pol} = \kappa - \Pi(\kappa-1) \quad , \qquad (3.12)$$

where κ is the adiabatic index of the gas mixture and Π is a "polytropic factor". Inserting equ. (3.12) into equ. (3.11), the expression

$$(T_\infty)_0 = T_i/\beta^{\frac{\kappa-1}{\kappa+\Pi/(1-\Pi)}} \tag{3.13}$$

can be obtained. It can be seen that $\Pi = 0$ describes a quasistatic, adiabatic expansion. With increasing Π the calculated temperature drop during the expansion decreases. As Π approaches unity, the calculated temperature drop vanishes and an isothermal expansion is described.

Now the initial saturation ratio at the end of the expansion,

$$(S_\infty)_0 = \frac{(p_{v,\infty})_0}{p_s((T_\infty)_0)} \quad , \tag{3.14}$$

can be obtained. Using the equation of state for ideal gases, the initial partial vapor density at the end of the expansion,

$$(\rho_{v,\infty})_0 = \frac{(p_{v,\infty})_0 \cdot M_v}{R.(T_\infty)_0} \tag{3.15}$$

and the initial partial carrier gas density at the end of the expansion,

$$(\rho_{g,\infty})_0 = (\rho_g)_N \cdot \frac{T_N}{p_N} \cdot \frac{p_0 - (p_{v,\infty})_0}{(T_\infty)_0} \tag{3.16}$$

can be calculated, where $(\rho_g)_N$ is the density of the carrier gas at temperature T_N and pressure p_N.

Based on the assumption that the ratio of the particle number concentration and the total gas density is constant during the expansion period, the relation

$$\frac{C_i}{C_o} = \frac{(T_\infty)_o}{T_i} \cdot \beta \qquad (3.17)$$

between the initial particle number concentration C_i before the expansion and the particle number concentration C_o at the end of the expansion can be derived.

4) LIGHT SCATTERING BY THE DROPLETS IN THE MEASURING CHAMBER

4.1 Light scattering by a sphere

Based upon Maxwell's electromagnetic theory Mie (19o8) and Debye (19o9) derived the theory of light scattering by a sphere, which is usually called Mie theory. Various treatments of the Mie theory may be found in Van de Hulst (1957), Kerker (1969), and Born, Wolf (1975). Here the results of the Mie theory are summarized, as far as they were used in the present investigations. Some numerical data are presented.
A homogeneous, isotropic and nonmagnetic sphere with radius a, dielectric constant ε^{int} and conductivity σ^{int} is considered, which is surrounded by a homogeneous, isotropic nonabsorbing and nonmagnetic medium with dielectric constant ε^{ext}. Incident upon the sphere is a plane, linearly polarized electromagnetic (light) wave with intensity I_0 and angular frequency ω . Droplet radius and wavelength of the incident wave are assumed to be large compared to atomic dimensions, so that the macroscopic Maxwell equations can be applied. Coherent and incoherent scattering by the considered media are assumed to be negligible compared to the scattering by the sphere.

A spherical coordinate system (r,θ,ϕ) is introduced with the origin at the center of the sphere. The direction $\theta = o$ is the direction of propagation of the incident wave and the direction $\theta = \pi/2, \phi = o$ is parallel to the electric field vector of the incident wave.

Scattering and absorption by the considered sphere are described by periodic solutions of Maxwell's equations inside and outside the sphere. In the absence of prescribed charge and current sources and assuming that the time dependence of the field vectors is given by $\exp(i\omega t)$, the time independent complex amplitudes $\vec{E}$, $\vec{H}$ of the field vectors satisfy two Maxwell equations in the time-free form +)

+) in SI-units

$$\operatorname{curl} \vec{E} = - k_m \vec{H}, \qquad (4.1 - 1)$$

$$\operatorname{curl} \vec{H} = k_e \vec{E}, \qquad (4.1 - 2)$$

where

$$k_e = i\omega\varepsilon + \sigma \ , \qquad (4.2 - 1)$$

$$k_m = i\omega\mu \quad . \qquad (4.2 - 2)$$

By taking divergences on both sides of equ. (4.1) it can be shown that solutions of equ. (4.1) automatically satisfy the remaining two Maxwell equations.

The field vectors can be expressed in terms of the well-known four-potential. However, for some applications it is more convenient to derive the field vectors from a different potential, the Hertz-potential, whose electric part was first introduced by Hertz (1889). The relation between the complex amplitudes $\vec{E}$, $\vec{H}$ of the field vectors and the complex amplitudes $\vec{\Pi}_e$, $\vec{\Pi}_m$ of the Hertz-potential can be expressed as

$$\vec{E} = \operatorname{curl} \operatorname{curl} \vec{\Pi}_e - k_m \operatorname{curl} \vec{\Pi}_m, \qquad (4.3 - 1)$$

$$\vec{H} = \operatorname{curl} \operatorname{curl} \vec{\Pi}_m + k_e \operatorname{curl} \vec{\Pi}_e. \qquad (4.3 - 2)$$

By inserting these expressions into equ. (4.1) it can be seen that $\vec{E}$, $\vec{H}$ are solutions of equ. (4.1)if $\vec{\Pi}_e$, $\vec{\Pi}_m$ are two solutions of the vector wave equation in the time-free form

$$\Delta\vec{\Pi} + k^2\vec{\Pi} = 0 \ , \qquad (4.4)$$

where the wave number k is given by

$$k^2 = - k_e k_m \ . \qquad (4.5)$$

In cases, where spherical coordinates are introduced, it is particularly useful to consider radial Hertz-vectors

$$\vec{\Pi}_e = \vec{r}\Pi_e \ , \qquad (4.6 - 1)$$

$$\vec{\Pi}_m = \vec{r}\Pi_m \ , \qquad (4.6 - 2)$$

where $\vec{r}$ is the radius vector from the origin. Inserting this potential into equ. (4.3) and using the identities

$$\Delta(\vec{r}\Pi) \equiv \vec{r}\Delta\Pi + 2 \ \mathrm{grad}\ \Pi \ , \qquad (4.7 - 1)$$

$$\mathrm{curl}\Delta(\vec{r}\Pi) \equiv \mathrm{curl}\ (\vec{r}\Delta\Pi), \qquad (4.7 - 2)$$

it can be shown that $\vec{E}$, $\vec{H}$ are solutions of equ. (4.1), if Π_e, Π_m are two solutions of the scalar wave equation in the time free form

$$\Delta\Pi + k^2\Pi = 0 \ . \qquad (4.8)$$

Inserting equ. (4.6) into equ. (4.3) and using equ. (4.7 -1) and (4.8) and the identity

$$\mathrm{div}(\vec{r}\Pi) - 2\Pi \equiv \Pi + \vec{r} \ \mathrm{grad}\ \Pi \ , \qquad (4.9)$$

equ. (4.3) can be rewritten for radial Hertz-vectors in the form

$$\vec{E} = \mathrm{grad}(\Pi_e + \vec{r} \ \mathrm{grad}\ \Pi_e) + k^2\vec{r}\Pi_e - k_m \ \mathrm{curl}(\vec{r}\Pi_m), \qquad (4.1o - 1)$$

$$\vec{H} = \mathrm{grad}(\Pi_m + \vec{r} \ \mathrm{grad}\Pi_m) + k^2 \ \vec{r}\Pi_m + k_e \ \mathrm{curl}(\vec{r}\Pi_e). \qquad (4.1o - 2)$$

By means of equ. (4.1o) the complex amplitudes $\vec{E}$, $\vec{H}$ of the field vectors can be expressed in terms of only two scalars Π_e, Π_m, the Debye-potentials. Debye (19o9) derived equ. (4.1o) in spherical coordinates. A connection

between Debye-potentials and radial Hertz-vectors has been pointed out by Sommerfeld (1927).

A physical interpretation of equ. (4.1o) can be given as follows. The electromagnetic field is represented as the sum of two subfields corresponding to the Debye-potentials Π_e and Π_m. Because of the identity $\vec{r}.\mathrm{curl}(\vec{r}\Pi) \equiv 0$ it can be seen that for the subfields corresponding to Π_e and Π_m the radial components of $\vec{H}$ and $\vec{E}$, respectively, vanish (transverse waves).

By means of equ. (4.1o) the problem of light scattering by a sphere can be reduced to the solution of equ. (4.8). In order to adapt the solutions of equ. (4.8) to the boundary conditions at the surface of the sphere, the Debye-potentials of the incident wave must be determined. In order to fulfill the boundary conditions, an additional wave, the scattered wave, must be superimposed upon the incident wave outside the sphere. The Debye-potentials of the wave inside the sphere and of the scattered wave can be expressed as solutions of equ. (4.8), which are of a similar form as the Debye-potentials of the incident wave. For physical reasons, the radial dependence of the wave inside the sphere can only be described by functions which remain regular at the origin. Furthermore, the radial dependence of the scattered wave must be given by functions, which describe an outgoing wave. These restrictions together with the boundary conditions at the surface of the sphere are sufficient for a unique determination of the Debye-potentials Π_e, Π_m. By inserting the solutions for Π_e, Π_m into equ. (4.1o), the complex amplitudes $\vec{E}$, $\vec{H}$ of the field vectors can be obtained rigorously.

The rigorous solution yields somewhat complicated expressions for the wave inside the sphere and for the scattered wave. In the present investigations only the scattered wave is considered at large distances from the center of the sphere. In this case the radial components of the field vectors are negligible, the scattered wave is transversal

and a considerable simplification of the theoretical expressions can be achieved.

In the vicinity of the forward direction $\theta = 0$ and the backward direction $\theta = \pi$, interference of incident and scattered wave occurs. It can be shown easily that the area of interference is of the order of $2\pi r\lambda$ and the corresponding angle is of the order of $\sqrt{2\lambda/r}$, where r is the distance from the center of the sphere. Only outside the interference regions the scattered wave can be separated from the incident wave. However, the angular range of these regions can be reduced arbitrarily by chosing sufficiently large observation distances.

The intensities of the linearly polarized components of the scattered wave, whose electric field vectors are perpendicular and parallel to the plane of observation, can be expressed as

$$I_\perp = I_o \frac{\lambda^2}{4\pi^2 r^2} i_\perp(m,\alpha,\theta)\sin^2\phi \,, \qquad (4.11 - 1)$$

$$I_\parallel = I_o \frac{\lambda^2}{4\pi^2 r^2} i_\parallel(m,\alpha,\theta)\cos^2\phi \,, \qquad (4.11 - 2)$$

respectively, where $\lambda = 2\pi/k^{ext}$ is the wavelength in the surrounding medium and r denotes the distance of the observer from the center of the sphere. $\alpha = 2\pi a/\lambda$ is the dimensionless size parameter of the sphere. The complex refractive index $m = n(1-in)$ of the sphere relative to the surrounding medium can be expressed as $m^2 = (k^{int}/k^{ext})^2 = k_e{}^{int}/k_e{}^{ext}$.

The intensity functions are given by

$$i_\perp = \left| \sum_{\ell=1}^{\infty} \frac{2\ell+1}{\ell(\ell+1)} \left[a_\ell(\alpha,m)\pi_\ell(\cos\theta) + b_\ell(\alpha,m)\tau_\ell(\cos\theta)\right]\right|^2, \qquad (4.12 - 1)$$

$$i_\parallel = \left| \sum_{\ell=1}^{\infty} \frac{2\ell+1}{\ell(\ell+1)} \left[a_\ell(\alpha,m)\tau_\ell(\cos\theta) + b_\ell(\alpha,m)\pi_\ell(\cos\theta)\right]\right|^2. \qquad (4.12 - 2)$$

The amplitude functions a_ℓ und b_ℓ can be expressed as

$$a_\ell(\alpha,m) = \frac{\Psi_\ell(\alpha)\,\Psi_\ell'(m\alpha) - m\,\Psi_\ell'(\alpha)\,\Psi_\ell(m\alpha)}{\zeta_\ell(\alpha)\,\Psi_\ell'(m\alpha) - m\,\zeta_\ell'(\alpha)\,\Psi_\ell(m\alpha)}\,, \qquad (4.13 - 1)$$

$$b_\ell(\alpha,m) = \frac{m\,\Psi_\ell(\alpha)\,\Psi_\ell'(m\alpha) - \Psi_\ell'(\alpha)\,\Psi_\ell(m\alpha)}{m\zeta_\ell(\alpha)\,\Psi_\ell'(m\alpha) - \zeta_\ell'(\alpha)\,\Psi_\ell(m\alpha)}\,, \qquad (4.13 - 2)$$

where

$$\Psi_\ell(x) = x.j_\ell(x)\,, \qquad (4.14 - 1)$$

$$\zeta_\ell(x) = x.h_\ell^{(2)}(x)\,, \qquad (4.14 - 2)$$

and $\Psi_\ell'(x)$, $\zeta_\ell'(x)$ are the derivatives of $\Psi_\ell(x)$, $\zeta_\ell(x)$ with respect to x. The spherical Bessel functions $j_\ell(x)$, spherical Neumann functions $n_\ell(x)$, and spherical Hankel functions $h_\ell^{(1)}(x)$, $h_\ell^{(2)}(x)$ can be defined according to the Rayleigh formulas as

$$j_\ell(x) = x^\ell \left(-\frac{d}{xdx}\right)^\ell \left(\frac{\sin x}{x}\right)\,, \qquad (4.15 - 1)$$

$$n_\ell(x) = -x^\ell\left(-\frac{d}{xdx}\right)^\ell\left(\frac{\cos x}{x}\right)\,, \qquad (4.15 - 2)$$

$$h_\ell^{(1)}(x) = j_\ell(x) + i\,n_\ell(x) = -i\,x^\ell\left(-\frac{d}{xdx}\right)^\ell\left(\frac{e^{ix}}{x}\right)\,, \qquad (4.15 - 3)$$

$$h_\ell^{(2)}(x) = j_\ell(x) - i\,n_\ell(x) = i\,x^\ell\left(-\frac{d}{xdx}\right)^\ell\left(\frac{e^{-ix}}{x}\right)\,. \qquad (4.15 - 4)$$

The spherical Bessel, Neumann, and Hankel functions are related to the half-integral-order Bessel, Neumann, and Hankel functions by

$$j_\ell(x) = \sqrt{\frac{\pi}{2x}}\; J_{\ell+1/2}(x)\,, \qquad (4.16 - 1)$$

$$n_\ell(x) = \sqrt{\frac{\pi}{2x}} \quad N_{\ell+1/2}(x) \ , \qquad (4.16 - 2)$$

$$h_\ell^{(1)}(x) = \sqrt{\frac{\pi}{2x}} \quad H^{(1)}_{\ell+1/2}(x), \qquad (4.16 - 3)$$

$$h_\ell^{(2)}(x) = \sqrt{\frac{\pi}{2x}} \quad H^{(2)}_{\ell+1/2}(x) \ . \qquad (4.16 - 4)$$

The angular functions π_ℓ and τ_ℓ can be expressed as

$$\pi_\ell(x) = \frac{d\, P_\ell(x)}{dx} \ , \qquad (4.17 - 1)$$

$$\tau_\ell(x) = x \frac{d\, P_\ell(x)}{dx} - (1-x^2) \frac{d^2 P_\ell(x)}{dx^2} \ . \qquad (4.17 - 2)$$

The Legendre polynominals $P_\ell(x)$ can be defined by

$$P_\ell(x) = \frac{1}{2^\ell\ \ell!} \quad \frac{d^\ell}{dx^\ell} (x^2 - 1)^\ell \ . \qquad (4.18)$$

The properties of the above functions are described in any of the standard mathematical books, e.g. Arfken (1971). For numerical calculations recurrence relationships are important.

In general, the scattered wave is elliptically polarized. However, as can be seen from equ. (4.11), the scattered wave is linearly polarized, if the plane of observation is perpendicular ($\phi = \pi/2$) or parallel ($\phi = 0$) to the electric field vector of the incident wave.

For $\phi = \pi/2$ the electric field vector of the scattered wave is perpendicular and for $\phi = 0$ it is parallel to the plane of observation.

For the case, where the incident wave is unpolarized, the scattering intensity I_u can be calculated by averaging of equ. (4.11) over ϕ . Using the relations $\langle \sin^2\phi \rangle = \langle \cos^2\phi \rangle = 1/2$, one obtains

$$I_u = I_0 \frac{\lambda^2}{8\pi^2 r^2} (i_\perp + i_\parallel) . \qquad (4.19)$$

The degree of polarization of the scattered light is given by

$$P = \left| \frac{i_\perp - i_\parallel}{i_\perp + i_\parallel} \right| . \qquad (4.2o)$$

In many cases it is important to determine the total energy, which is removed from the incident wave. The scattering cross section K_{sca} describes the total amount of energy, which is scattered by the sphere. The absorption cross section K_{abs} describes the total absorbed energy. The extinction cross section is defined as

$$K_{ext} = K_{sca} + K_{abs} . \qquad (4.21)$$

K_{ext} can be calculated by means of a general theorem, which is due to Van de Hulst (1949). According to this theorem K_{ext} is closely related to the complex amplitude of the scattered wave in the forward direction ($\theta = 0$). Applying the general theorem to the present case, the extinction efficiency $Q_{ext} \equiv K_{ext}/\pi a^2$ can be obtained as

$$Q_{ext}(\alpha,m) = \frac{2}{\alpha^2} \sum_{\ell=1}^{\infty} (2\ \ell+1)\ \mathrm{Re}\ (a_\ell + b_\ell), \qquad (4.22)$$

where Re denotes the real part.
By evaluating the Poynting vector of the scattered wave and integrating it over all directions Mie (19o8) obtained K_{sca}. The scattering efficiency $Q_{sca} \equiv K_{sca}/\pi a^2$ can be expressed as

$$Q_{sca}(\alpha,m) = \frac{2}{\alpha^2} \sum_{\ell=1}^{\infty} (2\ \ell+1)\ (|a_\ell|^2 + |b_\ell|^2). \qquad (4.23)$$

Finally, the absorption efficiency $Q_{abs} \equiv K_{abs}/\pi a^2$ can be calculated by inserting equ. (4.22) and (4.23) into equ. (4.21). For nonabsorbing spheres Q_{sca} is equal to Q_{ext} and accordingly Q_{abs} vanishes. For increasing α the extinction efficiency Q_{ext} approaches 2 in agreement

with a general theorem (extinction paradoxon). This is explained by the fact that in addition to the light intercepted by the sphere, there is a contribution to the extinction, which is due to the diffraction by the sphere. This additional contribution is important no matter how large the sphere is.

By means of equ. (4.11) - (4.23) the scattering properties of a sphere can be determined for arbitrary values of m and α . For small values of α and not too large values of $|m|$, i.e. for spheres, which are small compared to the wavelength of the incident wave, the above equations can be simplified considerably.

Using asymptotic approximations it can be shown that in this case the amplitude function a_1 is approximately given by

$$a_1 = \frac{2}{3} i \left(\frac{m^2 - 1}{m^2 + 2} \right) \alpha^3 . \qquad (4.24)$$

b_1 and a_2 are approximately $\propto \alpha^5$ and can be neglected. Inserting equ. (4.24) and the angular functions $\pi_1(\cos\theta) = 1$ and $\tau_1(\cos\theta) = \cos\theta$ into equ. (4.12), (4.19) and (4.2o) yields

$$I_u = I_o \frac{8\pi^4 a^6}{r^2 \lambda^4} \left| \frac{m^2 - 1}{m^2 + 2} \right|^2 . (1 + \cos^2\theta), \qquad (4.25)$$

$$P = \frac{\sin^2\theta}{1+\cos^2\theta} . \qquad (4.26)$$

These equations were first derived by Rayleigh (1871), in a different way.

For increasing values of α and m, more terms in equ. (4.12), (4.22) and (4.23) need to be taken into account, each term corresponding to

a particular partial wave. For different values of α , resonance for certain partial waves can be observed. With increasing order ℓ of the partial wave, the resonance peaks become sharper and accordingly higher-order partial waves occur only at discrete values of α .
As pointed out by Metz and Dettmar (1963), the magnetic resonances, corresponding to b_ℓ , are sharper than the electric resonances, corresponding to a_ℓ . The resonance peaks for a particular partial wave occur at nearly equidistant values of α . Furthermore, the first resonance peak is shifted towards higher values of α for increasing order ℓ of the partial wave. The contribution of higher-order partial waves is negligible for α-values below their first resonance peak. Accordingly, for particular values of α and m the summations in equ. (4.12), (4.22) and (4.23) have to be carried out until an order ℓ is reached, where the first resonance peak is located above the considered value of α . It turns out that the required number of summations is of the order of $|m|\alpha$. Therefore the numerical evaluations become increasingly complicated with increasing size of the sphere. Fortunately, for spheres, which are several orders of magnitude larger than the wavelength of the incident wave, light scattering can be described approximately by means of diffraction theory and geometrical optics.

Numerical light scattering calculations based upon Mie theory, have been performed by many authors, using digital electronic computers. The results for different refractive indizes have been tabulated, e.g. Penndorf (1956), Giese, et al.(1962), Denman, et al.(1966). For the present investigations, light scattering intensities were calculated by means of a computer program, which has been developed by Dave (1968, 1969 a, 1969 b) and is available as an IBM subroutine. In this program a_ℓ, b_ℓ, π_ℓ and τ_ℓ are calculated by means of recurrence relationships. In order to reduce the influence of error propagation in the course of the recurrence calculations, all the basic arithmetic is done in double precision. In upward recurrence calculations of the amplitude functions a_ℓ and b_ℓ , a numerical instability develops in certain situations. On the other hand, downward recurrence calculations of a_ℓ and b_ℓ always converge very rapidly and are insensitive to the assumed starting value. Therefore a_ℓ and b_ℓ are calculated by

means of a downward recurrence procedure, starting at $\ell > |m|\alpha$, where 0 is chosen as the initial value. The accuracy of the computed results was checked by comparison with data obtained from a different computer program. In this program a_ℓ, b_ℓ, π_ℓ and τ_ℓ are calculated directly, based on the definitions of the occuring functions. In all cases agreement of at least the first five significant figures was observed. Furthermore some results were compared with the data of Denman et al.(1966) and no difference was found.

In fig. 3, 4, 5 the intensity functions $i_\perp$ and $i_\parallel$ are shown for $m = 1{,}333$ as functions of α at the scattering angles $\theta = 15^o$, 45^o and $9o^o$, respectively. It can be seen that the curves are rather smooth at low values of α . With increasing α a ripple structure develops and some sharp spikes can be observed. This can be explained by the above mentioned resonance peaks for higher-order partial waves. The complexity of the curves increases with increasing scattering angle θ .

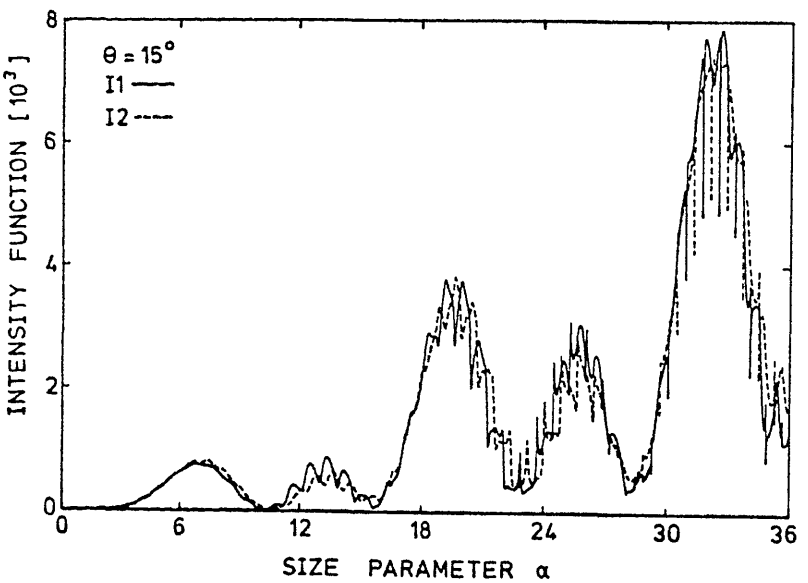

Fig. 3

Intensity functions $i_\perp$ (solid line) and $i_\parallel$ (broken line) as functions of α for $m = 1{,}333$ and scattering angle $\theta = 15^o$.

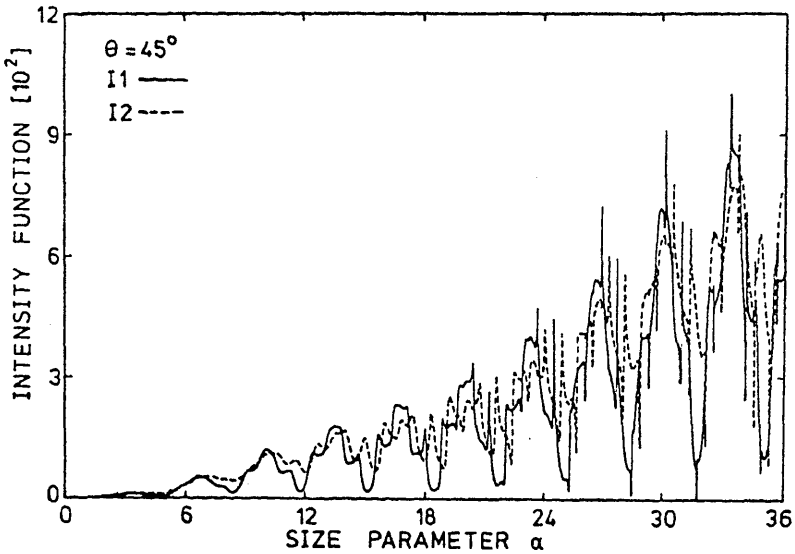

Fig. 4

As fig. 3 for θ = 45°

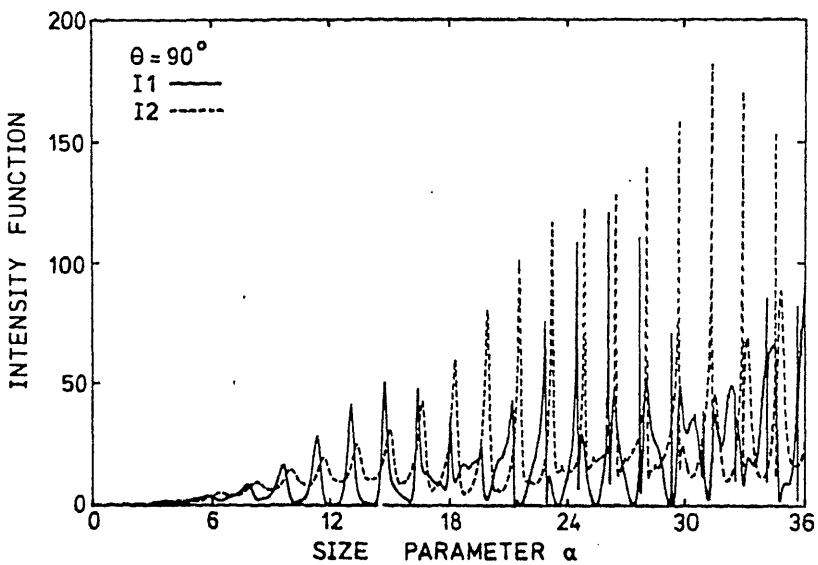

Fig. 5

As fig. 3 for θ = 90°.

Fig. 6, 7 show the intensity functions $i_\perp$ and $i_\parallel$ for m = 1,333 as functions of θ at the size parameters α = 3 and 3o, respectively. The comparatively smooth curves correspond to the superposition of several different partial waves. It turns out that the number of maxima is approximately equal to α . The curves for $i_\perp$ exhibit a somewhat more pronounced structure than the $i_\parallel$ -curves. For scattering angles close to the forward direction $\theta = 0$ the scattering intensity is much higher than for scattering angles around $\theta = \pi/2$. In the vincinity of the forward direction $\theta = 0$ and the backward direction $\theta = \pi$ it can be seen that $i_\perp \approx i_\parallel$. This ensures the continuity of the scattered intensity in the forward and backward direction. A three-dimensional plot of $i_\perp$ for m = 1,333 as a function of α and θ is shown in fig. 8.

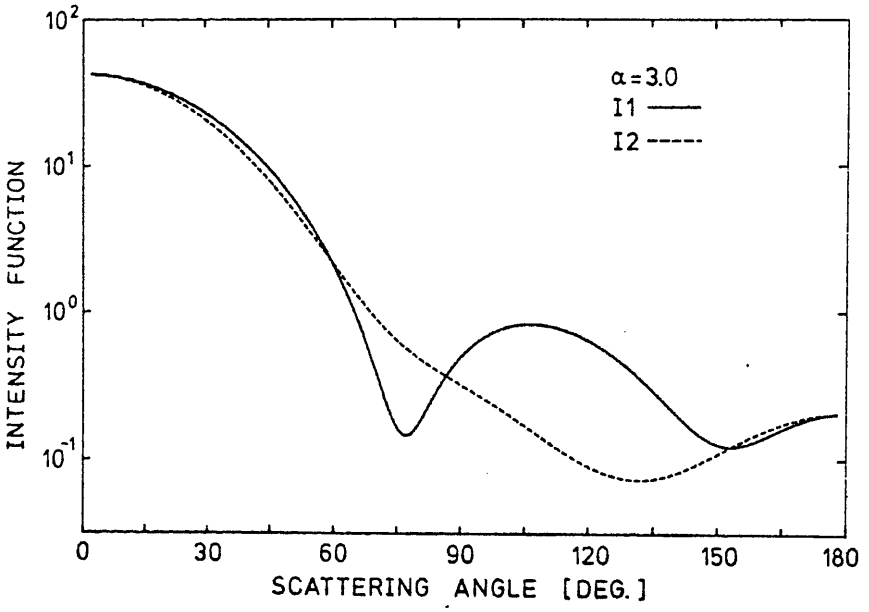

Fig. 6

Intensity functions $i_\perp$ (solid line) and $i_\parallel$ (broken line) as functions of θ for m = 1,333 and size parameter α = 3.

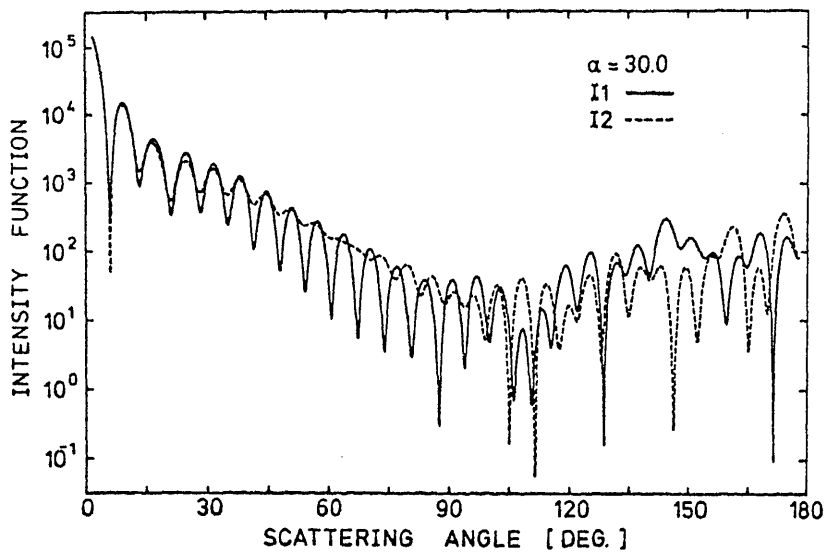

Fig. 7

As fig. 6 for α = 30.

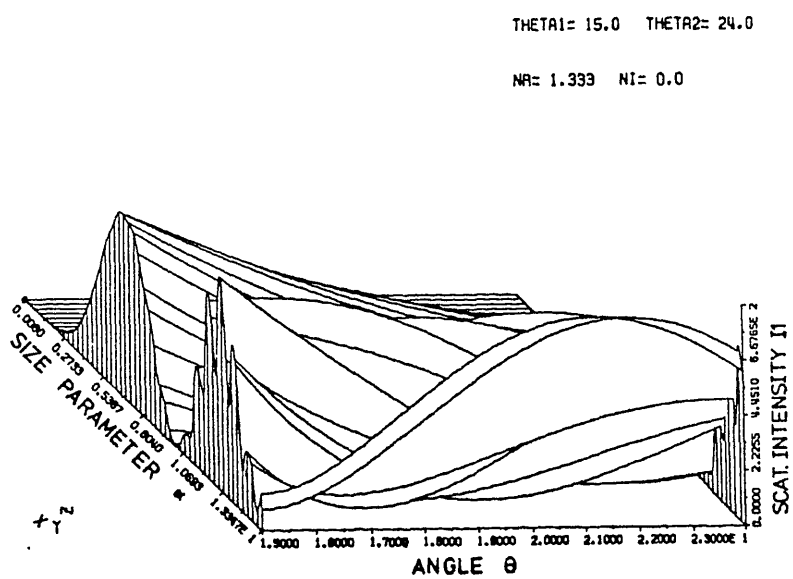

Fig. 8

Three-dimensional plot of $i_{\perp}$ as a function of α and θ for m = 1,333.

Fig. 9 illustrates the above mentioned resonance peaks for higher-order partial waves. The curves show the intensity functions $i_\perp$ for $m = 1{,}333$ as functions of the size parameter α for different scattering angles θ . In the considered α-interval a resonance peak can be observed. It can be seen that spikes occur at the same α-value for different scattering angles θ . However, due to interference with other partial waves, these spikes can be maxima or minima. At particular scattering angles the spikes disappear. In a three-dimensional plot, fig. 1o, a ridge can be observed at the α-value corresponding to the resonance peak.

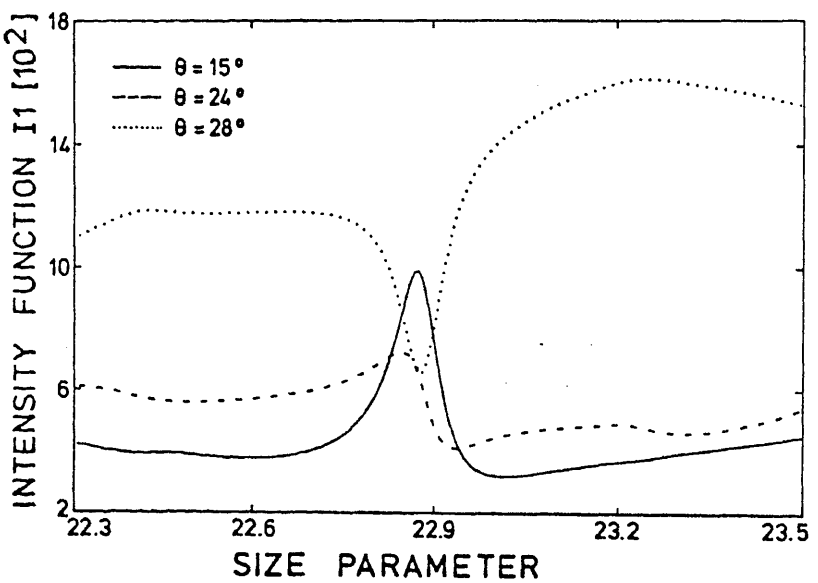

Fig. 9

Intensity functions $i_\perp$ as functions of the size parameter α for $m = 1{,}333$ and for scattering angles $\theta = 15^\circ$, 24° and 28°.

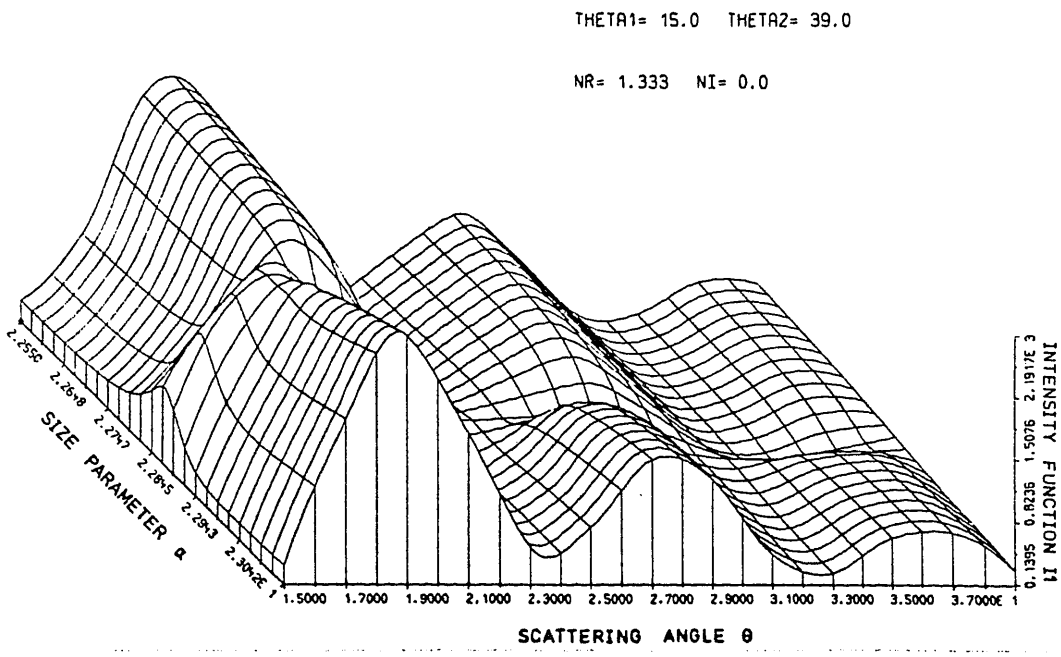

Fig. 10

Three-dimensional plot of $i_{\perp}$ as a function of α and θ for m = 1,333 and for α-values close to a resonance peak.

4.2 Scattering geometry

The droplets in the cylindrical measuring chamber are illuminated by a laser beam with diameter b. The total light flux, transmitted through the expansion chamber, is measured by an optoelement. Furthermore, the light flux, scattered by the droplets, is measured by a photomultiplier. The scattered light flux is defined by two stops, which are centered at a scattering angle θ_0 and determine the aperture ε of the light measuring system. The scattering angle θ_0 can be varied over a range from 15^0 (forward scattering) to 165^0 (backscattering).

Fig. 11 (not to scale) shows in principle the scattering geometry. The rectangular stop S_r with width w defines the section MV (scattering volume) of the laser beam LS, from where light is scattered into the photomultiplier PM. S_r is rectangular to ensure plane intersections of laser beam and observation beam. The circular stop S_c with diameter d and area $F_c = \pi d^2/4$ defines the light flux, scattered by each droplet inside the scattering volume MV, and entering the photomultiplier PM via the opal glass plate MG.

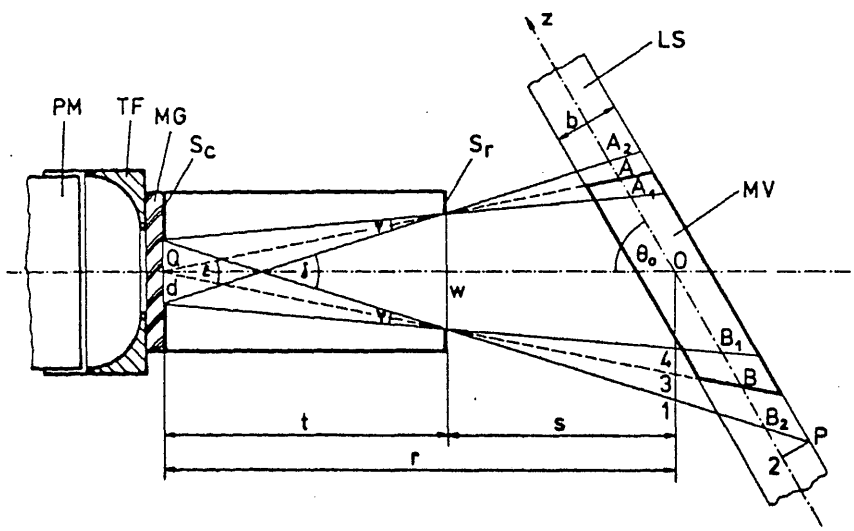

Fig. 11

Scattering geometry (not to scale) for light scattering measurements in the expansion chamber.

From fig. 11 it can be seen that the aperture ε is given by

$$\tan \frac{\varepsilon}{2} = \frac{w}{2t} \quad . \tag{4.27}$$

The length of the scattering volume is

$$L = \overline{OA} + \overline{OB} = r \sin \frac{\varepsilon}{2} \left[\frac{1}{\sin(\theta_o + \frac{\varepsilon}{2})} + \frac{1}{\sin(\theta_o - \frac{\varepsilon}{2})} \right]. \tag{4.28}$$

The scattering volume amounts to

$$V_s = \frac{\pi b^2}{4} \cdot L \quad . \tag{4.29}$$

The distance $\overline{OP}$ of the most distant point P of the scattering volume from the chamber axis can be determined from the equations

$$\overline{OI} = \frac{w}{2} \left[1 + \frac{(r-t)\ (d+w)}{wt} \right] \quad , \tag{4.3o-1}$$

$$\tan \frac{\delta}{2} = \frac{d + w}{2t} \quad , \tag{4.3o-2}$$

$$\overline{OB_2} = \overline{OI} \frac{\cos \frac{\delta}{2}}{\sin(\theta_o - \frac{\delta}{2})} \quad , \tag{4.3o-3}$$

$$\overline{B_2 2} = \frac{b}{2 \tan(\theta_o - \frac{\delta}{2})} \quad , \tag{4.3o-4}$$

$$\overline{OP} = \sqrt{(\overline{OB_2} + \overline{B_2 2}\ )^2 + b^2/4}. \tag{4.3o-5}$$

The actual dimensions of the experimental arrangement are

$r = 197$ mm
$t = 173$ mm
$d = 2$ mm
$w = 4$ mm
$b \cong 1{,}5$ mm.

Accordingly the aperture of the light measuring system is

$$\varepsilon = 1{,}32^{o}.$$

For a scattering angle $\theta_o = 15^o$ the scattering volume has a length of L = (8,44 + 9,2o) mm = 17,64 mm and amounts to V_s = 31,15 mm^3. The most distant point P has a distance

$$\overline{OP} = 13{,}o1 \text{ mm}$$

from the chamber axis, which is maller than the radius

$$\frac{D_{ch}}{2} = 2o \text{ mm}$$

of the expansion chamber.

Up to this point, the influence of the half-shade regions A_1A_2 and B_1B_2 has not been estimated. On the one hand, $\overline{AB}$ = L has been defined as the length of the scattering volume. On the other hand, the most distant point P of the scattering volume has been considered. Only inside the section A_1B_1 of the laser beam each droplet scatters light onto the whole circular stop S_c. The light scattered by each droplet inside the half-shade regions A_1A_2 and B_1B_2 only partly illuminates the circular stop S_c. Droplets outside the section A_2B_2 do not contribute at all to the light flux through stop S_c. For the calculations in section 4.3 it will be assumed that inside the section AB of the laser beam each droplet scatters light onto the whole circular stop S_c and outside this section the droplets do not contribute at all to the light flux through stop S_c. The so obtained light flux through stop S_c will be called calculated light flux as opposed to the actual light flux through stop S_c. The section AB will be considered as the scattering volume.

An estimate for the difference between calculated and actual light flux through stop S_c can be given as follows. The scattering intensity at the stop S_c, caused by all droplets inside a particular section MN of the laser beam, can be expressed as

$$I_s = C. \overline{MN} / R^2, \qquad (4.31\text{-}1)$$

where $\overline{MN}$ is the length of the section MN, R is the distance of the section MN from stop S_c and C is a proportionality factor. In general, C is dependent on the actual position of section MN, because the scattering intensity and the light extinction inside the measuring chamber vary over the angular range $\theta_o - \frac{\delta}{2}$ to $\theta_o + \frac{\delta}{2}$.

Accordingly, if all droplets inside the section MN scatter light onto the whole circular stop S_c, the light flux through S_c, scattered by all droplets inside the section MN, can be expressed as

$$\Phi_s = F_c \cdot C \cdot \overline{MN} / R^2 , \qquad (4.31\text{-}2)$$

where F_c is the area of stop S_c. The assumption, mentioned above, means that each droplet inside the sections AA_1 and BB_1 scatters light onto the whole stop S_c and the droplets inside the sections AA_2 and BB_2 do not contribute at all to the light flux through stop S_c. Actually, the light, scattered by each droplet inside the sections AA_1 and BB_1 only partly illuminates the stop S_c. However, after dividing section AA_1 into small segments, for each of these segments a corresponding segment of section BB_2 can be defined, so that droplets of corresponding segments together scatter light just onto the whole stop S_c. In order to compensate for the incomplete illumination of stop S_c by droplets from section AA_1, the scattering intensities at stop S_c, due to each two corresponding segments, would

have to be equal. As a consequence, also the total scattering intensities at stop S_c, due to the droplets of sections BB_2 and AA_1 would have to be equal. According to equ. (4.31-1), the total scattering intensities at stop S_c, due to the droplets of sections BB_2 and AA_1 can be expressed as $C_B\overline{BB_2}/\overline{QB}^2$ and $C_A\overline{AA_1}/\overline{QA}^2$, respectively. It can be seen that the total scattering intensity at stop S_c, due to the droplets of section BB_2 exceeds the total scattering intensity at stop S_c, due to the droplets of section AA_1, by an amount of $C_B.\overline{BB_2}/\overline{QB}^2 - C_A.\overline{AA_1}/\overline{QA}^2$. Accordingly, the incomplete illumination of stop S_c by droplets from section AA_1 will be <u>overcompensated</u> by droplets from section BB_2. Obviously, each droplet inside the section BB_2 will illuminate no more than half of the stop S_c. Therefore, the <u>additional</u> light flux through stop S_c, corresponding to the above mentioned <u>overcompensation</u> by droplets of section BB_2, does not exceed

$$\Phi_A = \frac{F_c}{2} \left(C_B \frac{\overline{BB_2}}{\overline{QB}^2} - C_A \frac{\overline{AA_1}}{\overline{QA}^2} \right) . \qquad (4.32\text{-}1)$$

With similar arguments it can be shown that the incomplete illumination of stop S_c by droplets from section BB_1 will be <u>undercompensated</u> by droplets from section AA_2. The <u>missing</u> light flux through stop S_c, corresponding to this <u>undercompensation</u> by droplets of section AA_2, does not exceed

$$\Phi_B = \frac{F_c}{2} \left(C_B \frac{\overline{BB_1}}{\overline{QB}^2} - C_A \frac{\overline{AA_2}}{\overline{QA}^2} \right) . \qquad (4.32\text{-}2)$$

Accordingly, the <u>actual</u> light flux through stop S_c is not <u>larger</u> than the <u>calculated</u> light flux by more than Φ_A and not <u>smaller</u> than the <u>calculated</u> light flux by more than Φ_B. The calculated scattered light flux can be expressed approximately as

$$\Phi_s = F_c \cdot C_o \frac{\overline{AB}}{\overline{QO}^2} = F_c . C_o . \frac{L}{r^2} . \qquad (4.33)$$

For the following, the maximum of the relative deviations of C_A and C_B from C_0 will be called $\Delta > 0$. Now according to equ. (4.32) the largest possible values for Φ_A and Φ_B can be expressed as

$$\Phi_A = \frac{F_c}{2} C_0 \left[(1 + \Delta) \frac{\overline{BB_2}}{\overline{QB}^2} - (1-\Delta) \frac{\overline{AA_1}}{\overline{QA}^2} \right], \tag{4.34-1}$$

$$\Phi_B = \frac{F_c}{2} C_0 \left[(1 + \Delta) \frac{\overline{BB_1}}{\overline{QB}^2} - (1 -\Delta) \frac{\overline{AA_2}}{\overline{QA}^2} \right]. \tag{4.34-2}$$

From equ. (4.33), (4.34) it can be concluded that the relative deviation of the actual light flux from the calculated light flux through stop S_c does not exceed.

$$\frac{\Phi_A}{\Phi_s} = \frac{r^2}{2L} \left[\frac{\overline{BB_2}}{\overline{QB}^2} - \frac{\overline{AA_1}}{\overline{QA}^2} + \Delta \left(\frac{\overline{BB_2}}{\overline{QB}^2} + \frac{\overline{AA_1}}{\overline{QA}^2} \right) \right], \tag{4.35-1}$$

$$-\frac{\Phi_B}{\Phi_s} = \frac{r^2}{2L} \left[\frac{\overline{AA_2}}{\overline{QA}^2} - \frac{\overline{BB_1}}{\overline{QB}^2} - \Delta \left(\frac{\overline{AA_2}}{\overline{QA}^2} + \frac{\overline{BB_1}}{\overline{QB}^2} \right) \right]. \tag{4.35-2}$$

From fig. 11 it can be seen that

$$\overline{QA} = r \frac{\sin \theta_0}{\sin(\theta_0 + \frac{\varepsilon}{2})} \tag{4.36-1}$$

$$\overline{QB} = r \frac{\sin \theta_0}{\sin(\theta_0 - \frac{\varepsilon}{2})} \tag{4.36-2}$$

$$\Psi \cong d / t \tag{4.36-3}$$

$$\overline{AA_1} \cong \overline{AA_2} \cong \frac{\Psi}{2 \sin \theta_o} (\overline{QA} - t) \tag{4.36-4}$$

$$\overline{BB_1} \cong \overline{BB_2} \cong \frac{\Psi}{2 \sin \theta_o} (\overline{QB} - t). \tag{4.36-5}$$

For the actual dimensions of the experimental arrangement and for a scattering angle $\theta_o = 15^o$ the following values are obtained:

$\overline{QA}$ = 188,89 mm

$\overline{QB}$ = 2o5,86 mm

$\overline{AA_1} \cong \overline{AA_2} \cong$ o,355 mm

$\overline{BB_1} \cong \overline{BB_2} \cong$ o,734 mm.

Accordingly, the volume of the half-shade regions amounts to approximately 12,3 % of the scattering volume.

The maximum relative deviation of the actual light flux from the calculated light flux, caused by the influence of the half-shade regions, can be calculated from equ. (4.35) for three different scattering angles θ_o as follows (Δ in %):

θ_o	$\Phi_A/\Phi_s \cong \Phi_B/\Phi_s$
15^o	(o.81 + o.o3oo .Δ) %
45^o	(o.22 + o.o3o5 .Δ) %
$9o^o$	o.o3o6 . Δ % .

From light scattering calculations the maximum relative variation $\pm \Delta$ of the scattering intensity over the angular range

$\theta_o - \frac{\delta}{2}$ to $\theta_o + \frac{\delta}{2}$ can be obtained for three different scattering angles θ_o and size parameters α as follows:

θ_o	α	Δ
15^o	6.83 (1.Max)	22,7 %
45^o	1o,o7 (3.Max)	12,7 %
$9o^o$	7,77 (4.Max)	18,1 % .

It can be concluded that the influence of the half-shade regions causes an error of less than $\pm$ 1,5 % for most practically important conditions.

4.3 Calculation of transmitted and scattered light fluxes

The total light flux Φ_{trans}, transmitted through the expansion chamber, and the scattered light flux Φ_{sca} for selectable, fixed scattering angles θ_0 were measured simultaneously as functions of time during the droplet growth process. On the other hand, Φ_{trans} and Φ_{sca} can be calculated for the above described scattering geometry by means of the Mie theory. For the following, the droplet concentration is assumed to be sufficiently small so that the mutual influence of the polarization fields of neighboring droplets and multiple scattering are negligible. Because the droplets are located randomly, no interference of scattered waves, originating from different droplets (dependent scattering) occurs. Accordingly, the total scattered intensity is the sum of the light intensities, scattered by each individual droplet. Furthermore it is assumed that the droplet aerosol has a unimodal size distribution with small relative standard deviation. As will be shown in section 5.3), under these assumptions the modal droplet radius a_M and the droplet number concentration C can be determined independently by comparison of experimental and theoretical values of the ratio Φ_{sca}/Φ_{trans}.

For calculation of Φ_{trans} the droplet aerosol is assumed at first to be strictly monodispersed. In order to determine the light extinction, caused by the droplets in the measuring chamber, a small segment of the laser beam is considered. $d\ell$ is the thickness and $f.d\ell$ is the volume of this segment, where f is a small part of the cross sectional area of the laser beam. According to the definition of the extinction cross section K_{ext}, one droplet removes the amount $I.K_{ext}$ from the incident light flux, where I is the intensity, incident upon the droplet.

The considered segment contains $C.f.d\ell$ droplets. Therefore the light flux, transmitted through this segment, is changed by the amount

$$d\Phi = - I.K_{ext}.C.f.d\ell \quad . \tag{4.37-1}$$

The corresponding change of the intensity is given by

$$dI = - I.K_{ext}.C.d\ell \quad . \tag{4.37-2}$$

The length of the laser beam inside the cylindrical expansion chamber is equal to the diameter D_{ch} of the chamber. Integration of equ. (4.37-2) over the length D_{ch} of the laser beam yields the equation

$$I_{trans} = I_o.\exp\,(-C.D_{ch}.K_{ext}) \tag{4.38-1}$$

for the transmitted intensity, where I_o is the primary intensity of the laser beam. In general, I_o varies over the cross section of the laser beam, the maximum of I_o being in the axis of the laser beam. Integration of equ. (4.38-1) over the cross section of the laser beam results in the expression

$$\Phi_{trans} = \Phi_o.\exp(-C.D_{ch}.K_{ext}) \tag{4.38-2}$$

for the transmitted light flux, where Φ_o is the primary light flux (power) of the laser beam. By generalization of equ. (4.38-2) for a droplet aerosol with normalized number size distribution p(a), the expression

$$\Phi_{trans} = \Phi_o.\exp(-C.D_{ch}.\int_0^\infty p.K_{ext}.da) \tag{4.39}$$

can be obtained.

For calculation of Φ_{sca} it is assumed that inside the section AB of the laser beam (fig. 11, 12) each droplet scatters light onto the whole circular stop S_c and outside this section the droplets do not contribute at all to the light flux through stop S_c. As shown in section

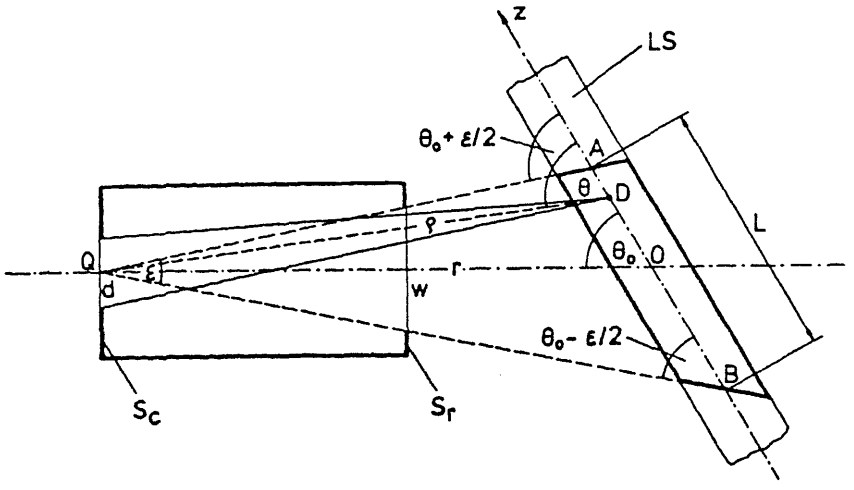

Fig. 12

Scattering geometry (not to scale) for calculation of the scattered light flux in the expansion chamber.

4.2), the so obtained calculated light flux is a good approximation for the actual light flux through stop S_c for most practically important conditions. The electric field vector of the linearly polarized incident wave is chosen to be perpendicular to the plane of observation ($\phi = \pi/2$). For the following, a z-coordinate is introduced in the axis of the laser beam (fig. 12), z = o being in the center O of the scattering volume .

The droplet aerosol is assumed at first to be strictly monodispersed. A single droplet D inside the scattering volume is considered (fig. 12). The intensity I_{dr} at stop S_c of the light, scattered by the droplet D, is determined by light scattering due to the droplet D and by light extinction inside the measuring chamber. From the entrance of the laser beam into the cylindrical expansion chamber until the exit of the scattered wave, the light passes over a distance, which is approximately equal to the diameter D_{ch} of the chamber. Therefore, according to equ. (4.11) and (4.38-1), the intensity I_{dr} can be

expressed as

$$I_{dr} = I_o \frac{\lambda^2}{4\pi^2 \rho^2} i_\perp(\theta) \exp(-C.D_{ch}.K_{ext}), \qquad (4.4o)$$

where I_o is the primary intensity of the laser beam, and ρ is the distance $\overline{QD}$ of the droplet D from stop S_c (fig. 12). As mentioned earlier, I_o generally varies over the cross section of the laser beam.

In equ. (4.4o) the scattered intensity is taken to be uniform over the area F_c of stop S_c. Accordingly, the flux Φ_{dr} through stop S_c, due to droplet D, is given as

$$\Phi_{dr} = I_{dr} \cdot F_c \quad . \qquad (4.41)$$

A volume element dv of the scattering volume V_s contains C.dv droplets. Therefore the light flux through stop S_c, due to all droplets inside dv, is given by $\Phi_{dr}.C.dv$. Integration over the scattering volume V_s yields the total scattered light flux Φ_{sca} through stop S_c, caused by all droplets inside the scattering volume:

$$\Phi_{sca} = C \cdot \int_{V_s} \Phi_{dr}\, dv. \qquad (4.42)$$

Inserting equ. (4.4o), (4.41) into equ. (4.42) and using equ. (4.38-2), the expression

$$\frac{\Phi_{sca}}{\Phi_{trans}} = \frac{\lambda^2}{4\pi^2} F_c.C.\int_L \frac{i_\perp(\theta)}{\rho^2}\, dz \qquad (4.43)$$

can be derived, where L is the length of the scattering volume (fig. 12). L can be calculated according to equ. (4.28).
It can be seen that the diameter b of the laser beam and the distribution of the primary light intensity I_o over the cross section of the laser beam do not enter the calculation of Φ_{sca}/Φ_{trans}, if

b is sufficiently small. For the evaluation of the integral in equ. (4.43) it can be assumed with good approximation that the droplet D is located on the axis of the laser beam (fig. 12). Then the linearization $\theta = \theta_o + (\varepsilon/L) \cdot z$ can be used for sufficiently small apertures ε, and by substitution of variables equ. (4.43) can be transformed into

$$\frac{\Phi_{sca}}{\Phi_{trans}} = \frac{\lambda^2}{4\pi^2} F_c . C . L \frac{1}{\varepsilon} \int_{\theta_o - \varepsilon/2}^{\theta_o + \varepsilon/2} \frac{i_\perp(\theta)}{\rho^2} d\theta \,, \qquad (4.44)$$

where the distance ρ can be expressed as

$$\rho^2 = r^2 - \frac{2 r L \cos\theta_o}{\varepsilon} (\theta - \theta_o) + \frac{L^2}{\varepsilon^2} (\theta - \theta_o)^2 . \qquad (4.45)$$

The aperture ε can be calculated according to equ. (4.27).

By generalization of equ. (4.44) for a droplet aerosol with normalized number size distribution p(a), the expression

$$\frac{\Phi_{sca}}{\Phi_{trans}} = \frac{\lambda^2}{4\pi^2} F_c . C . L \frac{1}{\varepsilon} \int_{\theta_o - \varepsilon/2}^{\theta_o + \varepsilon/2} \int_0^\infty p \frac{i_\perp(\theta)}{\rho^2} da \, d\theta \qquad (4.46)$$

can be obtained. For very small apertures ε the θ-integration need not be performed and equ. (4.46) reduces to

$$\frac{\Phi_{sca}}{\Phi_{trans}} = \frac{\lambda^2}{4\pi^2 r^2} \cdot F_c . C . L \int_0^\infty p . i_\perp(\theta_o) \, da . \qquad (4.47)$$

For numerical calculations p(a) was chosen to be a zeroth-order lognormal distribution

$$p(a) = \frac{1}{\sqrt{2\pi}\ \sigma\ a_M \exp(\sigma^2/2)}\ \exp\left[-\frac{(\log a - \log a_M)^2}{2\sigma^2}\right] , \quad (4.48)$$

where a_M is the modal radius and σ is the breadth parameter. For $\sigma^2 << 1$, σ is a good approximation for the relative standard deviation.

Fig. 13, 14 and 15 show Φ_{sca}/Φ_{trans} for a monodispersed aerosol as a function of the size parameter α, for $\theta_0 = 15^0$, m = 1,333, concentration C = 1 cm^{-3} and for apertures $\varepsilon = 1{,}32^0$, 8^0 and 15^0, respectively. By comparison with fig. 3 it can be seen that integration over an aperture of $\varepsilon = 1{,}32^0$ causes only small deviations from the unintegrated curve. At larger apertures stronger deviations can be observed. However, the ripple structure of the curves does not disappear. This is explained by the fact that resonance peaks occur at certain α-values irrespective of the scattering angle.

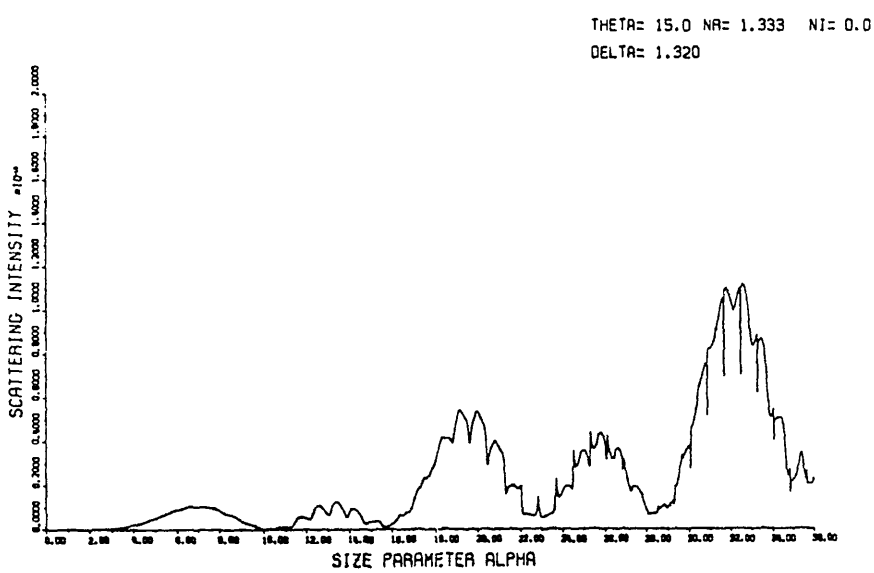

Fig. 13

Ratio of fluxes Φ_{sca}/Φ_{trans} as a function of the size parameter α for m = 1,333, $\theta_0 = 15^0$, concentration C = 1 cm^{-3} and aperture $\varepsilon = 1{,}32^0$. A monodispersed aerosol is assumed.

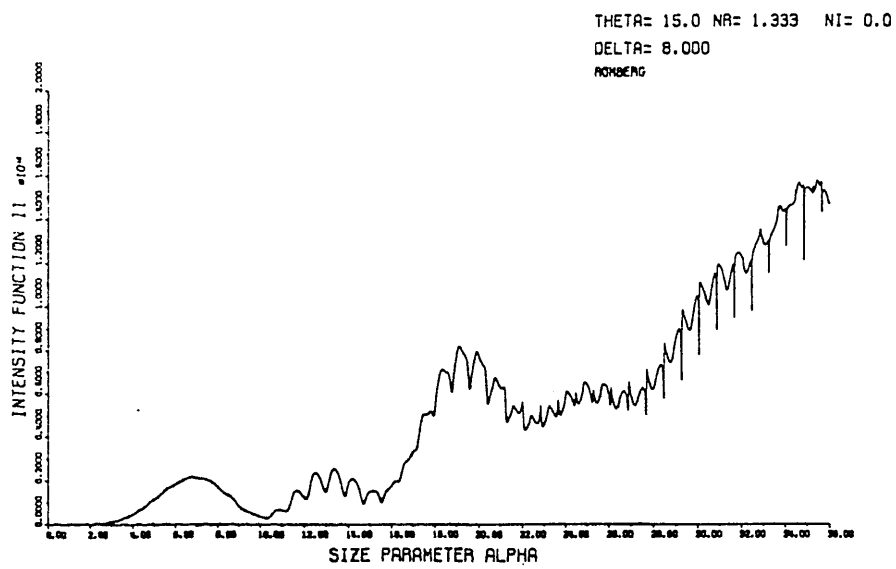

Fig. 14

As fig. 13, for $\varepsilon = 8^{o}$.

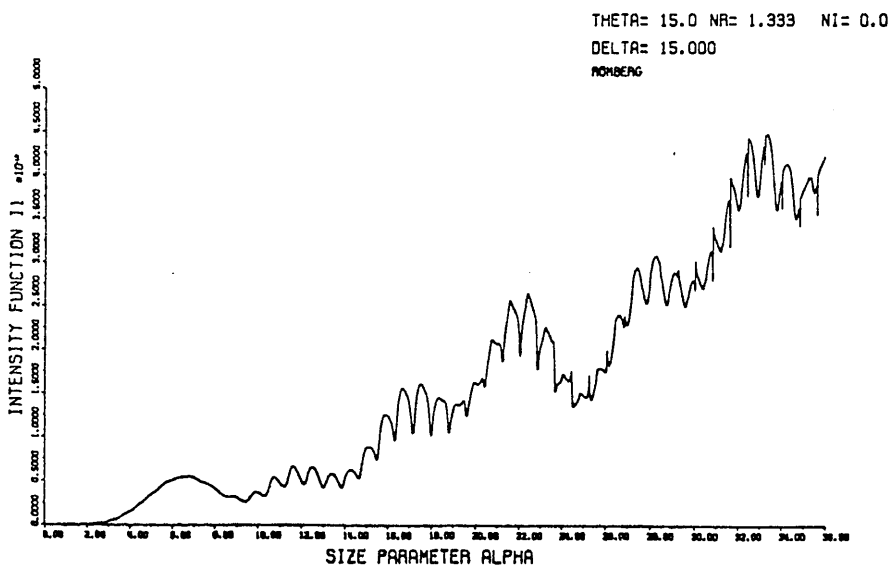

Fig. 15

As fig. 13, for $\varepsilon = 15^{o}$.

Accordingly, the ripple structure can only be smoothed by integration over a droplet size distribution. Fig. 16 shows Φ_{sca}/Φ_{trans} as a function of the modal size parameter α_M for $\theta_o = 15^o$, m = 1,333, C = 1 cm^{-3}, $\varepsilon = 1{,}32^o$ and for absolute standard deviations 1o nm and 3o nm. Comparison with fig. 13 shows that even at small absolute standard deviations several resonance peaks already disappear. At larger absolute standard deviations the ripple structure of the curves disappears completely.

In Fig. 17 the dependence of Φ_{sca}/Φ_{trans} on the scattering angle θ_o is demonstrated for modal size parameter α_M = 1o, m = 1,333, C = 1 cm^{-3} and $\varepsilon = 1{,}32^o$ for absolute standard deviations 1 nm and 25 nm. For highly monodispersed aerosols deep minima occur which become less pronounced as the standard deviation increases. Because these curves are very sensitive with respect to changes of α_M and/or σ, best fit procedures can be applied to determine α_M and σ independently (Kerker 1969).

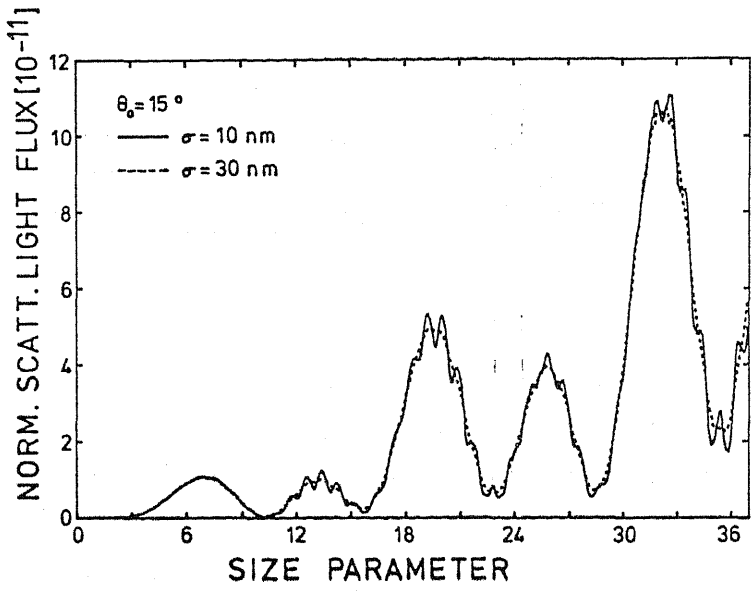

Fig. 16

Ratio of fluxes Φ_{sca}/Φ_{trans} as a function of the modal size parameter α_M for m = 1,333, $\theta_o = 15^o$, C = 1 cm^{-3}, $\varepsilon = 1{,}32^o$ and for absolute standard deviations 1o nm (solid line) and 3o nm (broken line). A zeroth order lognormal size distribution is assumed.

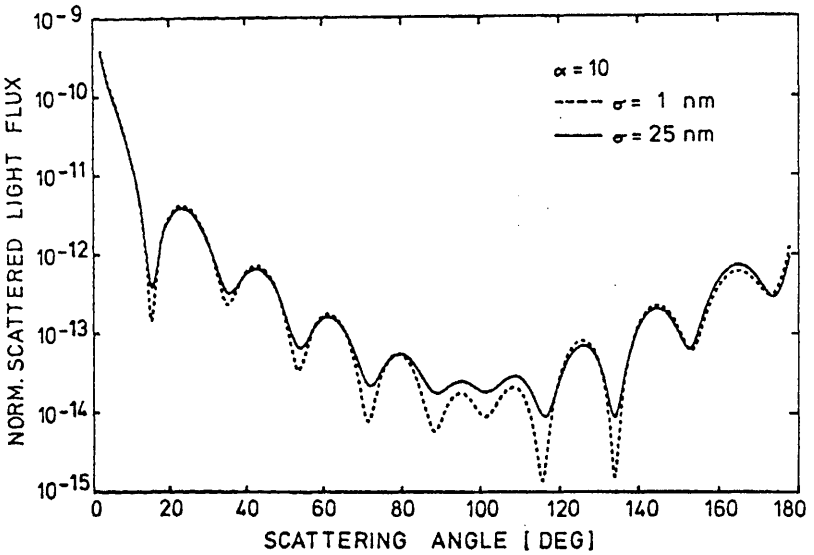

Fig. 17

Ratio of fluxes Φ_{sca}/Φ_{trans} as a function of the scattering angle θ_o for m = 1,333, α_M = 1o, C = 1 cm^{-3}, $\varepsilon = 1{,}32^o$ and for absolute standard deviations 1 nm (broken line) and 25 nm (solid line). A zeroth order lognormal size distribution is assumed.

5) DESIGN OF THE SIZE ANALYZING NUCLEI COUNTER SANC

The development of an experimental apparatus for investigations of condensation processes in supersaturated vapors was started more than ten years ago by Riediger (197o, 1971). Subsequently the expansion chamber was redesigned by Wagner (1974 a) in order to allow light scattering measurements over a wide range of scattering angles. Using a continuous-wave He-Ne laser as a light source, quantitative determinations of droplet size and concentration were performed. In order to ensure well-defined humidification of the condensation nuclei aerosol, the measuring cycle was newly designed by Pohl (1979 a). Furthermore Pohl developed an interface between the experiment and a digital computer. Complementary to this interface is a general-purpose interface, developed by Weber (1975) and Schindler (1975), which is integrated into the computer system. Presently a Ph.D. thesis on droplet size distributions and light scattering resonances is performed by W. Szymanski. Some of the recent results will be included in the present report.

5.1 Experimental arrangement

A pressure-defined expansion chamber is used for investigations of heterogeneous nucleation and droplet growth in supersaturated vapor. The principles of operation are described in section 3.1). Figure 18 shows a block diagram of the data acquisition and process control system of SANC.

The condensation process in the expansion chamber EXP is observed optically. The growing droplets are illuminated by a continuous-wave He-Ne laser. The light flux, transmitted through the expansion chamber, is measured by an optoelement OPT. The light flux scattered by the growing droplets under a fixed scattering angle, is monitored by a photomultiplier PM with a high-voltage

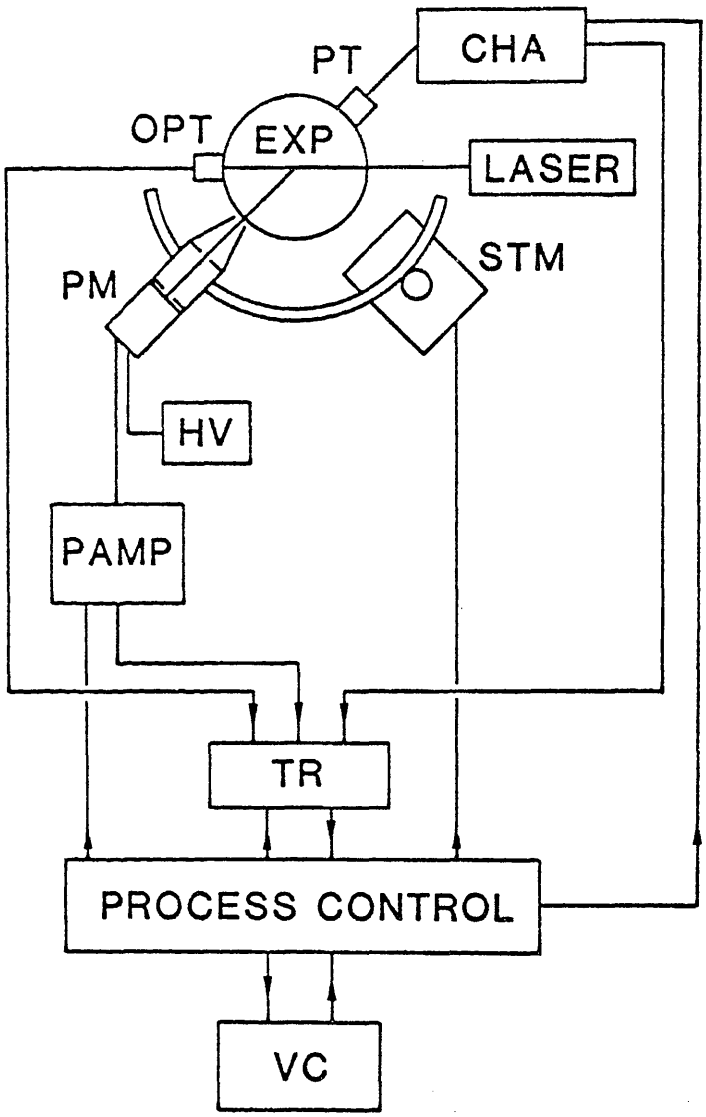

Fig. 18:
Data acquisition and process control system of SANC

power supply HV. The scattering angle can be varied over a range from 15^{0} to 165^{0} by means of a process controlled step-motor STM. The anode current of the PM is converted into a voltage signal and amplified by a process controlled amplifier PAMP. The scattered light flux varies over several orders of magnitude depending on the scattering angle and the droplet concentration.

Therefore it is necessary that the amplification of the PAMP can be adjusted automatically. The total pressure in the expansion chamber is measured by a fast piezoelectric pressure transducer PT in connection with a charge amplifier CHA.

The output signals of the optoelement OPT (transmitted light flux), the process controlled amplifier PAMP (scattered light flux), and the charge amplifier CHA (total pressure) are recorded simultaneously by a process controlled digital transient recorder TR. After a measuring cycle is completed, the recorded data are transferred into the computer and stored on magnetic tape. Furthermore, the scattering angle is measured by means of a calibrated potentiometer and the temperatures of humidifier (see below) and expansion chamber are determined.

5.2 Measuring cycle

In order to obtain good reproducibility, the measuring process is controlled by an electronic valve control unit VC (fig. 18) in connection with five solenoid valves. VC determines the timing of the experiment and interacts with the process control system. Fig. 19 shows a flow diagram of SANC.

At the beginning of each measuring cycle the expansion valve V2 is closed, inlet valve V1, separation valve V3, pressure release valve V5 are opened and two way valve V4 is in the position 1 - 3 (flush position). The expansion chamber EXP and the vessels R1, R2 are at atmospheric pressure. Condensation nuclei are generated in a condensation nuclei source CN. The nuclei aerosol is drawn through the humidifier HUM and the expansion chamber EXP by means of pump P1. Thus the expansion chamber is flushed with humidified condensation nuclei aerosol. The flushing flowrate can be adjusted by means of the needle valves NV1 and NV2, usually a flushing

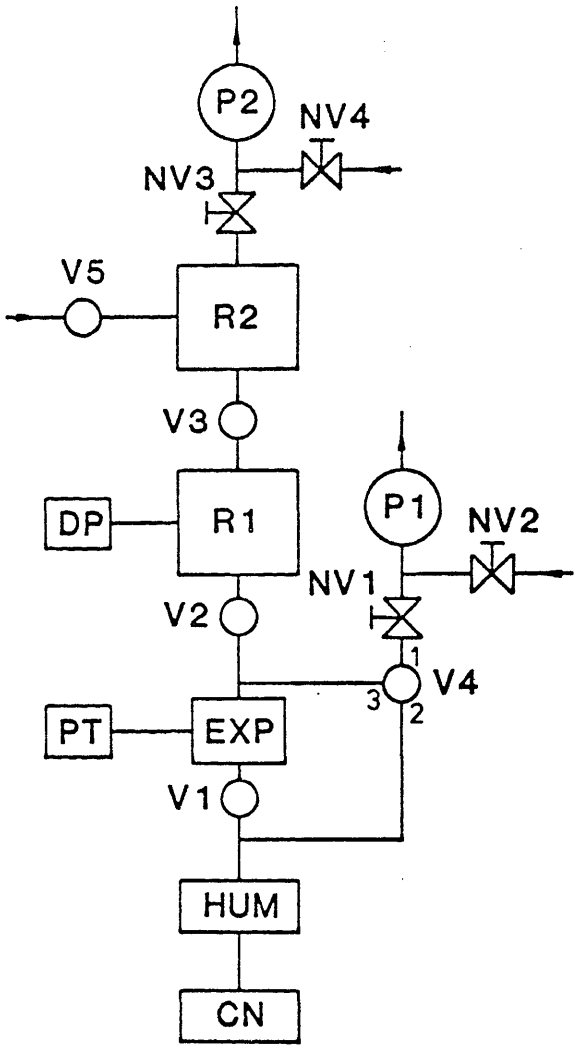

Fig. 19:
Flow diagram of SANC

flowrate of approx. 2 l/min is chosen. The flushing time can be varied between 7 and 65 s, usually a flushing time of approx. 2o s is set. The flushing time is terminated by switching of V4 into position 1 - 2 (bypass position). Simultaneously valve V5 is closed and evacuation of R1 and R2 by means of pump P2 is initiated.

Pump P1 in connection with the two-way valve V4 (bypass valve) ensures constant aerosol flow through the humidifier HUM during the whole measuring cycle and thereby a well-defined humidification of the nuclei aerosol. At no time during the measuring cycle valves V1 and V2 are open simultaneously. Accordingly, the flow conditions in the humidifier and thus the humidification of the nuclei aerosol are independent from the low-pressure system R1, R2.

The delay time of the aerosol in the expansion chamber from the switching of V4 into the bypass position until the closing of valve V1 (inlet valve) can be varied between 7 and 65 s, usually a delay time of approx. 2o s is set. During this time the aerosol in the expansion chamber reaches pressure and temperature equilibrium.

Before the end of the delay time a preset subpressure must be obtained in vessel R1. Therefore the subpressure in R1 is measured by a differential pressure transducer DP and compared with a preset value. When the preset subpressure is reached, valve V3 (separation valve) is closed thereby terminating the evacuation of R1. Now the pressure in R1 remains constant, vessel R2 is used as a buffer volume for pump P2. The pumping flowrate can be adjusted by proper setting of the needle valves NV3 and NV4. The subpressure in vessel R1 and accordingly the expansion ratio can be varied over a wide range.

Approximately 6 s after the inlet valve V1 has been closed, the expansion in the expansion chamber is initiated by opening of valve V2 (expansion valve). In order to obtain a fast pressure drop, V2 is opened by applying twice the normal operating voltage. During and after the expansion the actual measurements are performed. After a time interval of approximately o.7 s V2 is closed thus separating expansion chamber and humidifier from the low-pressure system R1, R2.

About 6 s after the expansion V5 and V3 are opened and R1, R2 are at atmospheric pressure again. Finally the bypass valve is switched into the flush position and the inlet valve is opened thereby starting the next measuring cycle.

5.3 Measuring principle

Figure 2o shows a typical set of experimental curves. The upper curve shows the total pressure in the expansion chamber and the lower curves show the transmitted and scattered light fluxes as functions of time. For technical reasons, the transmitted flux is shown inverted. A forward scattering angle of 15^{o} was chosen.

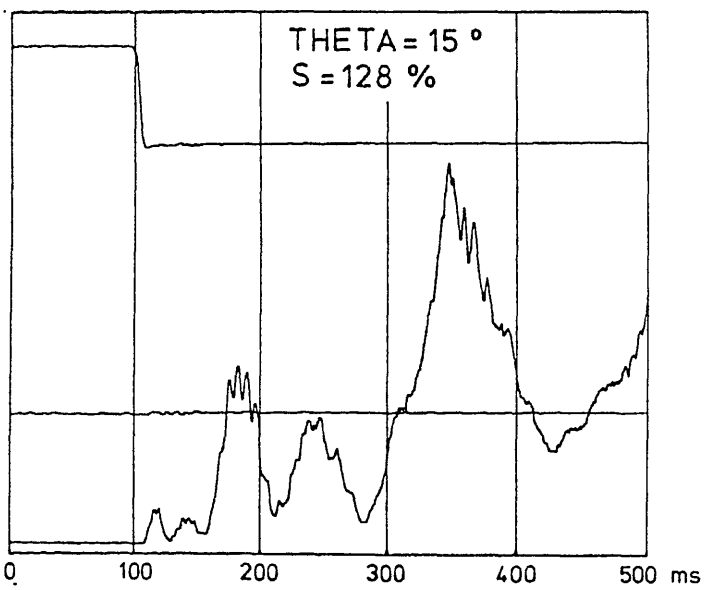

Fig. 2o:

Typical set of experimental curves: Total pressure, transmitted light flux and scattered light flux as functions of time. The transmitted flux is inverted. The scattering angle is 15^{o} in the forward direction.

It can be seen that the expansion process has a duration of 5 - 7 ms and is completed before the droplets grow to detectable sizes. Therefore the expansion process is assumed to by dry-adiabatic. A more detailed discussion of this point can be found in sections 8.2), 9.1) and 9.2). Accordingly the initial saturation ratio $(S_\infty)_0$ and the initial temperature $(T_\infty)_0$ at the end of the expansion can be calculated from experimentally determined thermodynamic parameters by means of the equations in section 3.3). The total pressure drop Δ_p can be obtained directly from the pressure vs. time curve. The initial total gas pressure p_i before the expansion in the expansion chamber is equal to the atmospheric pressure, which is measured by an absolute mercury barometer. The temperature T_B of the humidifier and the temperature T_i of the expansion chamber are determined by thermostats.

Comparison of the lower curve in fig. 2o (experimental scattered light flux) with the theoretical curves in fig. 13 and 16 shows good agreement (Wagner, 1973). Therefore it can be concluded that the droplet aerosol in the expansion chamber is quite monodispersed. A conceivable influence of multiple and dependent scattering can be ruled out for the present experimental conditions. A quantitative experimental determination of the droplet size distribution is described in section 8.1). This agreement of experimental and theoretical curves allows an independent quantitative determination of droplet size and concentration. To this end a one-to-one correspondence between experimental and theoretical light scattering extrema must be established. Three different methods seem feasible for this purpose (Wagner, 1975 b):

1) Identification of the first Mie maximum. This identification turns out to be rather simple and can be performed uniquely at low forward scattering angles. However, as can be seen from figures 3, 4, 5, the complexity of the Mie-curves increases,

the scattering intensities strongly decrease and therefore a unique determination of the first Mie maximum becomes more difficult with increasing scattering angle.

2) Comparison of light scattering data under various scattering angles. For scattering angles, where a unique identification of the first Mie maximum is difficult, particular light scattering extrema can be uniquely identified by comparison with light scattering curves for different scattering angles.

3) Measurement of a light flux vs. scattering angle curve at a specific droplet size by successive variation of the scattering angle during several measuring cycles. This method provides a conclusive test of the correct one-to-one correspondence between experimental and theoretical light scattering extrema.

In most cases scattering angles were chosen, where method 1) could be applied. In some cases method 2) was used as an additional test. In connection with the determination of the droplet size distribution (see section 8.1)) the one-to-one correspondence was verified by means of method 3).

After establishing the unique correspondence between experimental and theoretical light scattering extrema, droplet size and droplet concentration can be determined independently. From the position of the experimental light scattering extrema the droplet size at specific times can be obtained. On the other hand, from the height of the experimental maxima the droplet concentration can be evaluated. Particularly at high droplet concentrations, the light extinction in the expansion chamber must be taken into account. As explained in section 4.3), the scattered light suffers approximately the same extinction as the transmitted light. Therefore the effect of light extinction on the scattered light can be eliminated by

dividing the scattered light flux Φ_{sca} by the transmitted light flux Φ_{trans}. From the ratio of fluxes Φ_{sca}/Φ_{trans}, measured at a particular light scattering maximum, the droplet concentration C can be calculated according to equ. (4.44), (4.46) or (4.47). It should be stressed that the above described method for measurement of droplet concentration does not depend on any external standard or empirical calibration. Accordingly, the SANC can be regarded as an "absolute" condensation nuclei counter.

6) EXPERIMENTAL APPARATUS AND CALIBRATION

6.1 Mechanical equipment

6.1.1 Expansion chamber

The design of the expansion chamber was determined by the following features:

1) Constant and uniform temperature in the measuring volume,
2) Reproducible and uniform flushing of the chamber
3) Fast, nearly dry-adiabatic expansion
4) Wide range of scattering angles for light scattering measurements,
5) Small aperture of the measuring system for scattered light,
6) Negligible light reflexions inside the chamber volume
7) Prevention of mechanical vibrations of the chamber during and after the expansion
8) Possibility to insert a rubber membrane for separation of expansion chamber and low pressure system (see section 9.2)).

Figure 21 shows a top view and figure 22 a side view of the expansion chamber. The connector to the expansion valve is shown in figure 23.

The chamber is fixed on a table T, which is standing on an optical bench. The chamber consists of a lower part U, a middle part M, an upper part O and an outlet part D, which are connected by screws. In all these parts central holes of various diameters are provided, which form the aerosol inlet E, the chamber volume and the chamber outlet A. In U, M and O holes and rectangular channels L are provided for circulation of the thermostating liquid. The chamber volume on the one hand and the thermostating channel L on the other hand are sealed by means of teflon tape between T, U, M, O and D.

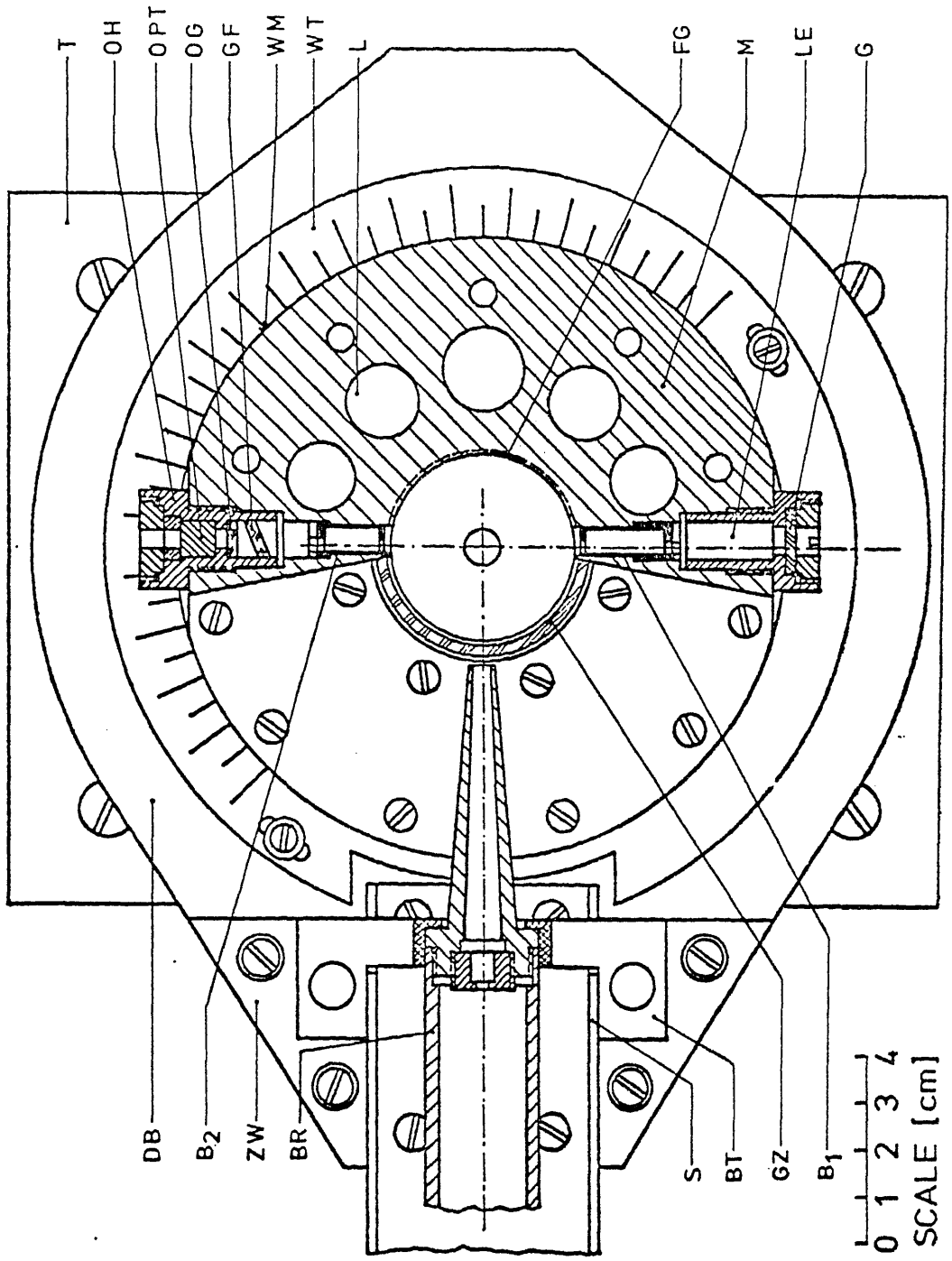

Fig. 21:

Top view of the expansion chamber

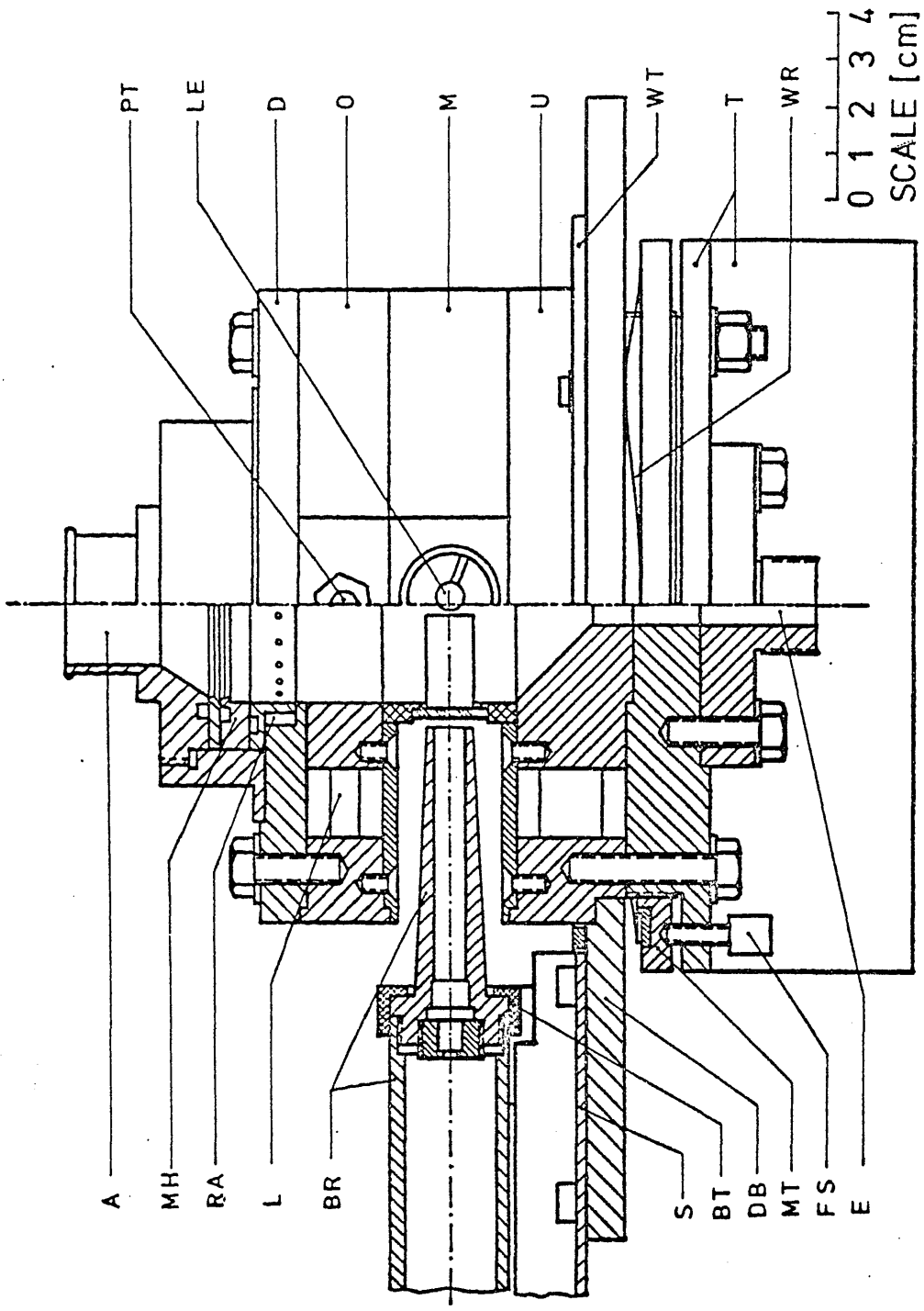

Fig. 22:

Side view of the expansion chamber

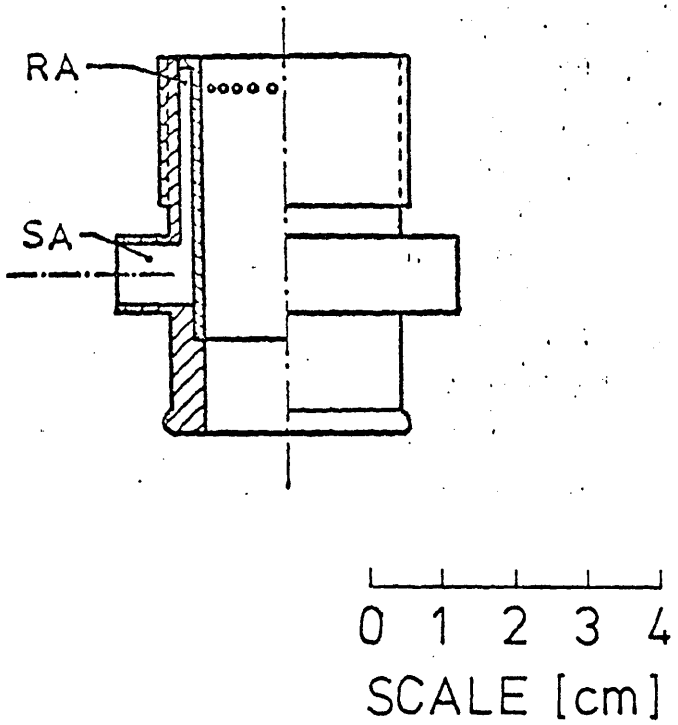

Fig. 23:
Connector C between PVC-tubing and expansion valve

On the bottom side of the table T a connector E is provided, which bears a thread for connection of the inlet valve to the expansion chamber. Furthermore a hole and a tubing connector (not shown in fig. 21, 22) form the inlet for the thermostating liquid.

Part U is the bearing for the support DB of the measuring system for scattered light. This system consists of a photomultiplier (not shown in fig. 21, 22) and a tube BR with several stops, which determine the aperture. DB can be rotated in order to set the

scattering angle. By means of a nut MT and a spring WR, the support DB is pressed against U. The nut MT can be fixed in a particular position by means of the screw FS. The actual scattering angle can be read off from an angular scale WT, which is adjustable relative to DB. The scattering angle can be set by hand or by means of a process controlled step motor (not shown in fig. 21, 22), which is attached to the table T. The step motor STM (Valvo, Philips, mod. PD 2o, 99o4 1122ooo1) is controlled by an electronic control unit (Valvo, Philips, mod. 99o4 131o3oo4) and powered by a 5 V power supply (Oltronix, mod. B 3oo D). A wheel on the motor axis is connected mechanically to a ten-turn potentiometer for precise determination of the scattering angle. The limiting angular positions of DB are electrically sensed by means of two microswitches. The ten-turn potentiometer and the microswitches are powered by the 1o V interface power supply (see section 6.4.2).

Part M bears a central hole with a diameter of 4 cm forming part of the chamber volume. As can be seen in fig. 21, a sector is removed from part M and thus the chamber volume can be observed optically through a glass cylinder GZ. The laser beam enters through a light inlet part LE with glass window G. The transmitted light flux is measured by the optoelement OPT installed in a support OH. Light scattering measurements can be performed over an angular range from 15^{o} to 165^{o}. The sensitive volume for light scattering is located in the center of the chamber volume sufficiently far away from the chamber walls so that wall effects are negligible (see sections 4.2) and 9.1)). In order to reduce light reflexions inside the chamber volume, the chamber wall bears a fine thread FG, which is painted flat black.

In part O the piezoelectric pressure transducer PT (Kistler, Mod. 7o31) is inserted just above the light inlet part LE. This pressure transducer has a rise time of 5 µs. An upper frequency

limit of 18o kHz is chosen at the charge amplifier CHA (Kistler, Mod. 5oo1). PT was calibrated against a Hg- and a H_2O-manometer with mirror scale and magnifying glasses. By proper readjustment of the charge amplifier (conversion factor = 53,75 pC/at) the deviations were reduced to less than $\pm$ o,2 % over a pressure range from 0 to o,65 bar. Thereby the excellent linearity of PT is demonstrated. In order to check, if changes of the gas temperature in the chamber have an effect on the pressure transducer PT, the transducer was thermally isolated for some experiments by means of silicone rubber. No differences could be observed and accordingly the silicone rubber was removed. At first, strong pressure oscillations immediately after the expansion had been observed, as can be seen from figure 24. These oscillations turned out to be sound vibrations due to the particular arrangement of expansion chamber, expansion valve and vessel R1. By inserting some damping material into R1, these sound vibrations have been practically eliminated, as shown in figure 25, without slowing down the pressure drop.

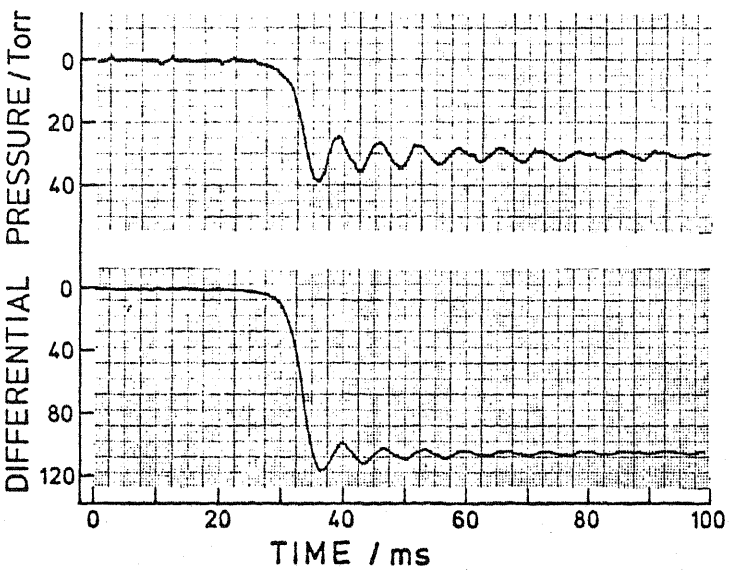

Fig. 24:

Pressure vs. time curves showing oscillations after the expansion.

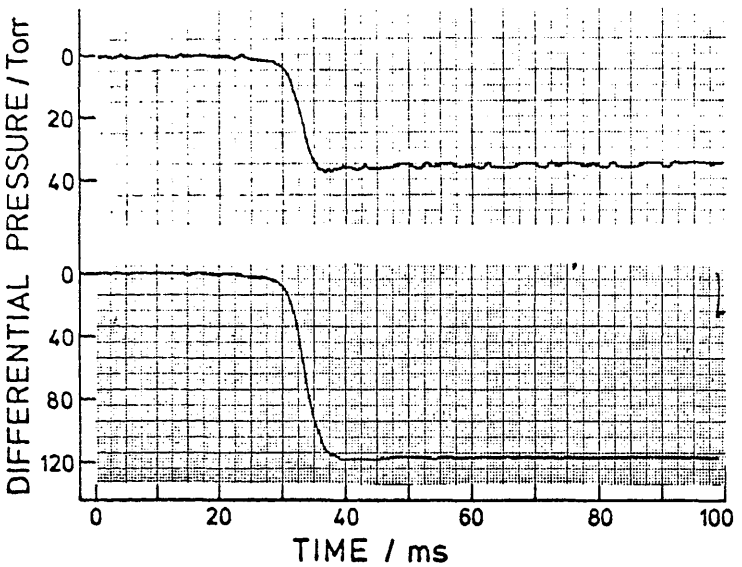

Fig. 25

Pressure vs. time curves after inserting damping material into R1.

The outlet part D essentially consists of the aerosol outlet, the connector A to the expansion valve and the outlet for the thermostating liquid. The expansion valve is connected to part A by means of PVC-tubing in order to prevent mechanical vibrations of the chamber during and after the opening of the expansion valve. The connector C between PVC-tubing and expansion valve is shown in figure 23. As can be seen in fig. 22 and 23, part D as well as connector C bear a number of small holes, a ring-channel RA and an aerosol outlet SA. By means of pump P1 (Leybold-Heraeus, mod. Minni A) the aerosol is drawn through these holes in order

to achieve uniform flushing of the chamber. For certain experiments a rubber membrane was inserted into the outlet part D by means of a support ring MH (see section 9.2)). If the rubber membrane was inserted, the chamber was flushed by drawing the aerosol through the holes in part D. Usually measurements are performed without using a rubber membrane. In this case it turned out that better reproducibility and uniformity of the aerosol in the chamber is achieved by drawing the aerosol through the holes in connector C. This procedure has the advantage that nearly the whole volume, all the way up to the expansion valve, can be flushed with fresh, humidified aerosol (see section 9.2)).

The expansion valve is connected to vessel R1. In R1 a well-defined subpressure is obtained prior to the expansion process by means of pump P2 (Rietschle, mod. RTE 2 DV). The pressure in R1 is measured by a strain-gauge-type differential pressure transducer DP (fig. 19) (Philips, Mod. PR 9356 ED/5o HM) in connection with a 1o V power supply (Delta Eletronika, mod. UD 15-1oo). The output signal of DP, which never exceeds 5o mV, is amplified by means of a chopper amplifier (Knick, Mod. MV). Then an offset correction of the amplified signal is performed and the chopping frequency is filtered by means of a two-stage passive filter. The required DC-voltages of ± 12 V for the offset correction circuit are provided by a NIM-chassis (Oltronix, mod. NIMPAC 9o-6). The amplification and the corresponding offset correction can be switched for two pressure ranges. In order to improve the reproducibility of the pressure measurement in R1, the differential pressure transducer is held at constant temperature. Thereby a reproducibility of the saturation ratio S_o in the expansion chamber better than ± o,1 % of S_o in the range S_o = 1o2 - 11o % and better than ± o,5 % of S_o in the range S_o = 11o - 35o % is achieved.

The volume of the expansion chamber amounts to approximately 131 cm^3, the vessel R1 has a volume of 315o cm^3, about 24 times as much as the chamber volume. Therefore changes of the total pressure in the expansion chamber after the expansion and during the droplet growth process will be negligible (see section 3.1)). Accordingly, the expansion chamber can be regarded as a pressure-defined chamber.

6.1.2 Humidifier

Before the condensation nuclei aerosol enters the expansion chamber, vapor saturation is achieved in a humidifier. All experiments, described in the present report, were performed with water vapor.

The humidifier consists of a rectangular vessel with a length of about 1 m. It is held at constant temperature by means of thermostating liquid, which is circulated around the outside of the vessel. The inside walls of the vessel are covered with teflon foil. Inside the vessel stands a gold-plated metal frame. Filter paper, as used in gas chromatography, is stretched over the metal frame. The bottom of the rectangular vessel is covered with distilled water in order to keep the filter paper wet. The total volume of the humidifier amounts to about 2ooo cm^3, the wet surface has a total area of approximately 29oo cm^2. Riediger (197o) performed gravimetric measurements of the humidity at the exit of the humidifier as a function of flowrate and temperature. Based on his results a temperature of 28°C and a flowrate of 2 l/min were chosen as standard conditions for most experiments.

In order to prevent losses of vapor in the connection tubes between humidifier, expansion chamber and expansion valve, these tubes, the inlet and the expansion valve are heated by means of two heating tapes, which are powered by two variable AC-power supplies. Using a pair of thermocouples, it is monitored that

the temperature of the connection tubes is higher than the temperature T_B of the humidifier.

A two-stage thermostating system was chosen. Two thermostats T1 and T2 (Lauda, mod. NB-D8/17, with Relais Box R2) are used for independent determination of the temperatures of humidifier and expansion chamber. For both thermostats the temperature regulation has PID-characteristics (proportional, integral, differential) (Lauda, PID-regulator R 25). The cooling coils of T1, T2 are held at a temperature slightly lower than the temperatures of humidifier and expansion chamber by means of a thermostat T3 (Lauda, mod. NB-D8/17, with Relais Box R2). In addition,T3 is used for thermostating the differential pressure transducer DP (fig. 19). The cooling coil of T3 is cooled by tap water.

For most experiments the chamber temperature was chosen to be somewhat higher than the humidifier temperature. This ensures a well-defined undersaturation in the expansion chamber before the expansion. The thermostats T1 and T2 are monitored continuously by measuring the temperature difference between chamber and humidifier using thermocouples, and recoding the data on a strip chart recorder. (Siemens, mod. M2-B186). It was found that the temperature variations of humidifier and chamber are smaller than $\pm$ o,o1^{o}C. The absolute temperatures were measured by calorimeter thermometers with a resolution of 1/1oo^{o}C. These thermometers have previously been calibrated against a standard Pt-resistance-thermometer at the Österreichisches Bundesamt für Eich- und Vermessungswesen with an accuracy better than $\pm$ o,o2^{o}C.

6.1.3 Aerosol generator

For measurements of droplet size distribution (section 8.1)) and droplet growth (section 8.2)) NaCl-particles were used as condensation nuclei. Figure 26 shows a schematic diagram of the

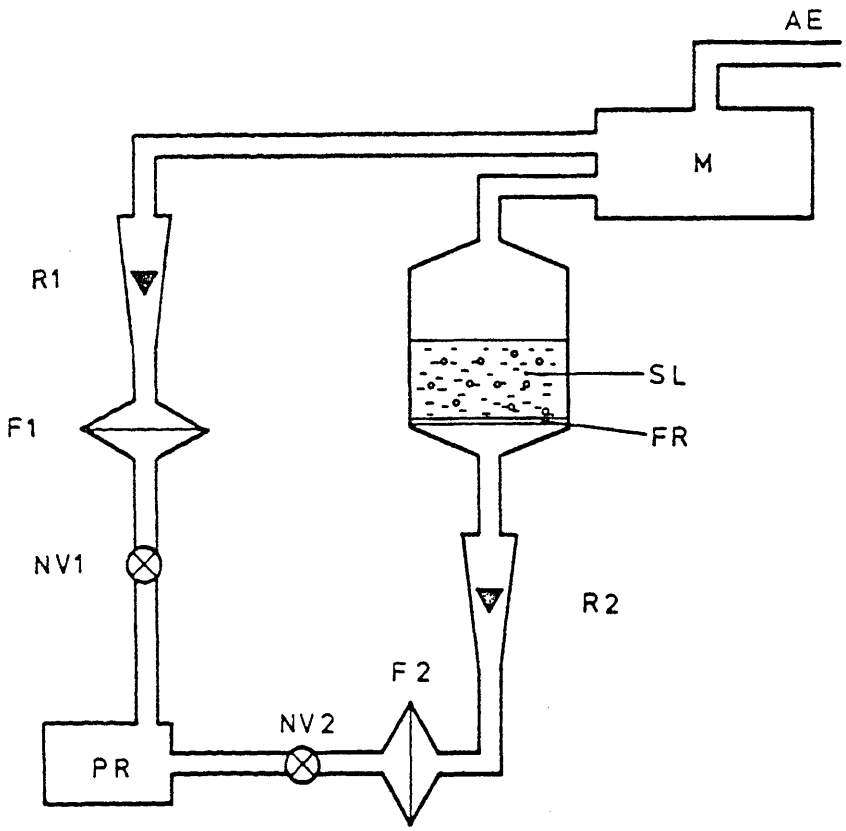

Fig. 26

Schematic diagram of the NaCl-aerosol generator.

NaCl-aerosol generator. Dry, oilfree compressed air flows from a compressor PR through a needle valve NV2, an absolute filter F2 and a flowmeter R2. Then the filtered air passes through fritted glass FR into an approximately 1 % NaCl-solution SL. The airbubbles reaching the liquid surface burst and produce solution droplets, which are carried away by the air flow. For reduction of the droplet concentration and for drying of the particles, filtered air is necessary. It is obtained from PR by filtering in filter F1. Aerosol and filtered air are mixed

in a 1o l-mixing vessel M and the solution droplets evaporate. The aerosol is available at the aerosol outlet AE. The concentration of the produced NaCl-aerosol can be varied from some 1oo to several 1oo.ooo cm^{-3} depending on the settings of the flowrates and needle valves. The concentration of the produced NaCl-aerosol is monitored continuously by means of a commercially available condensation nuclei counter (General Electric, Mod. CNC - 2) (Haberl, 1977). The variations of the number concentration readings were found to be smaller than $\pm$ 5 % during a time of 5 hours.

6.2 Optical arrangement

The geometry of the optical arrangement and the actual dimensions are presented in section 4.2). The calculations of the transmitted and scattered light fluxes according to the Mie-theory are described in section 4.3).

6.2.1 Light source

A continuous wave He-Ne laser (Spectra Physics, Mod. 12o in connection with exciter, mod. 256) is used as a light source. The light wavelength amounts to 632, 8 nm, the emitted power is approximately 5 mW. The full laser power is reached about 3o min after turn on. The emitted radiation corresponds to the transverse mode TEM_{oo}. At the exit of the laser the laser beam has a diameter of about o,65 mm (corresponding to the $1/e^2$-points). The laser beam has a divergence of 1,7 mrad. Using Brewster windows a linear polarization of the laser beam better than 1 : 1ooo is obtained. According to the specifications a long term power drift of about 5 % can occur. However, a possible influence of this power drift on the droplet concentration measurements is eliminated, because scattered and transmitted light fluxes are always measured simultaneously.

The laser beam enters the expansion chamber through a glass window G (fig. 21) and a tube B_1 with two inlet stops. The inlet stops prevent most of the light, scattered in the glass window G from entering the expansion chamber. The stops are positioned excentrically in the tube B_1 and can be adjusted by proper rotation of B_1.

6.2.2 Measuring system for transmitted light

After passing the expansion chamber the laser beam enters the measuring system for transmitted light through a tube B_2 with two outlet stops, which can be adjusted similar to the inlet stops. The total transmitted light flux is measured by means of an optoelement OPT. Before entering the optoelement, the laser beam is attenuated by means of a neutral density glass filter GF and then homogenized by opal glass plates OG. GF is inclined relative to the laser beam in order to prevent the reflected beam from returning into the chamber volume. The optoelement OPT (Centronic, type OSI 5 K) has a sensitive area of 5 mm^2, which is situated in a transistor housing together with an integrated operational amplifier which is powered by a $\pm$ 12 V power supply (Oltronix, Stabpac 3, 2 MV 15-o1). The output signal of OPT is inverted.

6.2.3 Measuring system for scattered light

Part of the light flux scattered by the droplets enters the measuring system for scattered light, which is shown in principle in figure 11. As described in section 4.2), the rectangular stop S_r and the circular stop S_c define the sensitive volume MV and the light flux, entering the photomultiplier PM. In addition, a third stop (not shown in fig. 11) between S_r and S_c eliminates most of the light, reflected and scattered by S_r and the inlet tubus. For quantitative measurements of the scattered light flux it is important to homogenize the light incident upon the photomultiplier because the sensitivity of the PM-cathode varies strongly over the cathode surface. Accordingly, after passing S_c the scattered light is homogenized by an opal glass plate MG in connection with a white teflon ring TF before entering the photomultiplier PM. Furthermore the diameter d of S_c must be determined precisely, because d^2 enters the light scattering calculations. Therefore d

was measured by means of an optical microscope with a calibrated ocular micrometer and an accuracy better than ± o,1 % was achieved. The photomultiplier PM (EMI, typ 9698 QB, ser. nr. 3168) has an S 2o cathode, which is suffiently sensitive to red light, and 9 dynodes. The high-voltage power supply HV (Keithley Instr., mod. 246 HV-supply) is usually set at 1 kV. The anode current is converted into a voltage signal and amplified by means of the programmable amplifier PAMP (see section 6.3.3)).

6.2.4 Alignment

Laser and expansion chamber stand on an optical bench. The laser is situated on an adjustable table. For alignment of the laser beam relative to the expansion chamber, the measuring system for transmitted light must be removed. Furthermore, the measuring system for scattered light must be replaced by a special stop and a plate with a central mark. Then the support DB (fig. 21) is turned to the angular positions 0^{o} and $18o^{o}$. Correct alignment of the laser is achieved, if in both positions the laser beam centrally passes the above mentioned stop and hits the mark on the above mentioned plate. Furtheremore, this ensures that the measuring system for scattered light is aligned on the support DB towards the center of rotation of DB. In addition, correct adjustment of the angular scale WT (fig. 21) relative to DB is verified.

The correct angular alignment of the optical arrangement can be checked by comparison between experimental and theoretical light scattering curves. It turns out that the fine structure of the light scattering curves is very sensitive to changes of the scattering angle. Fig. 27 shows the theoretical flux ratio Φ_{sca}/Φ_{trans}, calculated for the actual scattering geometry and for an absolute standard deviation of 12 nm as a function of

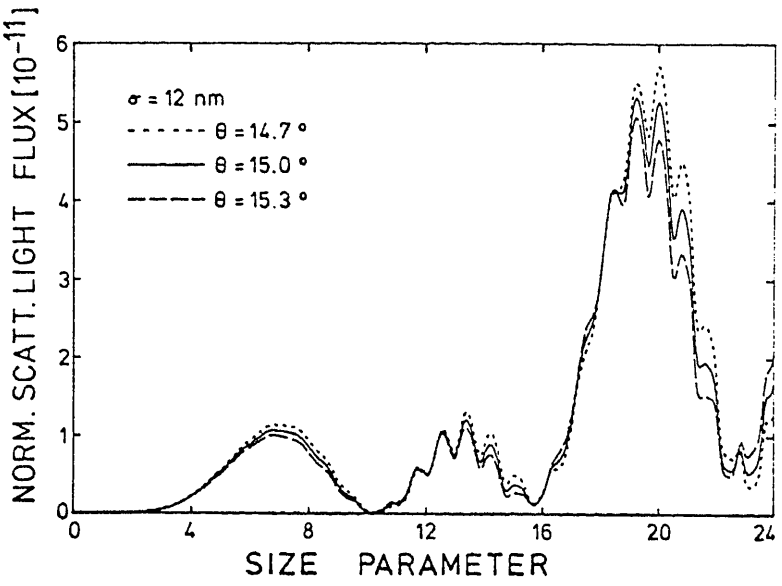

Fig. 27

Theoretical ratio of fluxes Φ_{sca}/Φ_{trans} for the actual scattering geometry and for an absolute standard deviation of 12 nm as a function of the size parameter α for scattering angles $\theta_o = 15^o$ (solid line), $\theta_o = 14.7^o$ and 15.3^o (broken lines).

the size parameter α for scattering angles $\theta_0 = 15^0$ (solid line), $\theta_0 = 14.7^0$ and 15.3^0 (broken lines). It can be seen that the relative height of the fine structure maxima at $\alpha = 18.46$ and $\alpha = 20.84$ is significantly different for the three scattering angles. Comparison with the average of 20 experimental light scattering curves for scattering angle $\theta_0 = 15^0$, presented in section 8.1), fig. 38, shows the correct alignment of the apparatus.

6.2.5 Relative calibration of optoelement and photomultiplier

For quantitative measurements of the ratio of fluxes Φ_{sca}/Φ_{trans}, the ratio of sensitivies (conversion factor) of optoelement OPT and photomultiplier PM must be determined. This can be done by measuring the incident laser power by means of optoelement and photomultiplier and then calculating the ratio of the obtained results. In this connection the measuring system for transmitted flux, consisting of optoelement OPT, opal glass plates OG and neutral density glass filter GF is considered as a measuring unit. For measurement of the laser power by means of the photomultiplier, the measuring system for transmitted flux must be removed and the photomultiplier must be brought into the angular position 0^{o}. To this end the conical inlet part of the tube BR, bearing the rectangular stop S_r, must be removed. In order to compensate for the extinction of the scattered light, caused by the glass cylinder GZ, a glass window of equal thickness was inserted in front of the photomultiplier. The circular stop S_c was removed in order to ensure, that the whole laser beam can enter the photomultiplier. The measuring system, consisting of photomultiplier PM, the white teflon ring TF, the opal glass plate MG and the above mentioned glass window is considered as a measuring unit.

The photomultiplier is much too sensitive for direct measurements of the laser power. Therefore the laser light intensity must be reduced by a factor of approximately $1o^6$ before the laser beam enters the PM-measuring system. This was achieved by two neutral density glass filters, each having an attenuation ratio of about $1o^3$. The actual attenuation ratios of the used neutral density glass filters were determined by means of the highly linear PM-measuring system and the values $2{,}592.1o^3$ (filter "4.1") and $2{,}537.1o^3$ (filter "4.2") were obtained.

The relative calibration of OPT-measuring system and PM-measuring system can now be performed. The total laser power was alternatively measured by means of OPT and PM. For measurements with PM, the two neutral density glass filters "4.1" and "4.2" were used for attenuation of the laser beam. The OPT-output (voltage) was then divided by the PM-output (current). Taking into account the attenuation ratios, the conversion factor 0,07717 V/A was calculated with an accuracy of about 1 %. This value was obtained with a high-voltage setting of 1 kV for the PM.

6.3 Electronical arrangement

6.3.1 Valve control VC

As described in section 5.2), the measuring cycle of the SANC is controlled by an electronic valve control unit VC. VC initiates the opening and closing of five solenoid valves according to a defined time schedule.

The valve control is designed in CMOS technology. The command and status signals for interaction with the process control system are TTL compatible. All electronic components of VC are built into a NIM plug-in unit. The required DC-voltage of 6 V is provided by the NIM-chassis.

The timing of VC is determined by a series of univibrators with different time constants. A detailed description of the univibrators is given by Pohl (1979 a). For most univibrators the time constant is set internally. However, the time constants, corresponding to flushing time and delay time (see section 5.2)) can be externally adjusted. The output of the last univibrator triggers the input of the first one and thereby a continuous operation of VC is obtained after the first univibrator has been activated by means of a start signal. The operation can be stopped by a reset signal, which causes a separation of all univibrators for a sufficiently long time, so that all univibrators are finally in their quiescent state. The activity of the different univibrators is indicated by light emitting diodes (LED's) on the front panel of the valve control VC.

The outputs of the univibrators trigger set- and reset-inputs of flip-flops. The outputs of the flip-flops in turn control relay-drivers and relays (Siemens, Erni, K2F - 6V 58 Ω/18oo T, K2P - 6 V 11o Ω/25oo T), which switch the solenoid valves.

Furthermore the relays control LED's on the front panel of the valve control VC, which, in connection with a block diagram, show the actual status of the measuring cycle. Each flip-flop corresponds to a particular solenoid valve and determines its status. Five solenoid valves are used: Inlet valve V1 (Herion, mod. B8N4), Expansion valve V2 (Herion, mod. C2222N3), Separation valve V3 (Herion, mod. 152o65o. 13oo), Two way valve V4 (Herion, mod. B8M2), Pressure release valve V5 (Herion, mod. B8N4). The normal operating voltage for the solenoid valves is 2o V Dc. As a special case, as described in section 5.2), the expansion valve V2 is opened by applying twice the normal operating voltage in order to obtain a fast pressure drop. The nominal tube diameter is 22 mm for the expansion valve and 8 mm otherwise.

In the special case of the separation valve V3, the set-input of the corresponding flip-flop is triggered, as usual, by the output of a univibrator, but the reset-input is triggered by a comparator. This comparator compares the pressure reading of the differential pressure transducer DP, which measures the pressure in vessel R1, with a preset reference voltage. If the DP-reading exceeds the reference voltage and accordingly the subpressure exceeds a particular value, the comparator triggers the reset-input of the flip-flop and the separation valve V3 is closed. Up to 11 reference voltages and accordingly expansion ratios can be preset by proper adjustment of 11 potentiometers. The particular potentiometer, which actually determines the expansion ratio, can be selected by means of a switch. The selected potentiometer is indicated by a corresponding LED on the front panel of the valve control VC.

For measurements under computer control the valve control VC interacts with the process control system. The computer provides command signals for start and reset and for selection of the potentiometer, which actually determines the expansion ratio. On the other hand, the valve control provides status information about the separation valve V3 and the inlet valve V1. Closing of V3 shows that the preset subpressure in R1 has been reached. In case this subpressure has not been reached, either the pumping flow rate or the delay time must be increased. Closing of V1 indicates that approximately 6 s later the expansion takes place and accordingly all measuring instruments must be activated. Finally, opening of V3 signalizes that one measuring cycle is completed and the obtained data can be transferred to tape.

6.3.2 Digital voltmeter DVM

The digital voltmeter DVM (Hewlett Packard, mod. HP 3474o A, in connection with display and BCD-module HP 34721 B, and multimeter HP 347o3 A) is used to measure constant or slowly varying signals, e.g. scattering angle (see section 6.1.1.)), or analog output of the General Electric Condensation nuclei counter (see section 6.1.3)). One out of 24 different analog signals can be connected to the input of the DVM by means of an analog-multiplexer, which is part of the interface PS 15/o2 (see section 6.4.2)).

For measurements under computer control, the DVM interacts with the process control system via status, command and data lines (see section 6.4.2)). In order to increase the reliability of the measuring results, two measurements are performed in immediate succession and the data are accepted only if the results differ by less than 2 %, otherwise the measuring process is repeated.

6.3.3 Programmable amplifier PAMP

A programmable amplifier PAMP was developed for conversion of the photomultiplier anode current into a voltage signal and subsequent amplification. The PAMP is powered by means of the NIM-chassis, which provides DC-voltages of ± 12 V. Furthermore a connection to the 1o V interface power supply (see section 6.4.2) is necessary for driving the input control circuitry. In order to keep the connection line between photomultiplier PM and PAMP as short as possible, the PAMP is fixed at the support DB of the measuring system for scattered light, just below the PM. The PAMP consists of three stages. The first stage is used for current-voltage conversion, the conversion factors o.1, 1 and 5 V/μA can be chosen. The resistors defining the conversion factors in stage 1 are switched by means of DIP Reed relais (C.P. Clare, mod. PRME 15oo5 AB). The second stage provides amplifications by factors 1, 2, 5, 1o, 2o and 5o. A fine adjustment of the amplification can be performed by means of the third stage with amplification factors 1, 1.2, 1.4, 1.6, 1.8 and 2. The resistors defining the amplifications of stage 2 and 3 are switched by means of CMOS-analog switches (Fairchild, mod. 4o16). Three switches for setting the above amplifications are provided on the front panel of the PAMP. The actual settings are indicated by light emitting diodes. The actual amplification factors were precisely measured by means of a digital voltmeter. Signal integrations with time constants o.7, 1.3 and 3.3 ms can be chosen by means of a switch.

6.3.4 Transient recorder TR

The measuring process has a duration of the order of 1oo ms. During this time total pressure, transmitted light flux and scattered light flux must be monitored simultaneously. For a sufficiently accurate determination of expansion ratio and initial supersaturation the total pressure drop must be measured

with an amplitude resolution of o.1 %. On the other hand, a unique identification of the light scattering extrema requires a time resolution of at least looo samples per channel. Accordingly, during each measuring interval, 3ooo lo-bit-datawords have to be processed corresponding to a transfer rate of 3o kHz. As the computer input rate has an upper limit of lo kHz, a fast intermediate storage device, the transient recorder TR (Biomation, wave form recorder lol5), had to be installed.

The TR has four identical input channels, each equipped with a separate input amplifier and a lo-bit analog-to-digital converter. As mentioned above, particularly the pressure signal, which is connected to the input of channel 3, has to be measured with high absolute accuracy. Therefore the input amplifier of channel 3 was calibrated for the sensitivities 2, 5 and lo V full scale by means of a digital voltmeter. The corrected full scale values 2.o1348, 5.o4755 and lo.1421 V, respectively, are taken into account for the numerical evaluation of expansion ratio and initial supersaturation.

Each of the input signals can be selected as the trigger signal. Because of the high reproducibility of the pressure signal, it is used for triggering of the TR. For measurement of the total pressure drop during the expansion, the pressure signal must be monitored already before the start of the actual expansion process (baseline determination). This can be achieved by using the TR in the "pre-trigger"-mode. In this mode the input signals are continuously monitored with the chosen sample rate. The memory is organized similar to a shift register, one "old" lo-bit information being lost with the recording of each "new" lo-bit-word. After the trigger condition occurs, the sampling process continues for a selectable number of lo-bit-words for each input channel and then recording is stopped. For most experiments a "delay" of 8oo words per channel is chosen, whereas a storage space of lo24 words per

channel is available. Accordingly, at the end of the recording process, 224 words per channel are still stored in the memory, which have been sampled before the trigger condition occured. Thereby the necessary baseline information is provided.

Three data output modes are available. The data are continuously displayed on a CRT-monitor (Tektronix, Monitor 6o4). Furthermore, the data can be plotted by means of an A4-plotter (Hewlett Packard, mod. HP 7o15 A), which is connected to the analog output of the TR. Finally, a digital output of the TR is available, which is used for transfer of the recorded data to the process control system and storage on magnetic tape. For measurements under computer control, the TR interacts with the process control system via status, command and data lines (see section 6.4.2)). A detailed description of this interaction can be found in Pohl (1979 a).

6.4. Digital interface

6.4.1 Computer configuration

The process control of the SANC is performed by means of a digital computer (Digital Equipment Corporation, mod. PDP 15/3o) with a 24 k 18-bit words core memory. Figure 28 shows a block diagram of the computer configuration. A number of peripheral

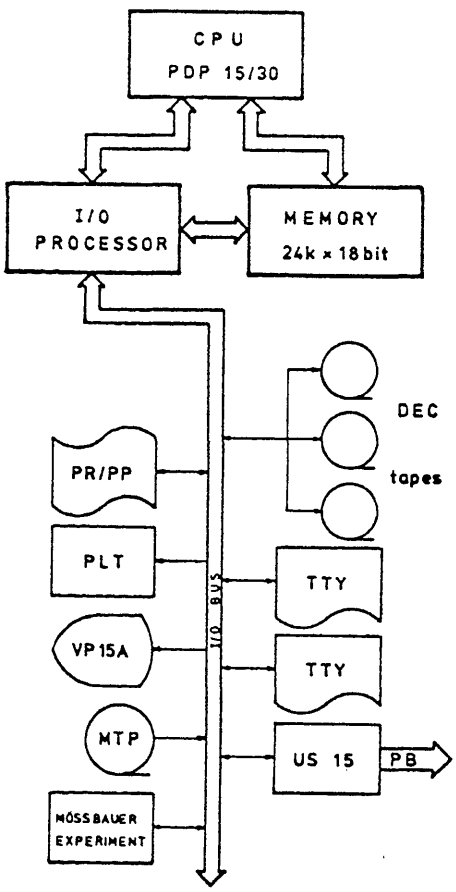

Fig. 28

Block diagram of the computer configuration

units is connected to the CPU via an I/O-bus and an I/O-processor. The periphery consists of 2 teletypes TTY, 3 DEC-tape units, a paper tape reader and paper tape punch PR/PP, a visual display VP 15 A, a plotter PLT and a general-purpose interface US 15.

One of the two teletypes TTY is situated besides the experimental apparatus. It is used for control and error messages and for data output. The second TTY is used during the data evaluation procedure. The three DEC-tape units are used as the mass storage device, having a storage capacity of about 145 k 18-bit words each. The monitor as well as user-programs and data are recorded on DEC-tapes. For the use of the PDP 15/3o as a process control computer, Weber (1975) and Schindler (1975) developed the general-purpose interface US 15. The US 15 hardware and supporting software are integrated into the computer system. A short description of the US 15 and the corresponding software is given by Pohl (1979 a). The process control of experiments is performed by means of the US 15 on the computer side in connection with a complementary user-interface PS 15 on the experiment side.

The above described system can be operated under two different monitors. The "Background - Foreground" - monitor (B/F-monitor) is designed for operation with two users simultaneously. It is particularly useful in connection with real-time data acquisition and process control. On the other hand, the "Advanced Software System" (ADSS-monitor) is designed for only one user and occupies less core memory. Therefore it is more suitable for calculations.

For the present application, the process control is performed by means of the PDP 15/3o under the B/F-monitor via the interface US 15 and a complementary user-interface PS 15/o2, which was developed by Pohl (1979 a). After some pretreatment, the experimental data are stored on DEC-tapes. The data reduction

is performed by means of the same computer, but under the ADSS-monitor.

6.4.2 The interface PS 15/o2

The experimental apparatus in connection with the digital interfaces is shown in principle in figure 29. The user-interface PS 15/o2 on the experiment side is connected to the general-purpose interface US 15 on the computer side by means of a peripheral bus PB, which has a length of about 7o m and consists of 6o doubly shielded line pairs. In order to avoid

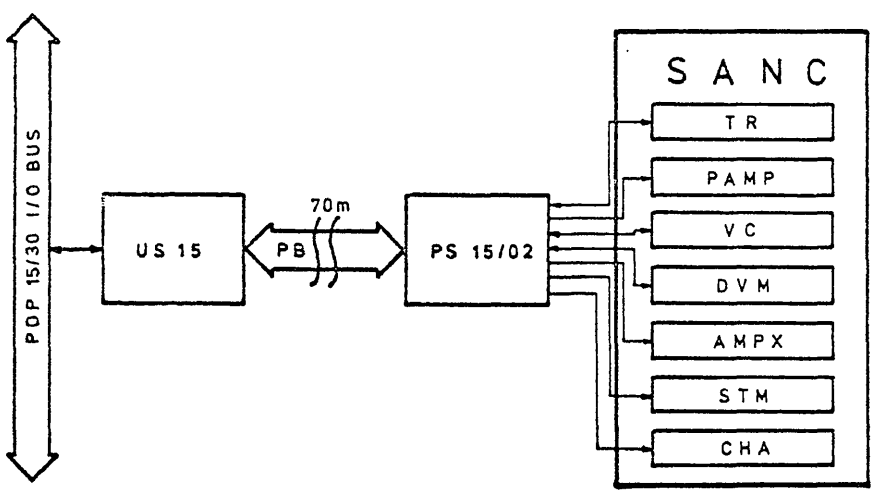

Fig. 29

Block diagram of the experimental apparatus in connection with the digital interfaces

a galvanic connection of US 15 and PS 15/o2, the signals are received by optically coupled isolators, which are part of the US 15 and the PS 15/o2, respectively.

Similar as the valve control VC, the user interface PS 15/o2 is designed in CMOS technology. Because most of the devices, controlled by the PS 15/o2, are designed in TTL technology, the corresponding signals have to be prepared properly. The practical realization of the PS 15/o2 was performed on one large motherboard (Augat, mod. 8136PG21) using the wire-wrap technique. The CMOS-components require a DC-voltage of 1o V, the circuits for conversion between 1o V (CMOS) and 5 V (TTL) level require a DC-voltage of 5 V. Both voltages are provided by a combined power supply (Chung Yu Electronics, mod. D-1o52).

The interface PS 15/o2 consists of three parts. In the first part the signal transfer by means of optically coupled isolators is performed. The second part consists of a status-command register and two data registers, which are complementary to the interface US 15. In the third part several interface circuits are provided to prepare the signals for interaction with the different experimental devices.

The first 9 bits of the status-command register form the status register. By means of the ninth status bit a particular device signalizes to the computer that the digital output of this device is ready for data transfer. After this bit has been set, the data transfer to the computer is performed. If a device does not provide a corresponding status signal, the reading process can be initiated by a command bit (see below), which sets the ninth status bit. By means of the remaining 8 status bits, general status information about the experiment is transferred to the computer. For example, the endpositions of the support DB (fig. 21) and the status of separation valve V3 and inlet valve V1

are signalized to the computer. Depending on the contents of an 18-bit mask register, which is integrated into the US 15, level changes of particular status bits can set a 1-bit flag register, which is also part of the US 15. This causes an interrupt of the normal sequence of operations and particular actions are performed depending on the actual status bit, which has caused the interrupt and on the actual status of the control program at the time, when the interrupt has occured. After these actions are completed, the normal sequence of operations is continued.

The second 9 bits of the status-command register form the command register. The ninth command bit signalizes data transfer from the computer to the experiment. It has a similar function as the ninth status bit for data transfer from the experiment to the computer. As mentioned below, for the present application no data transfer from the computer to the experiment is performed. Therefore the ninth command bit is not used. Because of the relatively large number of process controlled devices, the remaining 8 command-bits must be decoded. Therefore only four command bits are used actually for transferring commands from the computer to the experiment. The remaining four command bits are used as device address bits for identification of up to 16 different devices. A device, identified by the device address bits can be controlled by means of the above mentioned four command bits.

The transfer of experimental data from the experiment to the computer is performed by means of the 18-bit data-in register. The data are available in digital, bit-parallel form. Up to 16 different bit-parallel informations can be transferred via the same data-in register by means of a 16 : 1 multiplexer.

The select code for this multiplexer is formed by the above mentioned device address bits, which are part of the command register. Furthermore, these device address bits are sent to the computer as part of the data word via the data-in register and are used for identification of these data. Accordingly, the device address bits have three different functions:

1) Identification of a device, which is controlled by the four remaining command bits

2) The data output of the same device is connected to the data-in register by means of the 16 : 1 multiplexer

3) The device address code is sent to the computer as data identification code together with the data of the corresponding device.

The 18-bit data-out register can be used for data transfer from the computer to the experiment. For the present application this register is not used.

For interaction with the valve control VC, two device address codes are required. Command signals are provided for start and reset and for selection of one of the 11 potentiometers, which actually determines the expansion ratio (see section 6.3.1.)). On the other hand, two status signals are available from the valve control VC, which correspond to the status of the separation valve V3 and the inlet valve V1.

The operation of the digital voltmeter DVM is controlled by means of two signals. A command signal from the computer initiates the digitizing process. When the digitizing process is completed, a status signal is provided by the DVM, which sets the ninth status bit. Thereby, as described above, the data transfer to

the computer via the 18-bit data-in register is initiated. The data are transferred by means of 24 data lines. Therefore the transfer has to be performed in two steps and accordingly two device address codes are required. As mentioned in section 6.3.2.), up to 24 different analog signals can be digitized by the DVM in connection with an analog multiplexer AMPX. The AMPX is part of the PS 15/o2 and consists of 24 analog-switches, whose outputs are connected to the DVM-input. The actually activated analog-switch is specified by the contents of a 5-bit binary counter. The control of the AMPX requires reading of a 24-bit register and accordingly two device address codes. When the digital output data of the DVM are transferred to the computer, the particular setting of the analog multiplexer must be specified. Accordingly, it is not sufficient to include, as usual, the device address code into the data word. For the special case of the DVM the contents of the above mentioned 5-bit counter is used instead. Furthermore, a sixth bit is included into the data word identifying the first five bits as the contents of the five-bit counter.

The transient recorder TR is controlled by 4 command signals in connection with two device address codes. 3 status signals are provided by the TR. The input mode of the TR is initiated by the command signal "ARM". This signal starts the recording process. After the trigger condition has occured the sampling process is continued for a preset number of samples and then stopped (pre-trigger-mode, see section 6.3.4)). The status signal "Record Status" indicates, if the TR is in the input mode. The output mode of the TR is initiated by the command signal "output mode start" and stopped by the command signal "output mode stop". The status signal "output status" indicates, if the TR is in the output mode. When the output mode is initialized by means of the command signal "output mode start", simultaneously

the first 1o-bit data word is requested. When this 1o-bit data word is available at the digital output of the TR, a status signal "flag" is provided, which sets the ninth status bit. Thereby, as described above, the data transfer to the computer is initiated. Then the next data word is requested by the command signal "CMD". The status signal "flag" again signalizes, when this data word is available and thereby initiates the data transfer to the computer. The signals "CMD" and "flag" are used as "shakehand" signals for transfer of the recorded data to the computer. If the whole contents of the TR-storage is transferred to the computer, the output mode is automatically stopped after the transfer of the last 1o-bit data word.

The three stages of the programmable amplifier PAMP (see section 6.3.3.)) are controlled separately. The amplifications are set by means of 3 signal lines for stage 1, 6 signal lines for stage 2 and 6 signal lines for stage 3.

The step motor STM (see section 6.1.1.)) is controlled by two command signals. One command signal determines the direction of rotation, the other one initiates a single step.

The output signal of the charge amplifier CHA (see section 6.1.1.)) tends to show a drift. In order to obtain reproducible conditions, a "reset" must be performed before each measurement. This is achieved by short-circuiting of the CHA-input. For operation without computer control, this can be done manually by means of a switch. For measurements under computer control, a relay is provided in the PS 15/o2, which resets the CHA during the time, when no pressure measurement is performed.

The contents of the three 18-bit registers (status command, data-in, data-out) can be displayed alternatively by means of 18 LED's on the frontpanel of the PS 15/o2. Furthermore, 5 additional LED's on the front panel show the contents of the 5-bit binary counter, which specifies the particular setting of the analog multiplexer AMPX.

7) EXPERIMENTAL PROCEDURE AND DATA EVALUATION

7.1 Preparations for measuring series

Before a series of measurements is performed, the temperatures of humidifier and expansion chamber must be set at the temperature regulators of the corresponding thermostats. It turned out that a stabilizing period of several hours is required to obtain well-defined and reproducible conditions. Particularly the humidifier has a long relaxation time after a temperature change or some other disturbance has occured. Furthermore, the heating of the connection tubes between humidifer, expansion chamber and expansion valve must be turned on well in advance.

Depending on the actually planned experiment, the experimental parameters and the measuring sequence can be chosen accordingly. In order to prepare a measuring series under computer control ("on line"), usually a number of test measurements is performed without computer control ("off line"). Thereby the experimental conditions and parameters are determined. Then a file of initializing parameters is set up via the teletype, which is situated besides the experimental apparatus. One part of these initializing parameters corresponds to settings and data, which remain unchanged during the on-line-operation (e.g. identification code, TR-input-sensitivities, TR-timebase, atmospheric pressure, temperatures of humidifier and expansion chamber). The other part of the intializing parameters corresponds to settings, which have to be changed in a defined sequence in the course of the on-line-experiment. Up to 2o scattering angles and up to 5 groups of scattering angles can be selected. A group of scattering angles is determined by initial and final angle and by the number of equal angular intervals. Furthermore, up to 11 potentiometers can be

chosen, which actually determine the expansion ratio and supersaturation (see section 6.3.1)). Multiple choice of the same scattering angle or potentiometer-number is permitted. Finally, a number of repetitions can be chosen. During the on-line-experiment, this number of repetitions is performed for each setting of scattering angle and expansion ratio. For each selected scattering angle, sequentially all of the above determined expansion ratios are set before the scattering angle is changed. The initializing parameters are stored on the same DEC-tape, which is subsequently used for storage of the experimental data.

7.2 Measurements under computer control

After the file of initializing parameters has been set up, the on-line-operation can be started via the teletype. Immediately before the start, date and time can be entered. Furthermore it can be decided, if the scattered light signal is to be corrected with respect to the signal offset. In most cases this offset correction is performed. However, in the presence of large condensation nuclei the offset correction should not be applied. In addition, there is a choice between automatic PAMP-amplification setting and manual amplification setting via the teletype after each change of expansion ratio or scattering angle. Usually an automatic PAMP-amplification setting is chosen. However, for the measurements of Kelvin-equivalent size distributions (see section 8.3)), only the height of the first light scattering maximum is important and overrange at a later time is irrelevant. Therefore in this case the automatic PAMP-amplification setting is not required.

Immediately after the start of the on-line-operation, the valve control VC is brought into a defined initial condition by means of a reset-signal (see section 6.3.1)). Furthermore, the support DB of the measuring system for scattered light is rotated first to position 165^{o}, then to position 15^{o}. Both limiting angular positions are sensed electrically by means of microswitches. For each limiting position, the corresponding voltage, provided by the tenturn potentiometer, is measured by the DVM. In addition, the total number of steps of the step motor is determined. After a delay of 1 min, the actual measuring cycle is initiated by sending a start-signal to the valve control VC.

Before each measurement is performed, the PAMP-amplification, the scattering angle and the expansion ratio are set. The process-controlled measuring cycle is only continued, if the separation

valve V3 closes indicating that the required subpressure has been reached in the vessel R1. If so, closing of the inlet valve V1 causes an interrupt about 6 s before the actual measurements. Thereby charge amplifier CHA and transient recorder TR are activated and accordingly ready for measurement. After the measurements have been performed, opening of the separation valve V3 signalizes the end of the measurements. At this point, the setting of the scattering angle is checked. In case the scattering angle turns out to be incorrect, the recorded data are discarded. Now the charge amplifier CHA is brought into the reset-position. Subsequently the first 1o24 data words (scattered light) of the TR are read, the maximum value is determined, and by averaging over the first 3o data words the signal offset is calculated. If automatic PAMP-amplification-setting was requested, it is checked if the PAMP-amplification was correct with respect to the above maximum value. If it was not correct, the measurement is repeated with properly adjusted PAMP-amplification-setting. If the setting was correct, operation continues with reading the second 1o24 data words (transmitted light) of the TR. Simultaneously, the scattered light flux is normalized by means of the transmitted light flux and, if requested, an offset correction is performed. The primary laser flux is determined by averaging over 3o data words corresponding to the transmitted light flux before the expansion. Then the third 1o24 data words (total pressure) of the TR are read. These data are stored on DEC-tape, the first data word being set equal to 0 for identification. However, because of the high reproducibility of the pressure data, storage is only performed, if expansion ratio and/or scattering angle have been newly set. For each single measurement the total pressure drop in the expansion chamber is measured by averaging 3o data words corresponding to the pressure before, and 2oo data words corresponding to the pressure after the expansion. Thereby expansion

ratio and supersaturation are calculated for each single measuring run. Subsequently, the data corresponding to the normalized scattered light flux, are stored on DEC-tape, the first data word being set equal to 1 for identification. Then single experimental data (e.g. analog output voltage of the General Electric Condensation Nuclei Counter) are measured by means of the digital voltmeter DVM in connection with the analog multiplexer AMPX and transfered to the computer. Finally, all relevant single experimental data (e.g. scattering angle, expansion ratio, supersaturation, temperatures, TR-settings) are stored on DEC-tape for each single run, the first data word being set equal to 2 for identification.

After each single measuring run, a protocol is written on the teletype. This protocol includes the following parameters:

Identification code of the measuring series, run number, and repetition number,
temperature of humidifier,
temperature of expansion chamber,
initial pressure (atmospheric pressure),
measured scattering angle,
number of potentiometer determining the expansion ratio,
measured expansion ratio,
calculated initial temperature at the end of the expansion,
calculated initial saturation ratio at the end of the expansion,
actual conversion and amplification factor of the PAMP,
primary laser flux (in the same units as the scattered flux),
Relative measure of the total nuclei concentration (Analog output voltage of the General Electric Condensation Nuclei Counter).

Furthermore, in periodic time intervals date and time are written on the teletype.

7.3 Data evaluation

After a measuring series is completed, all relevant experimental data ("raw" data) are stored on DEC-tapes. For data output a teletype TTY, a visual display VP 15 A and a plotter PLT are available (see fig. 28).

As explained in section 5.3), for quantitative determination of droplet size and concentration a one-to-one correspondence between experimental and theoretical light scattering extrema is required. It turned out that a safe identification of the experimental extrema is very difficult without interaction with the experimentalist (pattern recognition problem). Therefore the data evaluation program is designed for interactive operation.

The software for data evaluation is presently divided into 6 program sections. In program section 1 ("display section") the raw data, which are stored on DEC-tapes, can be reviewed. The pressure and light data can be displayed on the visual display. The single data (e.g. scattering angle, expansion ratio), can be written on the teletype.

In order to reduce the influence of statistical fluctuations, usually the measurements were repeated several times with unchanged experimental conditions. In program section 2 ("mean value section") averages of experimental data from repeated measurements can be calculated. A further reduction of noise peaks can be achieved by numerical smoothing of raw or averaged light scattering curves, which is determined by a smoothing parameter. However, this procedure was usually not required. Raw or averaged light scattering curves can be displayed on the visual display or plotted. Furthermore, raw pressure curves can be displayed or plotted.

Maxima and minima of the raw or averaged light scattering curves can be located by means of a numerical searching routine. Depending on the choice of a special sensitivity parameter, more or less pronounced extrema can be recognized. Then the located extrema are indicated at the corresponding raw or averaged experimental light scattering curve, which is displayed on the visual display. If desired, an arbitrary number of the experimental light scattering data, for which extrema have just been located, can be written on the teletype. At the corresponding theoretical light scattering curve, the extrema are specified by identification numbers. By visual comparison the numerically located experimental extrema can either be identified by means of the above identification numbers or discarded. Thereby the one-to-one correspondence of theoretical and experimental light scattering extrema is obtained. For each of the identified experimental extrema identification number, position on the time axis and height are determined. These data can be written on the teletype. Furthermore, the expansion ratios,initial temperatures and initial supersaturations for the corresponding measuring runs are averaged. The results of this first step of the data reduction will be called "reduced" data. Each set of reduced data is identified by means of a selectable identification code ("work-ID"). If a set of reduced data corresponds to an averaged light scattering curve, it can be intermediately stored on the same DEC-tape, where the data evaluation software is recorded and part of the data from this set can be written on the teletype.

For further reference, intermediately stored reduced data can be permanently saved on the same DEC-tape, where the corresponding raw data are recorded. Storage and recall of the reduced data are performed in program section 5 ("store recall section").

Each set of reduced data consists of the following parameters:

- Work-ID
- Humidifier temperature T_B
- Chamber temperature T_i
- Scattering angle θ_0
- number of potentiometer, determining the expansion ratio
- averaged expansion ratio β
- averaged initial temperature $(T_\infty)_0$ at the end of the expansion
- averaged initial saturation ratio $(S_\infty)_0$ at the end of the expansion
- relative measure of the total nuclei concentration
- number of averaged runs
- number of identified maxima
- number of identified minima
- timebase setting of the transient recorder

Furthermore for each of the identified maxima and minima:

- identification number
- position on the time axis (transient recorder channel number)
- experimental light flux ratio Φ_{sca}/Φ_{trans}.

When a particular set of reduced data is saved or recalled, several informations about this set (e.g. work-ID, scattering angle, averaged expansion ratio, averaged initial supersaturation) can be written on the teletype.

In order to test the statistical significance of the experimental light scattering data, measuring runs must be considered, which were repeated several times with unchanged experimental conditions. A statistical evaluation of the raw light scattering data from these runs can be performed in program section 3 ("standard deviation section"). In this program section a set of raw experimental light scattering curves can be considered, which is identified by a selectable identification code. The extrema of the raw light scattering curves can be identified separately

for each single experimental run by means of a similar procedure as in the meanvalue section. This identification can be performed for different sets of raw light scattering curves. Then for each of the identified extrema corresponding to one of the above defined identification codes, meanvalues and standard deviations are calculated with respect to the time at which a particular extremum occurs and with respect to the height of this extremum. The results are written on the teletype. Thereby the statistical error of position and height of the experimental light scattering extrema can be estimated.

As described in section 8.2), droplet growth in supersaturated vapor was measured for different experimental conditions. The results were compared with various theoretical predictions. The corresponding numerical calculations and the comparison are performed in program section 4 ("droplet growth section"). Calculations can be performed without applying a transitional correction ("Maxwell"), or with the semiempirical transitional corrections according to equ. (2.79) ("Fukuta & Walter"), equ. (2.8o)("Smirnov") or according to a kinetic theory approach of Dahneke (1977) ("Dahneke"). Furthermore, the mutual influence of mass and heat flux in the vicinity of the droplets can either be neglected or taken into account by introducing the factors F_T from equ. (2.4o) ("thermal correction") and F_M from equ. (2.53) or (2.54) ("diffusional correction"). Finally, the calculations can be based on the analytical solution, equ. (2.91), (2.92) or the numerical solution of equ. (2.9o).

The droplet growth process is determined by the following experimentally obtained parameters:

Humidifier temperature T_B,
chamber temperature T_i,
initial total gas pressure p_i before the expansion (atmospheric pressure),

expansion ratio β ,
droplet concentration C_o at the end of the expansion,
condensation nuclei radius a_o
mass m_N of a soluble condensation nucleus,
molecular weight M_N of a soluble condensation nucleus,
Van't Hoff-factor i of a soluble condensation nucleus.

Before actual numerical droplet growth calculations are performed, all of the above data can be entered via the teletype. However, if the theoretical calculations are to be compared with the results of a particular measuring series, the parameters T_B, T_i and β can be read directly from the corresponding file of reduced data. The reduced data have been previously obtained in the "meanvalue section" and are identified by a particular work-ID. By means of the "store recall section" the reduced data can be recalled from the corresponding DEC-tape.

Besides the above mentioned experimentally obtained parameters, the following adjustable parameters can be entered via the teletype:

Humidification B (saturation ratio at the exit of the humidifier),
Polytropic factor Π ,
mass accomodation coefficient α_M,
thermal accomodation coefficient α_T,
thermal diffusion factor α .

The calculations result in a number of single data, which are written on the teletype, e.g.:

initial vapor pressure $p_{v,i}$ before the expansion ,
initial saturation ratio S_i before the expansion ,
initial number concentration C_i of the condensation nuclei before the expansion ,

gas temperature $(T_\infty)_0$ at the end of the expansion,
saturation ratio $(S_\infty)_0$ at the end of the expansion,
maximum droplet radius a_{max} at the end of the growth process,
maximum gas temperature T_{max} at the end of the growth process.

Furthermore, several quantities are calculated as functions of time and written on the teletype:

droplet radius a,
Knudsennumbers Kn_T, Kn_M ,
first order correction factors F_T, F_M ,
transitional correction factors β_T, β_M ,
analytical impedance terms N_T, N_M ,
mass flux I to one growing droplet ,
droplet temperature T_a ,
bulk gas temperature T_∞ in the expansion chamber ,
bulk vapor pressure $p_{V,\infty}$ in the expansion chamber ,
bulk saturation ratio S_∞ in the expansion chamber.

Some of these data can be displayed on the visual display or plotted.

Based on the above mentioned reduced data, the experimental droplet radius and concentration at specific times during the growth process can be evaluated. To this end, position and height of each of the identified extrema of the experimental light scattering curves are compared with the corresponding theoretical values. These theoretical "Mie reference" data are available on the same DEC-tape, where the data evaluation software is recorded. The resulting experimental data can be displayed on the visual display or plotted as points in droplet radius vs. time and droplet concentration vs. time diagrams. Furthermore these data can be written on the teletype.
For quantitative comparison of theoretical growth curves with experimental results, the experimental data points can be

displayed together with corresponding theoretical growth curves in droplet radius vs. time diagrams. The time scales of experimental and theoretical data can be matched by assuming the first experimental point to lie precisely on the theoretical curve. The sum of squares of the differences between experimental and theoretical data is calculated as a relative measure of the degree of coincidence of experimental points and theoretical growth curves.

As described in section 8.3), Kelvin-equivalent size distributions of the condensation nuclei aerosol were determined by measuring droplet concentrations at stepwise increasing supersaturations and otherwise unchanged conditions. The numerical evaluation of the experimental data is performed in program section 6 ("Aerosol distribution section"). First from the raw data, obtained for different supersaturations, the corresponding reduced data are evaluated by means of the "mean value section". The obtained sets of reduced data are intermediately stored on the same DEC-tape, where the data evaluation software is recorded. In the "aerosol distribution section" it is important that the sets of reduced data are entered in the order of increasing supersaturation. This can be achieved by evaluating the reduced data in the "mean value section" already in the correct sequence, identifying these sets of reduced data by the same work-ID. Referring to this work-ID in the "aerosol distribution section" causes these reduced data to be entered in the correct sequence automatically. However, usually it is easier to evaluate the reduced data in the sequence as the raw data are stored on the DEC-tape. In this case different work-ID's have to be chosen for each set of reduced data. In order to obtain a print out of the averaged supersaturations corresponding to the different work-ID's, the data can be saved using the "store recall section".

Then in the "aerosol distribution section" the sets of reduced data, each identified by an individual work-ID, can be entered sequentially in the order of increasing supersaturation. Then for each of these sets of reduced data, the droplet concentration and the Kelvin-equivalent diameter corresponding to the particular supersaturation are calculated. The droplet concentration as a function of the Kelvin-equivalent diameter yields a cumulative size distribution, which can be displayed or plotted as data points or as a polygon. By means of numerical differentiation a differential size distribution can be obtained, which can be displayed or plotted as a histogram. The corresponding numerical data can be written on the teletype.

8) EXPERIMENTAL RESULTS

As mentioned in section 6.1.2), all experiments reported here were performed with water vapor in air.

8.1 Size distribution of the droplet aerosol

The experimental investigations, described in the present report, were based on independent determination of droplet size and concentration by comparison of experimental and theoretical light scattering curves. As can be seen from fig. 13 and 16, the theoretical light scattering curves depend on the size distribution of the droplet aerosol. Accordingly, for accurate determinations of droplet size and concentration, theoretical light scattering curves are required, which correspond to the actual droplet size distribution in the expansion chamber. Therefore the droplet size distribution must be determined at different times during the droplet growth process. Part of the results, presented in the present section, is included in Szymanski et al. (1979, 198o).

As mentioned in section 4.3), the curves describing the light flux ratio Φ_{sca}/Φ_{trans} as a function of the scattering angle θ_o, are very sensitive with respect to changes of the modal size parameter α_M and/or the breadth parameter σ (see equ. (4.48)). Therefore these curves can be used for an optical determination of α_M and σ by means of a best-fit procedure ("inversion" of the light scattering data).

For measurements of the droplet size distribution, NaCl-particles were used as condensation nuclei. A description of the condensation nuclei generator is given in section 6.1.3). A nuclei concentration of about 1o ooo cm^{-3} and a supersaturation of 155 % were chosen. The scattered light flux was recorded as a function of time for scattering angles between 15^o and 165^o in steps of 5^o. Four repetitions were performed for each scattering angle. From all of the so obtained scattered flux vs. time curves, the scattered light flux was determined for a particular time t during the

droplet growth process. Thereby the scattered light flux was obtained as a function of the scattering angle at the time t. Figure 3o shows the experimental results for t = 64 ms.

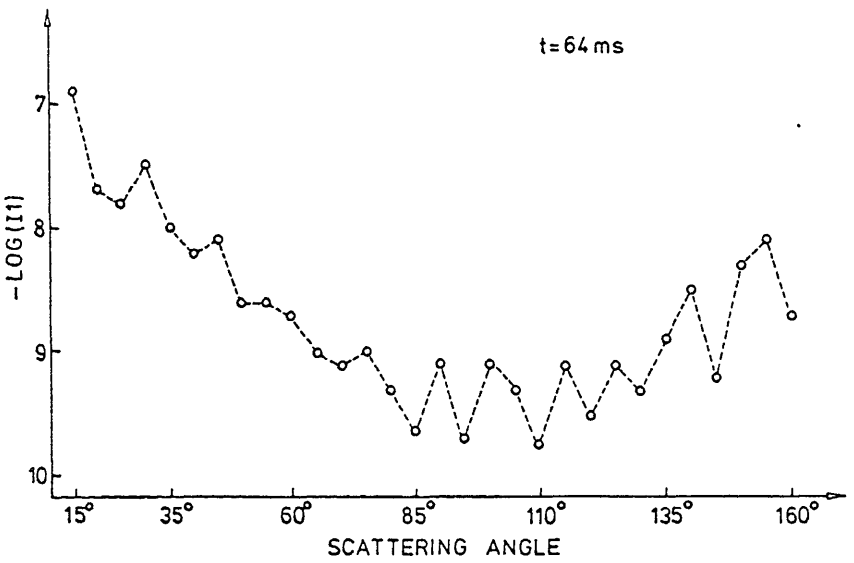

Fig. 3o

Experimental scattered light flux as a function of the scattering angle θ_o at a time t = 64 ms during the droplet growth process.

At this time a particular maximum of the scattered light flux vs. time curve for $\theta_o = 15^o$ has been observed. If the correspondence between experimental and theoretical light scattering extrema was correctly established, this maximum corresponds to a modal size parameter $\alpha_M = 13.38$. From the height of the experimental

maximum the approximate value C = 1o.1.1o^3 cm^{-3} of the droplet concentration can be derived.

For an independent, quantitative determination of α_M and σ at the time t during the growth process, an inversion of the experimental light scattering data must be performed. For the present investigations, the droplet size distribution was modeled by a zeroth-order lognormal distribution according to equ. (4.48). By systematic variation of α_M and σ and proper adjustment of the value for the droplet concentration C the best fit between experimental and theoretical data was obtained. The best fit is defined by the minimum of the sum of squares of the relative differences between experimental and theoretical data. The uniqueness of the best-fit procedure was extensively discussed by Kerker (1969). Figure 31 shows the experimental data of fig. 3o together with the theoretical curve corresponding to the best fit. Good agreement can be observed.

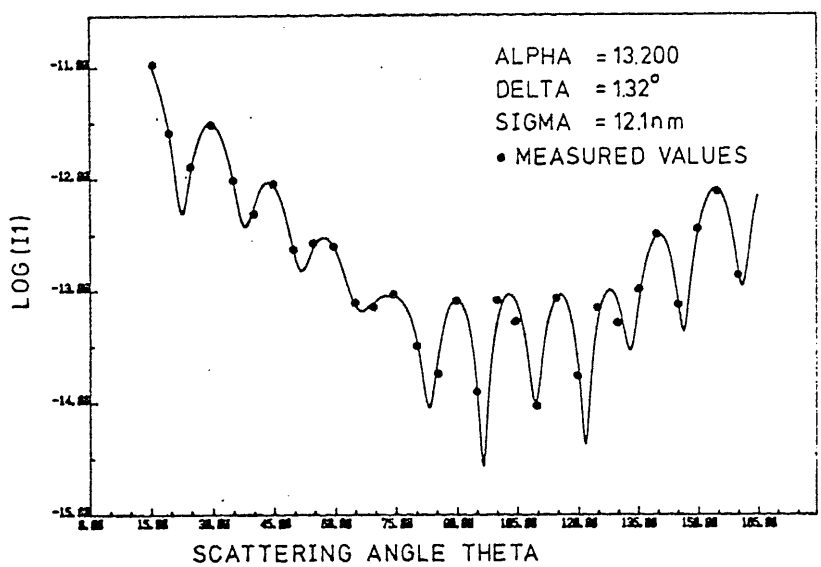

Fig. 31

Theoretical curve corresponding to the best fit. The experimental data of fig. 3o are indicated.

The best-fit procedure resulted in a modal size parameter $\alpha_M = 13.2o$, a breadth parameter $\sigma = o.91$ %, and a droplet concentration $C = 11.8.1o^3$ cm^{-3}. The values for α_M and C agree fairly well with the above mentioned values obtained from a maximum of the scattered flux vs. time curve at $\theta_o = 15^o$. Accordingly, the one-to-one correspondence between experimental and theoretical extrema of the scattered light flux vs. time curves is verified. This test corresponds to method 3), which is described in section 5.3).

The above described determination of α_M and σ has been performed for different times during the growth process. From the breadth parameters σ the corresponding absolute standard deviations of the droplet aerosol have been determined. Figure 32 shows the dependence of the absolute standard deviation on the modal size parameter α_M. It can be seen that the absolute standard deviation decreases with increasing droplet radius and accordingly the droplet aerosol becomes increasingly monodispersed during the growth process. This can be qualitatively explained by means of the droplet growth theory. Assuming, as a rough estimate, a quadratic growth law (see section 2.6.3)), it can be estimated that the absolute standard deviation of the droplet aerosol varies inversely proportional to the droplet radius.

Using the experimentally determined standard deviations of the droplet aerosol, the ratio of fluxes Φ_{sca}/Φ_{trans} can be calculated as a function of the modal size parameter α_M for different scattering angles θ_o. Thereby theoretical light scattering curves are obtained, which correspond to the actual experimental conditions in the expansion chamber. Figures 33, 34, 35, 36 und 37 show the theoretical light scattering curves for scattering angles 15^o, $3o^o$, 45^o, $6o^o$ and $16o^o$, respectively. The extrema

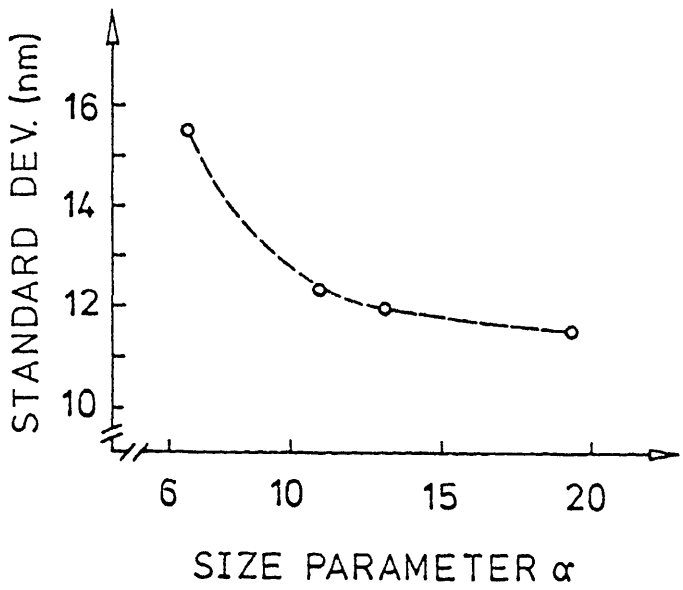

Fig. 32

Experimentally obtained absolute standard deviation as a function of the modal size parameter α_M.

of these curves are identified by means of identification numbers. As explained in section 7.3), these numbers are used for identification of the experimental light scattering extrema, which is performed in the "mean value section" of the data evaluation software. By comparison with the experimental scattered light flux vs. time curves, droplet size and concentration can be determined quantitatively.

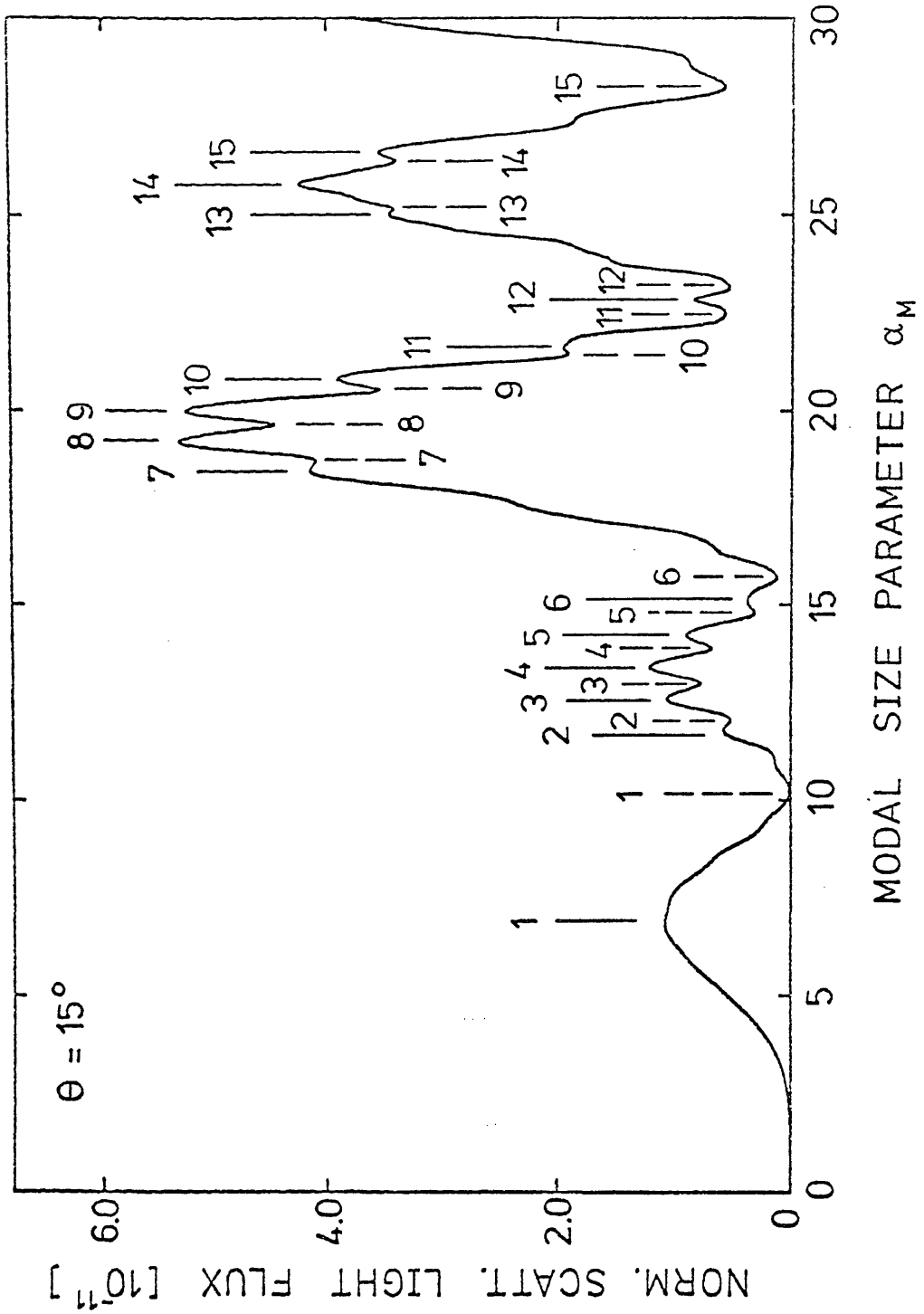

Fig. 33

Theoretical ratio of fluxes Φ_{sca}/Φ_{trans} as a function of the modal size parameter α_M, calculated for the actual experimental conditions in the expansion chamber and a scattering angle $\theta_o = 15^o$. The extrema are identified by identification numbers.

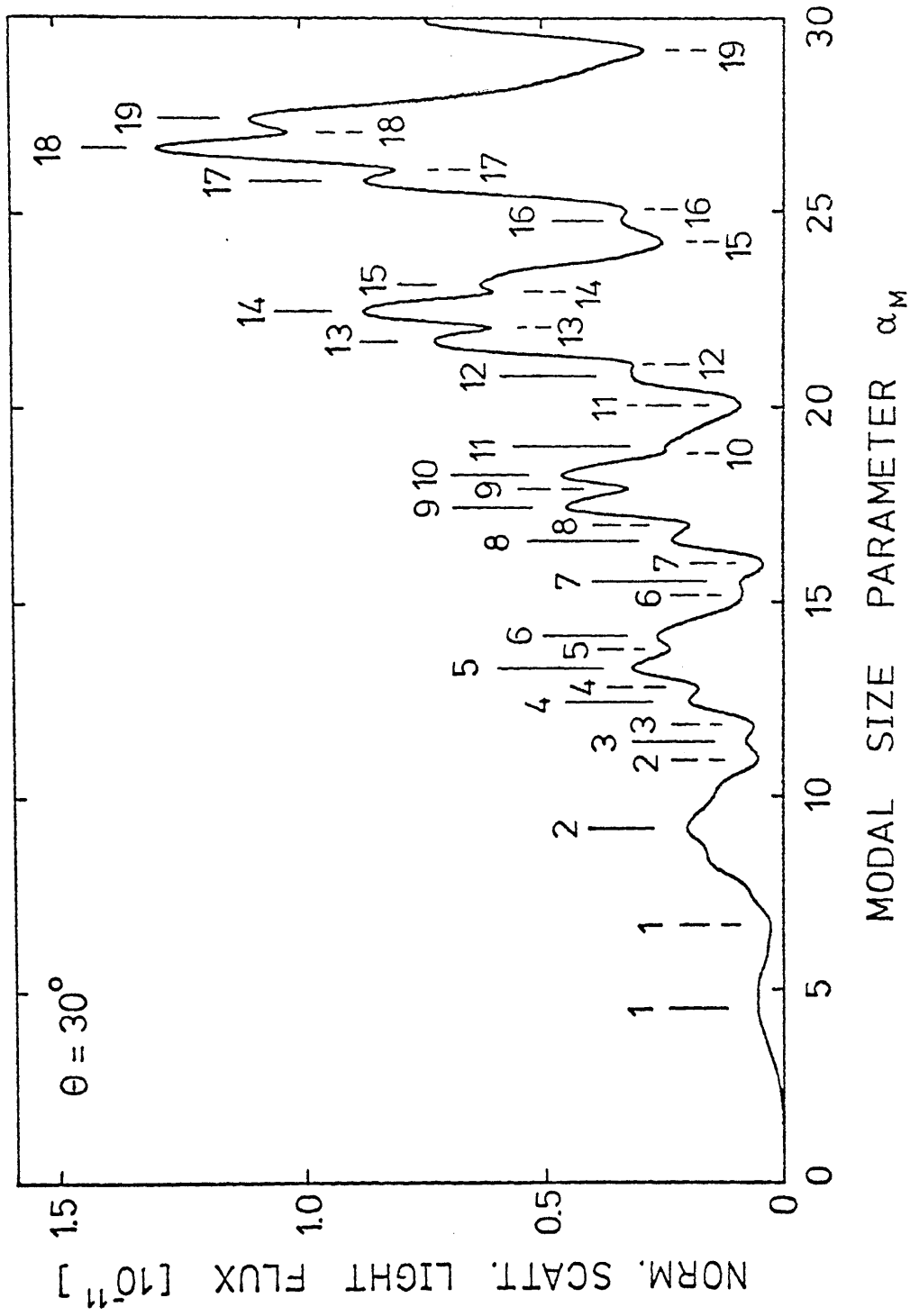

Fig. 34

As fig. 33 for $\theta_o = 30^\circ$

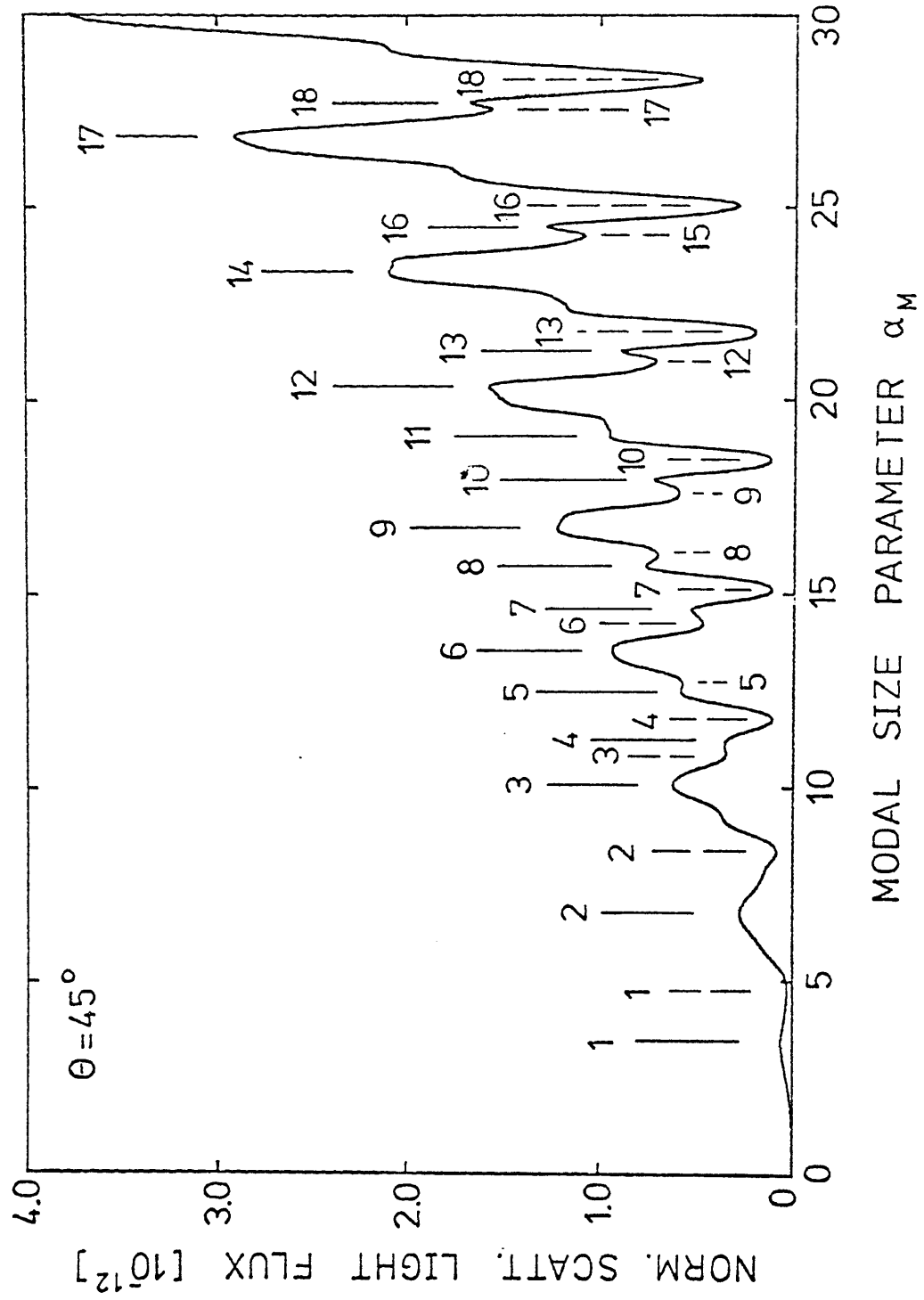

Fig. 35

As.fig. 33 for $\theta_o = 45^o$

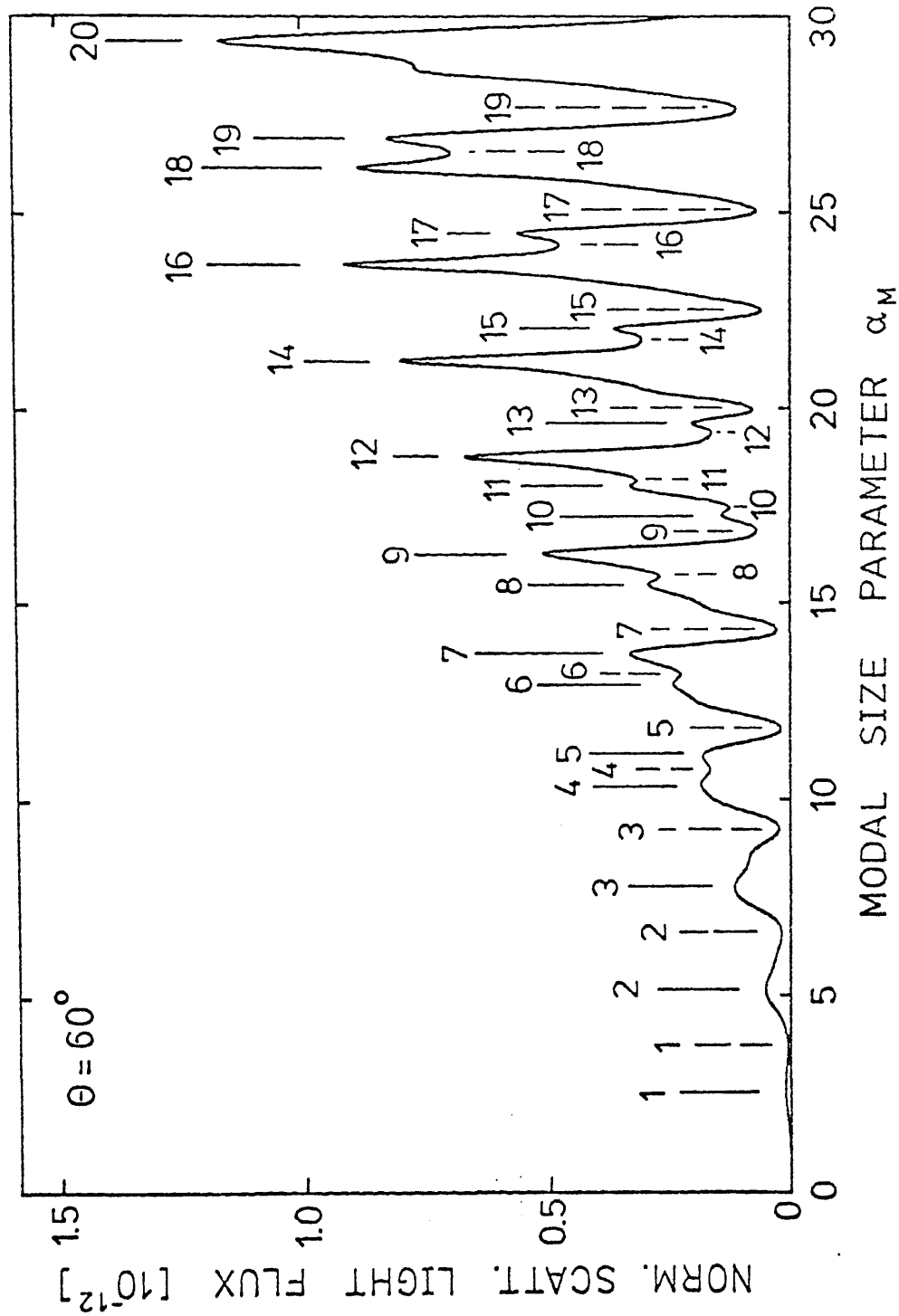

Fig. 36

As fig. 33 for $\theta_o = 60^o$

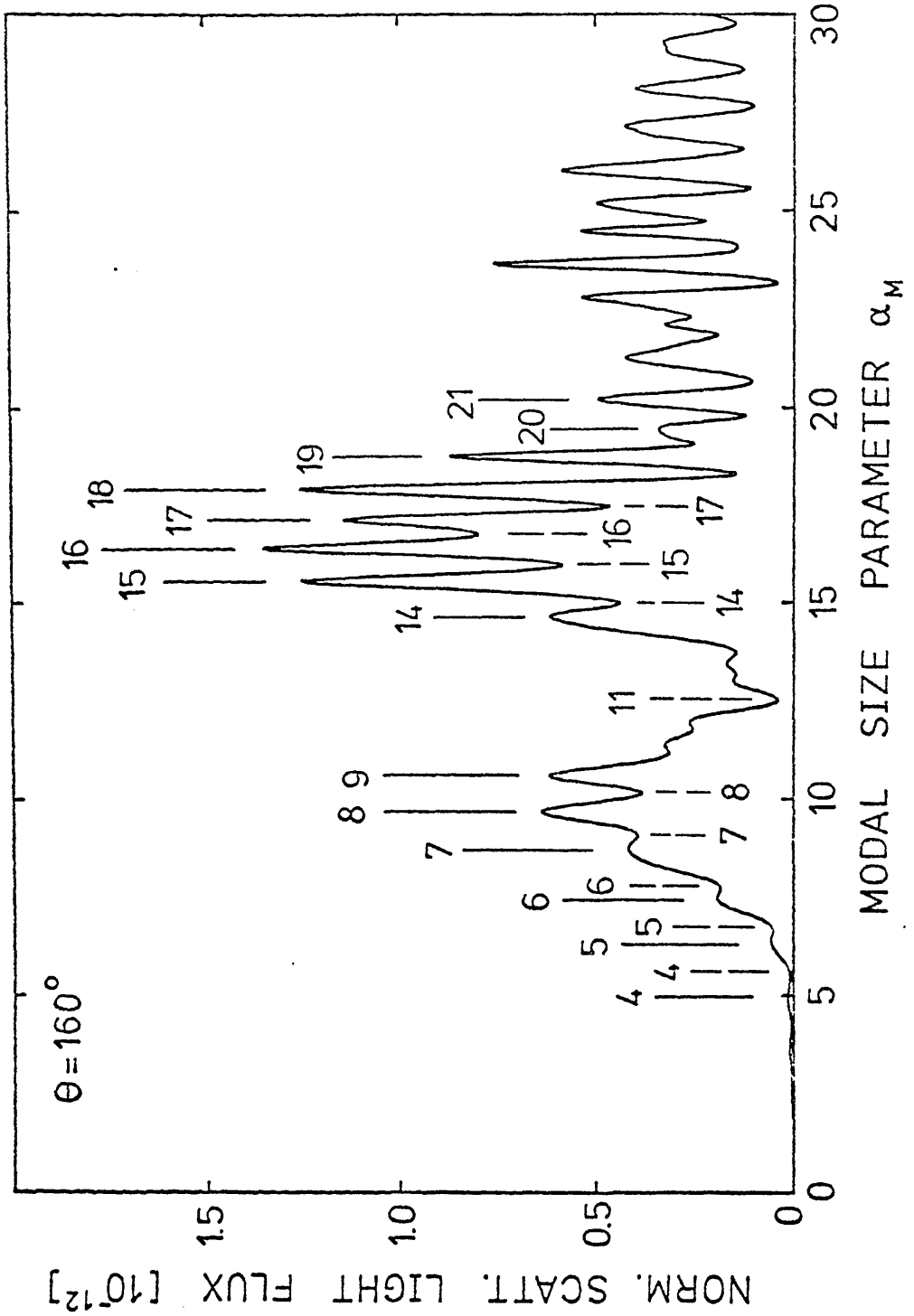

Fig. 37

As fig. 33 für $\theta_o = 160^o$

Figures 38, 39 and 4o show experimental light scattering curves for scattering angles 15^{o}, $3o^{o}$ and $16o^{o}$, respectively. The curves were obtained as the averages of 2o single experimental runs. Comparison with fig. 33, 34 and 37 shows good agreement. It can be seen that theoretically predicted resonance peaks for higher - order partial waves (e.g. at $\theta = 15^{o}$, $\alpha = 22.84$) can actually be verified experimentally.

A qualitative experimental observation of optical resonance has already been reported by Wood (19o2). A numerical investigation

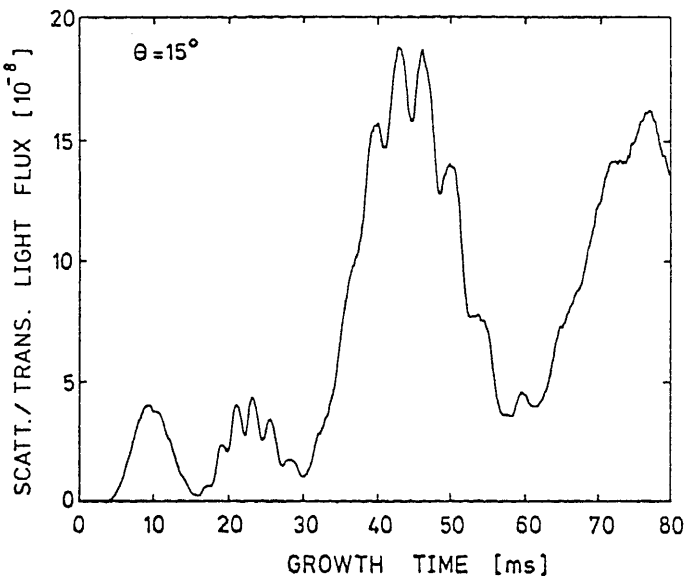

Fig. 38

Experimental ratio of light fluxes Φ_{sca}/Φ_{trans} as a function of time. Average over 2o single runs.
Scattering angle $\theta_o = 15^{o}$, saturation ratio $S_o = 153$ %
droplet concentration $C = 3.8.1o^{3}\ cm^{-3}$

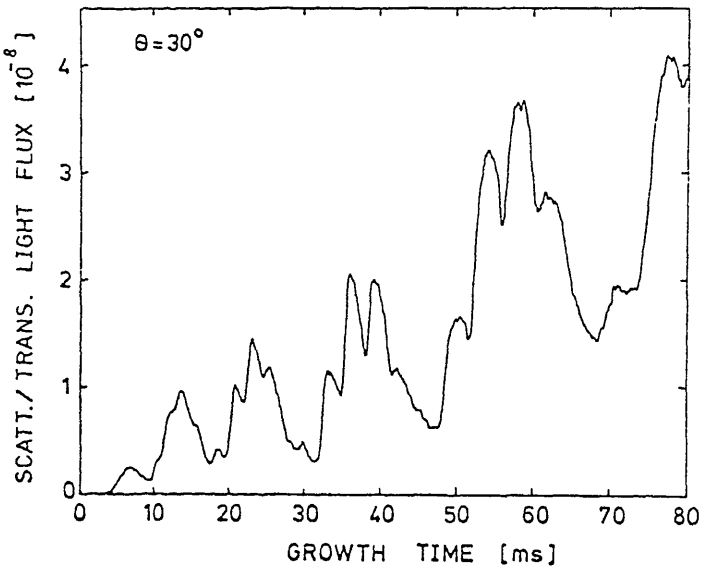

Fig. 39

As fig. 38 for $\theta_o = 30^o$.

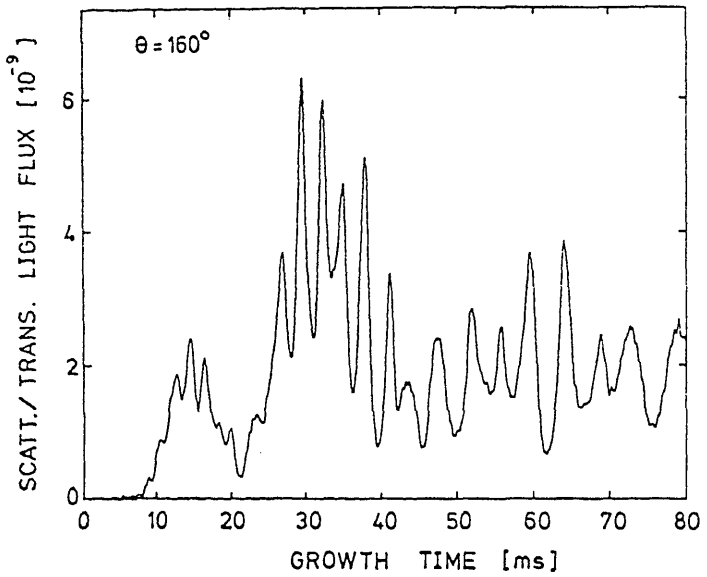

Fig. 40

As fig. 38 for $\theta_o = 160^o$.

of resonance peaks for the extinction cross section of spheres was performed by Chýlek (1976). Chýlek observed a basic period of the ripple structure. Furthermore it was found that absorption and nonsphericity strongly reduce the amplitude of resonance peaks. Ashkin and Dziedzic (1977) report measurements of the radiation pressure on dielectric spheres using optical-levitation techniques. Sharp resonances were observed for particular wavelengths in agreement with Mie-theory. As pointed out by Bennett and Rosasco (1978), optical resonances are important for the description of fluorescence and Raman scattering.

8.2 Measurements of droplet growth

Experimental investigations of droplet growth and evaporation have been performed by many authors. A number of different methods has been applied in order to obtain well-defined vapor pressures and thus saturation ratios in the measuring system. Furthermore, the observation of the droplets was based on various different principles.

In connection with measurements of the electron charge, Nestle (1932) investigated the evaporation of Hg-droplets in a vapor-saturated gas. Charged submicron Hg-droplets were injected into a Millikan-condenser. Rise and fall times of individual droplets were measured in immediate succession and from these measurements the droplet size was determined. The droplet mass was found to vary approximately linear with time in agreement with continuum droplet growth theory in connection with Kelvin's formula. Using published Hg-vapor pressure data, the diffusivity of Hg-vapor in CO_2, N_2 and Ar was estimated.

In a series of papers, Bradley et al. (1946), Birks and Bradley (1949) and Bradley and Shellard (1949) described measurements of the evaporation of drops in a vessel with vapor-absorbing walls. A single droplet with a diameter of the order of 1 mm was suspended on a quartz microbalance and the mass change of the droplet was measured. A number of organic liquids with very low volatility was considered. It was found that the droplet surface varied approximately linear with time in agreement with continuum droplet growth theory. After the corresponding vapor pressures were measured by means of an independent technique, the vapor diffusivities could be determined from the evaporation rates. Using very low total pressure (down to less than 1 torr), deviations from continuum droplet growth

theory were observed and agreement with Fuchs' (1934) semiempirical formula was obtained for mass accomodation coefficients close to unity. Similar observations were made by Monchick and Reiss (1954), who considered smaller droplets at somewhat higher pressures in a Millikan-condenser with vapor absorbing walls. Langstroth et al. (195o) studied the evaporation of single droplets with radii of about 1 mm, suspended in a chamber with vapor-absorbing walls, at atmospheric pressure. The droplet radii were measured by means of a microscope. Liquids with somewhat higher volatility, including water, were considered. The experimental evaporation rates were compared with the continuum theory of mass and heat transfer. Using published data for diffusion coefficients and vapor pressures, approximate agreement of theory and experiment was obtained. However, mechanically suspending the liquid droplet might have caused some systematic experimental error, particularly for liquids with higher volatility.

In order to avoid the mechanical suspension of the droplets, a new experimental technique was developed by Davis and Chorbajian (1974) and Chang and Davis (1976). A submicron charged droplet with low volatility was suspended in a chamber with zero bulk vapor pressure by means of an inhomogeneous electric field. The droplet size was determined by means of a best-fit procedure between experimental and theoretical light scattering intensities. At atmospheric pressure, a linear time-dependence of the droplet surface was observed. Approximate values for vapor pressures and diffusivities were determined from the evaporation data.

Experimental studies of droplet evaporation for low-volatility liquids are hampered by the insufficient knowledge of vapor pressures and diffusivities. Furthermore, significant errors can occur due to small amounts of high-volatility impurities. In order

to obtain reliable vapor pressure data and diffusivities for low-volatility liquids, Davis and Ray (1977) developed a method for calculating diffusivity and vapor pressure from continuum droplet evaporation rates, measured in three different carrier gases (He, N_2 and CO_2). Subsequently, this method was improved by Ray et al. (1979). Based upon this method, Davis and Ray (1978) performed measurements of droplet evaporation in the transition regime by varying the total gas pressure from o,o8 bar to atmospheric pressure. Good agreement with the theory of Loyalka (1973) was obtained.

In the above mentioned experiments, droplet evaporation was investigated. The bulk vapor pressure was either equal to the saturation vapor pressure or equal to zero. For many applications, however, droplet growth processes are important. Dennis (196o) investigated the growth rates of aqueous solution droplets in an air stream with controlled temperature and relative humidity. Various relative humidities over a range from 73 to 97 % were obtained by mixing of a dry and a saturated air stream with well-defined flowrates (divided flow method). A mechanically suspended solution droplet with a diameter of about 1 mm was observed by means of a microscope. The measured growth rates were compared with continuum droplet growth theory taking into account the production of latent heat, the ventilation, and the lowering of the vapor pressure above a solution. Fair agreement was obtained, the experimental growth rate being high by about 3o % for some solutions.

For measurements of the growth rate of pure liquid droplets, defined supersaturations must be obtained in the measuring system. Several methods have been used for this purpose. Coulier (1875) used the principle of adiabatic expansion in order to obtain supersaturated vapor. Aitken (189o/91) constructed the first

condensation nuclei counter. In the measuring chamber an adiabatic expansion was achieved by moving of a piston (volume-defined expansion chamber). For observing paths of ionizing particles, Wilson (1912) designed a volume-defined expansion chamber. Later, Wilson (1933) constructed a chamber, where the expansion was initiated by opening of a valve and thus connecting the chamber to a low-pressure system (pressure-defined expansion chamber). Some important features of expansion chambers were reviewed by Wilson (1951). Mettenburg, Kassner, and Rinker (1958) developed an expansion chamber for measurements of condensation nuclei concentrations and droplet growth. This chamber was later improved by Kassner, et. al. (1968 a).

Defined supersaturations can also be obtained in static downward diffusion chambers, as described by Langsdorf (1939). Studies of diffusional droplet growth in downward diffusion chambers have been performed by many authors, e.g., Gagin and Terliuc (1968), Gollub et al. (1973, 1974), Chodes et al. (1974). As pointed out by Vietti and Fastook (1975), these studies are complicated by the fact that "the nuclei must be introduced into a saturated environment, where in the time interval allowed for turbulence to subside, the droplets have grown a considerable amount". For measurements of homogeneous nucleation, Katz and Ostermier (1967) used a static upward diffusion chamber.

Expansion chambers have the advantage that supersaturations can be achieved nearly instantaneously, whereas static diffusion chambers work with time-independent supersaturations. Accordingly, droplet growth studies at relatively high supersaturations and growth rates were mostly performed by means of expansion chambers. On the other hand, static diffusion chambers are useful for obtaining low supersaturations, as occuring in the atmosphere.

Owe Berg and George (1968) investigated water droplet growth in a volume defined expansion chamber with an expansion time of about 2oo ms. The droplets were observed during the expansion by means of a high-speed film camera. However, no droplet growth could be detected. The droplet concentration was found to increase during the observation time the droplet aerosol being monodispersed at all times. Owe Berg and George concluded that "the growth of new droplets was too rapid to be resolved by the camera" and thus "5o μsec is a generous upper limit for the time of formation of condensate droplets 4 or 5 μ in diameter". As the known theories cannot explain these high growth rates, Owe Berg and Georg presume that the droplets "are formed by a chain-reaction type mechanism", the condensation nuclei serving as "chain initiators". However, Kassner, et al. (1968 b) point out that "it still requires the order of one millisec to increase the radius of a drop by one micron under the fastest conceivable physical meachnism". Schuster, et al. (1969) show that, due to the small sampling volume in the chamber used by Owe Berg and George, strong fluctuations of the observed droplet number will occur causing large statistical errors. Furthermore, Nix (1968) suspects that because of an insufficient resolution of the used optical system, the droplets will have caused a diffraction disc with a constant diameter between 3 and 4 μm. This would explain, why actual droplet growth has not been observed by Owe Berg and George.

For a correct interpretation of expansion chamber experiments, knowledge of the thermodynamic parameters in the measuring chamber during and after the expansion process is required (see section 3)). In order to investigate the thermodynamic processes in expansion chambers, Israel and Nix (1966 a,b) measured pressure and temperature in a Pollak condensation nuclei counter

using fast pressure and temperature transducers. Expansion times of the order of 1oo ms were found. Measurements with dry as well as with moist air resulted in a temperature decrease much smaller than expected for an adiabatic expansion. According to Israel and Nix this is caused by an irreversibility of the expansion. The experimental results of Israel and Nix were confirmed by Semonin and Hayes (1968). By means of light extinction measurements Israel and Nix observed the onset of water droplet growth already 7 ms after the start of the expansion. The actual saturation ratio in the expansion chamber of the Pollak-counter was found by Israel and Nix to be smaller than 1o2 % during the whole expansion process, whereas a saturation ratio of 27o % would be expected according to dry-adiabatic calculations (Nix, 1972). Nix (1968, 1972) concluded from the above results that the experimental droplet growth rate exceeds the theoretical prediction by a factor of about 1oo. Kassner, et al. (1968 b, c) discuss the difficulties in connection with temperature measurement using fine-wire thermometers in gases. The finite heat capacity of the wire and the steady heat production can cause erroneous temperature measurements, particularly during fast temperature changes. Finally, Kassner (1968 c) concluded that "in all probability it (the Pollak counter) is sufficiently adiabatic".

In order to measure droplet growth rates under reversible thermodynamic conditions, Nix (1968, 1969, 1972) develòped a new experimental technique. Instead of obtaining supersaturation by means of one single expansion, Nix achieved periodic changes of the saturation ratio by applying periodic pressure oscillations in a chamber with vapor-saturated air. Sinusoidal pressure oscillations with frequencies between 1 and 6o Hz and pressure amplitudes between 9 and 13 torr were obtained by means of an electronic wave generator in connection with an electrodynamic

pressure transducer. Corresponding peak saturation ratios between 1o4 and 1o8 % were calculated. The periodic growth and evaporation of single water droplets was optically observed. In order to achieve a sufficient time resolution, the considered droplets were kept on stationary elliptical orbits by introducing a slight unsymmetry of the flow conditions in the measuring chamber. By evaluating photographs of the droplets on their elliptical orbits Nix (1968) found that droplet growth only occurs during the periods of increasing supersaturations. Based on this observation Nix (1968) concluded that droplet growth is determined by a "slow" diffusion process, which depends on S and a "very fast" gaskinetic process depending on dS/dt. Later, Nix (1972) applied a light scattering technique for observation of the droplets. Thereby Nix found a sinusoidal droplet size change, the growth process occuring during nearly the whole period of supersaturation. However, no quantitative comparison with droplet growth theory was performed.

In order to test the droplet growth theory, quantitative measurements of the droplet size must be performed. Cohen (1969) first suggested a measuring technique based on illuminating the growing droplets and monitoring the intensity of the light, scattered by the droplets under a particular fixed scattering angle during the growth process. Cohen considered water droplets in a thermal diffusion cloud nuclei chamber at saturation ratios between 1oo,4 and 1o1 % and he measured the scattered light intensity under a scattering angle of $9o^{o}$. Because of the complexity of the obtained light scattering curves and the relatively low scattering intensities, a unique correspondence to the theoretical curves was not established and no quantitative comparison with droplet growth theory was performed. A similar experimental technique was used by Vietti and Schuster (1973 a, b) for measurements of water droplet growth in an expansion chamber at saturation ratios ranging from about 129 to 345 %. The saturation ratios were calculated assuming

dry-adiabatic conditions. The chosen expansion chamber was a duplicate of that used by Allard and Kassner (1965) with a chamber volume of about 1o l and expansion times of the order of 1oo ms. Re-evaporation nuclei from a previous homogeneous nucleation were used as condensation nuclei. The nuclei concentration were of the order of 1o cm^{-3}. At these very low concentrations the dry-adiabatic assumption appears to be justified. Vietti and Schuster chose a forward scattering angle of $3o^{o}$ and accordingly obtained less complicated experimental light scattering curves and higher scattering intensities than Cohen (1969). The correspondence between experimental and theoretical light scattering extrema was obtained by identification of the first Mie-peak. As pointed out by Carstens and Carter (1974 b),"the problem of initial conditions is important in using this technique. There is no guarantee that the first observed peak is actually the first Mie peak. This may be due to the possibility that the first peak, which is weak anyway, is not resolved. It may also be that the size distribution is just broad enough at the first peak, that it is washed out". In the experiments of Vietti and Schuster (1973 a, b) a "very monodisperse population of droplets" was observed. After the one-to-one correspondence between experimental and theoretical light scattering extrema was established,the droplet size at particular times during the growth process was determined from the position of the experimental light scattering extrema. The droplet growth was measured over a range of radii between o,45 and 1o μm. Fair agreement with several droplet growth theories was found, but mass accomodation coefficients as small as o,oo4 and simultaneously thermal accomodation coefficients of o,1 and less had to be assumed.

Using the same experimental technique, Carstens, et al. (1973) measured water droplet growth in Argon and found that a good theoretical fit to the experimental data can be obtained by

proper adjustment of the accomodation coefficients. It is emphasized that "a key step in the interpretation of the data lies in the identification of a specific Mie scattering peak". Subsequently, Carter and Carstens (1974) obtained "much better agreement" with the "conventional meteorological theory of drop growth" over a range of saturation ratios from 13o to 36o % assuming a thermal accomodation coefficient of unity and a mass accomodation coefficient of o,o23.

Wagner (1973) applied a similar experimental technique for quantitative measurement of water droplet growth. However, a smaller chamber volume of about 7o cm^3 was chosen and expansion times as short as 5 - 7 ms were thus achieved. Using different scattering angles in the range from 15^o to 165^o, a unique correspondence between experimental and theoretical light scattering peaks was established. Experimental droplet growth curves were obtained but no comparison with droplet growth theory was performed.

In order to extend the range of supersaturations, covered by the above mentioned expansion chamber experiments, Gollub et al. (1973, 1974) studied water droplet growth in a static downward diffusion chamber at saturation ratios not higher than 1o5 %. Condensation nuclei were entered into the chamber by means of a slow vertical downward flow of air, whose influence on the static supersaturation and temperature profiles in the chamber was negligible. The droplets, condensing on the condensation nuclei, fall through a sequence of known environments at a speed given by the sum of the mean flow speed and the terminal settling velocity of the droplets. For steady state conditions, the droplet radius and the corresponding fall velocity will only be functions of the height in the chamber. Gollub et al. (1973) described a technique for measuring the fall velocity of the droplets using "optical

heterodyne spectroscopy". Their method is applicable for droplets of radius larger than about 2 µm, because in this size range the influence of Brownian motion on the heterodyne spectrum is negligible. From measurements of the fall velocity at various heights, the droplet radius can be calculated as a function of height. Qualitative agreement with the theory of Fukuta and Walter (197o) was obtained for a mass accomodation coefficient of o,o2. After improving the experimental design, Gollub et al. (1974) obtained agreement with the theory of Fukuta and Walter for saturation ratios between 1o2 and 1o5 %, if mass and thermal accomodation coefficients are related by a particular equation, "but $\alpha = \beta = 1,o$ is not definitely excluded"."There appears to be a definite contrast" to the results of Vietti and Schuster (1973 a, b). However, strong deviations from theory were observed for saturation ratios smaller than 1o1,5 %. It should be mentioned that some uncertainty of the actual supersaturations is introduced by the presence of the cylindrical walls of the chamber.

Up to this point, most experiments, e.g. Vietti and Schuster (1973 a, b), were performed with extremely low droplet concentrations and thus the mutual influence of the growing droplet was assumed to be negligible. In order to study the influence of droplet concentration on the droplet growth process, Wagner (1974 b) measured water droplet growth in an expansion chamber at two different saturation ratios, varying the droplet concentration over a range from $5.1o^3$ to $5oo.1o^3$ cm^{-3}. Using the same technique as described above, the droplet size at particular times during the growth process was determined from the position of the experimental light scattering extrema. But furthermore, the droplet concentration was independently obtained from the height of the experimental light scattering maxima. It was found that the droplet growth is nearly unaffected by droplet concentration during the initial growth stages. However, later in the growth process, a stoppage of growth was observed depending on the actual droplet concentration.

This behaviour was qualitatively explained by the effects of vapor depletion and production of latent heat during droplet growth, but no quantitative comparison with corresponding droplet growth calculations was performed.

For calculation of droplet growth in droplet aerosols Wagner and Pohl (1975 a) as a first approximation used an analytical continuum droplet growth expression (Mason, 1971) without transitional corrections. The combined effects of vapor depletion and production of latent heat in the droplet aerosol were taken into account using the model of time dependent bulk parameters (see section 2.4.2)). Droplet radius, bulk temperature and bulk saturation ratio were calculated as functions of time for different initial saturation ratios and droplet concentrations. In qualitative agreement with the experimental results of Wagner (1974 b), the calculated droplet growth curves turned out to be insensitive with respect to the droplet concentration during the initial growth stages. Furthermore, a stoppage of growth is predicted depending on the actual droplet concentration. When the droplet radius approaches its final value, the calculated bulk saturation ratio approaches 1oo %. A quantitative comparison of experimental and theoretical growth curves was performed by Wagner (1975 b). The experimental growth rate was found to be somewhat smaller than theoretically predicted. As a possible explanation Wagner suggested insufficient humidification of the condensation nuclei aerosol. After assuming a certain value $< 1oo$ % for the relative humidity of the nuclei aerosol, good agreement with the experimental growth curves was obtained. The dependence of the droplet growth rate on the droplet concentration was correctly described by the used theory.

Vietti and Fastook (1974) reported about measurements performed in an expansion chamber, modified to produce small supersaturations.

Water droplet growth was observed at saturation ratios below 11Q % and droplet concentrations of no more than $1o^3$ cm^{-3}. In agreement with Wagner (1974 b) it was found that the growth process stopped at a certain terminal size. From comparison with theory Vietti and Fastook (1974) concluded that "theory agrees reasonably well with experiment during growth of the droplets, but does not predict the stoppage of growth".

Using a volume defined expansion chamber with a volume of 1 m^3, Vietti and Fastook (1975) measured water droplet growth in air for peak saturation ratios ranging from 1o2 to 1o5 %. Because of the large size of the chamber, the central portion of the chamber volume remains adiabatic for as long as 3o s. The expansion times were of the order of 3oo ms. Droplet concentrations of approximately 5oo cm^{-3} were chosen for all experiments. Again, stoppage of growth was observed at particular terminal droplet sizes. Based on the theory of Fukuta and Walter (197o) and taking into account vapor depletion and production of latent heat, droplet growth curves were calculated. The best overall agreement with the experimental data was obtained, if both accomodation coefficients were chosen to be unity. This is in contrast to the results, obtained by Vietti and Schuster (1973 a, b) for higher supersaturations. Vietti and Fastook (1975) conclude that the theory of Fukuta and Walter is valid for atmospheric conditions. At larger supersaturations, however, deviations occur and the experiments at larger supersaturations are regarded as "not similar". According to Vietti and Fastook that "places the larger supersaturation cloud chamber data as not applicable" with respect to atmospheric conditions.

The dependence of the droplet growth process on the carrier gas was studied by Vietti and Fastook (1976). Water droplet growth measurements in carbon dioxide were performed for saturation ratios between 1o1,7 and 1o3,5 %. It turned out that there is

"no specific value for the sticking coefficient which provides overall agreement during the later stages of the observed growing period". For droplets smaller than 2 µm radius, the mass accomodation coefficient α_M assumes values between 1 and 0,1. However, above 2 µm radius, α_M must be continually diminished to a value around 0,04. Vietti and Fastook suggest that the dehydration of bicarbonate is the principal mechanism for the observed reduction of droplet growth rate. In order to investigate the influence of the condensation nuclei on the growth process, Vietti (1978) produced different NaCl-particles by spraying aqueous salt solutions of different concentrations. It was found that α_M = 0,1 for pure water and α_M = 0,02 for the case, when 10^{-17} mol salt is present in each droplet.

Using a process controlled expansion chamber, Wagner and Pohl (1977 a,b) measured water droplet growth rates for different initial saturation ratios. Systematic deviations from the used droplet growth theory were observed, stronger deviations occuring at higher saturation ratios. A fit of the theoretical curves with the experimental data can be achieved by proper choice of the assumed humidification of the nuclei aerosol. However, smaller values of the humidification had to be assumed for higher saturation ratios. On the other hand, the measuring system was designed, so that the humidification of the nuclei aerosol is definitely independent from the chosen expansion ratio. This indicates that the dependence of the droplet growth rate on the supersaturation is not properly described by the applied theoretical model.

It appears from the above mentioned experiments that the deviations between theory and experiment are increasingly important for higher saturation ratios and growth rates. Furthermore, there is still much uncertainty about the actual values of the accomodation coefficients and their possible dependence on other physical parameters.

The investigations, described in the present section,are aimed towards a better understanding of the droplet growth process over a wide range of supersaturations. As a first step, single droplet growth theory was tested using droplet aerosols with low droplet concentrations. Later it is planned to study the mutual influence of the droplets in droplet aerosols with higher droplet concentrations. Furthermore, droplet growth processes for vapor/carrier gas-combinations other than water/air will be investigated.
Part of the results, reported in the present section, is included in Wagner and Pohl (1978 a, 1979).

Water droplet growth in the SANC-expansion chamber was measured for three different initial saturation ratios. NaCl-particles were used as condensation nuclei, which were produced by the aerosol generator, described in section 6.1.3). The nuclei concentration was chosen sufficiently small so that the growth process can be regarded with good approximation as single droplet growth for the considered measuring times (see below). As described in section 5.3), droplet size and concentration were obtained independently at specific times during the droplet growth process by comparison of experimental and theoretical light scattering curves . The following experimental parameters were chosen:

Identification code:	TURB 28.o1
Atmospheric pressure:	745 Torr
Humidifier temperature:	27,93°C
Chamber temperature:	28,53°C
Scattering angles:	15°, 45°
Expansion ratios:	1.o56, 1.257, 1.359
Initial saturation ratios:	12o %, 252 %, 354 %
Droplet concentration:	$4,6.1o^3$ cm^{-3}
Number of repetitions:	15.

The experimentally obtained droplet growth data are shown in fig. 41.

The above experimental results were compared with various theoretical predictions. The numerical calculations were performed in program section 4 of the data evaluation software, which is described in section 7.3). For the considered system water/air the following values were used (The subscripts L, v and g refer to liquid water, water vapor, and air, respectively, most values were taken from Landoldt-Børnstein):

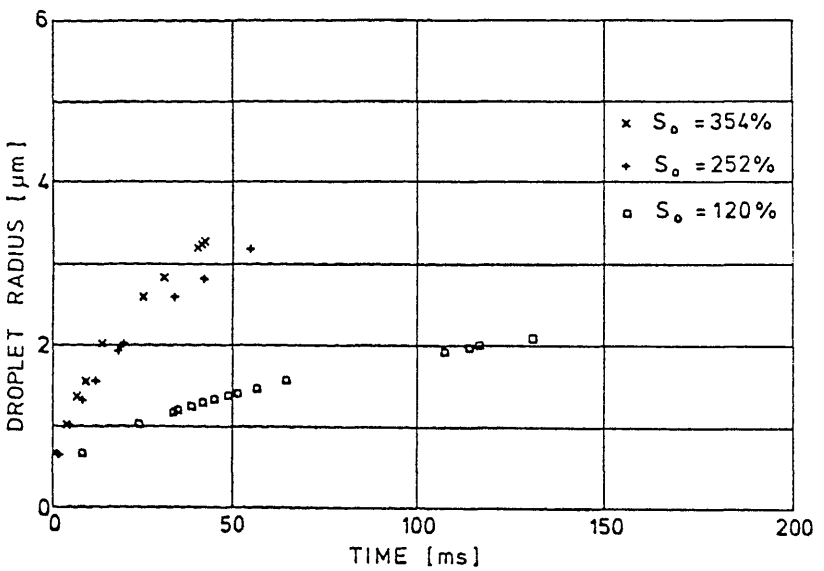

Fig. 41

Experimentally obtained droplet growth data from run TURB 28.01. Initial saturation ratios 120 %, 252 %, and 354 %, droplet concentration 4.6.10^3 cm^{-3}.

Constant values:

General gas constant:

$$R = 8,3147.1o^3 \text{ J kmol}^{-1} \text{ K}^{-1}$$

Molecular weights:

$$M_v = 18,o16 \text{ kg kmol}^{-1}$$

$$M_g = 28,96456 \text{ kg kmol}^{-1}$$

Air density at normal conditions (0^oC, 76o Torr):

$$(\rho_g)_N = 1,293o7 \text{ kg m}^{-3}$$

Specific heat capacities at constant pressure:

$$c_{p,v} = 1,86o.1o^3 \text{ J kg}^{-1} \text{ K}^{-1}$$

$$c_{p,g} = 1,oo5.1o^3 \text{ J kg}^{-1} \text{ K}^{-1}$$

Ratios of heat capacities (adiabatic indices):

$$\kappa_v = 1,343$$

$$\kappa_g = 1,4o2o.$$

Functions:

Saturation (equilibrium) vapor pressure:

$$\ln p_s(T) = A_1 - \frac{A_2}{T-A_3} - A_4 \ln T + A_5 T \qquad \text{(equ.(2.45))}$$

where

$$A_1 = 77,344913$$

$$A_2 = 7235,4247$$

$$A_3 = 0$$

$$A_4 = 8,2$$

$$A_5 = o,oo57113$$

p_s in N m^{-2}

T in K.

Specific enthalpy of water vapor:

$$h_v(T) = \gamma_v . T \qquad \text{(equ.(2.22-1))}$$

where

$$\gamma_v = 1,842.1o^3$$

h_v in J kg^{-1}

T in K.

Binary diffusion coefficient:

$$D(p_o,T) = D_N \left(\frac{T}{T_N}\right)^{\mu} \frac{p_N}{p_o} \qquad \text{(equ.(2.9))}$$

where

$D_N = 22,o7487.1o^{-6}$

$T_N = 273,16$

$p_N = 1o1324,72$

$\mu = 1,6658o$

D in $m^2\ s^{-1}$

T in K

p_o in $N\ m^{-2}$.

Thermal conductivity of the binary mixture:

$$K(p_v/p_g,T) = \frac{K_v}{1 + A_{vg}\ p_g/p_v} + \frac{K_g}{1 + A_{gv}\ p_v/p_g} \qquad \text{(from equ. (2.18))}$$

$$K_v = K_v^{(o)} + K_v^{(1)} \cdot T \qquad \text{(equ. (2.19-1))}$$

$$K_g = K_g^{(o)} + K_g^{(1)} \cdot T \qquad \text{(equ. (2.19-2))}$$

where:

$K_v^{(o)} = - 6,7194.1o^{-3}$

$K_v^{(1)} = 7,4857.1o^{-5}$

$K_g^{(o)} = 3,44o5.1o^{-3}$

$K_g^{(1)} = 7,5177.1o^{-5}$

$A_{vg} = o,556$

$A_{gv} = 1,189$

K in $W\ m^{-1}\ K^{-1}$

T in K.

Specific latent heat of vaporization for water:

$$L(T) = L^{(o)} + L^{(1)} \cdot T$$

where:

$L^{(o)} = 3,14566.1o^{6}$
$L^{(1)} = -2,36164.1o^{3}$
L in J kg^{-1}
T in K.

Molar heat capacity of air at constant volume:

$$C_{v,g}(T) = C_{v,g}^{(o)} + C_{v,g}^{(1)} \cdot T \qquad \text{(equ.(2.77)}$$

where

$C_{v,g}^{(o)} = 2o,4653.1o^{3}$
$C_{v,g}^{(1)} = 1,3o17$
$C_{v,g}$ in J $kmol^{-1}$ K^{-1}
T in K.

Density of liquid water:

$$\rho_L(T) = \rho_L^{(o)} + \rho_L^{(1)} \cdot T \qquad \text{(equ.(2.47))}$$

where

$\rho_L^{(o)} = 1o49,572$
$\rho_L^{(1)} = -\ o,1763$
ρ_L in kg m^{-3}
T in K.

Surface tension of the water - air - interface:

$$\sigma_{LV}(T) = \sigma_{LV}^{(o)} + \sigma_{LV}^{(1)} \cdot T \qquad \text{(equ.(2.46))}$$

where

$\sigma_{LV}^{(o)} = o,117296$
$\sigma_{LV}^{(1)} = -\ o,152362.1o^{-3}$
σ_{LV} in N m^{-1}
T in K.

First the experimental data were compared with droplet growth curves, calculated by means of equ. (2.91) (analytical solution). The correction factors β_M, β_T, F_M and F_T were not applied and thereby similar equations, as originally derived by Maxwell (1877), were obtained. As can be seen from fig. 42, the experimental droplet growth rates are significantly smaller than theoretically predicted by the uncorrected analytical solution over the considered range of saturation ratios. This could possibly be explained by an insufficient humidification of the nuclei aerosol in the humidifier. Assuming a humidification (saturation ratio at the exit of the humidifier) of 8o %, excellent agreement with the experimental data, corresponding to the intermediate supersaturation value, can be obtained, as can be seen in fig. 43. However, the experimental growth rate is still smaller than theoretically predicted for the high supersaturation value. On the other hand,

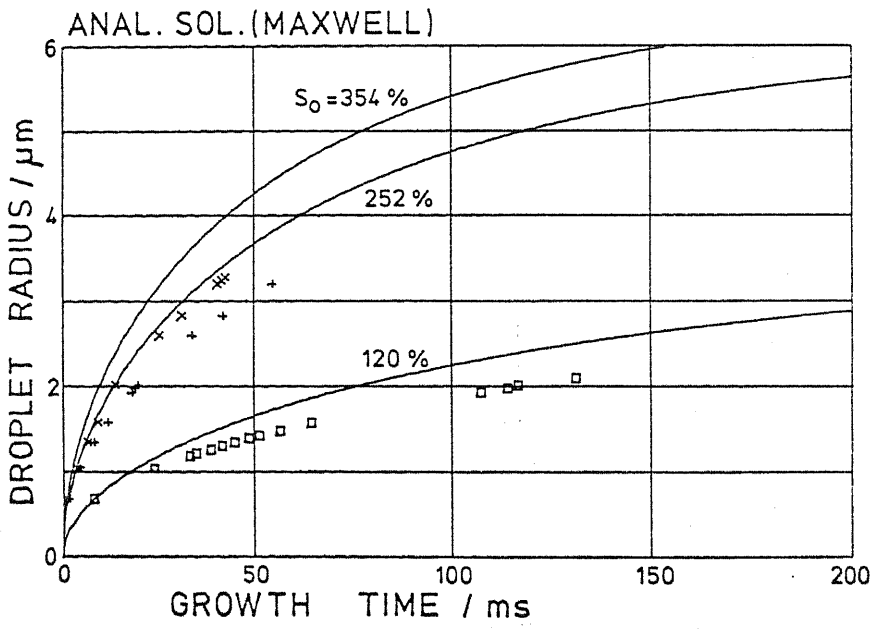

Fig. 42

Droplet growth curves, calculated for initial saturation ratios 12o %, 252 % and 354 % according to the analytical solution with no corrections applied (Maxwell). The corresponding experimental data are indicated.

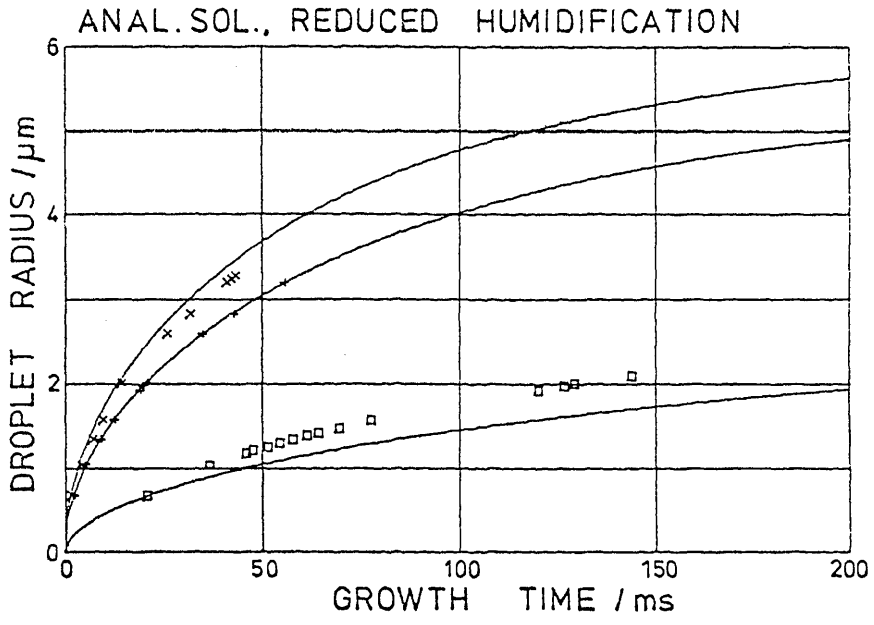

Fig. 43

Droplet growth curves, calculated according to the analytical solution with no corrections applied (Maxwell). A humidification of 80 % is assumed. The corresponding experimental data are indicated.

for the small supersaturation value, the experimental growth rate exceeds the theoretical one. In order to achieve agreement over the considered range of supersaturations, different humidifications would have to be assumed depending on the chosen supersaturation. However, this is unrealistic because the measuring cycle has been specifically designed, as explained in section 5.2), to provide a humidification of the nuclei aerosol, independent from the low-pressure system and thus from expansion ratio and supersaturation. Hence, the theoretical model does not properly describe the dependence of the droplet growth rate on the supersaturation (Wagner and Pohl, 1977 a, b).

Some improvement of the theoretical fit was achieved by introducing the transitional correction factors β_M and β_T in equ. (2.91). These factors were calculated according to the semiempirical expressions (2.79) ("Fukuta"), (2.8o) ("Smirnov") or according to Dahneke (1977). Fig. 44 shows the numerical results together with the corresponding experimental data for the initial saturation ratio of 354 %. The mass and thermal accomodation coefficients α_M, α_T were both chosen to be unity. For comparison, the uncorrected growth curve ("Maxwell") is included. The calculations according to Dahneke and Smirnov yielded very similar results, which could therefore not be indicated separately. As can be seen from fig. 44, the experimental growth rate is still significantly

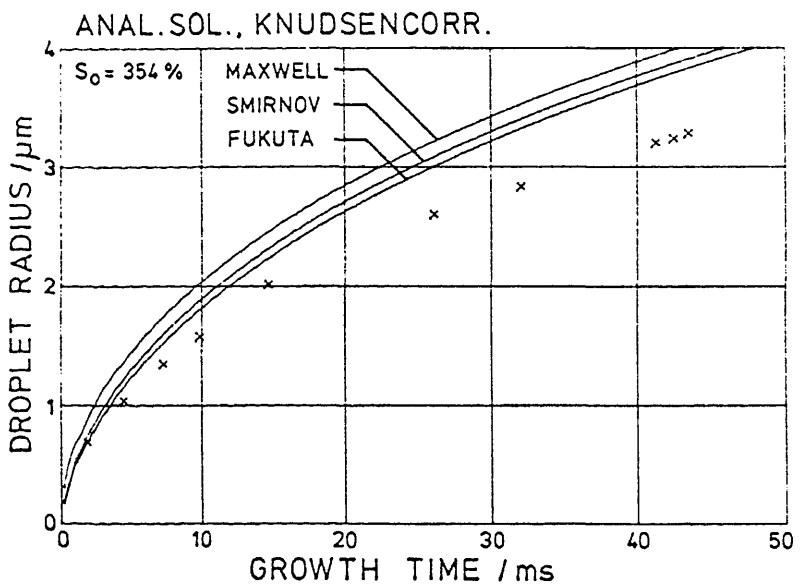

Fig. 44

Droplet growth curves, calculated for the initial saturation ratio 354 % according to the analytical solution with various transitional corrections applied ($\alpha_M = \alpha_T = 1$). The uncorrected curve (Maxwell) is included. The corresponding experimental data are indicated.

smaller than theoretically predicted. As suggested by many authors (see above), a better agreement could be obtained by assuming lower values for the accomodation coefficients. Fig. 45 shows the results for a mass accomodation coefficient α_M = o,2 and a thermal accomodation coefficient of unity. It can be seen that the theoretical curves can be forced to agree with the experimental data for small droplet radii. However, significant deviations still occur at larger droplet sizes. In this connection it should be mentioned that the transitional correction is insignificant for larger droplet sizes and accordingly small Knudsennumbers.

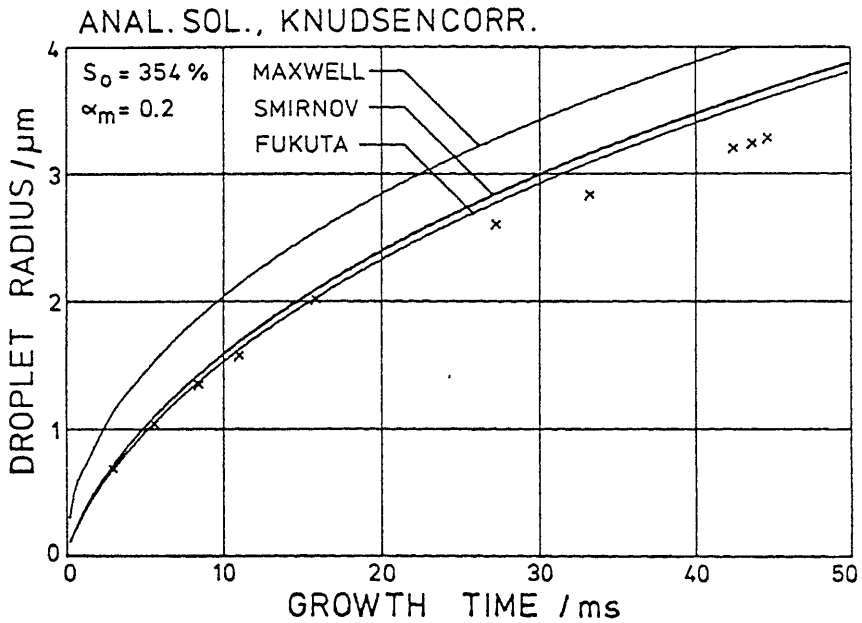

Fig. 45

As fig. 44 for α_M = o,2 , α_T = 1.

As mentioned in section 2.3.2), the transitional correction becomes less important with increasing droplet radius whereas the diffusional and thermal corrections are size-independent. By introducing the diffusional and thermal correction factors F_M and F_T in equ. (2.91) in addition to the transitional correction factors β_M and β_T, the curves of fig. 46 where obtained for the initial saturation ratio of 354 %. Mass and thermal accomodation coefficients α_M, α_T were both chosen to be unity. and the thermal diffusion factor α was chosen to be zero. Comparison with fig. 44 shows that the diffusional and thermal correction provides a significant improvement of the theoretical fit. This improvement was achieved without adjusting undetermined parameters.

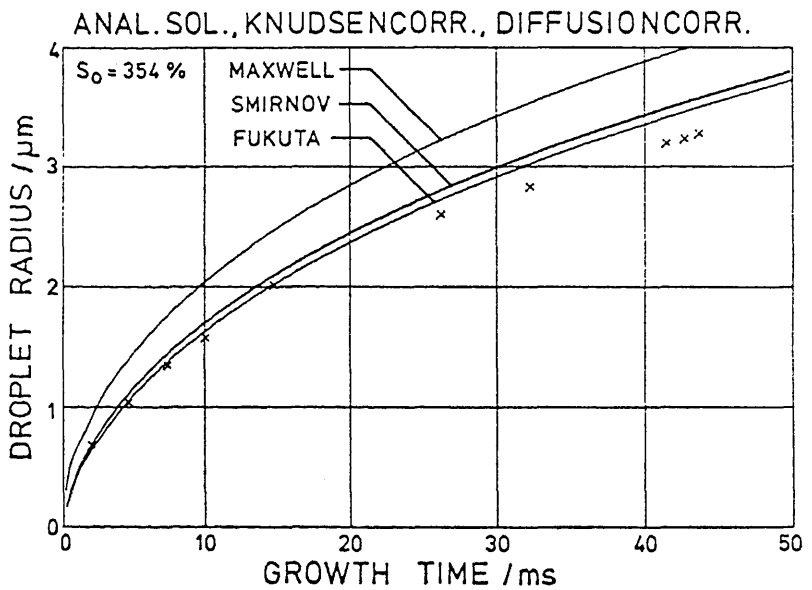

Fig. 46

As fig. 44 with diffusional and thermal corrections applied (α=0) in addition to the transitional corrections ($\alpha_M = \alpha_T = 1$).

While a satisfactory theoretical fit can be observed in fig. 46 for small droplet radii, significant deviations still occur at larger sizes. These deviations cannot be eliminated by chosing accomodation coefficients less than unity, because, as mentioned above, the transitional correction is insignificant for larger droplet sizes. A possible explanation for the remaining deviations could be the fact that equ. (2.91) for the mass flux was derived using an approximate expression for the equilibrium vapor pressure, as obtained from the equation of Clausius and Clapeyron. The correct temperature dependence of the equilibrium vapor pressure can be taken into account by numerically solving equ. (2.9o) to obtain T_a for different values of the droplet radius a (numerical solution). Fig. 47 shows droplet growth curves calculated for the initial saturation ratio 354 % by means of the numerical solution. Various transitional corrections with $\alpha_M = \alpha_T = 1$ as well as diffusional and thermal corrections with $\alpha = 0$ were applied. Good agreement with the experimental data can be observed. The transitional correction according to Smirnov seems to provide a somewhat better fit than Fukuta's expression. It should be emphasized that the theoretical curves of fig. 47 were obtained without adjusting undetermined parameters.

The above described numerical results were obtained taking into account the effects of vapor depletion and production of latent heat during the growth process (see section 2.4.2)). The influence of these effects on the growth curves is illustrated by means of fig. 48. The lower curve in fig. 48 was calculated taking into account vapor depletion and latent heat production for the droplet concentration of $4{,}6.1o^3$ cm^{-3} and using the transitional correction according to Smirnov. This curve is identical to the corresponding growth curve in fig. 47. The upper curve in fig. 48 was calculated similar to the lower curve, but assuming the droplet concentration to be zero and thereby neglecting the mutual

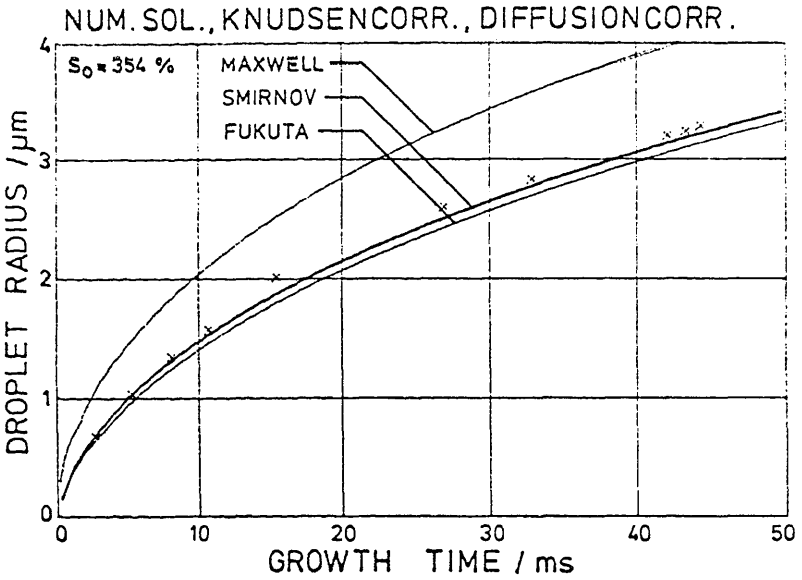

Fig. 47

Droplet growth curves, calculated for the initial saturation ratio 354 %, according to the numerical solution with various transitional corrections ($\alpha_M = \alpha_T = 1$) as well as diffusional and thermal corrections ($\alpha^M = 0$) applied. The uncorrected curve, based on the analytical solution (Maxwell) is included. The corresponding experimental data are indicated.

influence of the growing droplets. The small differences between the two curves in fig. 48 indicate that, as mentioned above, the droplet concentration was chosen sufficiently small so that the mutual influence of the growing droplets does not cause significant changes of the growth curves for the considered measuring times.

There is some uncertainty about the actual value of the thermal diffusion factor α. As mentioned in section 2.2.4), α is probably equal to 0.01 for the mixture of water vapor and air (Whalley, 1951, Katz and Mirabel, 1975). Generally, the absolute value of α is

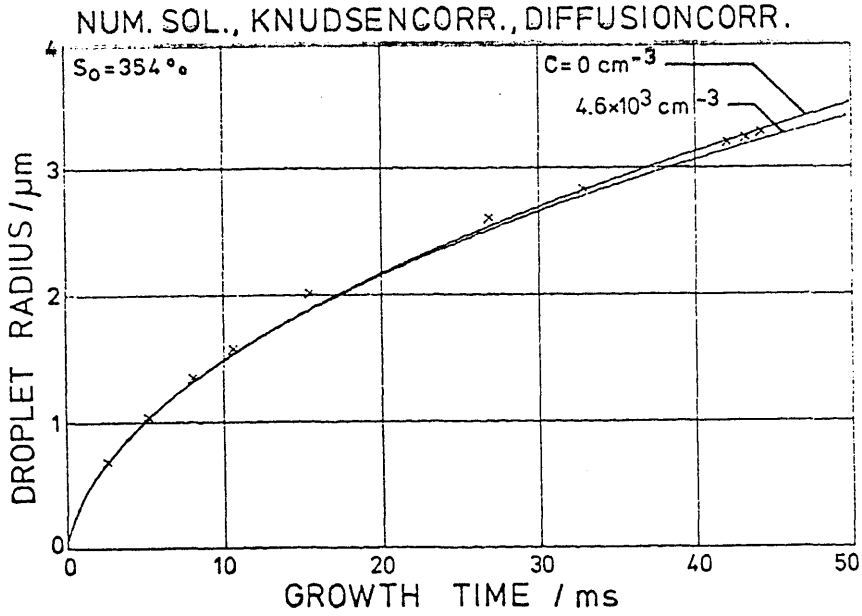

Fig. 48

Influence of the mutual interaction of the growing droplets on the growth process. The growth curves were calculated for the initial saturation ratio 354 % according to the numerical solution with all corrections applied. The lower curve corresponds to the actual experimental droplet concentration 4.6 .10^3 cm^{-3}, wheras the upper curve was calculated for zero droplet concentration. The corresponding experimental data are indicated.

assumed to be less than 0.6 (see section 2.2.2)). Fig. 49 shows the influence of thermal diffusion factor α on the growth curves. It can be seen that even thermal diffusion factors with unrealistically high absolute values cause only small changes of the growth curves. In order to test the chosen theoretical description of droplet growth for different initial supersaturations, the calculations were performed for the initial saturation ratios 120 %, 252 % and 354 %. Fig. 50 shows theoretical growth curves calculated by means of the numerical solution with the transitional correction according to Smirnov as well as diffusional and thermal corrections included. Both accomodation coefficients were

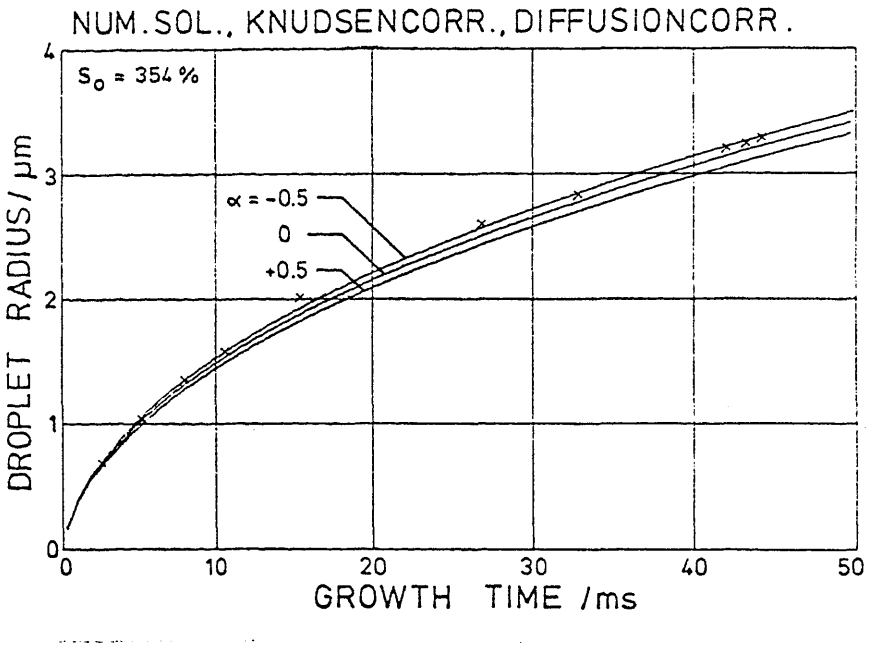

Fig. 49

Influence of the thermal diffusion factor α on the growth process. The growth curves were calculated for the initial saturation ratio 354 % according to the numerical solution with all corrections applied. The middle curve corresponds to α = 0, whereas the upper and lower curves were calculated for α = - 0.5 and α = + 0.5, respectively. The corresponding experimental data are indicated.

chosen to be unity and the thermal diffusion factor was set equal to zero. Satisfactory agreement with the experimental data can be observed for the considered range of supersaturations without making arbitrary assumptions. This indicates the internal consistency of the used theory.

For the above calculations the initial saturation ratios were determined assuming a reversible, quasistatic and dry-adiabatic expansion in the expansion chamber (see section 3.2)). The above mentioned consistency

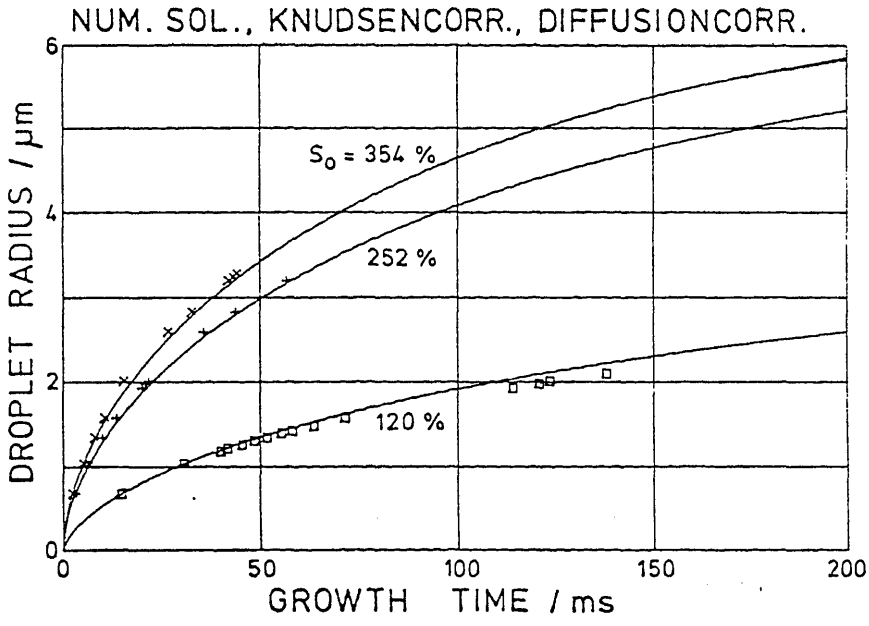

Fig. 5o
Droplet growth curves, calculated for initial saturation ratios 12o %, 252 % and 354 % by means of the numerical solution with the transitional correction according to Smirnov ($\alpha_M = \alpha_T = 1$) as well as diffusional and thermal corrections ($\alpha = 0$) applied. The corresponding experimental data are indicated.

of the theoretical results at different initial supersaturations and thus different expansion ratios suggests that these assumptions are justified for the present experimental conditions. The expansion can only be considered as dry-adiabatic, if changes of the saturation ratio during the expansion process, due to vapor depletion and production of latent heat, are negligible. Direct measurements of the saturation ratio during the growth process are difficult, as mentioned in section 2.4.3). However, based on the agreement of theoretical and experimental droplet growth rates it

can be assumed that the calculated time dependence of the bulk saturation ratio agrees with the actual experimental conditions. Fig. 2 in section 2.4.3) shows the bulk saturation ratio, calculated for the present experimental conditions and for the initial saturation ratio 354 % as a function of time during the growth process. The calculations were performed by means of the numerical solution with the Knudsen correction (Smirnov) and diffusional and thermal corrections included. It can be seen from fig. 2 that the changes of the bulk saturation ratio during the first 1o ms of the growth process are small. As shown in section 5.3) (see fig. 2o), the expansion process has a duration of 5 - 7 ms. This further supports the assumption of dry-adiabatic expansion. Accordingly it can be assumed as a good approximation that for the present experimental conditions the calculated initial saturation ratios actually occur in the expansion chamber at the end of the expansion. The assumption of reversible, quasistatic and dry-adiabatic expansion is further discussed in sections 9.1) and 9.2).

The above described results allow a number of conclusions as follows:

1) The assumption of quasi steady-state, which was made throughout the above described calculations, provides a good theoretical description of droplet growth processes for most practically important conditions. Accordingly, the duration of transient phenomena seems to be small compared to the typical growth times. This experimental result is in general agreement with most theoretical investigations of nonstationary droplet growth and evaporation (see section 2.1)).

2) Possible effects of incomplete mass or thermal accomodation at the droplet surface are not important for the description of the growth of pure water droplets in air, over a range of saturation ratios from 120 % to 354 % and for Knudsennumbers below about 0.3. The best theoretical fit with the experimental growth rates was always obtained by setting the mass as well as the thermal accomodation coefficient equal to unity. As mentioned in section 2.3.2) and in the present section, many authors assume mass accomodation coefficients α_M of the order of 0.03 and smaller, The value $\alpha_M = 0.036$, as obtained by Alty and Mackay (1935), was used by a number of authors. Fig. 51 shows the dependence of theoretical droplet growth curves on the choice of the mass accomodation coefficient α_M for the initial saturation ratio 354 % and for a thermal accomodation coefficient $\alpha_T = 1$. The calculations were based on the numerical solution with all corrections included. The best theoretical fit can be observed for $\alpha_M = 1$. For values of the mass accomodation coefficient $\alpha_M < 0.5$ significant deviations between theoretical and experimental growth rates can be observed and the value $\alpha_M = 0.03$ appeares to be definitely excluded. Accordingly, for the present experimental conditions the mass accomodation coefficient α_M for water was found to be larger than 0.5. As mentioned earlier, transitional effects and thus accomodation coefficients have a significant influence on the droplet growth process only at sufficiently large Knudsennumbers. Therefore a more precise determination of α_M can only be performed, if smaller droplets or lower gas pressures are considered.

3) The first order mutual interactions of mass and heat flux in the vicinity of the droplets have a significant influence on the droplet growth process. As opposed to the transitional

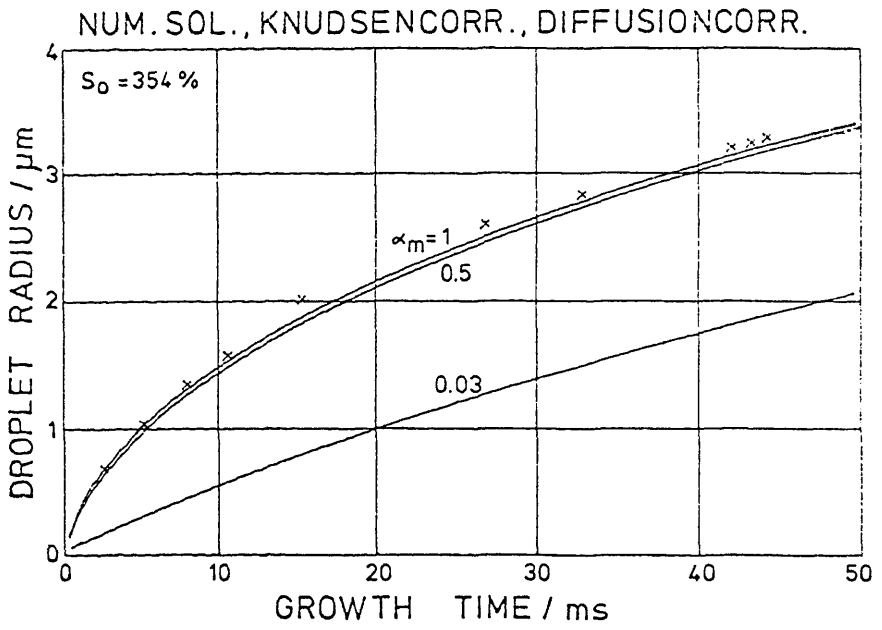

Fig. 51

Dependence of the growth curves on the choice of the mass accomodation coefficient α_M for the initial saturation ratio 354 % and for a thermal accomodation coefficient $\alpha_T = 1$. The calculations were based on the numerical solution with Knudsen correction (Smirnov) and diffusional and thermal corrections ($\alpha = 0$) included. The corresponding experimental data are indicated.

effects, the first order effects are not size dependent and thus are important even at larger droplet sizes, where the transitional effects are already negligible. In previous investigations, the first order effects have not been taken into account. This is consistent with the fact that most authors report experimental droplet growth rates smaller than theoretically predicted. In many cases the agreement was then achieved by chosing accomodation coefficients less than unity This might be an explanation, why low and very scattered values of the accomodation coefficients can be found in the literature. From the above described

calculations it can be concluded that thermal diffusion and the inverse process, the diffusion-thermo effect, are of minor importance for the droplet growth, at least for the system water/air. This result agrees with an estimate by Vietti and Fastook (1975). Furthermore the calculations showed that the Stefan flow is negligible. However, there are two first order effects which are important for droplet growth processes. The mass flux is smaller as compared to the usually applied zeroth order theory because the driving force for the mass flux is grad X_v and not gradρ_v. These gradients are proportional only for the case of uniform temperature, but high temperature gradients occur in the vicinty of the droplets (of the order of $15.1o^3$ K cm^{-1}, see section 2.4.3)). Furthermore, the heat flux is retarded because of the kinetic energy, which is carried with the diffusing vapor molecules. Both effects together cause a significant reduction of the theoretical droplet growth rate. For high supersaturations it was found that the analytical solution, equ. (2.91), which is based on an approximate expression for the saturation vapor pressure, significantly deviates from the experimental data. The numerical solution of equ. (2.9o), however, yields a good theoretical fit over the whole considered range of supersaturations. This indicates that using a simplified approximate expression for the equilibrium vapor pressure causes errors at high supersaturations. In most previous investigations, droplet growth was calculated by means of the analytical solution. This might be an explanation for the fact that Vietti (1973 a, b) found deviations between theory and experiment for high supersaturions, whereas Gollub et al. (1974)and Vietti and Fastook (1975) observed good agreement for low supersaturations. It can be concluded that droplet growth for atmospheric conditions at low supersaturations can be described sufficiently accurate by means of the analytical solution, equ. (2.91)). However, it is

important to include the diffusional and thermal correction factors F_M and F_T according to equ. (2.53), (2.4o) in addition to the transitional correction factors β_M and β_T. After inserting F_M and F_T into the analytical growth law, good agreement with experimental growth rates at low supersaturations is obtained without arbitrary adjustment of undetermined parameters.

8.3 Measurements of heterogeneous nucleation

Measurements of the number concentration of small aerosol particles can be performed by observing heterogeneous nucleation in supersaturated vapor. The aerosol particles act as condensation nuclei and the number of the condensing droplets can be measured. Assuming that each aerosol particle is activated as a condensation nucleus, the measured droplet concentration is equal to the particle number concentration.

The droplet concentration can be measured by means of a number of different techniques. In the "Pocket Dust-Counter", developed by Aitken (189o/91), the condensing droplets are visually counted. A similar measuring technique was used by Scholz (1932). Unfortunately, the visual counting technique is restricted to relatively small numbers of droplets and therefore large statistical errors of the measuring results can occur. In order to improve the statistical significance of the measured droplet concentrations, Nolan and Pollak (1946) designed a "photo-electric nucleus counter", where the light extinction, caused by the droplet aerosol in a cylindrical tube, is taken as a measure for the droplet concentration. This method requires an empirical calibration. At low concentrations the light extinction is very small and accordingly the concentration measurements are difficult in this range. More accurate results, particularly at low concentrations, can be obtained by measuring the light, scattered by the growing droplets. Condensation nuclei counters, based on the light scattering technique, were developed by Rich (1961), Haberl (1977), Bricard et al. (1976), and Agarwal and Sem (198o). The Size Analyzing Nuclei Counter SANC is also based on light scattering techniques (see section 5.3)).

Jaenicke (1975) suspected that in an expansion chamber a relative increase of the particle number concentration could occur due to the fact that the particles, because of their inertia, will not completely follow the gas movement during the expansion. This "expansion enrichment" would cause errors in the determination of the condensation nuclei concentration. In order to estimate the possible influence of this effect on the measurement of the actual particle number concentration, the relaxation time $\tau = m.B$ of an aerosol particle is considered, where m and B are the particle mass and mobility, respectively. For a particle with a diameter of 1 µm, the relaxation time is found to be of the order of 1 µs. On the other hand, typical expansion times are not shorter than a few ms. Therefore it can be concluded that particle inertia will have a negligible influence on the measurement of particle number concentrations.

In addition to the above theoretical estimate, the significance of the "expansion enrichment" was checked experimentally (Wagner and Pohl, 1978 b). Spray-dried Latex particles with a diameter of 0.48 µm were used as condensation nuclei. Number concentration measurements were performed by means of the SANC applying different expansion ratios under otherwise unchanged conditions. The lower curve of fig. 52 shows that the measured droplet concentrations decrease for increasing expansion ratio. Assuming that the condensation nuclei aerosol and the carrier gas are diluted in the same ratio during the expansion process, the initial nuclei concentration before the expansion can be calculated from the measured droplet concentration by means of equ. (3.17). The upper curve of fig. 52 shows that thereby initial nuclei concentrations are obtained, which are independent from the chosen expansion ratio. Accordingly, even for the used large condensation nuclei, an "expansion enrichment" could not be observed.

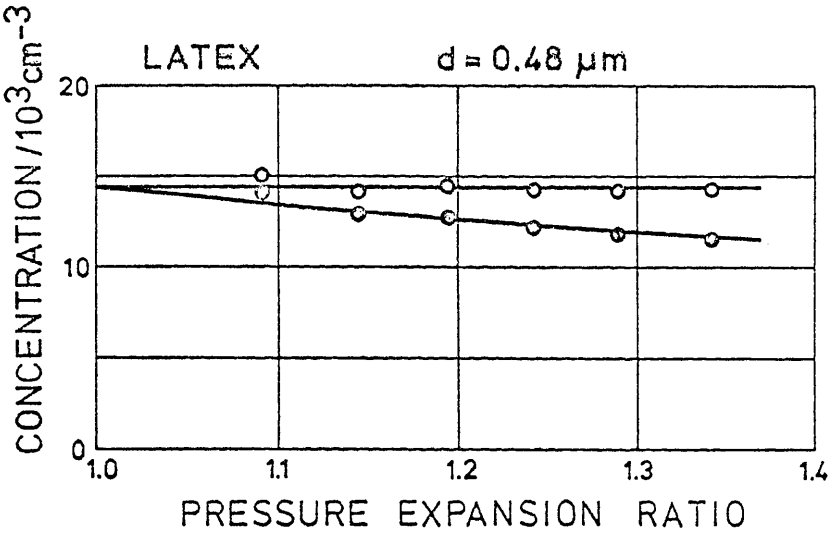

Fig. 52

Number concentrations, obtained at different expansion ratios. Lower curve: Uncorrected droplet concentration. Upper curve: Initial nuclei concentration before the expansion process, calculated by means of equ. (3.17).

Besides the measurement of aerosol number concentration, the aerosol particles can be classified with respect to their behaviour as condensation nuclei at different supersaturations. In this connection the aerosol particles are characterized by means of a Kelvin-equivalent diameter. This diameter is defined as the diameter of a pure water droplet which starts to grow at the same supersaturation as the particle. The relation between saturation ratio S and Kelvin equivalent diameter D_{equ} is given by the Kelvin-Gibbs equation

$$D_{equ} = \frac{4\,M\,\sigma}{R\,\rho\,T} \cdot \frac{1}{\ln S} \quad . \tag{8.1}$$

Fig. 53 shows the dependence of the Kelvin-equivalent diameter on the applied saturation ratio. The Kelvin-equivalent diameter is a measure for the geometrical size of the particles, but it also depends on the properties of the particle surface. If a water film is already adsorbed on the particle surface before super-saturation occurs, the particle will behave similar to a water droplet and the Kelvin-equivalent diameter will be a good approximation for the geometric diameter of the particle.

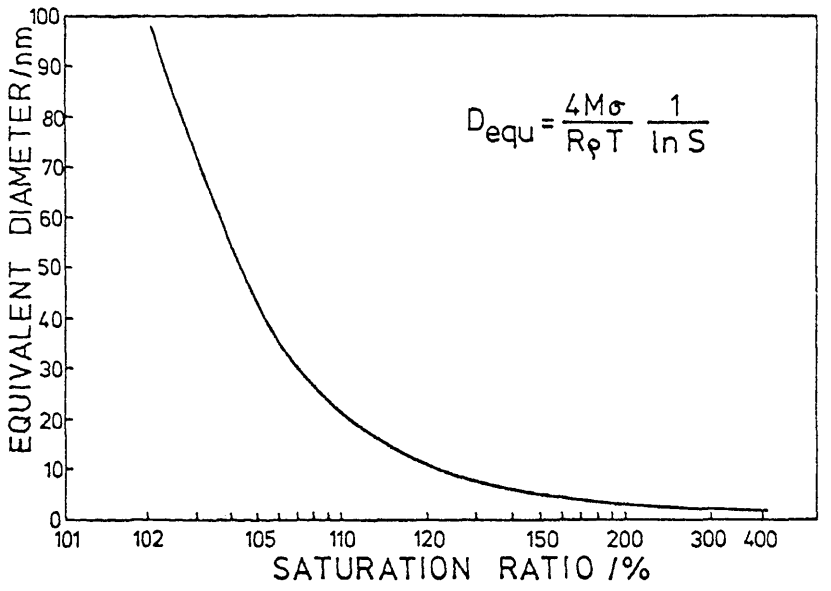

Fig. 53

Dependence of the Kelvin-equivalent diameter on the applied saturation ratio.

Rich (1955) already suggested to measure Kelvin-equivalent diameters by means of a modified Nolan-Pollak photo-electric nucleus counter. Katz and Kocmond (1973) investigated the size-supersaturation relationship and measured cumulative size distributions for NaCl-aerosols, using a thermal gradient diffusion chamber. Holländer et al. (1978) designed a "Humidity Gradient Condensation Nuclei Counter" for measurements of Kelvin-equivalent size distributions.
The size analyzing nuclei counter SANC can also be used for Kelvin-equivalent size distribution measurements. For this application, number concentration measurements are performed by means of the SANC with stepwise increasing saturation ratios and otherwise unchanged conditions. Thereby gradually smaller particles are activated as condensation nuclei and a cumulative Kelvin-equivalent size distribution is obtained. Differentiation of this cumulative distribution yields the corresponding differential Kelvin-equivalent size distribution of the nuclei aerosol in the form of a histogram.

This measuring technique was applied to size distribution measurements of the urban atmospheric aerosol in Vienna (Pohl and Wagner, 1978, 1979 b, 198o, Berner et al., 1979). In order to reduce short-term concentration fluctuations during the measuring time, the urban aerosol was drawn through a 2oo l-mixing vessel with a volume flow rate of about 1oo l min^{-1}. The connection tubes had a total length of about 6 m and a diameter of 7 cm. Part of the aerosol in the mixing vessel was drawn into the SANC. Simultaneous measurements by means of the General Electric Condensation Nuclei Counter were performed in order to monitor long-term drifts of the aerosol number concentration. The results of these reference measurements can be used for correction of the SANC-data.

The experimental conditions for the SANC-measurements were as follows:

Identification code:	SAIRRN2o1
	SAIRRN5o1
Dates: Wednesday, 1978-o9-o6, Sunday, 1978-o9-1o	
Humidifier Temperature:	$28^{o}C$
Chamber Temperature:	$28,5^{o}C$
Scattering angle:	15^{o}.

Light scattering curves were measured sequentially at 8 different expansion ratios, 2 repetitions being performed at each expansion ratio. A set of measurements for all chosen expansion ratios was repeated 4 times. Averages of the light scattering curves for all corresponding expansion ratios were taken. The droplet number concentrations were determined from the height of the first maximum. Fig. 54, 55 show the resulting Kelvin-equivalent size distribution of the urban aerosol in cumulative and differential form, as obtained on Wednesday, 1978-o9-o6. Fig. 56, 57 show the corresponding results, obtained on Sonday, 1978-o9-1o. It can be seen that the total aerosol number concentration was much higher on Wednesday, 1978-o9-o6. This can be explained by the fact that on this day an inversion occured in a height of about 5oo m. The measurements on Sunday, 1978-o9-1o, were performed under different meteorological conditions and significantly smaller total aerosol number concentrations were obtained. However, comparison of the differential size distributions, fig. 55, 57, shows that these distributions are quite similar, in spite of the different meteorological conditions. Maxima of the differential Kelvin-equivalent size distributions can be observed for diameters between 1o and 2o nm.

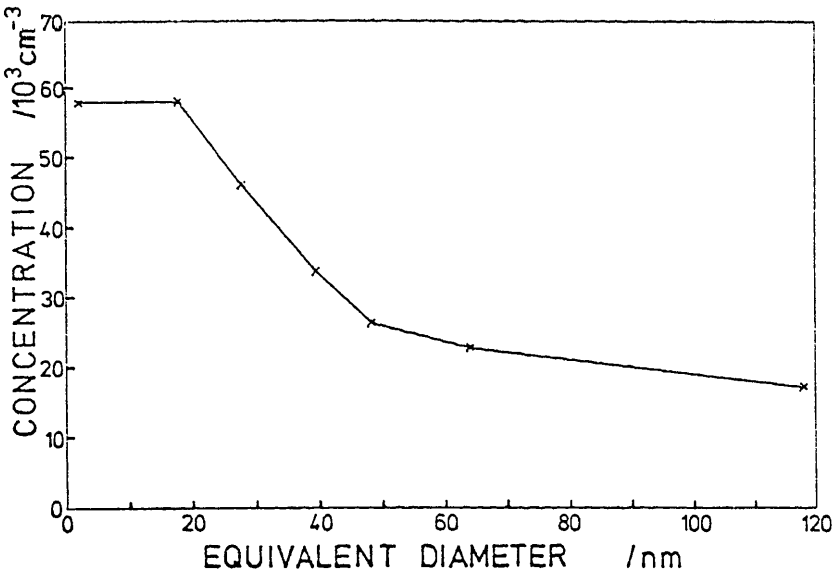

Fig. 54

Kelvin-equivalent size distribtuion of the urban aerosol in Vienna, Wednesday, 1978-09-06. Cumulative representation.

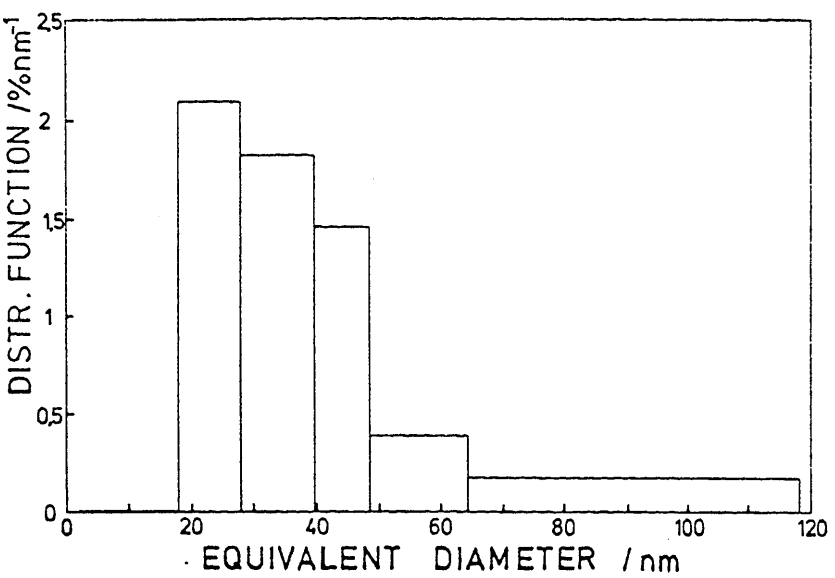

Fig. 55

As fig. 54, differential respresentation.

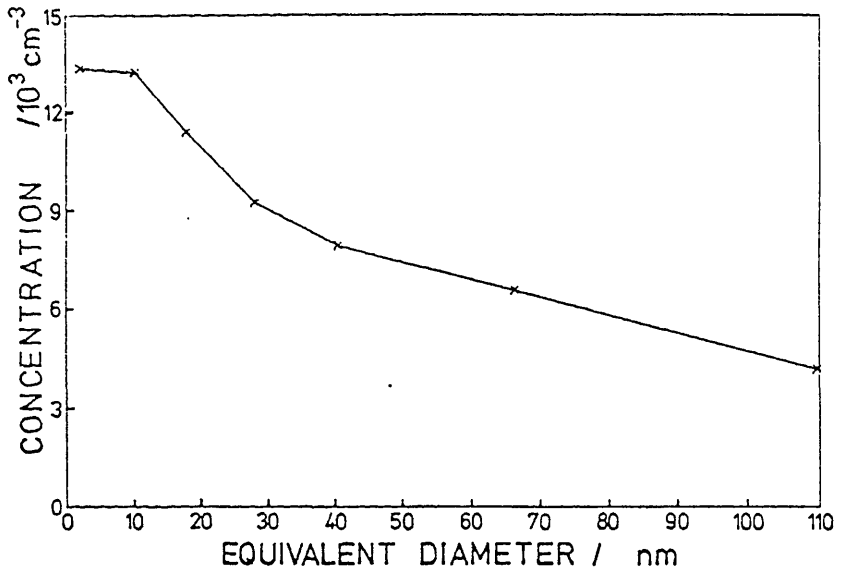

Fig. 56

As fig. 54, for Sunday, 1978-09-1o.

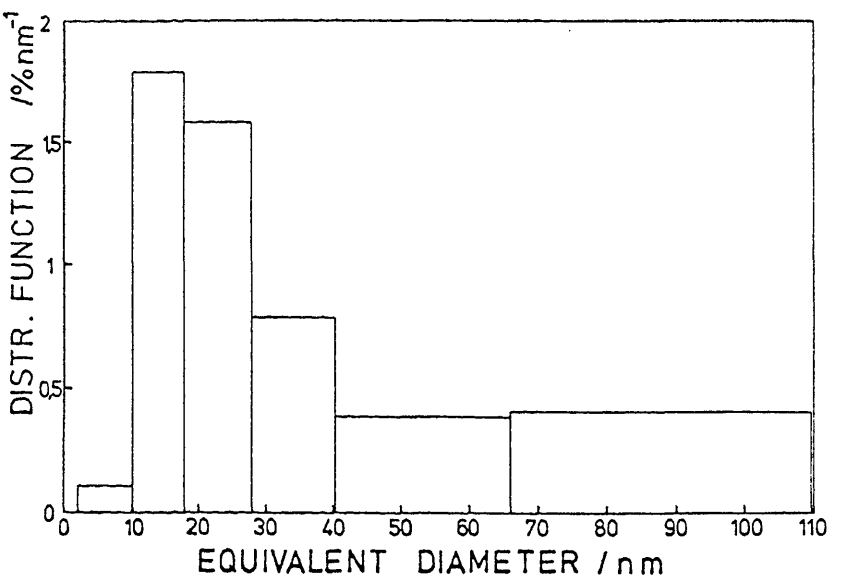

Fig. 57

As fig. 56, differential representation.

Whitby (1978) reported the results of size distribution measurements of atmospheric aerosols by means of an electrostatic aerosol mobility analyzer. For the California aerosol a maximum of the differential number size distribution at (13 ± 3) nm was found. This is in good agreement with the above described Kelvin-equivalent size distributions, although these measurements were based on completely different physical principles. The maximum of the size distribution in the size range around 1o nm is usually interpreted as the "Nucleation Mode" of the urban aerosol.

During a workshop, performed in Vienna, 1979,a comparison of the SANC with an electrostatic classifier, an aerosol electrometer and a number of different condensation nuclei counters was performed using well-defined aerosols. Fair agreement of the concentration readings of the different instruments was obtained. Furthermore, the Kelvin-equivalent diameters, as measured by the SANC, were found to be in satisfactory agreement with the particle diameters, as defined by the electrostatic classifier, for the case of DOP-particles. Some deviations were observed for NaCl-particles. Part of the results, obtained during this workshop, are included in Liu et al. (1979). During another workshop, performed in Vienna, 198o, these measurements have been extended towards smaller particle sizes, down to about 6 nm. A detailed description of the results of the above workshops will be presented elsewhere.

9) ACCURACY OF THE RESULTS

A number of experimental tests was performed in order to verify the assumptions, described in sections 2), 3) and 4).

9.1 Adiabatic expansion

For calculation of the initial thermodynamic conditions at the end of the expansion it is assumed that no heat and/or mass transport occurs from the chamber walls to the sensitive volume. An experimental test of this assumption was performed as follows.

Two different initial saturation ratios (relative humidities) in the measuring chamber before the expansion were chosen by appropriate setting of humidifier and chamber temperatures. Then for each of the two different initial saturation ratios before the expansion, a corresponding expansion ratio was selected to yield the same calculated supersaturation at the end of the expansion. The experimental droplet growth curves, obtained for both experimental conditions, were then compared. Fig. 58 shows the results for initial saturation ratios of 96.6 and 51.1 % before the expansion and corresponding expansion ratios 1.o57 and 1.245, resulting in a supersaturation of approximately 12o.5 % at the end of the expansion in both cases. Fig. 59 shows the results for the same two initial saturation ratios before the expansion, but for corresponding expansion ratios 1.359 and 1.597, resulting in a supersaturation of approximately 355 % at the end of the expansion in both cases. No significant differences of the experimental growth rates can be observed for measurements with the same supersaturation, although singificantly different expansion ratios had to be chosen for the different initial saturation ratios before the expansion.

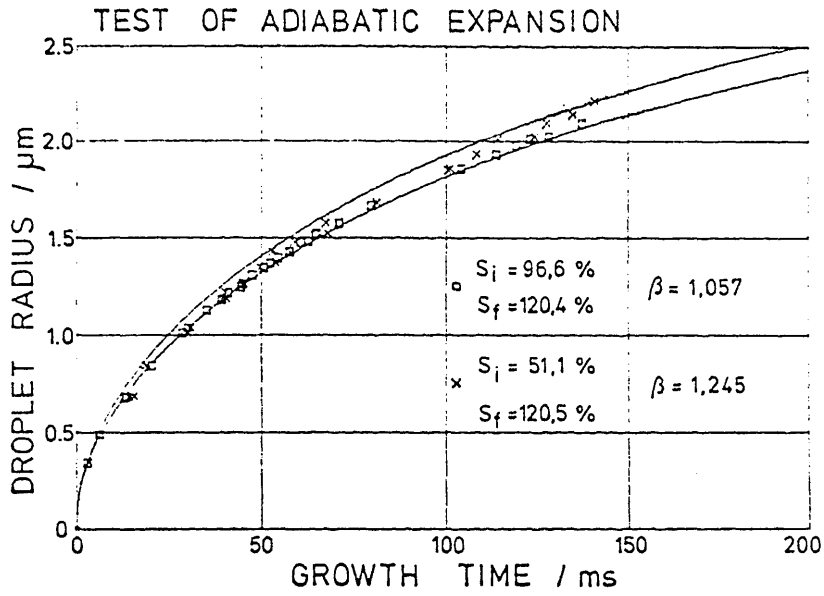

Fig. 58

Experimental droplet growth data for initial saturation ratios S_i = 96.6 and 51.1 % before the expansion and corresponding expansion ratios β = 1.057 and 1.245, resulting in calculated supersaturations S_f = 120.4 and 120.5 % at the end of the expansion.

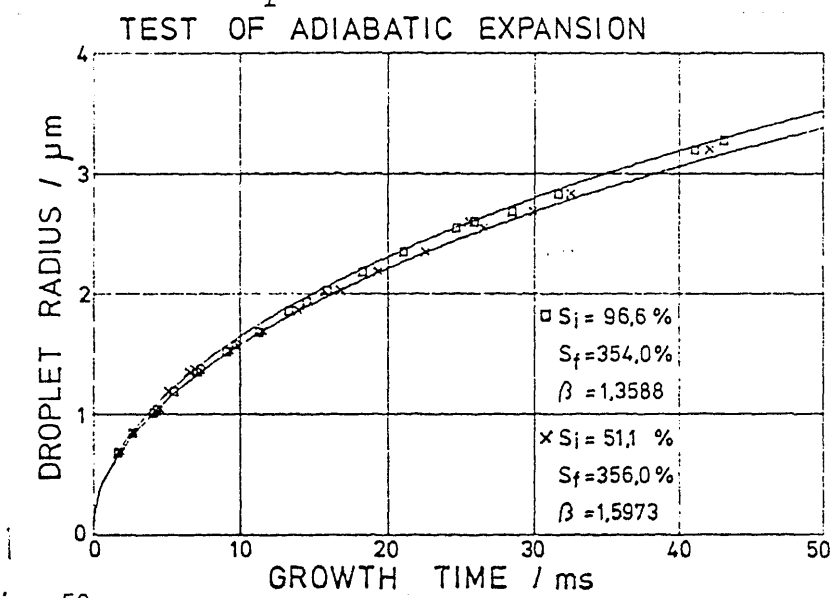

Fig. 59

As fig. 58 for expansion ratios β = 1.359 and 1.597, resulting in calculated supersaturations S_f = 354 and 356 % at the end of the expansion.

This result demonstrates that the actual supersaturation in the measuring chamber at the end of the expansion can be calculated with sufficient accuracy assuming dry-adiabatic expansion of an ideal gas mixture. Furthermore, possible influences of the chamber walls, caused by heat conduction, vapor diffusion, convection or turbulence, which are expected to be more important for higher expansion ratios, have not been observed and are thus negligible.

The changes of temperature and vapor pressure in the sensitive volume, caused by nonstationary diffusive heat and mass transfer from the chamber walls, can be calculated. Assuming an instantaneous expansion, Kassner et al. (1968 c) derived dimensionless expressions for the case of an infinite cylinder. For the system water vapor in air and for the actual dimensions of the SANC - expansion chamber a theoretical estimate proves the changes of temperature and vapor pressure in the sensitive volume to be much smaller than 1 % during the first 3oo ms after the end of the expansion. As mentioned earlier, the expansion time in the SANC expansion chamber is approximately 7 ms. Thus for the given experimental conditions the diffusive heat and mass transfer from the chamber walls to the sensitive volume are negligible during expansion and droplet growth.

9.2 Reversible quasistatic expansion without decomposition of the vapor-gas mixture

The expansion in the measuring chamber is assumed to be reversible quasistatic. Furthermore, the composition of the vapor-gas mixture is assumed to be unchanged during the expansion process. Both conditions are automatically fulfilled for a volume-defined expansion, initiated by a moving piston. However, in the SANC-measuring chamber a pressure-defined expansion is initiated by the opening of a valve. Strictly speaking, the opening of a valve causes an irreversible expansion and the composition of the vapor-gas mixture is not well-defined during the expansion process. For the present experimental conditions, the equivalence of pressure and volume defined expansions was tested by comparison of droplet growth rates, as obtained with pressure and volume defined expansions.

For measurements with volume defined expansions in the SANC expansion chamber, a thin, elastic rubber membrane was inserted into the outlet part D between measuring chamber and expansion valve (see section 6.1.1), fig. 22). Droplet growth measurements were performed with and without inserting the rubber memebrane under otherwise identical experimental conditions. Before each measurement was performed, the chamber was flushed at a flowrate of approx. 2 l/min. At first, in both cases, the chamber was flushed by drawing the aerosol through the same ring channel RA in part D (fig. 22). Using the rubber membrane, the measured droplet growth rates were found to be independent from the flushing time for flushing times above approx. 2o sec. However, for measurements without the rubber membrane, increasing growth rates were obtained for longer flushing times. Fig. 6o shows the experimental light scattering curves, obtained with and without the rubber membrane. The measurements without rubber membrane were performed with the longest available flushing time of 65 sec. Somewhat higher growth rates can be observed for measurements with rubber membrane (see fig. 6o).

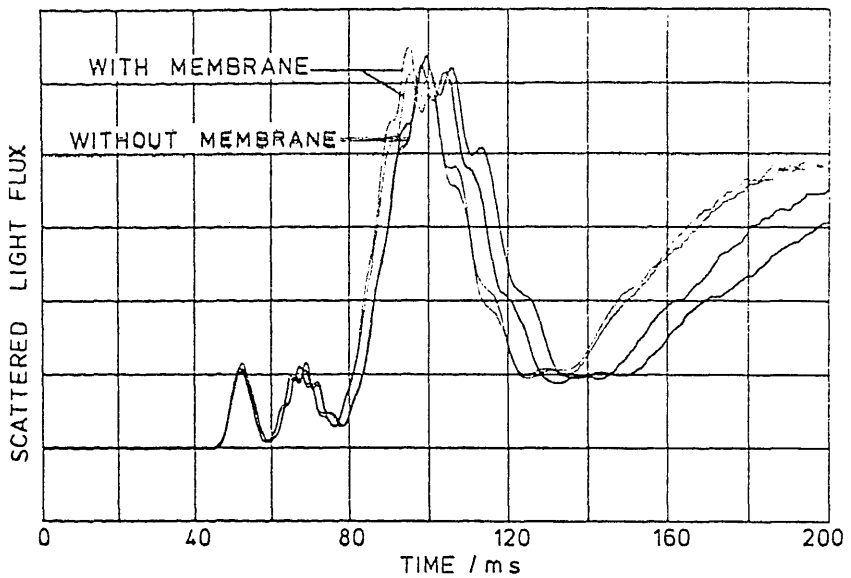

Fig. 6o

Experimental light scattering curves, obtained with and without inserting the rubber membrane. In both cases the chamber was flushed by drawing the aerosol through the same ring channel RA in part D (fig. 22).

In order to improve the chamber flushing, the aerosol was drawn through ring channel RA in connector C (fig. 23) for all further measurements without rubber membrane. Thereby, as described in section 6.1.1), nearly the whole volume, all the way up to the expansion valve, can be flushed with humidified aerosol. With this arrangement the measured droplet growth rates were found to be independent from the flushing time for flushing times above approx. 2o sec, no matter, if a rubber membrane was inserted or not. Fig. 61 shows a comparison of experimental light scattering curves, obtained with and without the rubber membrane, using the improved flushing arrangement in the latter case.

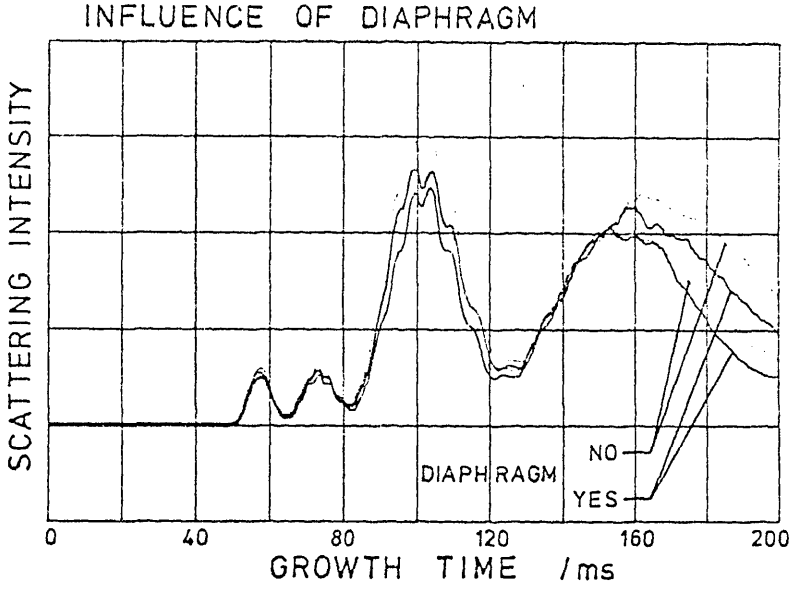

Fig. 61
As fig. 60, but for measurements without the rubber membrane the chamber was flushed by drawing the aerosol through the ring channel RA in connector C (fig. 23).

No significant differences can be observed. Thus it can be concluded that pressure and volume defined expansion are equivalent for the present experimental conditions. Accordingly, the pressure defined expansions, as usually obtained in the SANC measuring chamber by opening of a valve, can be regarded as reversible quasistatic and no significant decomposition of the vapor-gas mixture can be observed during the expansion process. In this connection it should be mentioned that Israel and Nix (1966 a, b) concluded from their measurements that the actual supersaturations in the pressure defined expansion chamber of a Pollak counter are smaller than calculated assuming a reversible quasistatic expansion. Israel and Nix considered the irreversibility of a pressure defined expansion as a possible explanation for these deviations. However, this explanation appears to be unlikely in view of the above described experimental results.

9.3 Humidification in the humidifier

In order to calculate the saturation ratio in the measuring chamber at the end of the expansion, the relative humidity (saturation ratio) B at the exit of the humidifier must be determined. Direct measurement of the relative humidity (Riediger, 1970, 1971) in the range close to 100 % with the required accuracy of better than $\pm$ 0.2 % is difficult. Therefore the flowrate through the humidifier was chosen sufficiently small so that the assumption B = 100 % appears to be justified.

A test of this assumption can be performed by means of droplet growth measurements, because droplet growth rates are strongly dependent on the supersaturation. As can be seen from equ. (2.91), the droplet growth rate depends on $(S_\infty - S_a)$, where S_a is close to unity for the present experimental conditions. Therefore the measured growth rates will be most sensitive with respect to changes of the saturation ratio S_∞, if small supersaturations are chosen. Accordingly, the saturation ratio S_∞ can be determined most accurately by comparison of experimental and theoretical droplet growth rates at small supersaturations. As shown in section 8.2), the droplet growth calculations are in good agreement with measured droplet growth rates over a wide range of supersaturations. However, possible inaccuracies of the used theoretical growth law have a comparatively small influence on the determination of the saturation ratio S_∞ for the case of small supersaturations. Thus the humidification of the humidifier can be tested by comparison of experimental and theoretical droplet growth rates at low supersaturations.

Fig. 62 shows a comparison of experimental and theoretical droplet growth data. Because of possible influences of the chamber walls on the growth process, the experimental data must be restricted

to a time interval of 2oo ms. Assuming complete humidification in the humidifier (B = 1oo %), an experimental saturation ratio of 1o2,93 % was obtained. It can be seen that droplet growth curves, calculated for saturation ratios, which differ from the experimental saturation ratio by no more than ± o.2 %, already deviate significantly from the experimental data. Thus it can be concluded that the humidification in the humidifier is better than 99.8 %.

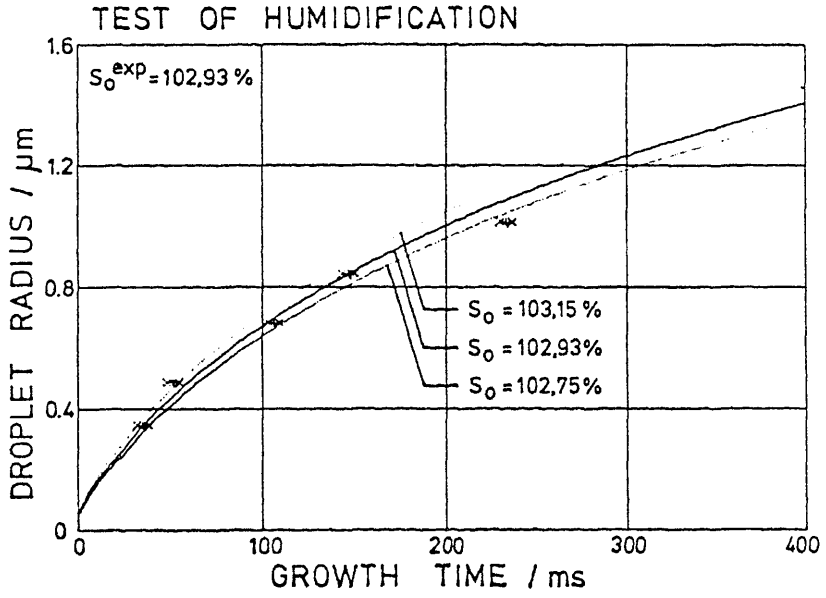

Fig. 62

Comparison of experimental and theoretical droplet growth data for an experimental saturation ratio of 1o2.93 %. The influence of slight changes of the saturation ratio on the theoretical curves is demonstrated.

9.4 Influence of the laser beam

For a quantitative comparison of experimental and theoretical droplet growth curves it is important that the laser beam does not influence the thermodynamic conditions in the measuring chamber. For the considered light wavelength of 632.8 nm, water does not show significant absorption. Accordingly, an influence of the laser beam is not expected. However, an experimental test was performed as follows (Wagner, 1974 a). A series of light scattering measurements was performed by means of light pulses instead of the usually applied continuous light. Light pulses with a pulselength of 100 μs were produced by means of a transverse Pockels cell, which was used as a fast shutter for the continuous wave laser. During a number of measuring cycles a light pulse was sent into the measuring chamber at the end of an adjustable delay time after the expansion and the scattered light pulse was measured. By means of systematic variation of the delay time during several measuring cycles with otherwise unchanged experimental conditions, the intensity of the scattered light was measured as a function of time. Fig. 63 shows the results for a scattering angle of 15^{o}, an expansion ratio of 1.37 and a droplet concentration of 5.10^{3} cm^{-3}. For the same experimental conditions a second measurement of the light scattering curve was performed with continuous light during one single measuring cycle. The corresponding result is shown in fig. 64. Comparison of fig. 63 and 64 shows no significant differences. Accordingly, an influence of the continuous laser beam on the droplet growth process has not been observed.

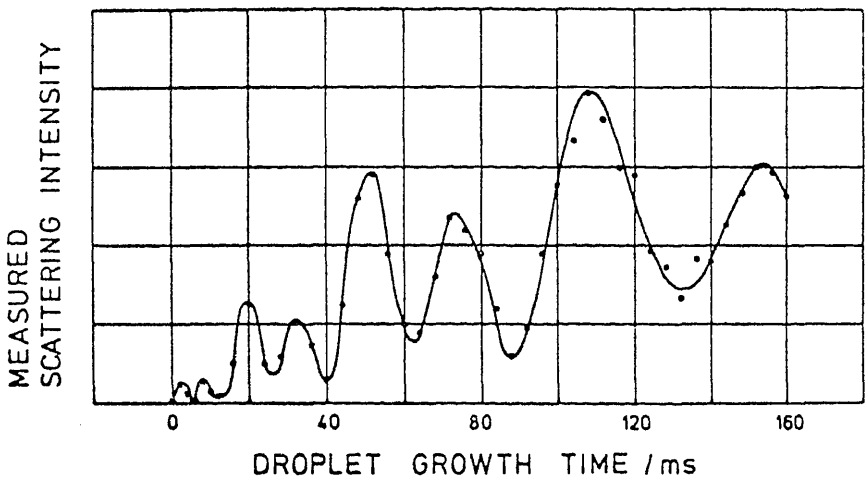

Fig. 63

Intensity of the scattered light, measured as a function of time by means of light pulses. Scattering angle 15^{o}, expansion ratio 1.37, droplet concentration 5.10^{3} cm^{-3}.

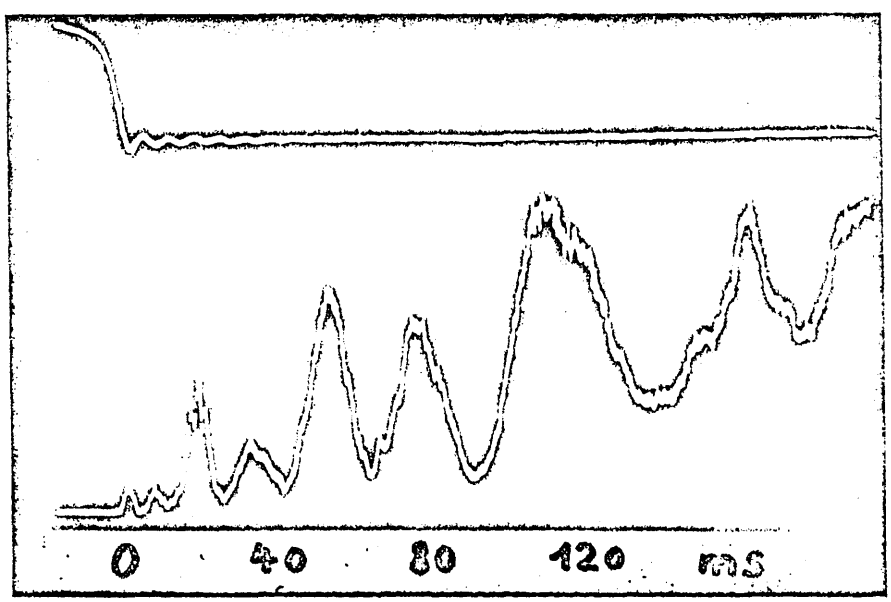

Fig. 64

As fig. 63, but measured with continuous light.

9.5 Quantitative test of the light measuring system

As described in section 5.3), the measurements of droplet concentrations in the SANC measuring chamber are based on the quantitative determination of the ratio of scattered light flux Φ_{sca} and transmitted light flux Φ_{trans}. The light flux Φ_{sca}, scattered by the droplets inside the scattering volume MV (fig. 11) and entering the measuring system for scattered light, is defined by the circular stop S_c (see section 4.2)). Therefore the diameter d of S_c must be determined precisely (see section 6.2.3)). The light flux Φ_{trans}, transmitted through the measuring chamber, is measured by the optoelement OPT (fig. 21, see section 6.2.2)), which was calibrated against the measuring system for scattered light (see section 6.2.5). The light intensity distribution over the cross section of the transmitted laser beam is quite different from the intensity distribution of the scattered light over the cross section of the circular stop S_c (fig. 11). Furthermore, both light intensity distributions will be quite inhomogeneous. Therefore it is important that the measurements of the light flux, entering the measuring system for scattered light, are independent from the actual light intensity distribution.

In order to test the measuring system for scattered light with respect to the independence from the light intensity distribution, measurements with two different circular stops S_c were compared. The diameters of the two stops were measured by means of an optical microscope with a calibrated ocular micrometer and the values $d_1 = (2.0086 \pm 0{,}0018)$ mm and $d_2 = (2.9860 \pm 0.0012)$mm were obtained. A dilute latex hydrosol, illuminated by the laser beam, was observed under a forward scattering angle of 45^o. The scattered light flux was found to be sufficiently time-independent after a stabilizing period of about 4 hours.

Measurements with the two different stops S_c resulted in an experimentally obtained light flux ratio of 2.19o5. On the other hand, the ratio of the cross sectional areas of the two circular stops S_c is 2.21oo. Accordingly, measured light flux and cross sectional area of the circular stop S_c were found to be proportional with an accuracy better than o.9 %. Hence measurements of the light flux entering the measuring system for scattered light, were found to be highly independent from the light intensity distribution over the cross section of the circular stop S_c. For all further measurements a stop S_c with about 2 mm diameter was used.

9.6 Dependence of the theoretical light scattering curves on different experimental conditions

The droplet concentrations in the SANC measuring chamber are determined by comparison of the height of experimental and theoretical light scattering maxima. The theoretical light scattering curves depend on the actual values of refractive index m of the droplets, breadth parameter σ of the droplet size distribution and scattering angle θ_o. Accordingly, the droplet concentration measurements are influenced by these parameters.

In order to estimate the errors of concentration measurements, caused by possible inaccuracies of the values for m,σ and θ_o, the influence of these parameters on the theoretical light scattering curves was checked numerically. The ratio of light fluxes Φ_{sca}/Φ_{trans} (see section 4.3)) was considered as a function of the size parameter α for different scattering angles. The height of the first and ninth maximum at forward scattering angle 15^o and of the ninth maximum at forward scattering angle $6o^o$ was calculated. The influence of slight variations of m, σ and θ_o on the height of the above light scattering maxima was determined. Fig. 65, 66, 67 and 68 show the dependence of the height of the considered light scattering maxima on the real and imaginary part of the refractive index m, the breadth parameter σ and the scattering angle θ_o, respectively. It can be seen that particularly the first maximum at forward scattering angle 15^o is only slightly influenced by changes of m, σ and θ_o. This maximum was chosen for most concentration measurements.

The real part of the refractive index m of water at the considered light wavelength λ = 632.8 nm varies between 1.3326 and 1.3295 for temperatures ranging from 0 to 40^oC according to the literature.

For the imaginary part of the refractive index m of water at the same wavelength the literature data are found to be smaller than $2.1o^{-6}$. The quantitative determination of the breadth parameter σ of the droplet size distribution is discussed in section 8.1). The accuracy of the scattering angle θ_o depends on the correct alignment of the laser beam relative to the expansion chamber. As shown in section 6.2.4), possible errors of the alignment are smaller than $\pm 0.3^o$.

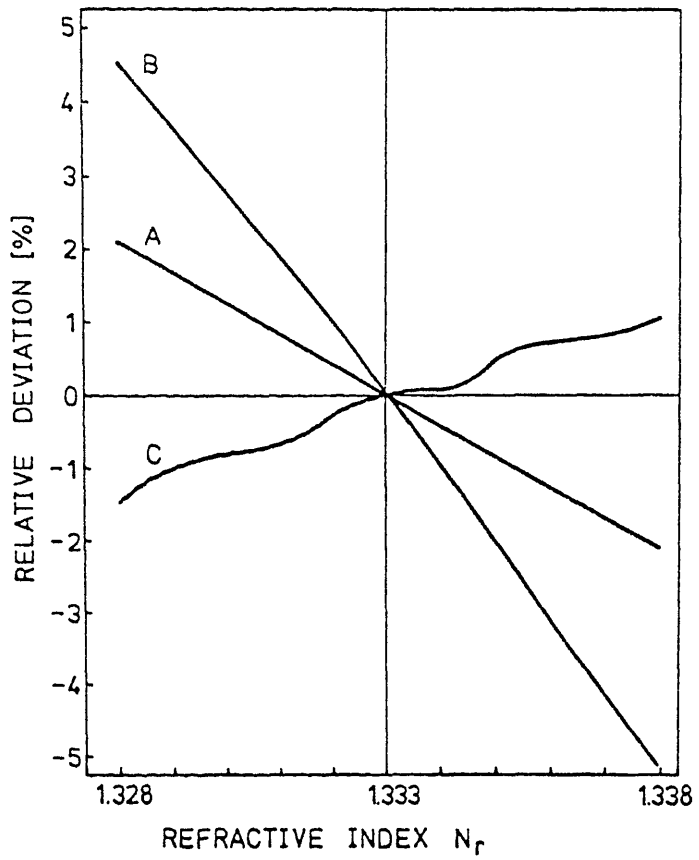

Fig. 65

Dependence of the height of different light scattering maxima on the real part of the refractive index n of the droplets. Curve A: $\theta_o = 15^o$, first maximum ($\alpha = 6.8$), curve B: $\theta_o = 15^o$, ninth maximum ($\alpha = 20.0$), curve C: $\theta_o = 60^o$, ninth maximum ($\alpha = 16.3$).

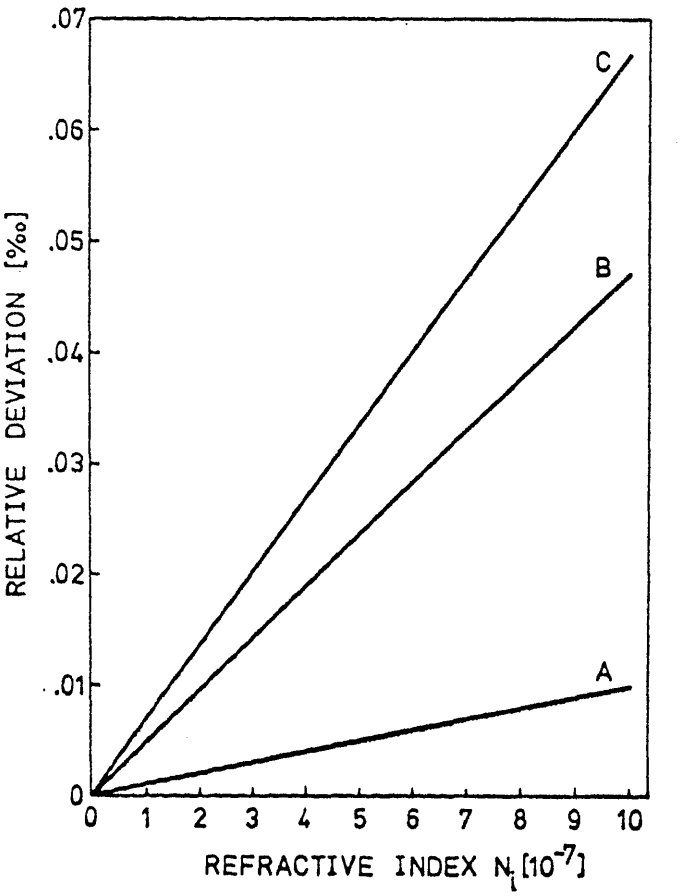

Fig. 66

As fig. 65 for the dependence on the imaginary part of the refractive index n of the droplets.

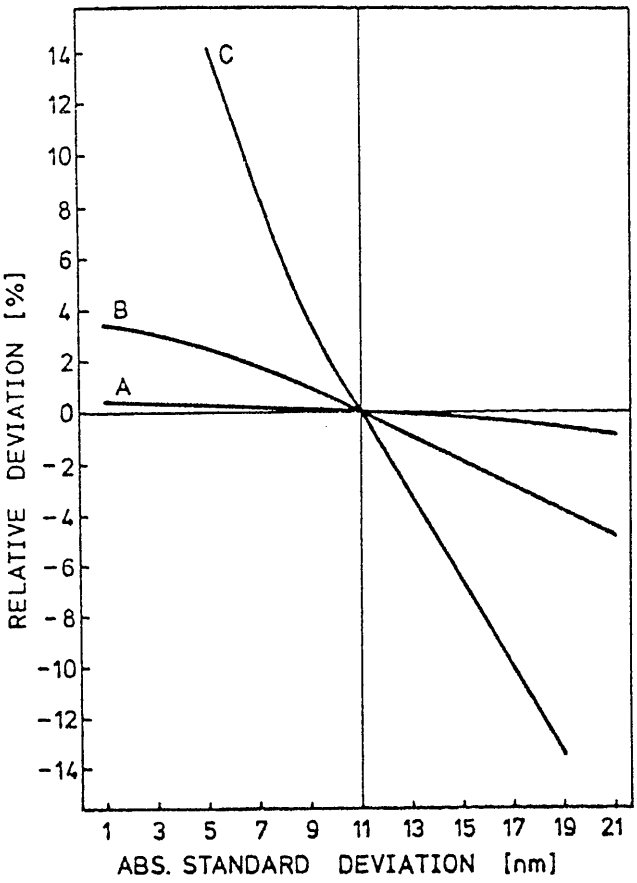

Fig. 67

As fig. 65 for the dependence on the breadth parameter σ of the droplet size distribution. A zeroth order lognormal size distribution is assumed.

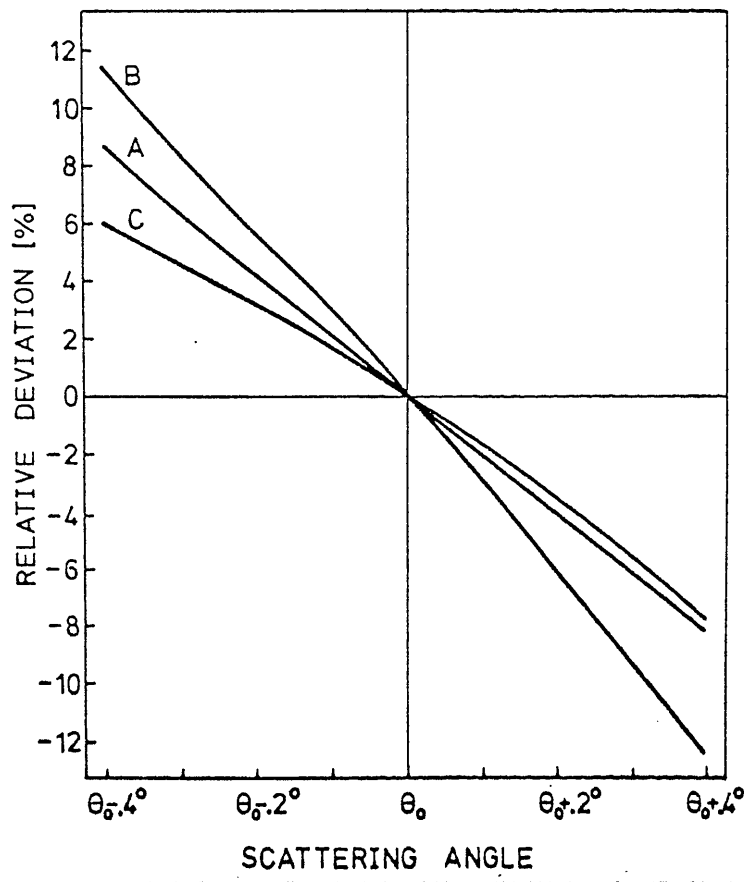

Fig. 68

As fig. 65 for the dependence on the scattering angle θ_o.

10) REFERENCES

Agarwal, J.K., and Sem, G.J. (1980), "Continuous Flow Single-Particle-Counting Condensation Nucleus Counter", J. Aerosol Sci. 11, 343.

Aitken, J. (1890/91), "On a Simple Pocket Dust-Counter" Proc. Roy. Soc. Edinburg 18, 39.

Akoy, E. (1971), "A Cloud Chamber Study for the Determination of Condensation Coefficient of Water", M.S. Thesis, Brown University, Providence, Rhode Island, U.S.A.

Allard, E.F., and Kassner, J.L., Jr. (1965), "New Cloud Chamber Method for the Determination of Homogeneous Nucleation Rates", J. Chem. Phys. 42, 1401.

Alty, T., and Mackay, C.A., (1935), "The Accomodation Coefficient and the Evaporation Coefficient of Water", Proc. Roy. Soc. London A 149, 104.

Arfken, G. (1971), "Mathematical Methods for Physicists", Academic Press, New York and London.

Ashkin, A., and Dziedzic, J.M. (1977), "Observation of Resonances in the Radiation Pressure on Dielectric Spheres", Phys. Rev. Lett. 38, 1351.

Bennett, H.S., and Rosasco, G.J. (1978), "Resonances in the efficiency factors for absorption: Mie scattering theory", Appl. Opt. 17, 491.

Berner, A., Lürzer, Ch., Pohl, F., Preining, O., and Wagner, P. (1979), "The Size Distribution of the Urban Aerosol in Vienna", Sci. Total Env. 13, 245.

Bhatnagar, P.L., Gross, E.P., and Krook, M. (1954), "A Model for Collision Processes in Gases. I. Small Amplitude Processes in Charged and Neutral One-Component Systems", Phys. Rev. 94, 511.

Birks, J., and Bradley, R.S. (1949), "The Rate of Evaporation of Droplets. II. The Influence of Changes of Temperature and of the Surrounding Gas on the Rate of Evaporation of Drops of di-n-butyl phtalate", Proc. Roy. Soc. A 198, 226.

Born, M., and Wolf, E. (1975), "Principles of Optics", Pergamon Press, Oxford, New York, Toronto, Sidney, Braunschweig. (fifth edition).

Bradley, R.S., Evans, M.G., and Whytlaw-Gray, R.W. (1946), "The Rate of Evaporation of Droplets. Evaporation and Diffusion Coefficients and Vapor Pressure of Dibutyl Phtalate and Butyl Stearate", Proc. Roy. Soc. London A 186, 368.

Bradley, R.S., and Shellard, A.D. (1949), "The Rate of Evaporation of Droplets. III. Vapour Pressures and Rates of Evaporation of Straight-Chain Paraffin Hydrocarbons", Proc. Roy. Soc. A198, 239.

Bricard, J., Delattre, P., Madelaine, G., and Pourprix, M. (1976), "Detection of Ultra-Fine Particles by Means of a Continuous Flux Condensation Nuclei Counter", in "Fine Particles" (B.Y.H.Liu, ed.), p. 566. Academic Press, New York, San Francisco, London.

Brock, J.R. (1966), "Diffusion to Particles in the Near Free Molecule Region", J. Colloid Interface Sci. 22, 513.

Brock, J.R. (1967 a), "Time Dependent Transfer Processes to Aerosol Particles in Noncontinuum Regions", J. Colloid Interface Sci. 23, 286.

Brock. J.R. (1967 b), "Highly Nonequilibrium Evaporation of Moving Particles in the Transition Region of Knudsen Number", J. Colloid Interface Sci. 24, 344.

Brown, P.S., and Arnason, G. (1973), "Efficient Numerical Integration of the Equations Governing Droplet Growth by Condensation", J. Atmos. Sci. 3o, 245.

Carstens, J.C., and Kassner, J.L., Jr. (1968), "Some Aspects of Droplet Growth Theory Applicable to Nuclei Measurements",J. Rech. Atmos. 3, 33.

Carstens, J.C., and Zung, J.T. (197o a), "Theory of Droplet Growth in Clouds. I. The Transient Stage of the Boundary - Coupled Simultaneous Heat and Mass Transport in Cloud Formation", J. Colloid Interface Sci. 33, 299.

Carstens, J.C., Williams, A., and Zung, J.T. (197o b), "Theory of Droplet Growth in Clouds: II. Diffusional Interaction between two Growing Droplets", J. Atmos. Sci. 27, 798.

Carstens, J.C., Carter, J.M., Vietti, M.A., and Schuster, B.G. (1973), "Droplet Growth Measurements in the One-Half to Ten Micron Size Range: Comparison with Theory", Trans. A.G.U. 54, 286.

Carstens, J.C., Podzimek, J., and Saad, A. (1974 a), "On the Analysis of the Condensational Growth of a Stationary Cloud Droplet in the Vicinity of Activation", J. Atmos. Sci. 31, 592.

Carstens, J.C., and Carter, J.M. (1974 b), "Current Meteorological Theory of Drop Growth by Condensation and Some Comparisons with Experiment", International Colloquium on Drops and Bubbles, California Institute of Technology and Jet Propulsion Laboratory, 28 - 3o. August 1974.

Carter, J.M., and Carstens, J.C. (1974), "Experimental Corroboration of the Conventional Meteorological Theory of Cloud Drop Growth by Laser Scattering", Trans. A.G.U. 55, 268.

Chang, R., and Davis, E.J. (1974), "Interfacial Conditions and Evaporation Rates of a Liquid Droplet", J. Colloid Interface Sci. 47, 65.

Chang, R., and Davis, E.J. (1976), "Knudsen Aerosol Evaporation", J. Colloid Interface Sci. 54, 352.

Chapman, S., and Cowling, T.G. (197o), "The Mathematical Theory of Non-Uniform Gases", Cambridge University Press, third edition.

Chodes, N., Warner, J., and Gagin, A. (1974), "A Determination of the Condensation Coefficient of Water from the Growth Rate of Small Cloud Droplets", J. Atmos. Sci. 31, 1351.

Chýlek, P. (1976), "Partial-wave resonances and the ripple structure in the Mie normalized extinction cross section", J. Opt. Soc. Am. 66, 285.

Cohen, A. (1969), "A Method for an Experimental Determination of the Growth Process of Water Droplets", Tellus 21, 736.

Coulier (1875), "Note sur une nouvelle propriété de l'air", J. Pharm. Chim. Paris (4) 22, 165.

Dahneke, B. (1977), private communication.

Dave, J.V. (1968), "Subroutines for Computing the Parameters of the Electromagnetic Radiation Scattered by a Sphere", Report No. 32o - 3237, p. 65. IBM Scientific Center, Palo Alto, California.

Dave, J.V. (1969 a), "Scattering of Visible Light by Large Water Spheres", Appl. Opt. 8, 155.

Dave, J.V. (1969 b), "Scattering of Electromagnetic Radiation by a large, absorbing Sphere", IBM J. Res. Develop. 13, 3o2.

Davis, E.J., and Chorbajian, E. (1974), "Measurement of Evaporation Rates of Submicron Aerosol Droplets", Ind. Eng. Chem. Fundam. 13, 272.

Davis, E.J., and Ray, A.K. (1977), "Determination of Diffusion Coefficients by Submicron Droplet Evaporation", J. Chem. Phys. 67, 414.

Davis, E.J., and Ray, A.K. (1978), "Submicron Droplet Evaporation in the Continuum and Noncontinuum Regimes", J. Aerosol Sci. 9, 411.

Debye, P. (19o9), "Der Lichtdruck auf Kugeln von beliebigem Material", Ann. Phys. (4), 3o, 57.

Delaney, L.J., Houston, R.W., and Eagleton, L.C. (1964), "The Rate of Vaporization of Water and Ice", Chem. Eng. Sci. 19, 1o5.

Denman, H.H., Heller, W., and Pangonis, W.J. (1966), "Angular Scattering Functions for Spheres", Wayne State University Press, Detroit.

Dennis, W.L. (196o), "The Growth of Hygroscopic Drops in a Humid Air Stream", Disc. Faraday Soc. 3o, 78.

Frisch, H.L., and Collins, F.C. (1953), "Diffusional Processes in the Growth of Aerosol Particles. II.", J. Chem. Phys. 21, 2158.

Frössling, N. (1938), "Über die Verdunstung fallender Tropfen", Gerlands Beitr. Geophys. 52, 17o.

Fuchs, N. (1934), "Über die Verdampfungsgeschwindigkeit kleiner Tröpfchen in einer Gasatmosphäre", Phys. Z. Sowjet. 6, 224.

Fuchs, N.A. (1958), "On the Theory of the Evaporation of Small Droplets", Sov. Physics - Tech. Physics 3, 14o (1958).

Fuchs, N.A. (1959), "Evaporation and Droplet Growth in Gaseous Media", Pergamon Press, London, Oxford, New York, Paris.

Fuchs, N.A. (1969), "Recent Progress in the Theory of Transfer Processes in Aerosols at Intermediate Values of the Knudsen Number", Proceedings of the 7th International Conference on Condensation and Ice Nuclei, Prague and Vienna, p. 1o, Academia, Prague.

Fuchs, N.A., and Sutugin, A.G. (1971), "High-Dispersed Aerosols", in "International Reviews in Aerosol Physics and Chemistry" (G.M. Hidy, and J.R. Brock, eds.), Vol. 2 ("Topics in Current Aerosol Research"), p. 1. Pergamon Press, Oxford, New York, Toronto, Sidney, Braunschweig.

Fukuta, N., and Walter, L.A. (197o), "Kinetics of Hydrometeor Growth from a Vapor-Spherical Model", J. Atmos. Sci. 27, 116o.

Fürth, R. (1942), "An Elementary Theory of Thermal Diffusion", Proc. Roy. Soc. London A 179, 461.

Gagin, A., and Terliuc, B. (1968), "A Modified Wieland-Twomey Thermal Diffusion Cloud Nuclei Counter", J. Rech. Atmos. 3, 73.

Giese, R.H., Debary, E., Bullrich, K., and Vinnemann, C.D. (1962), "Tabellen der Streufunktionen $i_1(\phi)$, $i_2(\phi)$ und des Streuquerschnittes $K(\alpha,m)$ homogener Kügelchen nach der Mie'schen Theorie", Abhandlungen der Deutsehen Akademie der Wissenschaften zu Berlin, p. 175. Akademie-Verlag, Berlin.

Gollub, J.P., Chabay, I., and Flygare, W.H. (1973), "Optical Heterodyne Measurement of Cloud Droplet Size Distributions", Appl. Opt. 12, 2838.

Gollub, J.P., Chabay, I., and Flygare, W.H. (1974), "Laser Heterodyne Study of Water Droplet Growth", J. Chem. Phys. 61, 2139.

Haberl, J.B. (1977), "A Linear Scale Aitken Nuclei Counter with Automatic Range Selection", J. Air Pollut. Control Assoc. 27, 146.

Hertz, H. (1889), "Die Kräfte elektrischer Schwingungen, behandelt nach der Maxwell'schen Theorie", Ann. Phys. Lpz. 36, 1.

Hickman K.C.D. (1954), "Maximum Evaporation Coefficient of Water", Ind. Eng. Chem. 46, 1442.

Hirschfelder, J.O., Curtiss, C.F., and Bird, R.B. (1954), "Molecular Theory of Gases and Liquids", John Wiley and Sons, Inc., New York, Chapman and Hall, Ltd., London.

Holländer, W., Schumann, G., and Schörmann, J. (1978), "A Condensation Nuclei Counter with Inherent Size Resolution Capability", in "Atmospheric Pollution 1978", Proceedings of the 13th International Colloquium, Paris, France (M.M. Benarie, Ed.) April 25 - 28, 1978, Elsevier, Amsterdam.

Israel, H., and Nix, N. (1966 a),"Thermodynamische Vorgänge im Kondensationskernzähler", Zeitschr. Geoph. 32, 175.

Israel, H. and Nix, N. (1966 b), "Thermodynamic Processes in the Condensation Nuclei Counter", J. Rech. Atmos. 2, 185.

Jaenicke, R. (1975), "Absolute, direkte und relative Kondensationskernzähler", Gesellschaft Aerosolforschung 3, 78.

Jeans, J. (1954) , "The Dynamical Theory of Gases", Dover Publications, New York.

Kassner, J.L., Jr., Carstens, J.C., Vietti, M.A., Biermann, A.H., Yue, P.C.P., Allen, L.B., Eastburn, M.R., Hoffman, D.D., Noble, H.A., and Packwood, D.L., (1968 a), "Expansion Cloud Chamber Technique for Absolute Aitken Nuclei Counting", J. Rech. Atmos. 3, 45.

Kassner, J.L., Jr., Carstens, J.C., and Allen, L.B. (1968 b), "The Myth Concerning the Condensation Nucleus Counters", J. Rech. Atmos. 3, 25.

Kassner, J.R., Jr., Carstens, J.C., and Allen, L.B. (1968 c), "Analysis of the Heat and Vapor Propagation from the Walls of the Nolan Pollak and Gardner Type Condensation Nucleus Counters", J. Atmos. Sci. 25, 919.

Katz, J.L., and Ostermier, B.J. (1967), "Diffusion Cloud Chamber Investigation of Homogeneous Nucleation", J. Chem. Phys. 47, 478.

Katz, J.L., and Mirabel, P. (1975), "Calculation of Supersaturation Profiles in Thermal Diffusion Cloud Chambers", J. Atmos. Sci. 32, 646.

Katz, U., and Kocmond, W.C. (1973), "An Investigation of the Size-Supersaturation Relationship of Soluble Condensation Nuclei", J. Atmos. Sci. 3o, 16o.

Kerker, M. (1969), "The Scattering of Light and Other Electromagnetic Radiation", Academic Press, New York, London.

Kirkaldy, J.S. (1958), "The Time-Dependent Diffusion Theory for Condensation on Spherical and Plane Surfaces", Can. J. Phys. 36, 446.

Langmuir, I. (1915), "The Dissociation of Hydrogen into Atoms. II. Calculation of the Degree of Dissociation and the Heat of Formation", J. Amer. Chem. Soc. 37, 417.

Langsdorf, A. (1939), " A Continuously Sensitive Diffusion Cloud Chamber", Rev. Sci. Instrum. 1o, 91.

Langstroth, G.O., Diehl, C.H.H., and Winhold, E.J. (195o), "The Evaporation of Droplets in Still Air", Can. J. Research A 28, 58o.

Lindsay, A.L., and Bromley, L.A. (195o), "Thermal Conductivity of Gas Mixtures", Ind. Eng. Chem. 42, 15o8.

Liu, B.Y.H., Pui, D.Y.H., McKenzie, R.L., Agarwal, J.K., Jaenicke, R., Pohl, F.G., Preining, O., Reischl, G., Szymanski, W., and Wagner, P.E. (1979), "Recent Experiments of the Working Group on Ultrafine Aerosols - the 1979 WUFA workshop", Gesellschaft Aerosolforschung 7, 245.

Loyalka, S.K. (1973), "Condensation on a Spherical Droplet", J. Chem. Phys. 58, 354.

Luchak, G., and Langstroth, G.O. (195o), "Applications of Diffusion Theory to Evaporation from Droplets and Flat Surfaces", Can. J. Research A 28, 574.

Mason, B.J. (1951), "Spontaneous Condensation of Water Vapor in Expansion Chamber Experiments", Proc. Phys. Soc. B 64, 773.

Mason, E.A., and Monchick, L. (1965), "Survey of the Equation of State and Transport Properties of Moist Gases", in "Humidity and Moisture", Vol. 3, p. 257, Reinhold.

Mason, B.J. (1971), "The Physics of Clouds", Clarendon Press, 2 nd ed.

Maxwell, J.C. (1877), "Diffusion", Encyclopedia Britanica 2, 82. Also included in "The Scientific Papers of James Clerk Maxwell", (W.D. Niven, ed.), Vol. 2, p. 625. The University Press, Cambridge, 189o.

Mettenburg, C.W., Kassner, J.L., Jr., and Rinker, D.A. (1958), "A Long Sensitive Time Cloud Chamber", Bull. Am. Phys. Soc. (II) 3, 3o2.

Metz, H.J., and Dettmar, H.K. (1963), "Zur Berechnung der Mie'schen Streukoeffizienten für reelle Brechungsindizes", Kolloid Z. Z. Polymere 192, 1o7.

Mie, G. (19o8), "Beiträge zur Optik trüber Medien, speziell kolloidaler Metallösungen", Ann. Phys. 25, 377.

Mills, A.F., and Seban, R.A. (1967), "The Condensation Coefficient of Water", Int. J. Heat Mass Transfer 1o, 1815.

Monchick, L., and Reiss, H. (1954), "Studies of Evaporation of Small Drops", J. Chem. Phys. 22, 831.

Mordy, W. (1959), "Computations of the Growth by Condensation of a Population of Cloud Droplets", Tellus 11, 16.

Narusawa, U., and Springer, G.S. (1975), "Measurements of Evaporation Rates of Water", J. Colloid Interface Sci. 5o, 392.

Neiburger, M., and Chien, C.W. (196o), "Computations of the Growth of Cloud Drops by Condensation Using an Electronic Digital Computer", in "Geophysical Monograph Series, publ. by the American Geophysical Union", (H.Weickmann, and W.E. Smith, eds.), Monograph No. 5, p. 191. Waverly Press, Baltimore.

Nestle, R. (1932), "Verdampfungserscheinungen an Quecksilberteilchen und ihr Einfluß auf die Messung des elektrischen Elementarquantums", Z. Phys. 77, 174.

Nix, N. (1968), "Kondensation und Verdampfung an künstlichen und natürlichen Aerosolen", Dissertation, Techn. Hochschule Aachen, BRD.

Nix, N. (1969), "Die Kondensation und Verdampfung an Einzelteilchen von Kleinaerosolen", Staub-Reinhalt. Luft 29, 188.

Nix, N. (1972), "Wachstumsgeschwindigkeiten von H_2O-Tropfen in Kondensationskernzählern", Arch. Met. Geoph. Biokl. . A 21, 3o7.

Nix, N., and Fukuta ,N. (1973), "Nonsteady - state Theory of Droplet Growth", J. Chem. Phys. 58, 1735.

Nolan, P.J., and Pollak, L.W. (1946), "The Calibration of a Photo-Electric Nucleus Counter", Proc. Roy. Irish Acad., Dublin 51 A, 9.

Owe Berg, T.G., and George, D.C. (1968), "Investigation of the Kinetics of Condensation", J. Geophys. Res. 73, 31o3.

Paul, B. (1962), "Compilation of Evaporation Coefficients", ARS J. 32, 1321.

Penndorf, R. (1956), "New Tables of Mie Scattering Functions for Spherical Particles", Geophysical Research Paper No. 45, Cambridge Air Force Research Center, Bedford, Massachusetts.

Pohl, F.G., and Wagner, P.E. (1978), "Kelvin-Äquivalentgrößenverteilung des urbanen Aerosols im submikroskopischen Bereich - Messung mit einer prozeßgesteuerten Expansionsnebelkammer", Gesellschaft Aerosolforschung 6, 184.

Pohl, F. (1979 a), "Zur Untersuchung der Wasserdampfkondensation in einer prozeßgesteuerten Expansionsnebelkammer und deren Anwendung zur Analyse des urbanen Aerosols", Ph.D. Thesis, University of Vienna.

Pohl, F.G., and Wagner, P.E. (1979 b), "Measurement of Size Distributions of Urban Aerosols in the Size Range Below o,1 µm", J. Aerosol Sci. 1o, 2o9.

Pohl, F.G., and Wagner, P.E. (198o), "Measurement of Kelvin-equivalent Size Distributions of Urban Aerosols", J. Phys. Chem. 84, 1642.

Pound, G.M. (1972), "Selected Values of Evaporation and Condensation Coefficients for Simple Substances", J. Phys. Chem. Ref. Data 1, 135.

Ray, A.K., Davis, E.J., and Ravindran, P. (1979), "Determination of Ultra-Low Vapor Pressures by Submicron Droplet Evaporation", J. Chem. Phys. 71, 582.

Rayleigh, Lord (1871), "On the Light from the Sky, its Polarization and Colour", Phil. Mag. 41, 1o7.

Reid, R.C., and Sherwood, T.K. (1966), "The Properties of Gases and Liquids", Mc Graw-Hill, New York, second edition.

Reiss, H., and La Mer, V.K., (195o), "Diffusional Boundary Value Problems Involving Moving Boundaries, Connected with the Growth of Colloidal Particles", J. Chem. Phys. 18, 1.

Reiss, H. (1951), "The Growth of Uniform Colloidal Dispersions", J. Chem. Phys. 19, 482.

Rich, T.A. (1955), " A Photo-Electric Nucleus Counter with Size Discrimination", Geofisica pura e appl. 31, 6o.

Rich, T.A. (1961), "A Continuous Recorder for Condensation Nuclei", Geofisica pura e appl. 5o, 46.

Richarz, F. (19o6), "Der Wert des Verhältnisses der beiden spezifischen Wärmen für ein Gemisch zweier Gase, insbesondere für ozonhaltigen Sauerstoff", Ann. Phys. 19, 639.

Riediger, G. (197o), "Ein automatischer Kondensationskernzähler mit Expansionsprogramm", Ph.D. Thesis, University of Vienna.

Riediger, G. (1971), "Ein automatischer Kondensationskernzähler mit Expansionsprogramm", Staub-Reinhalt. Luft 31, 237.

Sahni, D.C. (1966), "The Effect of a Black Sphere on the Flux Distribution in an Infinite Moderator", J. Nucl. Energy A/B 2o, 915.

Schäfer, K. (1932), "Verdampfungserscheinungen an Quecksilbertröpfchen", Z. Phys. 77, 198.

Schindler, H.M. (1975), "Ein Programmpaket zur Unterstützung von Datenerfassung und Prozeßsteuerung unter Verwendung einer universellen Schnittstelle", Ph.D. Thesis, University of Vienna.

Scholz, J. (1932), "Vereinfachter Bau eines Kernzählers", Meteorol. Z. 49, 381.

Schuster, B.G., Carstens, J.C., and Kassner, J.L., Jr. (1969), "Discussion of Paper by T.G. Owe Berg and Douglas C. George, Investigation of the Kinetics of Condensation", J. Geophys. Res. 74, 3447.

Sedunov, Y.S. (1974), "Physics of Drop Formation in the Atmosphere", John Wiley and Sons, New York, Toronto.

Semonin, R.G., and Hayes, C.F. (1968), "Thermodynamic Processes in a Rapidly Expanded Gas", J. Rech. Atmos. 3, 287.

Shankar, P.N. (197o), " A Kinetic Theory of Steady Condensation", J. Fluid Mech. 4o, 385.

Sinnarwalla, A.M., Alofs, D.J., and Carstens, J.C. (1975), "Measurement of Growth Rate to Determine Condensation Coefficients for Water Drops Grown on Natural Cloud Nuclei", J. Atmos. Sci. 32, 592.

Smirnov, V.I., (1971), "The Rate of Quasi-Steady Growth and Evaporation of Small Drops in a Gaseous Medium", Pure Appl. Geophys. 86, 184.

Sommerfeld, A. (1927), in "Riemann-Weber's Differential- und Integralgleichungen der Mechanik und Physik" (P. Frank and R.v. Mises, ed.), Vol. 2, p. 495. Vieweg, Brunswick.

Squires, P. (1952), "The Growth of Cloud Drops by Condensation", Australian J. Sci. Res. 5, 59.

Stefan, J. (1874), "Versuche über die Verdampfung", Wien Ber. 68, 385.

Stefan, J. (1881), "Über die Verdampfung aus einem kreisförmig oder elliptisch begrenzten Becken", Wien Ber. 83, 943.

Szymanski, W., Pohl, F.G., and Wagner, P.E. (1979), "Optische Bestimmung der Tröpfchengrößenverteilung während des Wachstumsprozesses in übersättigtem Wasserdampf", Gesellschaft Aerosolforschung 7, 128.

Szymanski, W., Pohl, F.G., and Wagner, P.E. (198o), "The Optical Determination of Droplet Size Distribution During a Growth Process in Supersaturated Vapor", J. Aerosol Sci. 11, 268.

Twomey, S. (1977), "Atmospheric Aerosols" (Development in Atmospheric Science, Vol. 7), Elsevier Sc. Publ. Comp., Amsterdam, Oxford, New York.

Van de Hulst, H.C. (1949), "On the Attenuation of Plane Waves by Obstacles of Arbitrary Size and Form", Physica 15, 74o.

Van de Hulst, H.C. (1957), "Light Scattering by Small Particles", Wiley, New York.

Vietti, M.A., and Schuster, B.G. (1973 a), "Laser Scattering Measurements of Droplet Growth in Binary Mixtures. I. H_2O and air", J. Chem. Phys. 58, 434.

Vietti, M.A., and Schuster, B.G. (1973 b), "Laser Scattering Measurements of Droplet Growth in Binary Mixtures. II. H_2O and Argon, H_2O and Helium", J. Chem. Phys. 59, 1499.

Vietti, M.A., and Fastook, J.L. (1974), "Water Droplet Growth in a Simulated Cloud Environment", Trans. A.G.U. 55, 268.

Vietti, M.A., and Fastook, J.L. (1975), "Water Droplet Growth in an Expansion Cloud Chamber Operating at Small Supersaturations", J. Rech. Atmos. 9, 181.

Vietti, M.A., and Fastook, J.L. (1976), "Water Droplet Growth in a Carbon Dioxide Atmosphere: A Case for Small Sticking Coefficient", J. Chem. Phys. 65, 174.

Vietti, M.A. (1978), "Water Droplet Growth on NaCl Nuclei", Conference on Cloud Physics and Atmospheric Electricity, American Meteorological Society, Issaquah, Washington, July 31 - Aug. 4,1978.

Volkov, F.G., and Golovin, A.M. (197o), "Thermal and Diffusion Relaxation of an Evaporating Droplet with Internal Heat Generation", Zhurnal Prikladnoi Matematiki i Tekhnicheskoi Fiziki 1, 78.

Wagner, P. (1973), "Optical Determination of the Size of Fast-Growing Water Droplets in an Expansion Cloud Chamber", J. Colloid Interface Sci. 44, 181.

Wagner, P. (1974 a), "Untersuchung des Tröpfchenwachstums in einer schnellen Expansionsnebelkammer", Ph.D. Thesis, University of Vienna.

Wagner, P. (1974 b), "Optische Bestimmung der Tröpfchenkonzentration in einer Expansionskammer bei Kondensation an verschiedenen Kernen", Gesellschaft Aerosolforschung, Bd. 2.

Wagner, P.E., and Pohl, F.G. (1975 a), "The Interdependence of Droplet Growth and Concentration. I. Theory of Droplet Growth and Applications on Condensation Nuclei Counters", J. Colloid Interface Sci. 53, 429.

Wagner, P.E. (1975 b), "The Interdependence of Droplet Growth and Condensation. II. Experimental Test of Droplet Growth Theory", J. Colloid Interface Sci. 53, 439.

Wagner, P.E., and Pohl, F.G. (1977 a), "Dynamic Processes in Condensation Nuclei Counters - Model Calculations and Experimental Test", Ninth International Conference on Atmospheric Aerosols, Condensation and Ice Nuclei, Galway, Ireland, 21. - 27. Sept. 1977.

Wagner, P.E., and Pohl, F.G. (1977 b), "Eine prozeßgesteuerte Anlage zur Untersuchung der Kinetik von Kondensationsvorgängen", Gesellschaft Aerosolforschung 5, 279.

Wagner, P.E., and Pohl, F.G. (1978 a), "Einsatz einer prozeßgesteuerten Expansionsnebelkammer zur Überprüfung neuerer Tröpfchenwachstumstheorien", Gesellschaft Aerosolforschung, 6, 147.

Wagner, P.E., and Pohl, F.G. (1978 b), "Eine prozeßgesteuerte Anlage zur Untersuchung der Kinetik von Kondensationsvorgängen", Staub-Reinhalt. Luft 38, 72.

Wagner, P.E., and Pohl, F.G. (1979), "Experimental Test of Recent Droplet Growth Theories by Means of a Process Controlled Expansion Cloud Chamber", J. Aerosol Sci. 1o, 2o4.

Wassiljewa, A. (19o4), "Wärmeleitung in Gasgemischen", Physik Z. 5, 737.

Weber, W. (1975), "Eine universelle programmierbare Schnittstelle für Datenerfassung in den Naturwissenschaften", Ph.D. Thesis, University of Vienna.

Whalley, E. (1951), "Thermal Diffusion in Hydrogen-Water Vapor Mixtures", J. Chem. Phys. 19, 5o9.

Whitby, K.T. (1978), "The Physical Characteristics of Sulfur Aerosols", Atmos. Environ. 12, 135.

Williams, A., and Carstens, J.C. (1971), "A Note Concerning the Interaction of Two Growing Water Droplets", J. Atmos. Sci. 28, 1298.

Williams, M.M.R. (1975), "Condensation and Evaporation of a Dilute Vapor on a Spherical Droplet", Z. Naturforsch. 3oa, 134.

Wilson, C.T.R. (1912), "On an Expansion Apparatus for Making Visible the Tracks of Ionising Particles in Gases and Some Results Obtained by its Use", Proc. Roy. Soc. A 87, 277.

Wilson, C.T.R. (1933), "On y New Type of Expansion Apparatus", Proc. Roy. Soc. A 142, 88.

Wilson, J.G. (1951), "The Principles of Cloud-Chamber Technique", Cambridge University Press.

Wood, R.W. (19o2), "On a Remarkable Case of Uneven Distribution of Light in a Diffraction Grating Spectrum", Phil. Mag. (Ser. 6) 4, 396.

Wright, P.G. (19o6), "On The Discontinuity Involved in Diffusion across an Interface (The Δ of Fuchs)", Disc. Faraday Soc. 3o, 1oo.